

3
2008

This is to certify that the
dissertation entitled

BIOCHEMICAL ANALYSIS OF THE CHLOROPLAST
DIVISION PROTEINS FTSZ1 AND FTSZ2

presented by

BRADLEY JESSE STANFORD CARNAHAN OLSON

has been accepted towards fulfillment
of the requirements for the

Doctoral degree in Biochemistry and Molecular
Biology

Debra Oskopcey
Major Professor's Signature

May 6, 2008
Date

PLACE IN RETURN BOX to remove this checkout from your record.
TO AVOID FINES return on or before date due.
MAY BE RECALLED with earlier due date if requested.

DATE DUE	DATE DUE	DATE DUE

BIOCHEMICAL ANALYSIS OF THE CHLOROPLAST DIVISION PROTEINS FTSZ1 AND FTSZ2

By

Bradley Jesse Stanford Carnahan Olson

A DISSERTATION

**Submitted to
Michigan State University
in partial fulfillment of the requirements
for the degree of**

DOCTOR OF PHILOSOPHY

Department of Biochemistry and Molecular Biology

2008

ABSTRACT

BIOCHEMICAL ANALYSIS OF THE CHLOROPLAST DIVISION PROTEINS FTSZ1 AND FTSZ2

By

Bradley Jesse Stanford Carnahan Olson

Chloroplast division in plants is mediated by FtsZ1 and FtsZ2, which are homologues of the bacterial cell division protein FtsZ. The bacterial FtsZ protein is thought to be the progenitor to tubulin. FtsZ is a GTP-dependent, filament-forming protein that encircles the bacterial division site. Similarly, plant FtsZ proteins encircle the mid-plastid. Plant FtsZ1 and FtsZ2 family proteins differ primarily at their C-termini with FtsZ2 proteins possessing a motif similar to those found in bacterial FtsZ that is responsible for binding to other bacterial cell division factors. In plants, this motif has been shown to bind to the chloroplast division protein ARC6, which may be involved in FtsZ filament remodeling. The focus of this dissertation is on understanding the composition of the *in vivo* FtsZ complex and understanding the function and topology of FtsZ protofilaments.

To understand the composition of the FtsZ complex *in vivo*, FtsZ was purified from pea stroma. Pea FtsZ1 and FtsZ2 co-fractionate with the chloroplast division proteins ARC3 and ARC6 when separated by sucrose density gradient, anion-exchange chromatography, size-exclusion chromatography and native polyacrylamide gel electrophoresis. In addition, a ZipA-antibody cross-reactive protein was found to co-fractionate with FtsZ1/FtsZ2/ARC3/ARC6-containing complexes. Data from these

experiments suggest that a minimal unit of FtsZ assembly is a complex containing FtsZ1, FtsZ2, ARC3, ARC6 and protein that cross-reacts with an antibody to *E. coli* ZipA. The identify of the ZipA cross-reactive protein was not able to be determined

Plant FtsZ2 contains a C-terminus similar to the ZipA-binding C-terminus of bacterial FtsZ. However, ZipA has not been identified in plants. A structural search algorithm was created find a chloroplastic protein that is structurally similar to ZipA or to identify the protein that cross-reacts with the *E. coli* ZipA antibody. This algorithm identified a strong ZipA candidate, Ssz1, which was found to be a stromal protein. A homozygous *ssz1* mutant has slightly fewer and enlarged chloroplasts. However, Ssz1 did not interact with FtsZ2 in the yeast two-hybrid assay. At this time Ssz1 can not be definitively linked to a role in chloroplast division.

To understand the biochemical properties of plant FtsZ, recombinant FtsZ1 and FtsZ2 were produced individually in *E. coli*. FtsZ1 and FtsZ2 were both found to be GTPases, but had approximately 15-fold lower GTPase activity than *E. coli* FtsZ. When mixed equally, FtsZ1 and FtsZ2 co-assemble into bundled ribbon-like structures. This result differs from *E. coli* FtsZ, which only assembles into single protofilaments when polymerized under similar conditions. Maximal FtsZ1/FtsZ2 co-assembly requires equal concentration of both proteins. In addition, a T7-loop mutant, FtsZ2D322A, was found to be a sub-stoichiometric competitive inhibitor of FtsZ1, but not FtsZ2. Together these results support an FtZ1/FtsZ2 heterofilament model similar to $\alpha\beta$ -tubulin.

Dedication

To my wife Valerie

ACKNOWLEDGMENTS

Special thanks to fellowship support from the Department of Biochemistry and Molecular Biology with a N. E. Tolbert Memorial fellowship and from the Michigan State University Plant Sciences fellowship program. In addition, special thanks to the MSU-DEO Plant Research Laboratory for supporting travel and professional development.

This work was supported by the National Science Foundation.

Jonathan Glynn, Aaron Schmitz, Dr. Cecilia Chi-Ham, Dr. Shin-ya Miyagishima, Dr. Stanislav Vitha and Dr. Yue Yang were invaluable resources to discuss ideas and for critical assessment of this work.

Thanks to Valerie Olson for editorial assistance

Special thanks to Dr. Alicia Pastor for training and support of electron microscopy

Dr. Robert Hausinger and Dr. Kenneth Keegstra deserve special thanks for supporting pursuit of external awards.

TABLE OF CONTENTS

List of Tables	x
List of Figures	xi
Key to Abbreviations.....	xiii
Introduction	1
Specific Aims.....	2
Bacterial cell division is best understood in <i>E. coli</i>.....	5
FtsZ	5
Tubulin biochemistry	6
<i>E. coli</i> FtsZ is structurally and biochemically similar to tubulin.....	10
FtsZ polymerization and structure.....	11
<i>E. coli</i> FtsZ GTP hydrolysis drives depolymerization.....	13
Cooperative assembly of bacterial FtsZ.....	15
Model of FtsZ polymerization.....	16
Regulation of Z-ring assembly and placement.....	19
Nucleoid occlusion positions the Z-ring in bacteria	19
Positioning of the Z-ring by the MinCDE system	20
ZipA and FtsA organize and anchor the Z-ring at the membrane	21
ZapA	22
EzrA	23
SulA	23
Chloroplast Division	24
Ultrastructural observations of chloroplast division	24
The stromal chloroplast division machinery.....	25
The eukaryotic-derived chloroplast division machinery	30
Perspective	32
<i>In vivo</i> quantitative relationship between plastid division proteins FtsZ1 and FtsZ2 and identification of ARC6 and ARC3 in a native FtsZ complex.....	33
Synopsis.....	34
Introduction.....	35
Experimental Procedures.....	37
Plant material	37
Chloroplast morphology phenotyping.....	38

Immunofluorescence labeling	38
Preparation of antibodies.....	39
Expression, purification and calibration of recombinant protein standards	40
Chloroplast isolation.....	43
Determination of chloroplast volume	43
Quantitative immunoblotting.....	44
Immunoprecipitation of in vitro FtsZ translation products before and after import into isolated intact chloroplasts	45
Isolation of an endogenous FtsZ complex by two-dimensional gel electrophoresis	47
Isolation and analysis of FtsZ-containing complexes from Arabidopsis and pea	48
Results	50
Specificity of Arabidopsis FtsZ antibodies	50
AtFtsZ2-2 functions in chloroplast division	51
Quantitative analysis of FtsZ levels in Arabidopsis chloroplasts	54
AtFtsZ proteins are stably associated following import into pea chloroplasts	64
FtsZ1 and FtsZ2 are in a stable complex in vivo	66
The native FtsZ complex also contains ARC6 and ARC3	76
Discussion.....	82
Supplementary Results	87
Preparation of Quantitative Immunoblotting Standards	87
Specificity of the ARC6 Antibody	88
Acknowledgments	89

Plant FtsZ1 and FtsZ2 are GTPases and Assemble into Heterofilaments that Bundle into Ribbons.....	90
Introduction.....	91
Experimental Procedures.....	98
Expression and purification of recombinant FtsZ proteins	98
Site-directed mutagenesis.....	103
GTP binding and hydrolysis assays	104
Polymerization assays.....	105
Results	107
Production and refolding of recombinant Arabidopsis FtsZ1-1 and FtsZ2-1	107
Both FtsZ1 and FtsZ2 bind and hydrolyze GTP	110
Do FtsZ1 and FtsZ2 assemble?.....	112
FtsZ1/FtsZ2 co-assembly EM and light-scattering.....	112
FtsZ1 and FtsZ2 homofilaments are unstable	120
FtsZ1/FtsZ2 co-polymer length correlates to GTPase activity.....	121
The critical concentration for polymerization	123

FtsZ1/FtsZ2 co-polymers are larger and more stable than E. coli FtsZ polymers	124
FtsZ1/FtsZ2 copolymers are not disassembled by GDP	127
Stoichiometric requirements for GTPase activity and polymerization	128
Adding additional FtsZ1 or FtsZ2 to FtsZ1/FtsZ2 polymerization assays decreases the extent of polymerization	128
FtsZ2-1 promotes lateral bundling of FtsZ1-1/FtsZ2-1 ribbons.....	129
FtsZ2D322A competitively inhibits the polymerization of FtsZ1	135
FtsZ2D322A inhibits the GTPase activity of FtsZ1, but not FtsZ2.....	136
Plant FtsZ and T7-loop mutants assemble into rings in E. coli.....	139
Discussion.....	139
Previous in vitro studies	139
FtsZ1 and FtsZ2 polymerize into heterofilaments.....	142
The in vivo stoichiometry of FtsZ1 and FtsZ2	144
Heterofilament bundling	146
FtsZ1/FtsZ2 are different than tubulin and bacterial FtsZ.....	147
Why do plants require two types of FtsZ?.....	148
Acknowledgements	149
The search for an analogue to the bacterial cell division protein ZipA by computational and experimental approaches.....	151
Introduction.....	152
Results	154
Chloroplasts contain a protein that cross-reacts with a ZipA antibody and co-fractionates with FtsZ during partial purification.....	154
Identification of a structural analogue to the bacterial cell division protein ZipA	158
Phenotype of a T-DNA insertional mutant for <i>ssz1</i>	163
Ssz1 is a Stromal Chloroplast protein	163
Removal of the Ssz1 homologue in <i>Synechococcus elongatus</i> does not disrupt FtsZ filament morphology.....	168
Ssz1 does not interact with FtsZ2 in the yeast-two hybrid assay.....	169
Discussion	176
Structure Similarity Search Algorithm Development	176
Materials and Methods.....	181
Generation of a <i>Ssz1</i> Δ strain of <i>Synechococcus</i> PCC 7942.....	181
Database of Putative Chloroplast Proteins for Threading.....	182
Threading of the Unknown Chloroplast Proteins	182
Growth Conditions of Plants.....	182
Microscopy of Fixed Arabidopsis Tissue	183
Genotype of SALK insertions in <i>Ssz1</i>	183
Yeast-two Hybrid Assay	184

Summary and Future Directions	189
Summary	190
Future Directions	191
Structural Search Algorithms.....	191
The protein that cross-reacts with the E. coli ZipA antibody	193
Chloroplast division protein purification from inclusion bodies	194
FtsZ biochemistry.....	196
Probing heterofilament formation by FtsZ1 and FtsZ2	196
FtsZ1 and FtsZ2 lateral interactions.....	200
The biochemical effects of ARC6 and ARC3.....	201
Concluding remarks	203
Appendix A	204
References	222

LIST OF TABLES

Table 2.1: Effects of whole plant age on FtsZ in Arabidopsis chloroplasts.....	60
Table 2.2: Comparison of FtsZ levels in actively dividing <i>E. coli</i> cells with those in chloroplasts of 3-week-old Arabidopsis	62
Table 3.1: GTP binding and hydrolysis properties of FtsZ1 and FtsZ2 compared to <i>E. coli</i> FtsZ.....	106
Table 4.1: Candidate proteins structurally similar to <i>E. coli</i> ZipA.....	161
Table 4.2: Residue contact comparison between ZipA bound to <i>E. coli</i> FtsZ and Ssz1 bound to the plant FtsZ2 C-terminus.....	167
Table 4.3: Summary of a yeast two-hybrid interaction assay between Ssz1 and FtsZ1	178

LIST OF FIGURES

Figure 1.1: Cartoon representation sequence similarity between plant FtsZ1, FtsZ2, bacterial FtsZ and α - and β -tubulin.....	4
Figure 1.2: Model of the assembly dynamics of <i>E. coli</i> FtsZ	18
Figure 2.1: Expression and purification of recombinant protein standards for quantitative analysis	42
Figure 2.2: Antibody specificity for AtFtsZ1-1, AtFtsZ2-1, and AtFtsZ2-2.....	52
Figure 2.3: Chloroplast morphology and AtFtsZ2-1 and AtFtsZ2-2 localization in WT Arabidopsis and <i>atftsZ2-1</i> and <i>atftsZ2-2</i> T-DNA insertional mutants	56
Figure 2.4: Linear ranges of detection of FtsZ protein standards and FtsZ in chloroplast lysates for quantitative immunoblotting.....	59
Figure 2.5: Quantitative analysis of molecular levels of FtsZ1 and FtsZ2 in wild-type Arabidopsis.....	63
Figure 2.6: Immunoprecipitation of in vitro [³⁵ S]-labeled AtFtsZ translation and import products by FtsZ-specific antibodies	68 & 70
Figure 2.7: FtsZ1 and FtsZ2 cofractionate in isolated pea chloroplasts	72
Figure 2.8: 2-D native SDS-PAGE separation of an endogenous protein complex from pea chloroplasts containing FtsZ1 and FtsZ2.....	74
Figure 2.9: Specificity of ARC6 Antibody.....	78
Figure 2.10: ARC6 and ARC3 are associated with a protein complex containing FtsZ1 and FtsZ2 in both pea and Arabidopsis.....	81
Figure 3.1: Sequence alignment of AtFtsZ1-1, AtFtsZ2-2 and <i>E. coli</i> FtsZ ...	94 & 95
Figure 3.2: GTPase kinetics of FtsZ1, FtsZ2, equally mixed FtsZ1/FtsZ2 and <i>E. coli</i> FtsZ	114
Figure 3.3: 90° Light-scattering polymerization assays of FtsZ1 and FtsZ2	117
Figure 3.4: Negative stain electron micrographs of FtsZ1 and FtsZ2	119

Figure 3.5: Critical concentration for FtsZ1/FtsZ2 polymerization monitored by 90° light-scattering	125
Figure 3.6: Light-scattering comparison of polymerization of <i>E. coli</i> FtsZ and FtsZ1 with FtsZ2 both at 5 μM in HMK buffer	126
Figure 3.7: Equally mixed FtsZ1 and FtsZ2 are not depolymerized by GDP	130
Figure 3.8: The effect of varying the ratio between FtsZ1 and FtsZ2, while keeping the total FtsZ concentration at 5 μM monitored by light-scattering.....	132
Figure 3.9: Inhibition of FtsZ1 polymerization by FtsZ2D322A.....	134
Figure 3.10: Inhibition of the GTPase activity of FtsZ1 and FtsZ2 by FtsZ2D322A in 2 mM GTP in a coupled GTPase assay.....	138
Figure 3.11: Fluorescence microscopy of plant FtsZs fused to GFP expressed in <i>E. coli</i>	142
Figure 3.12: Model of plant FtsZ protofilaments.....	150
Figure 4.1: FtsZ1, FtsZ2, ARC6 and a protein that cross-reacts with an antibody to <i>E. coli</i> ZipA cofractionate in sucrose density gradients, native PAGE and by hydrophobic interaction chromatography.....	156
Figure 4.2: Overview of the structural threading search algorithm used to identify a putative Arabidopsis chloroplastic protein with structural similarity to ZipA, Ssz1	159
Figure 4.3: Alignment of <i>E. coli</i> ZipA with its potential structural analogue in Arabidopsis	166
Figure 4.4: PCR analysis to identify a homozygous SALK_039451 mutant of in Ssz1	171
Figure 4.5: Comparison of WT and Salk 039451 cells.....	173
Figure 4.6: Chloroplast import assay of Ssz1	174
Figure 4.7: Immunolocalization of FtsZ in wild-type and Ssz1Δ <i>Synechococcus</i> PCC 7942	175
Figure 4.8: ClustalW alignment of plant and cyanobacterial Ssz1 homologues	186, 187 & 188

KEY TO ABBREVIATIONS

ATP	adenosine 5'-triphosphate
ABRC	Arabidopsis Biological Resource Center
Cc	critical concentration for assembly
C-terminus	carboxyl terminus of a protein
DDM	n-dodecyl- β -D-maltoside
Δ LS	change in light scattering
EM	transmission electron microscopy
EMS	ethyl methanesulfonate
E-site	exchangeable GTP binding site of tubulin
GDP	guanosine 5'-diphosphate
GDP-P _i	guanosine 5'-diphosphate with the hydrolyzed γ -P _i still bound to the protein
γ -P _i	γ -inorganic phosphate liberated from ATP or GTP
GTP	guanosine 5'-triphosphate
GTP γ S	guanosine-5'-O-(3-thiotriphosphate)

γ -TURC	γ -tubulin ring complex
His	histidine
IEM	inner envelope membrane
Min	minute(s)
MORN	membrane occupation nexus motif
MTOC	Microtubule organization complex
N-site	non-exchangeable GTP binding site of tubulin
N-terminus	amino terminus of a protein
OEM	outer envelope membrane
PAGE	polyacrylamide gel electrophoresis
PD-ring	plastid dividing ring
P _i	inorganic phosphate
PIP-5K	phosphatidyl inositol-5-phosphate kinase
QAAA	quantitative amino acid analysis of a protein
RuBisCo	ribulose 1-5-bisphosphate carboxylase/oxygenase
SDS	sodium dodecyl sulfate

sec

second(s)

sRuBP

small subunit of RuBisCo

CHAPTER ONE

INTRODUCTION

Specific Aims

Chloroplast division in plants is mediated by FtsZ1 and FtsZ2, which are homologues of the bacterial cell division protein FtsZ. The bacterial FtsZ protein is thought to be the progenitor to tubulin, and is a GTP-dependent, filament-forming protein that encircles the bacterial division site. Similarly, plant FtsZ proteins encircle the mid-plastid. Plant FtsZ1 and FtsZ2 family proteins differ primarily at their C-termini with FtsZ2 proteins possessing a motif similar to those found in bacterial FtsZ that is responsible for binding to other bacterial cell division factors. In plants, this motif has been shown to bind to the chloroplast division protein ARC6, which contains a DnaJ-like domain and may be involved in FtsZ filament remodeling, but it is unclear whether ARC6 forms a stable complex with FtsZ *in vivo*. The focus of this dissertation is on understanding the composition of the *in vivo* FtsZ complex and understanding the function and topology of FtsZ protofilaments.

The specific aims of this dissertation are:

Aim 1: Define the proteins that interact with FtsZ1 and FtsZ2 *in vivo*. FtsZ was purified from pea stroma and the composition of proteins that interact with FtsZ were defined. In Chapter 2, FtsZ levels were quantified in isolated Arabidopsis chloroplasts and FtsZ1 and FtsZ2 were found at a constant ratio of ~1:2. FtsZ was partially co-purified in a complex with the chloroplast division proteins ARC3 and ARC6 (chapter 2). The complex also contained a protein recognized by an antibody against *Escherichia coli*

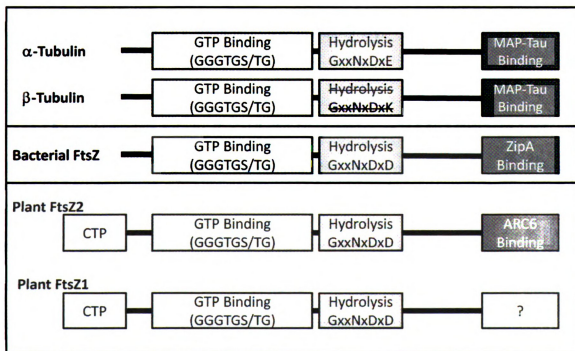
(*E. coli*) ZipA. A ZipA cross-reactive protein has been tightly linked to FtsZ-containing complexes and is discussed in Chapter 4.

Plant FtsZ2 proteins contain a C-terminal motif conserved with bacterial FtsZ (Figure 1.1). In bacteria, this motif specifically interacts with the bacterial cell division protein ZipA, but ZipA homologues have not been identified in plants. In an attempt to identify a putative ZipA-like protein, a structural search algorithm was created to derive structural similarity by threading a database of proteins of unknown function into the solved crystal structure of the FtsZ-interacting domain of ZipA. As discussed in Chapter 4, a strong candidate identified from this analysis, Ssz1, could not be definitively linked to a role in chloroplast division.

Aim 2: To determine the topology of the FtsZ1/FtsZ2 protofilament and define the biochemical properties of FtsZ1 and FtsZ2. Why do plants have two types of FtsZ, while bacteria only use one type of FtsZ? In Chapter 3, FtsZ1 and FtsZ2 are produced individually as recombinant proteins in *E. coli*, a significant technical advance. Because FtsZ proteins are evolutionary progenitors of tubulin, one possible hypothesis is that FtsZ1 and FtsZ2 have evolved in parallel into heterofilaments like tubulin. Despite both FtsZ1 and FtsZ2 being GTPases, maximal FtsZ1/FtsZ2 co-assembly requires equal concentration of both proteins, arguing for a heterofilament polymer topology. Moreover, the longitudinal, T7-loop mutant FtsZ2D322A was found to be a competitive inhibitor of FtsZ1, but not FtsZ2, further supporting an FtZ1/FtsZ2 heterofilament topology.

Figure 1.1: Cartoon representation of sequence similarity between plant FtsZ1, FtsZ2, bacterial FtsZ and α - and β -tubulin.

All proteins contain a glycine-rich N-terminal domain that binds GTP. All proteins, except β -tubulin have all residues required for GTP hydrolysis in their T7-loops. β -tubulin has a lysine substituted in its T7-loop that prevents hydrolysis in the α -subunit. $\alpha\beta$ -tubulin have C-terminal protease-sensitive extensions that bind regulatory proteins such as MAP-Tau. Bacterial FtsZ and plant FtsZ2 have similar C-terminal extensions that bind the cell division protein ZipA (Hale and de Boer 1997) and ARC6 (Maple et al. 2005), respectively. FtsZ1 has a plant-specific C-terminal extension that has no known interacting partner, but the entire FtsZ1 protein has been shown to interact with ARC3 in the yeast two-hybrid assay (Maple et al. 2005).



Bacterial cell division is best understood in *E. coli*

The stromal chloroplast division machinery is derived from the cell division machinery of the ancient cyanobacterial endosymbiont. Bacterial cell division is best understood in the Gram-negative bacterium *E. coli*. Cell division mutant screening in *E. coli* has been powerful for understanding the cell division mechanism of other bacteria including the Gram-positive bacteria *Bacillus subtilis* (*B. subtilis*). While the division mechanisms of *E. coli* and *B. subtilis* are similar, many functional details differ. Much of the difference between *E. coli* and *B. subtilis* division probably is because *B. subtilis* can undergo asymmetric cell division, termed sporulation. The division machinery of cyanobacteria is not well understood, but contains components found in both Gram-positive and Gram-negative bacteria and could represent a unique class of division machinery (Miyagishima et al. 2005). Because chloroplast division is derived from bacterial cell division, an understanding of bacterial cell division is essential for understanding the stromal chloroplast division machinery.

FtsZ

Bacteria contain tubulin-like cell-division proteins, called FtsZ (Erickson 1995, 1997) that assemble into a ring at mid-cell just after DNA replication and immediately before cell division. FtsZ contracts with the midcell division furrow as the cell-cycle progresses (Addinall et al. 1996; Bi and Lutkenhaus 1990a, 1991; den Blaauwen et al. 2003; Harry et al. 1999; Lin et al. 1997; Regamey et al. 2000). FtsZ has been proposed to be a scaffold for binding additional cell division proteins (Margolin 2000; Rothfield et al.

1999), but it also have been demonstrated to generate contractile force (Osawa et al. 2008).

Tubulin biochemistry

FtsZ is structurally and biochemically similar to tubulin despite sharing less than 10% sequence similarity. Due to a high degree of structural similarity (Löwe 1998; Lowe and Amos 1998) both proteins are believed to share a common ancestor (Erickson 1995, 1997; Nogales et al. 1998a). Tubulin biochemistry is well understood and the biochemistry of tubulin will be discussed as a foundation for understanding FtsZ biochemistry.

The basic subunit of tubulin is a $\alpha\beta$ dimer that are tightly bound and do not dissociate. Because α - and β -tubulin monomers are unstable alone, chaperone complexes assemble $\alpha\beta$ -tubulin dimers. Imbalanced expression of either α - or β -tubulin causes blocks in dimer assembly (Geissler et al. 1998; Hirata et al. 1998; Melki et al. 1996; Tian et al. 1999; Tian et al. 1996; Tian et al. 1997). Binding of GTP to $\alpha\beta$ -tubulin dimers causes assembly into microtubules. Microtubules are composed of longitudinally arranged, head-to-tail, repeating dimers of $\alpha\beta$ -tubulin that form heterofilaments (Tian et al. 1996). Tubulin heterofilaments laterally associate into tubes (Downing and Nogales 1998a, b, c; Nogales 2000).

Structures of $\alpha\beta$ -tubulin dimers have been generated to investigate how GTP binding and hydrolysis regulate tubulin assembly into microtubules (Nogales 1999, 2000; Nogales and Wang 2006; Nogales et al. 1999; Nogales et al. 1998b; Sackett 1995).

The N-terminus of α - and β -tubulin have a glycine-rich motif (GGGTGS/TG) called the tubulin signature motif found in a series of antiparallel β -sheets called a Rossman fold (Erickson 1995). The GTP binding characteristics of α - and β -tubulin differ in the ability to exchange fresh nucleotide. α -tubulin has a non-exchangeable GTP binding site called the N-site. The N-site is unable to exchange GTP because it is buried within the tight α/β dimer interface that does not dissociate (Menendez et al. 1998). In contrast, in unassembled tubulin the nucleotide binding site in the β -subunit is solvent-exchangeable and termed the E-site. However, the E-site becomes non-exchangeable when tubulin is assembled into filaments because of nucleotide burial in the interface between the α - and β -subunits in the heterofilaments (Menendez et al. 1998; Nogales et al. 1998a). FtsZ differs from tubulin because bound GTP is solvent-exchangeable within assembled filaments (Nogales 2000).

GTP is only hydrolyzed in the E-site of β -tubulin (Nogales 2000; Nogales and Wang 2006; Nogales et al. 1999; Nogales et al. 1998b). The GTP binding-site of β -tubulin is only GTPase competent when assembled with a second $\alpha\beta$ -tubulin dimer in a heterofilament. In the β -subunit, GTP is hydrolyzed by the T7-loop of α -tubulin from the second $\alpha\beta$ -tubulin dimer. The T7-loop contacts the γ -phosphate of the bound GTP, completing the active site in *trans* with an α -subunit. The β -tubulin T7-loop and FtsZ T7-loop have the consensus sequence GxxNx₂Dxx(E/D) (Löwe 1998; Lowe and Amos 1998; Nogales et al. 1998a). In a similar manner, the N-site GTP bound to α -tubulin is contacted by the T7-loop of the β -subunit within and individual $\alpha\beta$ -tubulin dimer, but the T7-loop of the β -subunit cannot promote GTP hydrolysis because its consensus is

GxxNx_DxxK, having a lysine substituted for an acidic residue (Nogales et al. 1998a). The inability of α -tubulin to hydrolyze GTP stabilizes the α/β dimer interface, preventing dissociation, and maintaining tubulin as a strict α/β dimer.

Because tubulin GTPase active sites are formed in *trans*, tubulin filament ends are biochemically different. Microtubules grow quickly at their plus-ends and more slowly on their minus ends. The plus end of $\alpha\beta$ -tubulin is always a β -subunit with its exposed E-site bound to GTP. The plus end grows by binding to the T7-loop-containing C-terminal interface of an incoming α -subunit dimerized with a β -subunit, thus re-creating a new GTP-bound β -subunit on the plus side. In contrast, the minus-end contains the T7-loops of α -tubulin, which are not GTP bound. Incoming $\alpha\beta$ -tubulin dimers cannot assemble at the minus end; this process is kinetically unfavorable.

The minus end of a tubulin filament is composed primarily of α -tubulin. The current model is that strong lateral contacts between α -subunits stabilize the minus end (Nogales et al. 1999). In contrast, lateral interactions between β -subunits are strong when GTP is bound, but weak when GTP is hydrolyzed to GDP (Derry et al. 1998; Tanaka-Takiguchi et al. 1998). $\alpha\beta$ -tubulin filaments are thus stable when the plus end is bound to GTP (Derry et al. 1998; Tanaka-Takiguchi et al. 1998). GTP hydrolysis is not required for tubulin assembly and the rates of GTP hydrolysis vary considerably in different types of tubulin (Dougherty et al. 1998; Vandecandelaere et al. 1999), but generally the GTPase activity of tubulin is slower than the rate of polymerization. Thus, $\alpha\beta$ -tubulin plus-ends contain primarily GTP, but as the GTPase activity catches up with

polymerization, the polymer becomes prone to disassembly due to destabilized lateral interaction between β -subunits at the plus-end in a process termed “dynamic instability”. When examined by EM, destabilized GDP-bound β -tubulin subunits show individual filaments curling away from the microtubule (Nogales 2000). Dynamic instability of $\alpha\beta$ -tubulin leads to an interesting assembly phenomenon called treadmilling (Margolis and Wilson 1998; Waterman-Storer and Salmon 1998). If $\alpha\beta$ -tubulin lacks new incoming GTP-bound dimers to continue assembly, growth stops and when all the GTP is hydrolyzed within the β -subunits, the microtubule disassembles. However, in the presence of sufficient GTP, $\alpha\beta$ -tubulin dimers released from the minus end can exchange their hydrolyzed GDP for a new GTP and re-assemble at the plus end, thus dynamically maintaining the tubulin polymer, a process called treadmilling. Experimentally, fluorescently labeled tubulin added to treadmilling filaments will rapidly traverse from the plus to minus end (Waterman-Storer and Salmon 1998).

Tubulin assembly is rate-limited at nucleation. *In vivo*, tubulin is nucleated by specialized complexes called “microtubule organizing complexes” (MTOCs). *In vitro*, a high critical concentration (abbreviated as C_c) of tubulin is typically required to grow microtubules ($\sim 7 \mu\text{M}$). Stabilization agents such as DEAE-dextran or the microtubule inhibitor taxol are often required to stabilize and promote tubulin assembly *in vitro* due to the high tubulin C_c . The best-described MTOC is the γ -tubulin ring complex (γ -TURC). γ -TURC is a large, 2.2 MDa complex that can directly nucleate microtubules (Moritz et al. 1995; Zheng et al. 1995). Recently, γ -TURC was shown to accomplish this by directly

stabilizing α -tubulin at microtubule minus ends (Kollman et al. 2008) and is a key regulator of tubulin polymerization *in vivo*.

Tubulin assembly is regulated by several types of microtubule-associated proteins (MAPs). The best-characterized MAPs are MAP-Tau proteins, which promote tubulin assembly. MAP-Tau proteins are unstructured, negatively charged proteins that bind the positively charged C-termini of $\alpha\beta$ -tubulin (Chau et al. 1998) that are solvent accessible in assembled microtubules (Sackett et al. 1985). MAP-Tau likely inhibits GTP hydrolysis by stabilizing the interaction between $\alpha\beta$ -tubulin dimers and possibly allosterically slowing the hydrolysis of GTP by an unknown mechanism (Chau et al. 1998). Finally, many microtubule-destabilizing proteins have been described. Katanin is a microtubule severing factor essential for releasing microtubules from centrosomes (Ahmad et al. 1999; Hartman et al. 1998; Lohret et al. 1998; McNally et al. 1996; McNally and Thomas 1998). Katanin severs microtubules, releasing GDP-capped microtubules from within assembled polymers that are unstable and rapidly depolymerize. Stathmin is a tubulin depolymerization factor that promotes tubulin disassembly by directly binding $\alpha\beta$ -tubulin dimers to promote GTP hydrolysis by an unknown mechanism (Belmont and Mitchison 1996 ; Howell et al. 1999).

E. coli FtsZ is structurally and biochemically similar to tubulin

FtsZ is key to initiating bacterial cell division. FtsZ binds and hydrolyzes GTP in a glycine-rich motif near the N-terminus similar to the GTP-binding motif in tubulin (de Boer et al. 1992a; Mukherjee et al. 1993; RayChaudhuri and Park 1992). The presence

of a tubulin-like GTP-binding site in the N-terminus of *E. coli* FtsZ suggested FtsZ might be a bacterial version of tubulin.

FtsZ polymerization and structure

FtsZ and tubulin only share ~10% sequence similarity, but evidence was growing that FtsZ might be similar to tubulin. Supporting this hypothesis was the finding that recombinant FtsZ forms multimers when separated by native PAGE (Mukherjee and Lutkenhaus 1994). Electron microscopy of FtsZ in the presence of GTP shows long thin filaments reminiscent of tubulin (Mukherjee and Lutkenhaus 1994). Moreover, use of the non-hydrolysable GTP analogue GTP γ S also results in FtsZ assembly, further suggesting that, as in tubulin, GTP binding, but not GTP hydrolysis, is required for assembly (Mukherjee and Lutkenhaus 1994). FtsZ assembly is protein concentration dependent like tubulin assembly with a Cc of ~0.5-1 μ M (Mukherjee and Lutkenhaus 1994).

The first structural link between FtsZ and tubulin came from 3D-reconstruction of electron micrographs of tubulin and FtsZ. From this study, the structure of assembled tubulin and FtsZ were found to have nearly identical structures and arrangement of monomers within filaments (Erickson et al. 1996). However, the structural similarity between bacterial FtsZ and tubulin was fully realized when *Methanococcus jannaschii* FtsZ was crystallized and found to have a nearly identical structure to tubulin, despite less than 10% sequence similarity (Löwe 1998; Lowe and Amos 1998). Interestingly, the primary difference between tubulin filaments and the proposed FtsZ filament model is

that the FtsZ nucleotide-binding site is partially solvent-accessible while tubulin GTP binding sites are non-exchangeable when polymerized (Löwe 1998; Lowe and Amos 1999; Nogales et al. 1998a; Small and Addinall 2003). Mechanistically, this means that tubulin is only able to exchange GTP at its plus-ends, whereas FtsZ can maintain polymer stability by exchanging GDP for fresh GTP within assembled filaments (Lu et al. 2000).

GTP-assembled FtsZ protofilaments are unstable *in vitro* and rapidly depolymerize within 10-20 minutes (Mukherjee and Lutkenhaus 1999). The inclusion of CaCl_2 and DEAE-dextran is typically required to stabilize protofilaments and promote lateral bundling between protofilaments (Mukherjee and Lutkenhaus 1994, 1999; Scheffers et al. 2000; Yu and Margolin 1997). CaCl_2 is used to stabilize FtsZ polymers because it mimics MgCl_2 , which is required for GTP hydrolysis. Thus, CaCl_2 stabilizes FtsZ filaments because it is a competitive inhibitor of GTP hydrolysis. The advantage of CaCl_2 stabilization of FtsZ polymers is that the effect is reversible by chelating CaCl_2 with EGTA. The mechanism by which DEAE-dextran promotes FtsZ polymerization and bundling is unknown.

The polymerization dynamics of *E. coli* FtsZ can be measured in real time by 90° light scattering (Mukherjee and Lutkenhaus 1999). This technique utilizes a spectrofluorimeter with excitation and emission monochromators set at 350 nm, and detects the diffraction of light at a 90° angle using a narrow slit width. 90° light scattering has the advantage that it tolerates high protein concentration, but due to the wavelength of light used for diffraction it can only detect filaments larger than short

oligomers. FtsZ nucleation into dimers is not detectable with this technique (Mukherjee and Lutkenhaus 1999). Despite this limitation, light scattering has proven to be a powerful technique for monitoring FtsZ polymerization in real-time (Mukherjee and Lutkenhaus 1999).

EM has shown that GTP-FtsZ forms single, long, straight filaments that can laterally associate to form sheets in the presence of the stabilizing DEAE-dextran (Erickson et al. 1996; Lu et al. 2000; Mukherjee and Lutkenhaus 1994). Assembly of FtsZ stimulates GTP hydrolysis by the completion of the active site in *trans* similar to tubulin (Scheffers and Driessen 2001; Scheffers et al. 2002; Wang and Lutkenhaus 1993). Following GTP hydrolysis and γ -P_i dissociation, GDP-FtsZ polymers adopt a curved conformation that is believed to be less stable than straight filaments, leading to rapid disassembly (Erickson and Stoffler 1996; Lu et al. 2000; Romberg et al. 2001).

E. coli FtsZ GTP hydrolysis drives depolymerization

GTP binding promotes FtsZ assembly into filaments, but GTP hydrolysis is not required for polymerization since GTPase inhibitors such as GTP γ S and CaCl₂ promote polymerization. This suggested that GTP hydrolysis promotes depolymerization of FtsZ filaments similar to the regulation of tubulin stability. The structural similarity between FtsZ and tubulin predicts that the association of two monomers would complete FtsZ active sites. This hypothesis is supported by the conserved GxxNx₂Dxx(D/E) motif in the T7-loop of bacterial FtsZ. To test if an FtsZ GTPase active site is formed in *trans*, Scheffers et al. created a series of T7-loop mutations in *E. coli* FtsZ that were tested for

GTPase activity with the wild-type protein. The T7-loop mutants were found to be sub-stoichiometric competitive inhibitors of GTP hydrolysis and polymerization but did not affect GTP binding (Scheffers et al. 2002). Moreover, these mutants did not interfere with the ability of FtsZ to assemble into cell division rings when expressed at low levels *in vivo*, but when expressed at high levels block cell division (Redick et al. 2005). These results confirmed that FtsZ has an active site composed of two monomers and is mechanistically similar to tubulin.

The GTPase activity of FtsZ is ~50-times faster (Huecas et al. 2007b; Romberg and Mitchison 2004) than that of MAP-free tubulin (David-Pfeuty et al. 1977). Within ~10 min. of polymerization *in vitro*, *E. coli* FtsZ filaments begin to rapidly disassemble (Mukherjee and Lutkenhaus 1999) as the ratio of available GTP/GDP is reduced (Small and Addinall 2003). This leads to the question, how are FtsZ polymers maintained with a fast GTPase activity? A key difference between tubulin and FtsZ is nucleotide binding. Once tubulin polymerizes, the bound nucleotide can no longer be exchanged for free GTP in solution. Because tubulin has a slow GTPase activity, polymerization can continue for a significant period until the GTPase activity catches up with the polymer in a process called “dynamic instability”. However, FtsZ maintains polymer stability by exchanging nucleotide within assembled protofilaments (Mingorance et al. 2001; Small and Addinall 2003). Thus, instead of re-assembling FtsZ plus-ends, FtsZ regenerates straight, stable polymers by directly exchanging nucleotide within the polymer (Figure 1.2). Because FtsZ polymers can exchange nucleotide, FtsZ is sensitive to the ratio of

GTP/GDP. High GDP concentration favors FtsZ depolymerization (Small and Addinall 2003).

FtsZ filaments contain mostly GDP and the hydrolyzed γ -P_i (Scheffers and Driessen 2002). Polymerized FtsZ is able to exchange hydrolyzed GDP+P_i for GTP unlike polymerized tubulin, where the nucleotide is non-exchangeable (Huecas and Andreu 2004; Huecas et al. 2007a; Huecas et al. 2007b; Romberg and Levin 2003; Scheffers and Driessen 2002; Small and Addinall 2003). Although FtsZ and tubulin crystal structures are similar, there are considerable differences in the active site. Notably, in the interface between monomers adjacent to the bound GTP in FtsZ is the T3-loop that makes contact with the GTP γ -phosphate. In tubulin, the T3-loop prevents nucleotide exchange with solvent, but in FtsZ, the T3-loop is shorter and allows solvent access to the nucleotide (Diaz et al. 2001). In FtsZ, loss of the γ -P_i after GTP hydrolysis causes displacement of the T3-loop away from the nucleotide binding site and likely induces protofilament curvature (Diaz et al. 2001). This conformation is believed to be less stable than straight protofilaments (Diaz et al. 2001; Erickson and Stoffler 1996; Erickson et al. 1996; Huecas and Andreu 2004; Mukherjee and Lutkenhaus 1994, 1998; Oliva et al. 2004) and ultimately leads to depolymerization (Figure 1.2).

Cooperative assembly of bacterial FtsZ

FtsZ was initially thought to assemble isodesmically because it assembles into single filaments even though FtsZ has an apparent C_c for assembly, which does not support isodesmic assembly (Gonzalez et al. 2005; Romberg et al. 2001). Dimerization

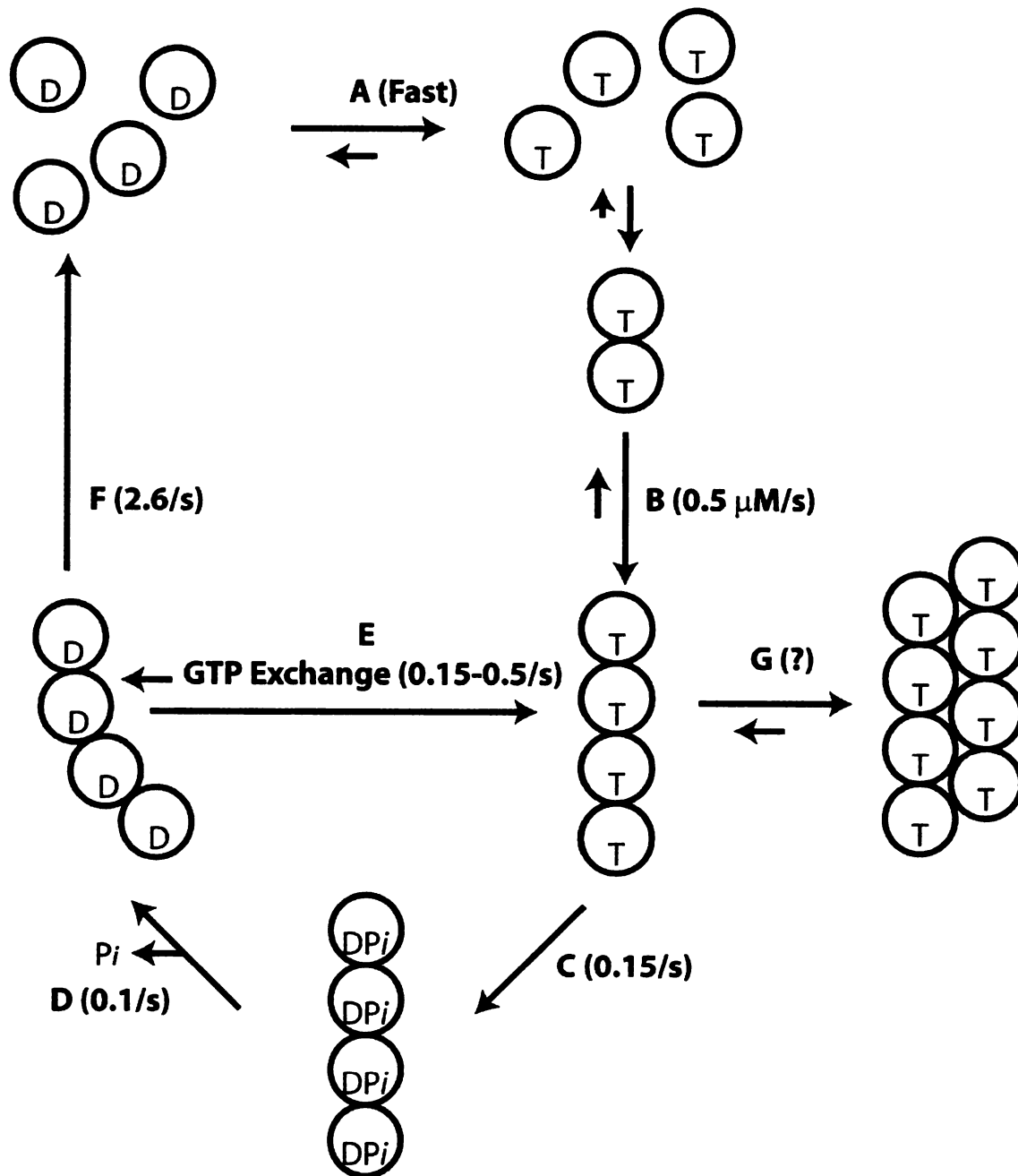
of GDP-FtsZ requires GTP (Rivas et al. 2001; Rivas et al. 2000), while GDP-FtsZ dimerization and assembly is kinetically disfavored (Huecas and Andreu 2004). Like tubulin, the emerging model of FtsZ polymerization suggests the minimal subunit for assembly is a dimer (Chen and Erickson 2005). Despite FtsZ only forming single-stranded filaments (which predicts isodesmic assembly)(Gonzalez et al. 2005; Romberg et al. 2001) FtsZ assembles cooperatively (Caplan and Erickson 2003; Chen et al. 2005; Huecas and Andreu 2003; Huecas et al. 2007a). The precise mechanism of FtsZ cooperative assembly is still unclear, but recent work suggests that conformational switches within FtsZ upon polymerization may self-stabilize protofilaments (Huecas et al. 2007a; Huecas et al. 2007b).

Model of FtsZ polymerization

In vitro, unassembled FtsZ is GDP-bound. When GTP is available, FtsZ rapidly exchanges nucleotide, forming GTP-FtsZ (Figure 1.2A). GTP-FtsZ cooperatively assembles into protofilaments (Figure 1.2B) with a rate of $\sim 0.5 \mu\text{M sec}^{-1}$ (and an off rate of 1.2 sec^{-1}) (Huecas et al. 2007b). However, there is evidence that FtsZ is assembled from dimers of FtsZ and not monomers (Chen et al. 2005; Huecas et al. 2007a). If FtsZ is indeed assembled from dimers, this explains why single-filament FtsZ assembly is cooperative (Chen et al. 2005; Huecas et al. 2007a; Rivas et al. 2001; Rivas et al. 2000; Romberg et al. 2001; Sossong et al. 1999)(Figure 1.2). Within protofilaments GTP hydrolysis is $\sim 0.13 \text{ sec}^{-1}$ (Figure 1.2C) and is the rate limiting step of the polymerization cycle (Romberg and Mitchison 2004).

Figure 1.2: Model of the assembly dynamics of *E. coli* FtsZ.

This model is adapted from (Huecas et al. 2007b; Romberg and Levin 2003; Romberg and Mitchison 2004). FtsZ molecules are indicated by circles and the nucleotide-bound state of bacterial FtsZ is indicated by “T” for GTP, “DPi” for GDP-Pi, and “D” for GDP. (A) GDP/GTP exchange in monomers is fast in solution. (B) GTP-FtsZ dimers rapidly assemble into straight protofilaments. (C) After GTP hydrolysis, FtsZ filaments are GDP-Pi-FtsZ bound and still straight and (D) Pi release is rapid. (E) Protofilaments can be maintained as straight polymers by a relatively slow nucleotide exchange within the polymer. (G) FtsZ protofilaments are believed to laterally associate, but it is unknown how this affects FtsZ kinetics since laterally associated FtsZ is not observed *in vitro*. (F) Curved GDP-FtsZ is unstable and rapidly disassembles. (H) GTP-FtsZ can also presumably laterally associate, but this has not been demonstrated under physiological conditions.



Following hydrolysis, FtsZ is in the GDP-P_i-FtsZ state and P_i release has a rate of 0.1 sec⁻¹ (Figure 1.2D)(Huecas et al. 2007b; Romberg and Mitchison 2004); P_i release results in FtsZ curved filaments, which rapidly disassemble (Romberg et al. 2001). Polymerized filaments disassemble when the γ-P_i dissociates, leaving FtsZ GDP-bound, with a rate of ~2.6 sec⁻¹ (Figure 1.2F)(Huecas et al. 2007b). However, GTP can exchange within the assembled filament to maintain the assembly (Figure 1.2E)(Lu et al. 2000; Mingorance et al. 2001; Romberg and Mitchison 2004). Bundling of bacterial FtsZ is believed to occur, but has not been observed under physiological conditions and it is unclear how lateral association between FtsZ filaments would affect polymerization kinetics (Figure 1.2G).

Regulation of Z-ring assembly and placement

Nucleoid occlusion positions the Z-ring in bacteria

Z-ring assembly is negatively regulated by the presence of the bacterial nucleoid. In order for the cell division apparatus to assemble at mid-cell the nucleoid must be duplicated and separated toward the poles, which leaves a small nucleoid-devoid furrow in the middle of the cell where FtsZ can assemble (Rothfield et al. 2005; Woldringh et al. 1990). The nucleoid occlusion model predicts the presence of a Z-ring inhibitory factor that uniformly binds the nucleoid. Recently, SlmA and Noc were found to be DNA binding proteins required for cell-division (Bernhardt and de Boer 2005; Marston et al. 1998). Double SlmA/Noc mutants are lethal, suggesting both have critical roles in cell division. Both SlmA and Noc are located to the polar side of the nucleoid. SlmA and Noc

are predicted to be FtsZ inhibitors, but biochemical roles in Z-ring assembly have not been described.

Positioning of the Z-ring by the MinCDE system

The position of the Z-ring at mid-cell is controlled not only by nucleoid occlusion, but also by a system of three proteins, MinC, MinD and MinE, collectively termed the Min system. Mutations in components of the Min system result in “mini” cells from improper placement of the Z-ring (de Boer et al. 1989a, 1992b). Because the cells divide before the nucleoid is properly segregated, they are typically anucleate (de Boer et al. 1989a, 1992b). Min proteins are found in Gram-negative (e.g. *E. coli*) and Gram-positive bacteria (e.g. *B. subtilis*) as well as cyanobacteria (Mazouni et al. 2004) and homologues of MinD and MinE, but not MinC, are found in plants (Aldridge et al. 2005).

MinC is a direct inhibitor of FtsZ assembly (Hu et al. 1999; Levin et al. 2001; Marston and Errington 1999; Pichoff and Lutkenhaus 2001). However, MinC lacks spatial site selection. MinC heterodimerizes with the membrane recruitment factor MinD (Hu and Lutkenhaus 1999; Raskin and de Boer 1999a, b). The balance between MinCD heterodimers and FtsZ is essential for proper cell division. For example, hyper-accumulation of MinC leads to blocked cell division, which can be overcome by an overproduction of FtsZ (Bi and Lutkenhaus 1990b; Justice et al. 2000; Levin et al. 2001). MinC is composed of two domains; the N-terminal domain directly inhibits FtsZ assembly (Hu and Lutkenhaus 2001). The N-terminus of MinC is connected by a linker to

the C-terminal domain that heterodimerizes with MinD (Cordell et al. 2001; Hu and Lutkenhaus 2000; Szeto et al. 2001).

MinE is a topological specificity factor for MinCD. MinE restricts the FtsZ-inhibitory activity of MinCD to the poles in *E. coli* (Fu et al. 2001; Hu and Lutkenhaus 1999; Raskin and de Boer 1999a, b; Rowland et al. 2000) by forming a MinE-ring that caps MinCD to the polar region (Fu et al. 2001; Hale et al. 2001; Raskin and de Boer 1997; Shih et al. 2002). MinE rapidly cycles between the poles of the *E. coli* cell, rapidly assembling and disassembling with a periodicity of approximately 1-2 min (Raskin and de Boer 1999b). Assuming a simple oscillator model for pole-to-pole movement of MinCDE would result in a time averaged accumulation of MinCDE at the poles (Rothfield et al. 2005), suggesting that the determinant for polar localization is dependent upon intrinsic assembly properties of MinE, although direct evidence of this does not exist.

Gram-positive bacteria such as *B. subtilis* lack MinE and instead use DivIVA to recruit MinCD to the poles. MinE dynamically oscillates between the cell poles, whereas *B. subtilis* DivIVA is statically localized to the cell pole (Edwards et al. 2000). DivIVA is believed to be targeted specifically to a lipid or protein domain at the cell pole (Rothfield et al. 2005), thus explaining its static polar localization.

ZipA and FtsA organize and anchor the Z-ring at the membrane

In bacteria, FtsZ proteins are anchored to the membrane by two proteins, ZipA and FtsA; the latter is in the same structural super-family as actin/HSP70 proteins (Bork et al. 1992; van den Ent and Lowe 2000). Both ZipA and FtsA interact with the extreme

C-terminus of *E. coli* FtsZ (Addinall and Lutkenhaus 1996; Hale and de Boer 1999; Hale and de Boer 1997; Haney et al. 2001; Liu et al. 1999; Wang et al. 1997; Yan et al. 2000) and anchor the FtsZ ring to the inside of the cell membrane (Hale and de Boer 1997). Both FtsA and ZipA are required for interaction with downstream cell division proteins (Pichoff and Lutkenhaus 2002). The crystal structure of ZipA complexed with the carboxyl terminus of FtsZ has been solved (Mosyak et al. 2000). Based on the quaternary structure of tubulin (Li et al. 2002) the ZipA/FtsZ interacting domain is believed to stick out of FtsZ polymers (Löwe 1998; Lowe and Amos 1999). Despite the conservation of the ZipA/FtsZ binding motif in FtsZ2 (Figure 1.1), neither ZipA nor FtsA have been identified in plants, but both functions are essential to bacterial cell division.

ZapA

ZapA promotes the assembly of FtsZ and is found in many bacteria, but is not essential for proper cell division (Gueiros-Filho and Losick 2002). ZapA was identified in *B. subtilis* by a novel genetic screen. Constitutive overexpression of MinD results in loss of topological specificity of MinC, an FtsZ assembly inhibitor, inhibiting Z-ring assembly throughout the cell. This MinD overexpressor was transformed with an overexpression library and screened for cell lines that were able to overcome the constitutive block in FtsZ assembly and would thus be FtsZ assembly factors (Gueiros-Filho and Losick 2002). This screen resulted in the identification of ZapA, (*yshA*) which is a relatively short protein (85 amino acids) and was found to co-localize to Z-rings. ZapA is required for proper cell division only in the absence of EzrA and DivIVA, both of which regulate Z-ring

dynamics (Gueiros-Filho and Losick 2002). ZapA has a functionally equivalent ortholog in *E. coli* called YgfE (Small et al. 2007).

EzrA

EzrA is found only in Gram-positive bacteria such as *B. subtilis* and is a negative regulator of Z-ring assembly. Loss of EzrA function results in Z-rings that mis-localize to the cell pole (Levin et al. 1999). EzrA contains a transmembrane domain that localizes it to the cell membrane, but EzrA is also associated with the Z-ring. The GTPase activity of FtsZ is slightly enhanced by EzrA, even though GTP binding is reduced (Chung et al. 2007). EzrA destabilizes Z-rings by interacting with the C-terminus of FtsZ near the conserved C-terminal motif, suggesting EzrA is a negative regulator of FtsZ. Thus a working model is that FtsA, a positive regulator of assembly, and EzrA compete to regulate Z-ring formation (Singh et al. 2007)(Gram-positive bacteria do not have ZipA).

SulA

SulA is a negative regulator of FtsZ assembly that is not essential for proper cell division. SulA prevents cell division in response to various cell damage signals (Higashitani et al. 1997; Huang et al. 1996; Justice et al. 2000; Mukherjee et al. 1998). SulA is interesting because it blocks FtsZ assembly by binding the T7-loop, or the hydrolysis loop, effectively acting as a filament cap by preventing the addition of new GTP-bound subunits. The effect of SulA can be mimicked by mutating the T7 loop, which blocks GTP hydrolysis but not GTP binding (Redick et al. 2005; Scheffers et al. 2002).

Chloroplast Division

Ultrastructural observations of chloroplast division

Electron microscopy of fixed plant and algal chloroplasts has been a powerful tool for observing the ultrastructure of dividing plastids. These experiments have identified electron dense rings, termed PD rings. An inner PD-ring is found adjacent to the stromal side of the inner-envelope membrane (IEM). A outer PD-ring is found on the cytosolic side of the outer-envelope membrane (OEM)(Leech et al. 1981). An inter-membrane space localized middle PD-ring has also been observed, but only in the alga *Cyanidioschyzon merolae* (Miyagishima et al. 2001a). It is unknown if plants also have a middle PD-ring.

After the discovery of stromal FtsZ rings in chloroplasts (discussed below) (Vitha et al. 2001) a logical hypothesis was that the inner PD-ring is composed of FtsZ, but it was later found that the FtsZ ring assembles much earlier. Additionally, the inner PD-ring is probably dependent on FtsZ assembly at mid-plastid (Kuroiwa et al. 2002; Miyagishima et al. 2001a). FtsZ probably assembles before of the inner PD-ring, which in turn promotes assembly of the middle PD ring (in *C. merolae*) and finally the outer PD-ring assembles at the site of chloroplast division. The inner and middle PD-rings disassemble after constriction and prior to completion of fission (Miyagishima et al. 2001a), but the outer ring stays intact through completion of division. The composition of the PD-rings is still unknown. Preliminary biochemical studies of the outer PD-ring

found it to be composed of a ~56 kDa filament forming protein with an unknown sequence or identity (Miyagishima et al. 2001b).

The stromal chloroplast division machinery

FtsZ

Supporting the endosymbiotic origin of chloroplasts (Gray 1993) was the finding that plants contain chloroplast-targeted homologues of the bacterial cell division protein FtsZ (Osteryoung et al. 1998; Osteryoung and Vierling 1995). Bacteria typically have one type of FtsZ, but plants have two phylogenetically distinct families of FtsZ, FtsZ1 and FtsZ2. Arabidopsis contains three nuclear-encoded FtsZ genes: one FtsZ1 gene, *AtFtsZ1-1*, and two FtsZ2 genes, *AtFtsZ2-1* and *AtFtsZ2-2*. In Arabidopsis, *AtFtsZ2-1* and *AtFtsZ2-2* are genetically redundant (Aaron Schmitz, unpublished observation). All three Arabidopsis FtsZs are targeted to the chloroplast stroma by cleavable transit peptides (McAndrew et al. 2001; McAndrew et al. 2008). FtsZ1 may associate with thylakoids early in development (El-Kafafi et al. 2008). Plant FtsZ2 proteins are more similar to bacterial FtsZ proteins and have the conserved C-terminal motif (Figure 1.1) that in bacteria binds to ZipA and FtsA. In plants, the FtsZ2 C-terminal motif binds to the chloroplast division protein ARC6 (Maple et al. 2005) through a discrete portion of ARC6 that may be structurally similar to the FtsZ binding domain of ZipA (Jonathan Glynn, unpublished). FtsZ1, which lacks this conserved domain, does not bind ARC6 (Maple et al. 2005). In contrast to FtsZ2, FtsZ1 proteins have shorter C-termini and there are no known proteins that bind FtsZ1 C-termini. However, FtsZ1 is distinguished from FtsZ2 by

specifically binding the chloroplast division protein ARC3, but not ARC6 (Maple et al. 2005).

In *E. coli*, blocked cell division, such as caused by mutations in *FtsZ*, results in long, filamentous, multinucleate cells with evenly spaced Z-rings (Addinall et al. 1996). Blocked chloroplast division results in fewer enlarged chloroplasts (Osteryoung et al. 1998; Osteryoung and Vierling 1995; Stokes et al. 2000). Loss of function or overexpression of any of the three Arabidopsis *FtsZ* genes leads to blocked chloroplast division, which suggests stoichiometric interaction between the *FtsZ* proteins may be important for function (Osteryoung et al. 1998; Stokes et al. 2000).

Similar to bacterial *FtsZ*, plant *FtsZ* proteins are localized to rings at mid-plastid that encircle the site of division on the stromal side of the IEM of the chloroplast (Vitha et al. 2001). Moreover, using double-stain immunofluorescence microscopy, *FtsZ1* and *FtsZ2* are found precisely co-localized (within the resolution limit of immunofluorescence microscopy) to the same division rings at mid-plastid (Vitha et al. 2001). *FtsZ* rings have been found to be remodeled in less than 30 sec (Vitha et al. 2005) similar to the dynamics of *E. coli FtsZ in vivo* (Stricker et al. 2002). Disruption of *FtsZ* levels leads to defects in *FtsZ*-ring morphology (Vitha et al. 2001). Loss of *FtsZ1* function results in long disorganized *FtsZ2* filaments throughout the chloroplasts, whereas the loss of *FtsZ2* results in short disorganized *FtsZ1* filaments in the plastid (Stokes et al. 2000; Vitha et al. 2001; Yoder et al. 2007). Because the *FtsZ2*-interacting

protein ARC6 (discussed below) may promote FtsZ2 organization, it is unclear if the long FtsZ2-filaments are a property of FtsZ2, or a result of ARC6 promoting FtsZ2 assembly.

ARC6 is a homologue of Ftn2

ARC6 was identified as having a role in chloroplast division in a series of T-DNA insertion lines with enlarged chloroplasts. In *arc6* mutants, plants typically have only one enlarged chloroplast that takes up much of the available cytosolic volume (Pyke and Leech 1994). The gene encoding *ARC6* was identified as a homologue of the cyanobacterial cell division gene *Ftn2* (Koksharova and Wolk 2002) found in the *arc6* mapping interval (Vitha et al. 2003). *ARC6* is a transmembrane protein that contains an N-terminal DnaJ-like co-chaperone motif, which is in the chloroplast stroma, while the C-terminus extends into the intermembrane space.

ARC6 has been found to interact specifically with the conserved C-terminal motif found in plant FtsZ2 proteins, but not FtsZ1 family proteins (Maple et al. 2005). Immunolocalization of FtsZ in the *arc6* mutant shows disorganized Z-filaments throughout the entire plastid, but the lines overexpressing *ARC6* have hyper-stabilized Z-filaments that form spirals at mid-plastid, suggesting *ARC6* organizes and stabilizes Z-rings (Vitha et al. 2003) by binding the C-terminus of FtsZ2 (Maple et al. 2005; McAndrew et al. 2008).

AtMinD and AtMinE

Chloroplasts have homologues of MinD and MinE, but lack an obvious homologue of MinC. Because not all bacteria use the Min system, the functional

consequences of missing MinC are unknown (Barak and Wilkinson 2007; Lutkenhaus 2007; Margolin 2002; Rothfield et al. 2005). MinD and MinE were first found in plants by BLAST searches (Colletti et al. 2000; Itoh et al. 2001; Maple et al. 2002). In the plastid, MinD and MinE specify proper symmetric division of the plastid and loss of MinD or overexpression of MinE leads to asymmetric plastid division, resulting in heterogeneous plastid sizes. As in bacteria, the opposite experiment of overexpression of MinD or loss of MinE results in blocked plastid division (Colletti et al. 2000; Fujiwara et al. 2004; Maple et al. 2002).

AtMinD has been reported to bind and hydrolyze ATP like its bacterial counterpart (Hu and Lutkenhaus 2001), and is stimulated by AtMinE (Aldridge et al. 2005). In bacteria, MinD and MinE homodimerize and heterodimerize together and the same is true for AtMinD and AtMinE, suggesting functional conservation (Maple et al. 2005; Maple and Moller 2007b). *In vivo*, the mutant *arc11* has a mutation in the AtMinD dimerization motif resulting in misplacement of the division furrow and heterogeneously-sized and multiply constricted chloroplasts (Fujiwara et al. 2004) again suggesting the Min system is functionally conserved in chloroplast division. However, many functional details of the Arabidopsis Min system remain unknown.

ARC3

ARC3 was identified in a mutant screen for plants with fewer enlarged chloroplasts (Pyke and Leech 1994) and the *arc3* mutation was cloned by map-based cloning (Shimada et al. 2004). The N-terminus of ARC3 contains an FtsZ-like, glycine-

rich, GTP binding domain and a eukaryotically derived C-terminal repeat MORN (membrane occupation and nexus) motif followed by a domain similar to a phosphatidylinositol-5-phosphate kinase (PIP-5K) domain. However, biochemical activity of these domains has not been described. Moreover, the PIP-5K domain lacks key residues required for catalytic activity (Maple et al. 2007). ARC3 localizes to a mid-plastid ring (Shimada et al. 2004) and specifically interacts with FtsZ1, but not FtsZ2 proteins (Maple et al. 2007) and can be partially purified in a salt-stable complex with FtsZ1, FtsZ2 and ARC6 (McAndrew et al. 2008). Curiously, immunofluorescence labeling of FtsZ in *arc3* mutants shows multiple parallel Z-rings (Glynn et al. 2007) and multiple parallel division furrows (Maple and Moller 2007a, b). This suggests a role for ARC3 in Z-ring positioning similar to that of MinC, although its mid-plastid localization by immunofluorescence suggest that ARC3 positioning of Z-rings is mechanistically different than that of MinC (which is polar localized in bacteria). However, the biochemical effect of ARC3 on plant FtsZ filaments is unknown.

AtSulA/GC1

In response to DNA damage in bacteria, FtsZ filaments are capped and depolymerized by the cell division inhibitor SulA. A weak homologue of SulA, AtSulA (also called GC1) has been identified in plants (Maple et al. 2004; Raynaud et al. 2004a). AtSulA is a transmembrane protein that does not assemble into a ring at mid-plastid (Maple et al. 2004). In contrast to other chloroplast division proteins, AtSulA does not form rings or other sub-plastidic localized structures, but instead is found diffusely throughout the IEM. Loss of AtSulA leads to blocked chloroplast division, but it is

unclear if overexpression leads to blocked chloroplast division (Maple et al. 2004; Raynaud et al. 2004a). Bacterial SulA proteins interact with FtsZ to block the GTPase activity by capping Z-filaments blocking incoming subunits to complete a trans-GTPase active site (Bi and Lutkenhaus 1993). However, AtSulA does not interact with either FtsZ1 or FtsZ2 in yeast-two-hybrid assays and no other functional information exists for AtSulA/GC1. Recently it has been argued that AtSulA may be only weakly similar to bacterial SulA and may have other roles in chloroplast division (Maple and Moller 2007b). Immunolocalization of FtsZ in AtSulA mutants will be essential to assignment of AtSulA function.

The eukaryotic-derived chloroplast division machinery

ARC5/CmDnm2

ARC5 and its homologue in the alga *C. merolae*, CmDnm2, were identified simultaneously and are plant-specific dynamin proteins (Gao et al. 2003; Miyagishima et al. 2003b). CmDnm2 was identified by sequence similarity to CmDnm1 which is involved in *C. merolae* mitochondrial division. In contrast to mitochondrial localized CmDnm1, CmDnm2 was found to localize to the cytosolic side of the chloroplast division site in *C. merolae* (Miyagishima et al. 2003b). Interestingly, CmDnm2 is found to only localize to the chloroplast division site during the process of fission and is not a part of cytosolic PD-rings (Kuroiwa et al. 2002; Miyagishima et al. 2001a). Furthermore, CmDnm2 stays associated with the division furrow late into division long after the FtsZ ring has disassembled (Miyagishima et al. 2003b)

ARC5 was identified in an ethyl methanesulfonate (EMS) mutant screen for *Arabidopsis* plants with defects in chloroplast division having altered chloroplast morphology (Pyke and Leech 1994). In the *arc5* mutant, chloroplasts are dumbbell-shaped suggesting *ARC5* may have a role in completing chloroplast division (Pyke and Leech 1994; Robertson et al. 1996). *ARC5* is a dynamin-like protein that localizes to a ring outside the mid-plastid division furrow (Gao et al. 2003). Dynamin proteins are known to be involved in cellular membrane fission and fusion and most notably are involved in mitochondria fission (Bleazard et al. 1999; Ingerman et al. 2005; Tieu and Nunnari 2000; Tieu et al. 2002). CmDnm2 rings have been isolated and found to exert force on optical tweezers supporting the idea that *ARC5/CmDnm2* provide the external force of chloroplast division (Yoshida et al. 2006).

PDV1/PDV2

PDV1 was identified as an *ARC5* phenocopy mutant in a population of EMS mutagenized *Arabidopsis* plants. Plants contain two types of PDV proteins, *PDV1* and *PDV2*. Mutation in either *PDV1* or *PDV2* gene show defects in late-stages of chloroplast division, often having dumbbell shaped chloroplasts in mutant lines. *pdv1/pdv2* double mutants show an additive, more severe defect in chloroplast division (Miyagishima et al. 2006). *ARC5-GFP* localizes to mid-plastid rings in *pdv1* and *pdv2* mutants, but not in the *pdv1/pdv2* double mutant. These results suggest that *PDV1* and *PDV2*, though partially redundant, may work together to recruit *ARC5* to the division site (Miyagishima et al. 2006). However, the biochemical roles of *PDV1* and *PDV2* in chloroplast division are unknown.

Perspective

Bacterial cell division has been a useful model for the discovery of several chloroplast division proteins such as FtsZ1, FtsZ2, MinDE and others. However, the biochemical properties of plant homologues of bacterial cell division proteins are not well understood. In the case of plant FtsZs, there is reason to believe their fundamental properties may vary from those of bacterial FtsZ, primarily because there are two-types of FtsZ in plants. Moreover, many of the key FtsZ regulatory proteins such as ZipA, FtsA and MinC have no obvious homologues in chloroplasts, further complicating our understanding of chloroplast division. The work described below seeks to understand the composition of the stromal FtsZ complex and to define the functional properties of plant FtsZ1 and FtsZ2 and determine if the FtsZ1/FtsZ2 filament topology is a heterofilament or homofilament.

CHAPTER TWO

***IN VIVO* QUANTITATIVE RELATIONSHIP BETWEEN PLASTID DIVISION PROTEINS FTSZ1 AND FTSZ2 AND IDENTIFICATION OF ARC6 AND ARC3 IN A NATIVE FTSZ COMPLEX.**

McAndrew, R. S*, B. J. S. C. Olson*, D. Kadirjan-Kalbach, C. L. Chi-Ham, S. Vitha, J. E.

Froehlich and K. W. Osteryoung

Biochemical Journal (2008). 412: 367-368

*These authors contributed equally to this work

B. J. S. C. Olson contributed the following data:

Figures 2.7, 2.10 and 2.11

Confirmation of the data reported in Figure 2.8

B. J. S. C. O also co-wrote the discussion, contributed other major portions of the manuscript, and submitted the manuscript for publication in consultation with K. W. Osteryoung.

Synopsis

FtsZ1 and FtsZ2 are phylogenetically distinct homologues of the tubulin-like bacterial cell division protein FtsZ that play major roles in the initiation and progression of plastid division in plant cells. Both proteins are components of a mid-plastid ring, the Z-ring, which functions as a contractile ring on the stromal surface of the chloroplast inner envelope membrane. FtsZ1 and FtsZ2 have been shown to interact, but their *in vivo* biochemical properties are largely unknown. To gain insight into the *in vivo* biochemical relationship between FtsZ1 and FtsZ2, we investigated their molecular levels in wild-type *Arabidopsis thaliana* plants and endogenous interactions in *Arabidopsis* and pea. Quantitative immunoblotting and morphometric analysis showed that the average total FtsZ concentration in chloroplasts of 3-week-old *Arabidopsis* plants is comparable to that in *E. coli*. FtsZ levels declined as plants matured, but the molar ratio between FtsZ1 and FtsZ2 remained constant at approximately 1:2, suggesting this stoichiometry is regulated and functionally important. Density gradient centrifugation, native gel electrophoresis, gel filtration and co-immunoprecipitation experiments show that a portion of the FtsZ1 and FtsZ2 in *Arabidopsis* and pea chloroplasts is stably associated in a complex of ~200-245 kDa. This complex also contains the FtsZ2-interacting protein ARC6, an inner envelope membrane (IEM) protein, and analysis of density gradient fractions suggests the presence of the FtsZ1-interacting protein ARC3. Based on the mid-plastid localization of ARC6 and ARC3 and their postulated roles in promoting and inhibiting chloroplast FtsZ polymer formation, respectively, we hypothesize that the FtsZ1/FtsZ2/ARC3/ARC6 complex represents an

unpolymerized, IEM-associated pool of FtsZ that contributes to the dynamic regulation of Z-ring assembly and remodeling at the plastid division site *in vivo*.

Introduction

The essential cell division protein FtsZ is a polymer-forming, tubulin-like GTPase found in most prokaryotes (reviewed in (Margolin 2005a; Michie and Lowe 2006; Romberg and Levin 2003)). Prior to cytokinesis, FtsZ assembles at the mid-cell division site, just inside the cytoplasmic membrane, to form a contractile ring termed the Z-ring. The *in vivo* molecular structure of the Z-ring is unknown, but *in vitro* studies suggest it is built from overlapping segments of short protofilaments composed of FtsZ monomers assembled end-to-end and stabilized at the division site through interactions with accessory factors (Anderson et al. 2004; Chen et al. 2005; Chen and Erickson 2005; Redick et al. 2005). Mutations in *FtsZ* disrupt cell division, resulting in the formation of long, multi-nucleate bacterial filaments. The Z-ring in *Escherichia coli* and *Bacillus subtilis* contains 30-35% of the total FtsZ, but is constantly remodeled by exchange of subunits with a cytoplasmic FtsZ pool in a dynamic process that requires the GTPase activity of FtsZ (Anderson et al. 2004; Redick et al. 2005; Stricker et al. 2002). FtsZ concentration is critical for its cell division activity (Sossong et al. 1999; Wang and Lutkenhaus 1993). Alterations in FtsZ levels or in the stoichiometry between FtsZ and other division proteins cause lethal blocks in cell division *in vivo*, and FtsZ polymerization and GTPase activity are concentration-dependent *in vitro* (Dai and Lutkenhaus 1992; Dewar et al. 1992; Hale and de Boer 1997; Takada et al. 2005). FtsZ is known to interact

with several other proteins that are recruited to the ring in a defined order, but the physiologically relevant sub-complexes deployed to the division site *in vivo* and the mechanisms regulating Z-ring dynamics in bacteria remain unclear (Margolin 2005b; Michie and Lowe 2006; Pradel et al. 2006; Romberg and Levin 2003).

Consistent with the endosymbiotic origin of chloroplasts, plants possess nuclear-encoded, plastid-targeted homologues of bacterial FtsZ (Osteryoung et al. 1998; Osteryoung and Vierling 1995). Most prokaryotes, including the cyanobacterial relatives of chloroplasts, have a single form of FtsZ; however, plants contain two distinct FtsZ protein families, FtsZ1 and FtsZ2, both of which are required for the proper division of plastids (McAndrew et al. 2001; Osteryoung et al. 1998; Stokes et al. 2000). Similar to their bacterial counterparts, FtsZ1 and FtsZ2 colocalize to a mid-plastid Z-ring in the chloroplast stroma adjacent to the inner envelope membrane. The Z-ring assembles prior to the ordered recruitment of other sub-assemblies of the division complex and constricts throughout plastid division (McAndrew et al. 2001; Miyagishima et al. 2001c; Vitha et al. 2001). Recently, FtsZ1 and FtsZ2 have been shown to interact separately with the chloroplast division proteins ARC3 and ARC6, respectively (Maple et al. 2005; Maple et al. 2007), and may interact with other novel components of the chloroplast division machinery (Glynn et al. 2007; Maple et al. 2007). Thus, FtsZ1 and FtsZ2 are functionally distinguished in part by distinct protein-protein interactions.

Several lines of evidence suggest that FtsZ1 and FtsZ2 function in a complex. They are tightly colocalized to rings in immunofluorescence labeling experiments in both

wild type plants and in chloroplast division mutants in which FtsZ filament morphology is perturbed (Fujiwara and Yoshida 2001; McAndrew et al. 2001; Vitha et al. 2003; Vitha et al. 2001). FtsZ1 and FtsZ2 interact directly, both individually and with each other, in yeast two-hybrid and bimolecular fluorescence complementation assays (Maple et al. 2005). FtsZ1 is not absolutely required for plastid division since *ftsZ1* null mutants in *Arabidopsis* are viable (El-Kafafi et al. 2008; Yoder et al. 2007), but a change in the level of either FtsZ1 or FtsZ2 perturbs plastid division (Osteryoung et al. 1998; Raynaud et al. 2004b; Stokes et al. 2000; Strepp et al. 1998), suggesting their stoichiometry relative to one another and/or to other division factors such as ARC3 and ARC6 is important for normal plastid division *in vivo*.

As an important foundation for understanding the roles of FtsZ1 and FtsZ2 in chloroplast Z-ring dynamics, we are investigating their *in vivo* biochemical properties. In the studies described here, we report endogenous FtsZ1 and FtsZ2 protein levels and molar ratios in chloroplasts of the model plant *Arabidopsis thaliana*. In addition, we show that FtsZ1 and FtsZ2 in pea and *Arabidopsis* chloroplasts are stably associated in a native complex that also contains ARC6; analysis in pea indicates that the complex contains ARC3 as well. These studies are the first in which the *in vivo* quantitative relationship between chloroplast FtsZ proteins and their interactions with accessory factors have been investigated in wild-type plants.

Experimental Procedures

Plant material

Arabidopsis thaliana ecotype Columbia (Col-0) plants were grown as in (Stokes et al. 2000). Pea plants (*Pisum sativum* var. Little Marvel) were grown in vermiculite as in (Bruce et al. 1994). The mutant lines SALK_134970 and SALK_050397, carrying T-DNA insertions in the *AtFtsZ2-1* and *AtFtsZ2-2* genes were identified in the Salk Institute Genomic Analysis Laboratory database (<http://signal.salk.edu/cgi-bin/tdnaexpress>) (Alonso et al. 2003) and obtained from the Arabidopsis Biological Resource Center (<http://www.arabidopsis.org/abrc/>). The positions of the T-DNA inserts were confirmed by sequencing of PCR products amplified from the mutants using the T-DNA left border primer LBb1 (5'-GCGTGGACCGCTTGCTGCAACT-3') and either an *AtFtsZ2-1*-specific primer (5'-AGGGGGTTCGTGGGATATCTG-3') or *AtFtsZ2-2*-specific primer (5'-TATTGTGTGAATTTGCTGCC-3'). Individuals homozygous for the T-DNA insertions were identified by segregation analysis.

Chloroplast morphology phenotyping

Leaf tissue was prepared for microscopic analysis and viewed with a BH-2 (Olympus) microscope as described (Osteryoung et al. 1998; Pyke et al. 1991).

Immunofluorescence labeling

Fixation, embedding and immunofluorescence labeling of leaf and floral bud tissue with antibodies specific for *AtFtsZ1-1*, *AtFtsZ2-1* and *AtFtsZ2-2* was performed as described (Vitha et al. 2001). Specimens were viewed with a Leica DMR A2 microscope (Leica Microsystems, Wetzlar, Germany) and images were processed as described (Vitha et al. 2003).

Preparation of antibodies

Polyclonal antipeptide antibodies specific for AtFtsZ1-1 (1-1 antibodies) and AtFtsZ2-1 (2-1A antibodies) were generated previously (Stokes et al. 2000). The same procedure was used to generate and affinity-purify antipeptide antibodies against AtFtsZ2-1 (2-1B antibodies) and AtFtsZ2-2 (2-2 antibodies) using synthesized peptides corresponding to amino acid residues 367-380 (TRRRSSSFRESGSVEI) of AtFtsZ2-1 and 244-261 (EGRRAVQAQEGLAALRD) of AtFtsZ2-2, respectively. Affinity-purified 1-1, 2-1B and 2-2 antibodies were concentrated to 1.7, 1.2, and 2.8 mg/ml, respectively. The specificity of the 2-1A antibody was maximized by pre-absorbing IgG-enriched 2-1A serum on an AtFtsZ2-2 peptide column prior to affinity purification on a 2-1A peptide column (Stokes et al. 2000). 2-1A antibodies were concentrated to 1.3 mg/ml in PBS (140 mM NaCl, 3 mM KCl, 10 mM Na₂HPO₄, 2 mM KH₂PO₄).

ARC6 antibodies were raised against amino acids 216-482 created from a XhoI-DraI fragment of the ARC6 cDNA (At5g42480) ligated into the XhoI-SmaI site of the expression vector pJC40 (Clos and Brandau 1994) resulting in a C-terminally His-tagged ARC6. This ARC6 fragment does not include the conserved J-like domain (Vitha et al. 2003). Recombinant proteins were expressed in *E. coli* Rosetta (DE3) pLysS cells (Novagen) with 1 mM IPTG and purified by Ni-affinity chromatography (Novagen). Antiserum produced in New Zealand White rabbits (Covance Research Products, Denver, PA) was affinity-purified over a 1 ml protein-A column (Pierce); the column was washed with PBS, and bound antibodies eluted in 0.2M glycine, pH 1.85. After buffering the

eluted antibody in Tris-HCl with a final pH of 7.4, the eluate contained 0.72 mg/ml protein. Affinity-purified antibodies were diluted 1:4900 for immunoblotting.

An antibody to ARC3 (Shimada et al. 2004) was obtained from Dr. Hiroshi Shimada and verified for specificity by immunoblotting using extracts from wild type *Arabidopsis* (Col-0) and *arc3* mutant plants, extracts from *E. coli* expressing recombinant ARC3-His, and purified ARC3-HIS (not shown).

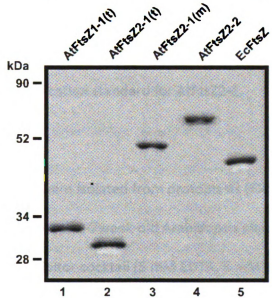
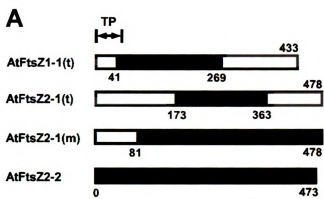
Expression, purification and calibration of recombinant protein standards

Quantitative immunoblotting standards were created from fragments of the *AtFtsZ1-1*, *AtFtsZ2-1*, and *AtFtsZ2-2* cDNAs encoding partial or full-length proteins as shown (Figure 2.1A) expressed in *E. coli* as N-terminal 10-histidine-tagged fusion proteins. Recombinant proteins were produced as described (Stokes et al. 2000) except that *AtFtsZ2-2* was produced in C43(DE3) cells (Miroux and Walker 1996) (Avidis) and the mature *AtFtsZ2-1* construct (*AtFtsZ2-1(m)*) was expressed from pDB328 in C41(DE3) cells (de Boer et al. 1989b; Hale and de Boer 1997). Soluble recombinant proteins were purified from cell lysates by Ni-affinity chromatography and their purity was evaluated by SDS-PAGE (Figure 2.1B). The purified proteins (>95% pure) were lyophilized, resuspended in storage buffer (50 mM Tris-HCl, pH 8, 1 mM EDTA, 1 mM 4-(2-aminoethyl) benzenesulfonyl fluoride (AEBSF), 10% glycerol), and stored at -20°C .

FtsZ protein concentration was determined by the BCA and Bradford assays (Olson and Markwell 2007) calibrated against purified *E. coli* FtsZ (Supplementary Figure 2.2B, lane 5) quantified as described (Lu et al. 1998). Protein standards were

Figure 2.1: Expression and purification of recombinant protein standards for quantitative analysis

(A) Schematic diagram of recombinant protein sequences expressed in *E. coli* for use as quantification standards. Numbers on right indicate lengths in amino acid residues of pre-proteins encoded by full-length cDNAs (McAndrew et al. 2001). Arrow above indicates approximate length of transit peptides (TP). Residues encoded by recombinant protein constructs (black bars) were 41-269 for truncated AtFtsZ1-1(t), 173-363 for AtFtsZ2-1(t) (25), 81-478 for mature AtFtsZ2-1(m) (Stokes et al. 2000), and 1-473 for AtFtsZ2-2. (B) Coomassie-stained gel showing recombinant AtFtsZ1-1(t), AtFtsZ2-1(t), AtFtsZ2-1(m), and AtFtsZ2-2 proteins (lanes 1-4, respectively, ~1 mg protein/lane) resolved by SDS-PAGE. Recombinant proteins were analyzed and calibrated for protein concentration and purity relative to recombinant *E. coli* FtsZ (lane 5). Approximate molecular masses are indicated on the left.



adjusted to 1 mg/ml, diluted serially (500 to 2.5 ng in 10 μ l), and processed on immunoblots probed with FtsZ-specific primary antibodies and [125 I]donkey-anti-rabbit secondary IgG (8.8 μ Ci/ μ g, GE Healthcare) to generate standard curves (Supplementary Figure 2.3) for quantitative analysis of plant FtsZ levels (described below). Standard curves were constructed based on the linear range of detection of radioactive signals. Data generated from the fusion proteins labeled AtFtsZ2-1(m) and AtFtsZ2-1(t) in Figure 2.1 yielded nearly identical standard curves (not shown); therefore, AtFtsZ2-1(t) was used subsequently as the quantification standard for AtFtsZ2-1.

Chloroplast isolation

Arabidopsis chloroplasts were isolated from protoplasts (Fitzpatrick and Keegstra 2001) prepared from whole shoots of 3-7week-old Arabidopsis plants and all steps after isolation included a protease inhibitor cocktail (5 mM EDTA, 5 mM EGTA, 0.05 mg ml $^{-1}$ 1-chloro-3-tosylamido-7-amino-2-heptanone, 1 mM benzamidine HCl, 5 mM ϵ -amino-*N*-caproic acid, 1 μ M leupeptin, 1 μ M pepstatin A, and 1 mM AEBSF). Pea chloroplasts were isolated from leaves of 7-9 day-old plants as described previously (Bruce et al. 1994). All steps included a protease inhibitor cocktail (Sigma P2714). Chlorophyll content of chloroplast suspensions was determined as in (Arnon 1949) and chloroplast concentration (organelles/ml) was determined using a hemacytometer.

Determination of chloroplast volume

Chloroplasts isolated from 3-week old Arabidopsis plants were immobilized by mixing chloroplasts in import buffer 1:1 with warm low-melting-point agarose, 0.2%

(w/v) in import buffer, and cooling the suspension on a slide under a cover glass. 3-D images of chlorophyll autofluorescence (excitation 488 nm, emission 600-700 nm) were acquired using a Zeiss LSM 5 PASCAL confocal microscope (Carl Zeiss) equipped with a 60x/1.4 oil immersion objective. After correction for refractive index mismatch between the immersion oil and the specimen, the effective voxel size was 0.089 μm in the XY, and 0.43 μm in the Z direction, yielding a voxel volume of $3.4 \times 10^{-3} \mu\text{m}^3$. Image stacks were opened using ImageJ ver. 1.34 software (<http://rsb.info.nih.gov/ij>), filtered (Median, radius = 4), set to auto-threshold, and voxels for each chloroplast were counted using the VoxelCounter plug-in (<http://rsb.info.nih.gov/ij/plugins/voxel-counter.html>). Volume was calculated as the number of voxels multiplied by voxel volume. Plastid circumference was measured from image stacks that were rotated using the VolumeViewer plug-in (<http://rsb.info.nih.gov/ij/plugins/volume-viewer.html>) to show the plastid projection along the longest axis of the plastid, which corresponds to the plastid cross-section at mid-length. The circumference of this projection was then measured in ImageJ. A total of 66 chloroplasts were measured to determine average volume.

Quantitative immunoblotting

Isolated chloroplasts in import buffer were solubilized by addition of 2X Laemmli sample buffer (1:1) (Laemmli 1970), and diluted with 1X Laemmli sample buffer to various chlorophyll concentrations. Immunoblotting on PVDF was performed as previously described (McAndrew et al. 2001) except that blots were incubated overnight

with 1-1 (1:6000), 2-1A (1:5000), or 2-2 (1:6000) antibodies in TBSTG which is composed of TBS (50 mM Tris-HCl, pH 7.4, 200 mM NaCl) with 0.2% [v/v] Tween 20, 0.25% (v/v) fish gelatin (Sigma-Aldrich). Following washing, blots were incubated for 4 h in TBSTG containing ^{125}I -donkey-anti-rabbit IgG (8.8 $\mu\text{Ci}/\mu\text{g}$, GE Healthcare), at 2-3 $\mu\text{Ci}/42.5 \text{ cm}^2$. Blots were washed, dried, and placed on phosphorimager screens for periods ranging from 1-16 h, then digitized with a phosphorimager (Personal FX, Bio-Rad) and QUANTITY ONE software (Bio-Rad). Three identical blots containing a duplicate set of serially diluted standards and chloroplast lysate proteins were developed concurrently with signal intensities showing less than 10% (\pm S.D.) variation. FtsZ concentrations in chloroplast lysates were determined within the linear range of the standards Figure 2.4 and showed <10% (\pm S.D.) variation between replicate blots. The results of these quantitative immunoblots were combined with microscopic measurements to estimate the number of FtsZ molecules per chloroplast.

Immunoprecipitation of in vitro FtsZ translation products before and after import into isolated intact chloroplasts

Affinity-purified 1-1 (8 mg), 2-1A (10 mg), 2-1B (10 mg), and 2-2 (10 mg) antibodies were separately coupled to CarboLinkTM Gel (Pierce) agarose beads, as recommended by the manufacturer, with a coupling efficiency of ~85-90%. Coupled antibodies (A-beads; ~8.5 ng antibodies/ μl beads), pre-conditioned with 0.1 M glycine, pH 2.5, and equilibrated in TBS plus 0.02% (w/v) thimerosal, were used in immunoprecipitation assays as a 1:1 (bead:buffer) slurry. 2-1A and 2-1B antibodies

were coupled to beads and mixed together (1:1) prior to use for immunoprecipitation of AtFtsZ2-1.

AtFtsZ1-1, AtFtsZ2-1, or AtFtsZ2-2 were translated in the presence of [³⁵S]-Met and imported into pea chloroplasts as previously described (McAndrew et al. 2001). Import reactions contained 2.1 X 10⁶, 2.0 X 10⁶, and/or 3.3 X 10⁶ dpm of radiolabeled AtFtsZ1-1, AtFtsZ2-1, and AtFtsZ2-2, respectively, and intact pea chloroplasts (150 μg chlorophyll) in a final volume of 900 μl. Control assays were performed using the nuclear-encoded, small subunit of RuBisCO (SSU). Following import, chloroplasts were treated with thermolysin to degrade non-imported proteins (Cline et al. 1984), re-isolated through 40 % (v/v) Percoll, and washed in import buffer. Intact chloroplasts (75-100 μg chlorophyll) were either solubilized in 2X Laemmli sample buffer for SDS-PAGE, or resuspended in 200 μl of buffer containing 25 mM HEPES-KOH, pH 8.0, 4 mM MgCl₂ and protease inhibitors (5 mM EDTA, 5 mM EGTA, 1 mM benzamidine HCl, 5 mM ε-amino-*N*-caproic acid, 1 μM leupeptin, 1 mM AEBSF) and placed on ice for 30 min before initiating immunoprecipitation reactions.

Radiolabeled translation products were immunoprecipitated directly from *in vitro* translation reactions (48 μl containing ~120,000 dpm/μl), as described (Anderson and Blobel 1983), using FtsZ-specific A-beads (100 μl of 1:1 slurry, ~5 ng antibody μl⁻¹). Imported proteins (~1.0 x 10⁵ dpm/reaction) were immunoprecipitated from chloroplast lysates, as described (Nielsen et al. 1997), with the following modifications. Briefly, 1 ml of IP-DDM buffer (25 mM HEPES, pH 7.5, 50 mM NaCl, 2 mM EDTA, 2 mM EGTA, 0.2 mM

n-dodecyl- β -D-maltoside (DDM, Anatrace) and protease inhibitors) was added to the chloroplast lysate (200 μ l), followed by addition of FtsZ-specific A-beads (100 μ l of 1:1 slurry). Reactions were incubated (~12 h, 4 °C) on a rocking table. Beads were collected by centrifugation (10,000 *g*, 15 s), washed three times with IP-DDM, and once in buffer with no detergent (50 mM Tris, pH 7.5, 150 mM NaCl, 2 mM EDTA, 2 mM EGTA). Bound proteins were eluted by addition of 2X Laemmli sample buffer (no dye) and incubation at 80 °C (5 min) and collected as above. Beads were washed once in water and combined eluants were analyzed by SDS-PAGE and fluorography.

Isolation of an endogenous FtsZ complex by two-dimensional gel electrophoresis

Intact pea chloroplasts (~2.3 mg chlorophyll/ml) were lysed in buffer containing 50 mM Tris, pH 7.5, 50 mM MgCl₂, 50 mM KCl, 50 mM NaCl, 0.2 mM DDM, supplemented with protease inhibitors. The lysate was incubated on ice (30 min) and passed several times through a syringe fitted with a 25-gauge needle. Stromal protein complexes (400 μ g total protein) were recovered in the supernatant following centrifugation (17,000 *g*, 45 min, 4 °C), mixed 1:1 with native-PAGE sample buffer (40% (w/v) sucrose, 1 M Tris, pH 8.0, 5% (w/v) bromophenol blue, 0.6 mM PMSF) and immediately resolved on native gradient gels (4-20% resolving, 4% stacking, 4°C) (Weigel and Glazebrook 2002). Molecular mass marker complexes ranging from 66-669 kDa (GE Healthcare) were run in parallel for estimating masses of unknown complexes. FtsZ migration in native gels was determined from immunoblots of adjacent duplicate lanes

probed with FtsZ-specific antibodies. Putative complexes containing FtsZ proteins were excised from native gels stained with 0.05% aqueous Coomassie Brilliant Blue G Colloidal (Sigma-Aldrich), solubilized by maceration of the gel slices in Laemmli sample buffer, and separated by 10% SDS-PAGE in the second dimension. Pea chloroplast stromal proteins (7 μ g) were loaded onto adjacent lanes as controls. FtsZ1 and FtsZ2 proteins were detected by immunoblotting as described (McAndrew et al. 2001).

Isolation and analysis of FtsZ-containing complexes from Arabidopsis and pea

Chloroplasts isolated from pea were lysed hypotonically in lysis buffer (50 mM HEPES-KOH pH 8.0, 4 mM MgCl₂, 1 mM DDM) and passed through a 25-gauge needle several times. Insoluble material was removed by centrifugation (16,000 *g*, 10 min, 4 °C). All buffers used for lysis and subsequent analysis contained protease inhibitors. Soluble proteins in isolated pea chloroplasts (50-100 mg chlorophyll) were resolved by sedimentation through a sucrose density gradient (5-20% (w/v), in lysis buffer, 130,000 *g*, 12 h, 4 °C) and collected in 24 fractions. Gradient fraction proteins were precipitated with 80% ice cold acetone, dried, resuspended (1:20) in Laemmli buffer, and analyzed by SDS-PAGE and immunoblotting using antibodies raised against AtFtsZ1-1, AtFtsZ2-1 (McAndrew et al. 2001), and ARC6 (Figure 2.9). In a separate series of experiments, a similar gradient was fractionated into 13 fractions and examined for FtsZ2 and ARC3 (Shimada et al. 2004) . Molecular mass standards (66-669 kDa, GE Healthcare) dissolved in lysis buffer were applied to a separate sucrose gradient, and run in parallel. Protein

peaks in gradient fractions were detected by UV absorbance at 280 nm and the standard curve is shown in Supplementary Figure 2.6A.

To investigate the co-fractionation of radiolabeled, imported Arabidopsis AtFtsZ1-1 and ARC6, both AtFtsZ1-1 and ARC6 were translated in the presence of [³⁵S]-Met as described above and imported independently into isolated pea chloroplasts. Chloroplasts were treated with thermolysin (Cline et al. 1984), reisolated through 40% Percoll in import buffer, and disrupted in lysis buffer. Proteins were resolved in parallel through identical sucrose density gradients, collected in fractions, precipitated with 80% acetone, dried, and resuspended 1:100 (v/v) in Laemmli buffer. 10 µl from each of two sequentially collected fractions were combined and resolved by SDS-PAGE. Following electrophoresis the gel was soaked for 1 h in 20% (w/w) 2,5-diphenyloxazole (PPO) in dimethylsulfoxide (DMSO), washed with water and dried for autoradiography.

To investigate the stability of FtsZ-containing complexes, sucrose gradient fractions containing FtsZ were pooled in sets of two, dialyzed in lysis buffer with protease inhibitors, and concentrated by ultrafiltration (Amicon Ultra 15, 30,000 MWCO; Millipore). Proteins from the concentrated pool (~50 µg total protein) were applied to a Q-sepharose (GE Healthcare) anion exchange column (1 ml bed volume) equilibrated with 50 mM HEPES-KOH pH 8.0, 4 mM MgCl₂. Proteins were eluted at 1 ml/min in a linear gradient (0-1M NaCl) applied over 100 min. Fractionated proteins were acetone-precipitated and FtsZ1, FtsZ2 and ARC6 were detected by immunoblotting.

Because it was difficult to estimate accurately the molecular mass of the FtsZ containing complex in sucrose density gradients, chloroplast stromal proteins prepared in lysis buffer were applied to a Superdex 200 10/300 GL column (GE Healthcare) equilibrated in lysis buffer (containing 1 mM DDM) and eluted at a flow rate of 0.5 ml/min; 178, 0.2 ml fractions were collected. Fractions were acetone-precipitated and examined by immunoblotting with FtsZ1 and FtsZ2 antibodies. The column was standardized with HMW calibration markers (GE Healthcare) prepared in lysis buffer and the molecular mass of the complex was calculated based on a standard curve (Figure 2.11). The retentions of the standards differed slightly in the presence and absence of DDM (not shown).

Results

Specificity of Arabidopsis FtsZ antibodies

Arabidopsis thaliana contains one *FtsZ1* gene, *AtFtsZ1-1* (At5g55280), and two *FtsZ2* genes, *AtFtsZ2-1* (At2g36250) and *AtFtsZ2-2* (At3g52750). Previously, we produced antipeptide antibodies against *AtFtsZ1-1* (1-1 antibodies) and *AtFtsZ2-1* (2-1 antibodies) that specifically target FtsZ1 and FtsZ2 in plant extracts (Vitha et al. 2001). For the studies described here, to ensure discrimination between *AtFtsZ2-1* and *AtFtsZ2-2*, which share ~82% amino acid identity, we generated and affinity-purified new antibodies against a peptide from *AtFtsZ2-2* (2-2 antibodies), and further purified our previously generated 2-1 antibodies (Stokes et al. 2000; Vitha et al. 2001). Antibody specificity was established by immunoblotting of leaf extracts (Figure 2.2) prepared

from WT Arabidopsis plants, transgenic plants expressing antisense constructs for either *AtFtsZ1-1* or *AtFtsZ2-1* (Osteryoung et al. 1998), and a homozygous *atftsZ2-2* knockout mutant (described below).

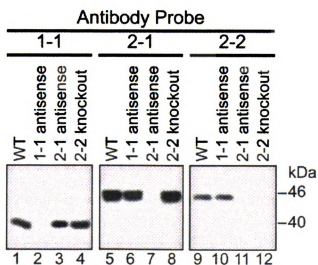
Consistent with previous results (Stokes et al. 2000; Vitha et al. 2001), the 1-1 antibodies recognized a single protein of ~40 kDa in WT plants, *AtFtsZ2-1* antisense plants and *atftsZ2-2* knockout mutants that was not detected in *AtFtsZ1-1* antisense plants (Figure 2.2, lanes 1-4) or in a mutant null for *AtFtsZ1-1* (Yoder et al. 2007). Likewise, the 2-1 antibodies detected two closely migrating proteins of about 45 and 46 kDa in all extracts except those of the *AtFtsZ2-1* antisense line (Figure 2.2, lanes 5-8). The 2-2 antibodies recognized a single protein in WT and *AtFtsZ1-1* antisense plants (lanes 9 and 10) that was not detected in the *AtFtsZ2-2* knockout mutant (lane 12). These results demonstrate the specificity of the 1-1, 2-1 and 2-2 antibodies for *AtFtsZ1-1*, *AtFtsZ2-1* and *AtFtsZ2-2*, respectively. In addition to establishing antibody specificity, the results shown in Figure 2.2 revealed that the *AtFtsZ2-1* antisense transgene (Osteryoung et al. 1998) silenced both *AtFtsZ2-1* (lane 7) and *AtFtsZ2-2* (lane 11) and that the two closely migrating proteins recognized by the 2-1 antibodies (Stokes et al. 2000; Vitha et al. 2001) (lanes 5, 6 and 8) are both products of the *AtFtsZ2-1* gene.

AtFtsZ2-2 functions in chloroplast division

Prior studies (Osteryoung et al. 1998; Vitha et al. 2001; Yoder et al. 2007) have established unequivocal roles for *AtFtsZ1-1* and *AtFtsZ2-1* in plastid division in Arabidopsis. To determine whether *AtFtsZ2-2* is also a functional plastid division gene,

Figure 2.2: Antibody specificity for AtFtsZ1-1, AtFtsZ2-1, and AtFtsZ2-2 protein

(A) Immunoblot analysis of proteins (1 mg fresh leaf tissue/lane) from WT Arabidopsis plants (WT, lanes 1, 5, and 9), transgenic plants carrying antisense constructs for *AtFtsZ1-1* (lanes 2, 6, and 10) or *AtFtsZ2-1* (lanes 3, 7, and 11), and knockout mutants with a T-DNA insertion in the *AtFtsZ2-2* gene (lanes 4, 8, and 12) were probed with affinity-purified antibodies raised against peptide sequences from AtFtsZ1-1 (lanes 1-4), AtFtsZ2-1 (lanes 5-8), and AtFtsZ2-2 (lanes 9-12). The two proteins detected by the AtFtsZ2-1 antibodies are consistently detected in Arabidopsis extracts (McAndrew et al. 2001; Stokes et al. 2000). Approximate molecular masses are shown.



we characterized a T-DNA insertional mutant of *AtFtsZ2-2* (SALK_050397). We also characterized a T-DNA insertion allele of *AtFtsZ2-1* (SALK_134970). We sequenced the annotated T-DNA insertion sites (<http://signal.salk.edu/cgi-bin/tdnaexpress>) (Alonso et al. 2003) and confirmed their positions in intron 4 after nucleotide 1363 for the *atftsZ2-1* mutant, and in exon 4 after nucleotide 1417 for the *atftsZ2-2* mutant (Figure 2.3A). *AtFtsZ2-2* protein was not detected by immunoblotting at any stage of development in the *atftsZ2-2* mutant (Figure 2.2, lane 12), indicating that the *atftsZ2-2* T-DNA insertion allele is null. *AtFtsZ2-1* and *AtFtsZ1-1* levels were unaffected in the *atftsZ2-2* mutant (Figure 2.2, lanes 4 and 8). In homozygous *atftsZ2-1* individuals, *AtFtsZ2-1* protein was not detected in plants grown from the original seed stock obtained from the ABRC, but *AtFtsZ2-1* proteins were often detected in progeny of these plants and in later generations (not shown). We conclude that *atftsZ2-1* is a knockdown allele of *AtftsZ2-1* with variable expression, probably due to the location of the T-DNA insertion in an intron (Figure 2.3A).

Chloroplast morphology in fully expanded leaf mesophyll cells of four-week-old *atftsZ2-1* and *atftsZ2-2* mutants was examined by light microscopy (Osteryoung et al. 1998) and compared with that in WT plants (Figure 2.3B). In the *atftsZ2-1* mutant, chloroplast morphology was highly variable. Large and small chloroplasts were frequently observed in the same cells (Figure 2.3C) and chloroplast number was reduced, often to one per cell. Related phenotypes have been reported in *AtFtsZ2-1* antisense plants (Osteryoung et al. 1998; Raynaud et al. 2004b). Chloroplast division defects were less pronounced in the *atftsZ2-2* mutant (Figure 2.3D), but quantitative

analysis showed that these chloroplasts were visibly larger and fewer in number than those in cells of comparable size from WT plants (Figure 2.3B) (A. Schmitz and K. W. Osteryoung, unpublished), indicating impaired chloroplast division. The difference in severity of division defects in the *atftsZ2-1* and *atftsZ2-2* mutants may reflect their respective contributions to the total FtsZ2 pool, as described below.

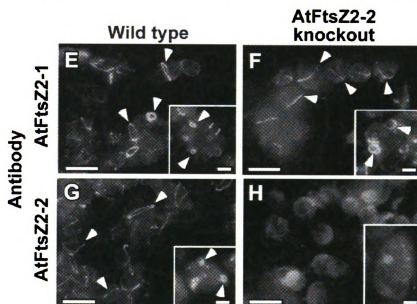
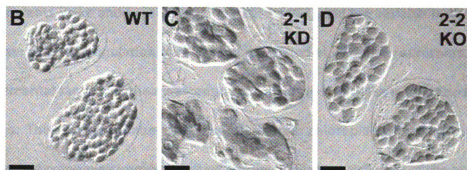
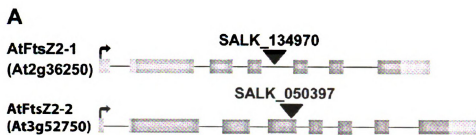
To further define the role of AtFtsZ2-2 in chloroplast division, we investigated its localization by immunofluorescence labeling. In green chloroplasts of fully expanded leaves, AtFtsZ2-2 was detected in mid-plastid ring structures in WT plants, but not in the *atftsZ2-2* knockout mutant (Figure 2.3, G and H, respectively). AtFtsZ2-2 also localized to rings in small non-green plastids of young floral buds (Figure 2.3G, inset). The absence of AtFtsZ2-2 in the enlarged chloroplasts of *atftsZ2-2* mutants did not interfere with ring formation by either AtFtsZ2-1 (Figure 2.3F) or AtFtsZ1-1 (not shown), which is consistent with the mild division defect observed in the *atftsZ2-2* plants. Taken together, the localization of AtFtsZ2-2 to a mid-plastid ring in WT plants and the reduced chloroplast division capacity of the *atftsZ2-2* knockout mutants indicate that AtFtsZ2-2, like AtFtsZ2-1, is a functional chloroplast division protein. These results also suggest that AtFtsZ2-1 and AtFtsZ2-2 are at least partially redundant

Quantitative analysis of FtsZ levels in Arabidopsis chloroplasts

AtFtsZ levels were measured by quantitative immunoblotting in chloroplasts isolated from whole rosettes of plants ranging in age from 3-7 weeks.

Figure 2.3: Chloroplast morphology and AtFtsZ2-1 and AtFtsZ2-2 localization in WT Arabidopsis and *atftsZ2-1* and *atftsZ2-2* T-DNA insertional mutants

(A) Positions of T-DNA insertions in mutant alleles of *AtFtsZ2-1* (At2g36250) and *AtFtsZ2-2* (At3g52750). (B-D) Chloroplast morphology in leaf mesophyll cells of WT Col-0 (B), and homozygous *atftsZ2-1* knockdown (KO; C) and *atftsZ2-2* knockout (KO; D) mutants. (E-G) Immunofluorescence labeling of AtFtsZ2-1 (E and F) and AtFtsZ2-2 (G and H) in leaf mesophyll cells and floral buds (insets) of WT plants (E and G) and *atftsZ2-2* knockout mutants (F and H). FtsZ rings are indicated by arrowheads. AtFtsZ2-1 and AtFtsZ2-2 colocalize in WT (E and G). In the *atftsZ2-2* knockout mutant, AtFtsZ2-1 forms rings (F) and AtFtsZ2-2 is not detected (H). In all panels, the bar = 20 μ m.



Preliminary blots established the linear working range for the purified FtsZ recombinant protein standards (Fig S2) and the range over which FtsZ protein levels and chlorophyll content were linearly correlated in leaf extracts (~7-15 μg chlorophyll; Figure 2.4B). Leaves, leaf cells and chloroplasts in older plants are on average larger than those in younger plants (Pyke and Leech 1994; Pyke et al. 1991), but are variable in size at any given age; thus the population of chloroplasts isolated at each age represents a developmental range and the measurements performed on these populations represent averages. The average number of FtsZ molecules per chloroplast at each plant age was estimated by combining immunoblotting results with measurements of the average number of chloroplasts per unit chlorophyll in isolated chloroplast suspensions (Table 2.1). In 3-week-old plants, the average number of FtsZ molecules per chloroplast was $101,200 \pm 6000$, with a molar distribution of approximately 33% AtFtsZ1-1, 47% AtFtsZ2-1, and 20% AtFtsZ2-2. Although total FtsZ levels declined 10-fold between 3 and 7 weeks, the molar ratio between FtsZ1 and FtsZ2 remained at approximately 1:2 (Figure 2.5), suggesting this stoichiometry in chloroplasts may be important for FtsZ function. The ratio between AtFtsZ2-1 and AtFtsZ2-2 was also somewhat stable (Table 2.1). Comparison of signals on immunoblots suggests FtsZ1-to-FtsZ2 ratios may be similar in pea, tobacco and spinach (Vitha et al. 2001) (not shown), but we lack the protein standards and knowledge of complete *FtsZ* gene complement required for rigorous quantitative analysis in other species. Previous calculations by Lu et al. (Lu et al. 1998) have shown there are ~15,000 FtsZ molecules in an average log-phase *E. coli*

Figure 2.4: Linear ranges of detection of FtsZ protein standards and FtsZ in chloroplast lysates for quantitative immunoblotting

(A) Average densities (CNT/mm²) of phosphorimager signals, within 10% (\pm S.D.) agreement after 2 h exposures, were recorded from immunoblots of recombinant protein standards AtFtsZ1-1(t) (circles), AtFtsZ2-1(t) (squares), and AtFtsZ2-2 (triangles) probed with FtsZ-specific primary antibodies and ¹²⁵I-secondary antibodies, and plotted relative to total protein (ng). FtsZ standards demonstrated reproducible linearity over the protein ranges shown: 10-83.5 ng, 10-65 ng, and 10-62.5 ng, for AtFtsZ1-1(t), AtFtsZ2-1(t), and AtFtsZ2-2, respectively. (B) To determine the limits of quantitative immunoblotting relative to plant sample load, total FtsZ (ng) in chloroplast lysates of known chlorophyll content (μ g) were extrapolated from the standard curves shown in (A). The linear range of chlorophyll (μ g), relative to that of the FtsZ standards, is 7.5-20 μ g/lane for AtFtsZ1-1 (circles) or AtFtsZ2-1 (squares), and 10-20 μ g/lane for AtFtsZ2-2 (triangles). Experiments were repeated four times in duplicate and data was averaged from separate blots containing both standards and plant extracts generating signals within 10% (\pm S.D.) agreement.

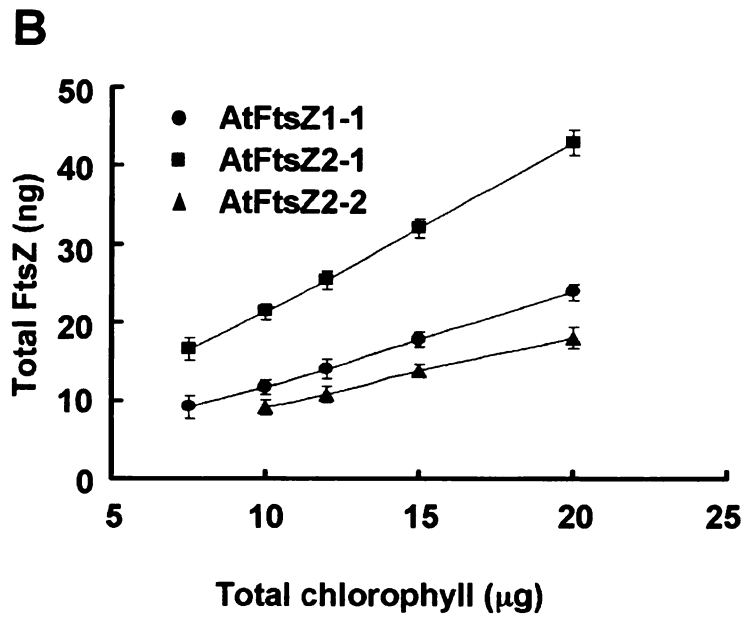
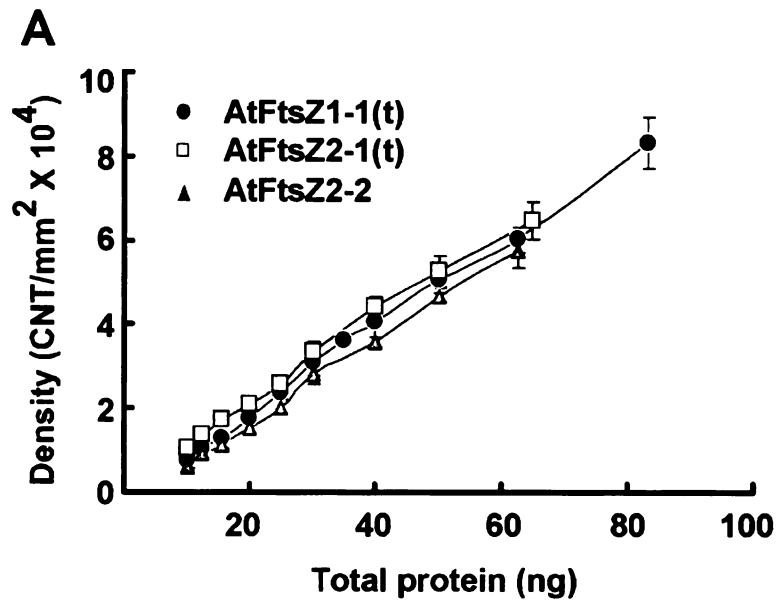


Table 2.1: Effects of whole plant age on FtsZ in Arabidopsis chloroplasts

Plant age (weeks) ^a	FtsZ levels (average molecules/ chloroplast) ^b				Molar ratio (1-1:2-1:2-2)
	AtFtsZ1-1	AtFtsZ2-1	AtFtsZ2-2	Total FtsZ	
3	33,100	47,700	20,400	101,200	1:1.4:0.6
3.5	27,100	45,500	19,500	92,100	1:1.6:0.7
4	20,500	25,900	11,100	57,500	1:1.3:0.5
5	6,900	12,000	3,600	22,500	1:1.3:0.5
7	3,500	5,100	2,100	10,700	1:1.4:0.6

^a Time (weeks post-germination) of plant harvest and chloroplast isolation.

^b FtsZ molecular levels were calculated from ng FtsZ/chloroplast, and based on molecular masses of 40, 45, and 46 kDa, respectively, for AtFtsZ1-1, AtFtsZ2-1, and AtFtsZ2-2. (Molecular averages did not vary by more than 8% (\pm S.D.).)

cell, which if assembled end-to-end, could in theory form a protofilament encircling the cell's circumference ~20 times.

We combined our measurements of chloroplast FtsZ levels with morphometric measurements to compare FtsZ levels in chloroplasts isolated from 3-week-old *Arabidopsis* plants with those in *E. coli* (Table 2.2). The average circumference of the short axis of these chloroplasts at midpoint, measured from 3-D image stacks, was $19.1 \pm 2.3 \mu\text{m}$. Assuming FtsZ monomer dimensions equivalent to those of bacterial FtsZ, 4-4.5 nm long and ~5 nm wide (Gonzalez et al. 2003; Löwe 1998; Lu et al. 2000; Romberg et al. 2001), the average ~101,200 total molecules of FtsZ in chloroplasts of 3-week-old plants (Table 2.1) could theoretically encircle the plastid division site ~21-23 times, close to the estimate of 20 times calculated for *E. coli* FtsZ (Lu et al. 2000). Although only 30% of the total FtsZ in *E. coli* is in the Z-ring (Stricker et al. 2002) and the *in vivo* molecular structures of the bacterial and chloroplast Z-rings are not yet known, these calculations suggest that FtsZ levels and overall ring structure in the cell and organelle are comparable with respect to their sizes and the dimensions of their division sites.

We estimated the average FtsZ concentration in chloroplasts of 3-week-old plants. Confocal microscopy indicated that the average volume of chloroplasts isolated from these plants was $131 \pm 55 \mu\text{m}^3$. If the stroma, in which FtsZ1 and FtsZ2 are localized (McAndrew et al. 2001), occupied the entire chloroplast volume, then the average total FtsZ concentration would be ~1.28 μM . Because the thylakoids occupy a considerable proportion of the chloroplast volume (Musser and Theg 2000),

Table 2.2: Comparison of FtsZ levels in actively dividing *E. coli* cells with those in chloroplasts of 3-week-old Arabidopsis.

Species	Cell/Organelle circumference ^b (μm)	Total FtsZ (molecules)	Polymer length ^d (μm)	Division site encircled ^e (# times)	Reference
<i>E. coli</i> (log phase cells) ^a	3.03	15,000	64	~20	(Lu et al. 1998)
<i>A. thaliana</i> (chloroplasts) ^a	21.23	101,200	435	~21	This work

^a The majority of chloroplasts in 3-week-old seedlings or log phase *E. coli* cells are actively dividing.

^b Circumference was calculated as $2\pi r$, for an *E. coli* cell with ~0.48 μm radius or *A. thaliana* chloroplast with a ~3.37 μm radius, respectively.

^c The length of FtsZ polymers was calculated as the total molecules of FtsZ multiplied by FtsZ monomer length, ~4.3 nm (Gonzalez et al. 2003; Romberg et al. 2001).

^d The number of times FtsZ polymers theoretically encircle the division site was calculated by dividing polymer length (μm) (end-to-end assembly) by cell or organelle circumference (μm).

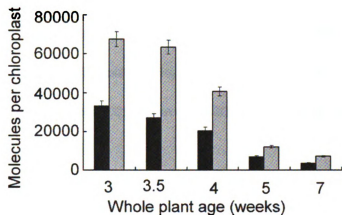


Figure 2.5: Quantitative analysis of molecular levels of FtsZ1 and FtsZ2 in wild-type Arabidopsis

Total FtsZ1 (black bars) and FtsZ2 (gray bars) in Arabidopsis chloroplasts were determined for plants of different ages. Total molecular levels of FtsZ were 101,200 (± 5050), 92,930 (± 4650), 57,310 (± 2860), 18,690 (± 940), and 10,720 (± 540) in chloroplasts of 3-, 3.5-, 4-, 5-, and 7-week-old plants, respectively. Error bars are \pm S.D.

this value represents a minimum concentration; if the stroma represents 50% of the total volume, as has been reported, the concentration would be twice this, or 2.56 μM . These values are within the range of concentrations required for both cooperative assembly (0.3-3 μM) and full GTPase activity (0.5-2 μM) of *E. coli* FtsZ *in vitro* (Anderson et al. 2004; Caplan and Erickson 2003; Chen et al. 2005; Redick et al. 2005; Rueda et al. 2003).

AtFtsZ proteins are stably associated following import into pea chloroplasts

FtsZ1 and FtsZ2 tightly co-localize to rings *in vivo* (McAndrew et al. 2001; Vitha et al. 2003) and recombinant and GFP-fused forms of FtsZ1 and FtsZ2 interact in yeast and transgenic plants (Maple et al. 2005). To begin investigating *in vivo* interactions between FtsZ1 and FtsZ2, we performed a series of immunoprecipitation assays on radiolabeled precursor (p) AtFtsZ1-1, AtFtsZ2-1, and AtFtsZ2-2 proteins generated by *in vitro* translation in the presence of [³⁵S]-Met that were subsequently imported into isolated pea chloroplasts to yield processed, mature (m) import products (McAndrew et al. 2001). Following import, chloroplasts were treated with protease to remove unimported precursors and reisolated. Radiolabeled precursor and imported mature proteins were detected by SDS-PAGE and autoradiography (shown for p-AtFtsZ1-1 and m-AtFtsZ1-1 in Figure 2.6A).

For immunoprecipitation experiments, 1-1, 2-1, and 2-2 antibodies coupled to agarose beads were incubated with either radiolabeled mature proteins present in post-

import chloroplast lysates or radiolabeled precursor proteins. Analysis of bound (B) and unbound (U) fractions showed that all radiolabeled AtFtsZ proteins, both precursor (Fig 4B, lanes 1, 2, 7 and 9 and not shown) and mature (Fig 4B, lanes 3, 8, 10 and not shown) forms, were immunoprecipitated by their corresponding antibodies. Due to the complexity of the experiments, only a subset of the results is shown in Figure 2.6. In control assays, radiolabeled, imported RuBisCO small subunit (SSU) was not precipitated by any of the AtFtsZ antibodies (shown for 1-1 antibodies in Figure 2.6B, lanes 5 and 6), and neither agarose beads alone (not shown) nor pre-immune IgG coupled to agarose beads (PI) pulled down any of the radiolabeled AtFtsZ proteins (shown for m-AtFtsZ2-2 incubated with PI in lane 12).

To investigate FtsZ interactions, radiolabeled AtFtsZ precursors were first incubated with pea chloroplasts in combinations of two: AtFtsZ1-1 and AtFtsZ2-2, AtFtsZ2-1 and AtFtsZ2-2, or AtFtsZ1-1 and AtFtsZ2-1. In all cases, co-import of both proteins was observed (Figure 2.6C, lanes 1-3, respectively). Following import and recovery of intact chloroplasts, equal amounts (μCi) of radiolabeled mature proteins in chloroplast lysates were incubated with FtsZ-specific antibodies and analyzed as above. The results indicated that any two coimported AtFtsZ proteins (Figure 2.6C, lanes 1-3) were coprecipitated ($\sim 10\text{--}20\%$ yield) by antibodies specific for either protein (Figure 2.6C, lanes 4-9). In contrast, when two precursor proteins were incubated together with any of the FtsZ antibodies, only the radiolabeled protein recognized by the antibody was precipitated ($\sim 5\%$ yield) (not shown). In experiments in which all three AtFtsZ proteins were coimported, all three mature proteins could be coprecipitated by any one FtsZ-

specific antibody (~12-30% yield) indicating their interaction in a stable complex (Figure 2.6D). Moreover, coimported AtFtsZ2-1 and AtFtsZ2-2 (Figure 2.6E), as well as singly imported AtFtsZ2-1 (not shown), could be pulled down by the FtsZ1 antibody. These results show that the imported Arabidopsis FtsZ2 proteins associate with the endogenous pea FtsZ1 *in organello*.

FtsZ1 and FtsZ2 are in a stable complex in vivo

Ultracentrifugation experiments were used to examine whether FtsZ1 and FtsZ2 are in a complex *in vivo* as suggested by the coimport/coimmunoprecipitation experiments. Chloroplasts from 7-9 day-old pea leaves were lysed in the presence of DDM to partially solubilize the membranes and the soluble protein fraction was sedimented through a 5-20% sucrose gradient. Gradient fractions were analyzed by immunoblotting. Replicate experiments showed that FtsZ1 and FtsZ2 primarily cosedimented in the upper region of the gradient in a mass range between ~215-240 kDa (Figure 2.7A). The association between FtsZ1 and FtsZ2 was further examined by pooling the peak FtsZ-containing density gradients fractions and subjecting them to anion exchange chromatography, where both proteins co-eluted at ~300-400 mM NaCl (Figure 2.7B). The DDM-solubilized chloroplast proteins were also separated by size exclusion chromatography and the fractions examined by immunoblotting (Fig 5C). Consistent with the sedimentation analyses, both FtsZ1 and FtsZ2 co-eluted in fractions corresponding to a mass range of 213-243 kDa.

Figure 2.6: Panels A and B, Immunoprecipitation of *in vitro* [³⁵S]-labeled AtFtsZ translation and import products by FtsZ-specific antibodies

AtFtsZ1-1, *AtFtsZ2-1* and *AtFtsZ2-2* cDNAs were translated *in vitro* with [³⁵S]-Met to produce precursor proteins and imported into isolated pea chloroplasts to yield processed, mature proteins. Following import, chloroplasts were treated with thermolysin and reisolated. Immunoprecipitation reactions, carried out using 1-1, 2-1, 2-2 or preimmune (PI) antibodies coupled to agarose beads, were performed directly on the *in vitro* translation mixture for precursor proteins (p-1-1, p-2-1, p-2-2, precursor *AtFtsZ1-1*, *AtFtsZ2-1* and *AtFtsZ2-2*, respectively) and on soluble chloroplast fractions for mature proteins (m-1-1, m-2-1, m-2-2, mature *AtFtsZ1-1*, *AtFtsZ2-1* and *AtFtsZ2-2*, respectively). Translation, import and immunoprecipitation products were detected by SDS-PAGE and autoradiography. (A) p-*AtFtsZ1-1* (lane 1) and m-*AtFtsZ1-1* (lane 2). (B) Precursor (lanes 1-2, 7, 9) or individually imported (lanes 3-6, 8, 10-12) proteins were immunoprecipitated with the antibodies shown above panel and proteins either bound (B) or unbound (U) to the antibody beads are shown. All precursor and mature proteins were specifically bound by their corresponding antibodies, which did not recognize SSU. *AtFtsZ2-1* is a doublet as previously reported (Vitha et al. 2003). In a control experiment, imported SSU was detected only in the unbound fraction after immunoprecipitation with 1-1-antibodies (lanes 5-6).

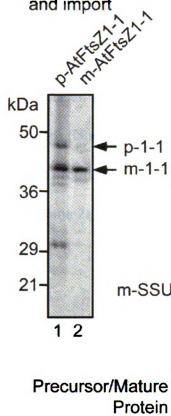
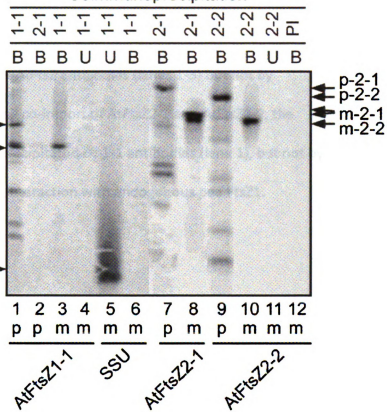
AIn vitro translation
and import**B**Antibody used for
Coimmunoprecipitation

Figure 2.6 (Continued):

(C) Pairs of the precursor AtFtsZ proteins were co-imported into pea chloroplasts and the mature proteins (left panel in C) immunoprecipitated with the FtsZ antibodies indicated. (D) All three AtFtsZ proteins were co-imported into chloroplasts and immunoprecipitated with the different AtFtsZ antibodies (lanes 1-3) but not by uncoupled beads (lane 4). (E) Following co-import of AtFtsZ2-1 and AtFtsZ2-2, the mature import products could be co-precipitated by 1-1 antibodies (lane 1), but not by PI antibodies (lane 2), indicating their interaction with endogenous pea FtsZ1.

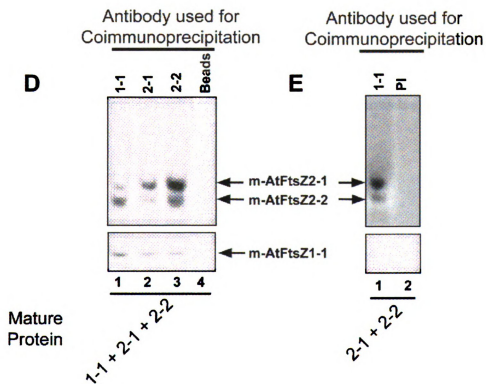
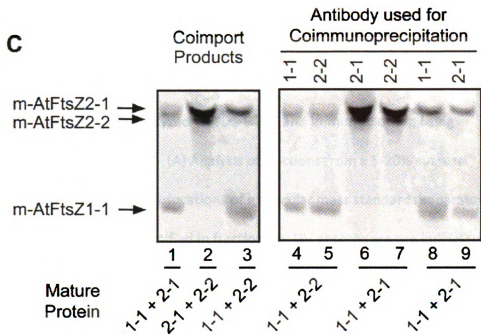
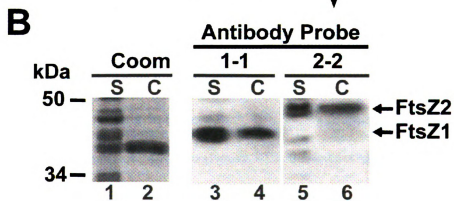
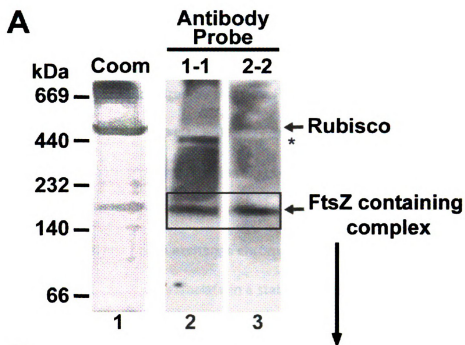


Figure 2.7: FtsZ1 and FtsZ2 cofractionate in isolated pea chloroplasts

Isolated intact pea chloroplasts were lysed hypotonically in the presence of DDM and soluble proteins were fractionated as indicated. Proteins in the fractions shown were acetone-precipitated and analyzed by SDS-PAGE and immunoblotting using AtFtsZ1-1 and AtFtsZ2-1 antibodies. (A) Analysis of fractions from a 5-20% sucrose density gradient. Approximate peak locations of molecular mass standards separated in a parallel sucrose gradient and identified in fractions by UV absorbance are indicated. FtsZ1 and FtsZ2 cosedimented in a mass range of ~215-240 kDa. (B) The peak FtsZ-containing fractions (5-8) from panel A were pooled and subjected to anion-exchange chromatography using a 0-1 M NaCl elution gradient. FtsZ1 and FtsZ2 coeluted in 300-400 mM NaCl. (C) Soluble proteins from chloroplasts lysed in the presence of DDM were fractionated by gel filtration chromatography. Immunoblots of the subset of fractions (0.2 ml) near the FtsZ complex peak are shown. The standard curve is shown in Figure 2.1.

Figure 2.8: 2-D native SDS-PAGE separation of an endogenous protein complex from pea chloroplasts containing FtsZ1 and FtsZ2

(A) Isolated intact pea chloroplasts were lysed hypotonically in the presence of DDM and soluble proteins were separated by native PAGE through a 4-20% gradient gel. Replicate samples loaded onto the same gel were Coomassie-stained (lane 1) or analyzed by immunoblotting with AtFtsZ1-1 (lane 2) and AtFtsZ2-2 (lane 3) antibodies. Relative to the molecular mass markers (left), the native RuBisCO complex (550 kDa, right) migrated at an apparent mass of ~470 kDa and a complex containing only FtsZ1 migrates just below this mass (indicated by *). A putative complex containing pea FtsZ1 and FtsZ2 (boxed) migrated at an apparent mass of ~200 kDa. (B) The putative FtsZ1- and FtsZ2-containing complex (C) was excised from the Coomassie-stained native gel shown in panel A and separated by SDS-PAGE in the second dimension. Pea chloroplast stromal proteins (S) were loaded in adjacent lanes as controls. Replicate samples loaded onto the same gel were Coomassie-stained (lanes 1 and 2) or analyzed by immunoblotting with AtFtsZ1-1 (lanes 3 and 4) or AtFtsZ2-2 (lanes 5 and 6) antibodies. Migration of molecular mass markers and FtsZ proteins are indicated on the left and right, respectively.



In a separate approach, protein complexes from intact pea chloroplasts were separated by native-PAGE using 4-12% gradient gels (Figure 2.8A, lane 1). A distinct band that resolved at ~200 kDa was recognized by both the FtsZ1 and FtsZ2 antibodies (Figure 2.8A, lanes 2-3). Notably, the 550 kDa RuBisCO complex [57] migrated with an apparent mass of ~470 kDa, indicating the mass of the FtsZ1- and FtsZ2-containing complex was probably underestimated by this method. Based on the results of native PAGE, density gradient centrifugation and anion exchange chromatography, we conclude that endogenous pea FtsZ1 and FtsZ2 associate in a stable, discrete complex *in vivo* with a mass between ~200 and 245 kDa.

The native immunoblots also showed smearing of the FtsZ1 and FtsZ2 signals, suggesting the presence of larger FtsZ-containing complexes or assembled protofilaments of various lengths (Figure 2.8A, lane 2). In addition, FtsZ1 was detected in a well-resolved complex of ~440 kDa (Figure 2.8A, asterisk) that did not contain detectable FtsZ2; however a similarly sized complex was not evident in the pea density gradient or size-exclusion chromatography fractions (Figure 2.7A, 5C). The composition of this FtsZ1-containing complex was not further investigated in this study.

In a bid to identify other proteins associated with the FtsZ1- and FtsZ2-containing complex, the ~200 kDa band resolved by native PAGE was excised from the native gel and analyzed by SDS-PAGE (Figure 2.8B). While FtsZ1 and FtsZ2 were readily detectable

by immunoblotting, neither was stained by Coomassie, precluding visual detection of other proteins potentially associated with the complex.

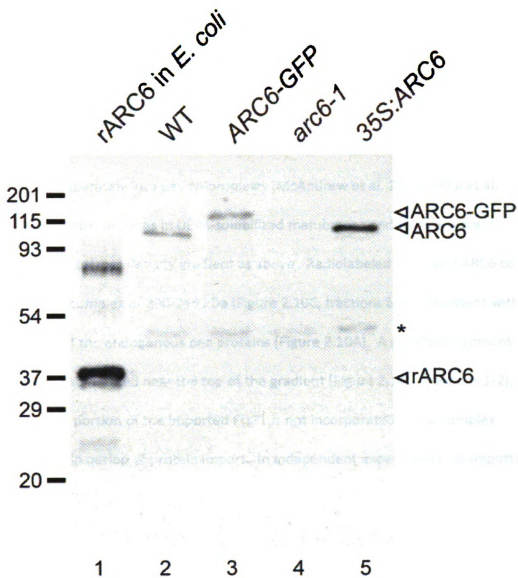
The native FtsZ complex also contains ARC6 and ARC3

Interaction assays have shown that FtsZ1 and FtsZ2 interact with the chloroplast division proteins ARC3 and ARC6, respectively (Maple et al. 2005; Maple et al. 2007). To ask whether FtsZ, ARC6 and/or ARC3 can be detected in an endogenous complex, DDM-solubilized chloroplast proteins from 7-10 day-old pea plants were fractionated on sucrose density gradients and analyzed by immunoblotting using antibodies against Arabidopsis ARC6 (Figure 2.9) and ARC3 (Shimada et al. 2004). The anti-ARC6 antibodies detected two cross-reactive pea proteins of ~100 kDa, similar to the mass of ARC6 (Vitha et al. 2003). The doublet could be indicative of posttranslational modification. A significant portion of the smaller protein sedimented at the bottom of the gradient, suggesting it is membrane-associated (Figure 2.10A, fraction M), as is ARC6 (McAndrew et al. 2001; Vitha et al. 2003). Within the gradient, this protein co-sedimented with the peak FtsZ1- and FtsZ2-containing fractions at ~215-240 kDa (Figure 2.10A, fractions 5-8).

In a separate experiment, immunoblots of density gradient fractions were probed with antibodies against FtsZ1, FtsZ2, ARC6 and ARC3. As in Figure 2.10A, FtsZ1, FtsZ2 and the putative pea ARC6 co-sedimented at 215-240 kDa (not shown).

Figure 2.9: Specificity of ARC6 Antibody

Immunoblot analysis shows immunoreactivity of anti-ARC6 with the recombinant ARC6 immunogen (rARC6, lane 1) and proteins (1 mg fresh tissue/lane) from WT Arabidopsis plants (WT, lane 2), transgenic plants carrying ARC6-GFP (lanes 3) the *arc6-1* mutant (lane 4), and overexpressed *35S:ARC6* (lane 5). Approximate molecular masses are indicated at the left.

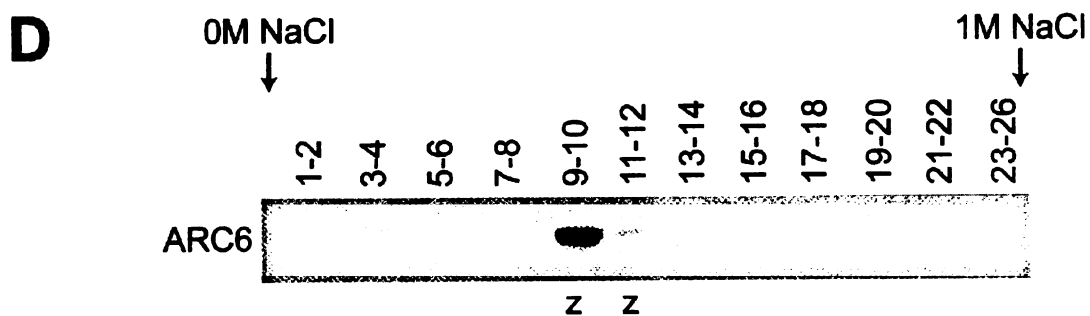


The ARC3 antibody detected two closely migrating proteins of ~75 kDa, presumably pea ARC3, that cosedimented with FtsZ1 and FtsZ2 (Figure 2.10B). These results suggest that the stable FtsZ1- and FtsZ2-containing complex also contains ARC6 and ARC3. To confirm co-sedimentation of FtsZ and ARC6, Arabidopsis [³⁵S]-AtFtsZ1 and [³⁵S]-ARC6 were imported separately into pea chloroplasts (McAndrew et al. 2001; Vitha et al. 2003). Subsequently, proteins in DDM-solubilized membranes and stroma were fractionated on a sucrose density gradient as above. Radiolabeled FtsZ1 and ARC6 cofractionated in a complex of 200-245 kDa (Figure 2.10C, fractions 5-8), consistent with cofractionation of the endogenous pea proteins (Figure 2.10A). A significant amount of imported FtsZ1 sedimented near the top of the gradient (Figure 2.10C, fractions 1-2), suggesting that a portion of the imported FtsZ1 is not incorporated into a complex during the ~30 min period of protein import. In independent experiments, co-imported ARC6, FtsZ1 and FtsZ2 could be co-immunoprecipitated from post-import chloroplast lysates with FtsZ1 or FtsZ2 antibodies (R. M. McAndrew, J. E. Froehlich and K. W. Osteryoung, unpublished).

To investigate the stability of protein associations in the native pea complex, sucrose density gradient fractions containing FtsZ1, FtsZ2 and ARC6 (Figure 2.7A and 2.10A, fractions 5-8) were separated by anion-exchange chromatography (Figure 2.7B and 2.10D) and fractions analyzed by immunoblotting with ARC6 antibodies. The peak FtsZ-containing fractions (Figure 2.10D, indicated by “z”, equivalent to fractions 9-12 in Figure 2.7B) were also found to contain the ~100 kDa ARC6 protein.

Figure 2.10: ARC6 and ARC3 are associated with a protein complex containing FtsZ1 and FtsZ2 in both pea and Arabidopsis

(A) The pea stromal sucrose density gradient fractions shown in Figure 2.7 were also subjected to immunoblotting for ARC6. Proteins from fractions containing FtsZ1 and FtsZ2 (Figure 2.6) are shown in lanes labeled below with "Z". Although ARC6 co-fractionates with FtsZ, a significant amount of ARC6 was found in the membrane fraction "M". (B) Fractions from separate sucrose density gradient were examined by immunoblot for FtsZ1, FtsZ2 (Vitha et al. 2001) ARC6 and ARC3 (Shimada et al. 2004). The lanes indicated with a "Z" co-fractionated with FtsZ1, FtsZ2 and ARC6 (not shown) and the MW of these fractions is 200-245 kDa. (C) Anion-exchange chromatography fractions depicted in Figure 2.6C were also analyzed by immunoblotting with anti-ARC6 and found to co-fractionate with FtsZ (marked with a "Z"). (D) Autoradiogram of [³⁵S]-AtFtsZ1-1 and [³⁵S]-ARC6 imported into pea chloroplasts, DDM lysed and soluble proteins separated on a sucrose density gradient. The peak containing AtFtsZ1-1 and ARC6 in fractions 5-6 has a mass of 210-240 kDa.



This demonstrates not only that FtsZ1, FtsZ2 and ARC6 are associated in a complex, but also that this complex is stable at high ionic strength, suggesting tight and specific interactions within the complex.

Discussion

FtsZ1 and *FtsZ2* arose by duplication and divergence of an ancestral *FtsZ* of cyanobacterial origin (McAndrew et al. 2001; Osteryoung et al. 1998; Rensing et al. 2004; Stokes and Osteryoung 2003; Vaughan et al. 2004). The functional significance of this divergence is not fully understood, but recent findings showing that FtsZ2 interacts specifically with ARC6 (Maple et al. 2005) and FtsZ1 with ARC3 (Maple et al. 2007) suggest the acquisition of distinct binding activities for FtsZ1 and FtsZ2. However, the interaction assays performed to date have been carried out in yeast and transgenic plants overexpressing FtsZ1 or FtsZ2. In the work described here, we have begun to investigate the composition of an endogenous FtsZ-containing complex as well as FtsZ1 and FtsZ2 levels in WT plants. Such studies are critical for extrapolating the results of other types of experiments to the *in vivo* system.

We have shown previously that suppression and overexpression of *AtFtsZ1-1* or *AtFtsZ2-1* in *Arabidopsis* perturb Z-ring morphology and cause dose-dependent defects in chloroplast division (Osteryoung et al. 1998; Stokes et al. 2000; Vitha et al. 2001). These results suggest that the stoichiometry between FtsZ1 and FtsZ2 could be an important aspect of their activity *in vivo*. Consistent with this possibility, we have found in the present study that, although individual and total FtsZ levels in *Arabidopsis* leaves

decline as plants mature between 3 and 7 weeks, their relative contributions to the average FtsZ pool remain similar: AtFtsZ1-1 constitutes ~30% of the total FtsZ pool while AtFtsZ2-1 and AtFtsZ2-2 together constitute ~70% (Table 2.1). This translates into a molar ratio of about 1:2 between FtsZ1 and FtsZ2. The high amino acid identity between the AtFtsZ2-1 and AtFtsZ2-2 (~81% for the full-length proteins and ~85% for the predicted mature forms), along with our finding that *AtFtsZ2-2*, like *AtFtsZ2-1* (Vitha et al. 2001), encodes a functional, ring-forming chloroplast division protein (Figure 2.3), suggest that AtFtsZ2-1 and AtFtsZ2-2 have biochemically equivalent functions within the FtsZ2 pool. We hypothesize that the relatively mild phenotype of the *atftsZ2-2* knockout mutant (Figure 2.3D) reflects the loss of only about 30% of the total FtsZ2 in this mutant. The significance of 1:2 ratio between FtsZ1 and FtsZ2 is not yet clear, however. Recent studies show that, *in vitro*, recombinant FtsZ1 is capable of assembling into polymers and filaments independently of FtsZ2 (El-Kafafi et al. 2005; Lohse et al. 2006), and vice versa (Olson and Osteryoung 2007). In addition, we have found that FtsZ2 can be detected in mid-plastid rings in an *atftsZ1-1* null mutant, though only in the tiny proplastids of meristematic tissue and not in differentiated chloroplasts (Yoder et al. 2007). Together, these results indicate that the 1:2 ratio in Arabidopsis does not reflect a stoichiometric requirement for FtsZ polymerization *per se*. More likely, a balance between FtsZ1 and FtsZ2, and/or a balance between these proteins and other plastid division factors, may be critical for proper regulation of Z-ring morphology, position and dynamics *in vivo*. Our finding that FtsZ1 and FtsZ2 can complex with ARC3 and ARC6 *in vivo* is consistent with this idea.

FtsZ levels have been rigorously quantified only in *E. coli* (Lu et al. 1998). The high degree of sequence conservation between chloroplastic and prokaryotic FtsZs (Stokes and Osteryoung 2003; Vaughan et al. 2004) strongly suggests structural and mechanistic conservation as well. Consistent with this expectation, our measurements indicate that the average FtsZ concentration in chloroplasts of three-week-old plants, in which leaves are still actively expanding and chloroplasts actively dividing (Pyke and Leech 1994; Pyke et al. 1991), is similar to that in the cytoplasm of log-phase *E. coli* cells (Lu et al. 1998). Somewhat surprising was our hypothetical calculation (Table 2.1) suggesting that the average number of FtsZ molecules in chloroplasts at this stage of development is comparable to the amount of FtsZ present in dividing *E. coli* cells with respect to the average dimensions of their division sites. This may be coincidental; we only measured the mid-plastid circumference in mesophyll cells of three-week-old plants, and molecular levels of FtsZ relative to the dimension of the chloroplast division site could be different in other cell types and at other stages of development. Nevertheless, the potential similarity between chloroplasts and *E. coli* in this regard is intriguing and worthy of further comparison.

We have found that FtsZ1, FtsZ2, ARC6 and ARC3 associate in a native complex in pea and Arabidopsis. The isolated complex is robust—it remains intact during several size fractionation procedures as well as during anion exchange chromatography (Figure 2.10), and ARC3 also remains associated during anion exchange chromatography (not shown). The estimated mass of the complex, between ~200 and 245 kDa, is consistent with the calculated molecular masses of the mature forms (i.e., lacking chloroplast

transit peptides) of FtsZ1, FtsZ2, ARC3 and ARC6, which in Arabidopsis are 39, 45, 75 and 81 kDa, respectively (though ARC6 often migrates at ~100 kDa in SDS gels; Supplementary Figure 2.5). A complex containing these proteins in a 1:1:1:1 stoichiometry would be ~240 kDa. Based on yeast-two-hybrid, *in vivo* FRET, and bimolecular fluorescence complementation assays reported by Maple et al. (Maple et al. 2005; Maple et al. 2007), we would predict direct interactions within the native complex between ARC6 and FtsZ2, FtsZ2 and FtsZ1, and FtsZ1 and ARC3. Other compositions and stoichiometries are also possible; for example, complexes containing subsets of these proteins in different stoichiometries could co-elute at similar molecular weights, though the co-elution of the four proteins during anion exchange chromatography (Figure 2.7B, 2.10C) suggests their association in a single stable complex. Further analysis of the composition, stoichiometry and protein-protein interactions within the ~200-245 kDa complex will be important for fully defining its structure and functional role in chloroplast division.

The bacterial Z-ring is proposed to consist of short, overlapping FtsZ protofilaments bundled at the cell membrane (Margolin 2005b; Stricker et al. 2002). Protofilaments within the ring are rapidly remodeled by exchange of subunits with a cytoplasmic FtsZ pool, allowing the ring to be dynamic (Anderson et al. 2004; Chen et al. 2005; Stricker et al. 2002). Preliminary evidence suggests that chloroplast Z-rings and filaments exhibit similar dynamics (Vitha et al. 2005). However, the presence in the FtsZ1- and FtsZ2-containing complex of ARC6, an inner envelope membrane (IEM) protein (Vitha et al. 2003), as well as the stability and relatively small mass of the

complex (Figure 2.10A), implies that it represents an IEM-associated FtsZ pool that is not polymerized or readily exchangeable. Further, the mid-plastid localization of ARC6, FtsZ1, FtsZ2 and at least a portion of the ARC3 (Maple et al. 2007; Shimada et al. 2004; Vitha et al. 2003; Vitha et al. 2001) suggests that the complex may be associated with the plastid division site *in vivo*. The complex contains only a fraction of the FtsZ in the chloroplast, however, and multiple pools of FtsZ presumably exist in the chloroplast, as indicated by the “smearing” of the FtsZ1 and FtsZ2 signals on native immunoblots (Figure 2.8), broad sedimentation patterns in density gradients (Figure 2.7A), and detection of the ~440 kDa FtsZ1-containing complex (Figs. 5C, 6A). It is conceivable that the latter represents a pool of FtsZ1 recently reported to be associated with thylakoid membranes in Arabidopsis (El-Kafafi et al. 2008). Although the distribution of FtsZ1 and FtsZ2 between the stromal and membrane fractions of the chloroplast has been variously reported in the literature, perhaps due to differences developmental stage, growth conditions, or isolation procedures (El-Kafafi et al. 2005; El-Kafafi et al. 2008; Glynn et al. 2007; McAndrew et al. 2001), the data consistently suggest that a significant fraction of the chloroplast FtsZ is soluble. If, as proposed in bacteria, the chloroplast Z-ring is composed of rapidly remodeled protofilaments, then it seems likely that the bulk of the FtsZ in the ring and the exchangeable fraction would be soluble.

What might the function of the FtsZ1/FtsZ2/ARC6/ARC3-containing complex be?

In bacteria, Z-ring dynamics are regulated by the balanced activity of several Z-ring assembly and disassembly factors (Margolin 2005b). In chloroplasts, ARC6 has been shown to promote and stabilize chloroplast FtsZ filament formation *in vivo*, suggesting it

is an assembly factor (Vitha et al. 2003), and ARC3 has been postulated to have an activity related to that of MinC, which inhibits FtsZ polymer assembly in bacteria (Glynn et al. 2007; Hu et al. 1999; Maple et al. 2007). We speculate that the complex plays a role in regulating FtsZ polymer assembly and remodeling adjacent to the IEM. ARC6 and ARC3 could antagonistically regulate polymer formation at the division site, facilitating Z-ring dynamics. The complex could also comprise a nucleation or other pre-assembly complex, perhaps resembling the role of microtubule organizing centers in regulating microtubule dynamics (Raynaud-Messina and Merdes 2007). Further analysis of the complex will yield a clearer picture of its functional significance.

Supplementary Results

Preparation of Quantitative Immunoblotting Standards

To establish a baseline for investigating the stoichiometric relationship between FtsZ1 and FtsZ2, we carried out quantitative immunoblotting to determine their molecular levels in chloroplasts of Arabidopsis. Standard curves (Figure 2.1A) were constructed from immunoblots of purified FtsZ recombinant proteins (Supplementary Figure 2.2) resolved by SDS-PAGE and probed with the corresponding FtsZ-specific primary antibody and ¹²⁵I-labeled secondary antibodies. Comparable to the linear range of standards used to quantify *E. coli* FtsZ (Lu et al. 1998), the linear ranges of detection for the recombinant Arabidopsis FtsZ standards were 10-83.5 ng/lane for AtFtsZ1-1, 10-65 ng/lane for AtFtsZ2-1, and 10-62.5 ng/lane for AtFtsZ2-2 (Figure 2.1A). To establish a reliable range for measuring FtsZ proteins in chloroplasts, we took advantage of the fact

that the amount of chlorophyll in chloroplast suspensions was directly proportional to the number of chloroplasts, and therefore, to the amount of FtsZ protein per chloroplast. Chloroplast lysates of determined chlorophyll content were analyzed by immunoblotting with ¹²⁵I-labeled secondary antibodies, and the amount of each AtFtsZ protein was extrapolated from the standard curves (Figure 2.1A). AtFtsZ protein levels exhibited a linear correlation with chlorophyll content in samples containing ~7-15 µg chlorophyll (Figure 2.1B).

Specificity of the ARC6 Antibody

Following affinity purification, the ARC6 antibodies recognized a protein migrating at ~100 kDa in leaf extracts from WT Arabidopsis plants and plants overexpressing ARC6 from the 35S promoter (Figure 2.1, lanes 2 and 4). Although this is higher than the mass of ~81 kDa predicted for ARC6 lacking its predicted transit peptide (amino acids 1-67), import of Arabidopsis [³⁵S]-ARC6 into pea chloroplasts also produces an import product of ~100 kDa, suggesting ARC6 migrates aberrantly during SDS-PAGE separation (Vitha et al. 2003). In plants expressing an ARC6-GFP fusion protein, the antibodies also reacted with a slightly larger protein (Figure 2.1, lane 3) that was also detected by an anti-GFP antibody (not shown). In contrast, the antibodies demonstrated no immunoreactivity to a protein corresponding to ARC6 in the *arc6-1* mutant (Figure 2.1, lane 4), in which a premature stop-codon severely truncates the *ARC6* gene product (Vitha et al. 2003). These results demonstrate that the anti-ARC6

antibodies specifically recognize ARC6 in Arabidopsis. They also indicate that *arc6-1* is a null allele of *ARC6*.

Acknowledgments

We thank Harold P. Erickson for *E. coli ftsZ* expression plasmids and antibodies specific for bacterial FtsZ, Piet de Boer for the plasmids used to construct expression vectors for recombinant AtFtsZ proteins, Kathy Schegg for synthesis of peptides, Hiroshi Shimada for providing the ARC3 antibody, the Salk Institute Genomic Analysis Laboratory for providing the sequence-indexed Arabidopsis T-DNA insertion mutants, Jonathan Glynn for producing the ARC6 antibody, and Aaron Schmitz, Jonathan Glynn and Yue Yang for helpful comments on the manuscript. This work was supported by grants from the National Science Foundation to K.W.O and by Michigan State University N. E. Tolbert and Plant Sciences Fellowships to B.J.S.C.O.

CHAPTER THREE

PLANT FTSZ1 AND FTSZ2 ARE GTPASES AND ASSEMBLE INTO HETEROFILAMENTS THAT BUNDLE INTO RIBBONS

Bradley J. S. C. Olson and Katherine W. Osteryoung

This work is being submitted for publication

B. J. S. C. Olson performed all the experiments and wrote in consultation with Katherine
W. Osteryoung

Introduction

Chloroplasts are endosymbiotically derived from cyanobacteria and the chloroplast division machinery is derived from the cyanobacterial endosymbiont. FtsZ is essential for proper bacterial cell division and is one of the earliest markers of the bacterial cell division site. Owing to the endosymbiotic origin of chloroplasts, FtsZ is also required for proper chloroplast division (McAndrew et al. 2008; Osteryoung and McAndrew 2001; Osteryoung and Pyke 1998; Osteryoung et al. 1998; Osteryoung and Vierling 1995; Stokes et al. 2000; Yoder et al. 2007). Bacteria typically have one type of FtsZ, but plants have two families of nuclear-encoded, plastid-targeted homologues of bacterial FtsZ, named FtsZ1 and FtsZ2 (Osteryoung et al. 1998; Osteryoung and Vierling 1995). Moreover, the evolution of FtsZ1, lacking a conserved bacterial C-terminal domain, has been speculated to be important for the establishment of endosymbiotic plastids (Miyagishima et al. 2003a).

Loss of FtsZ function in bacteria leads to blocked cell division resulting in filamentous, multinucleate cell. Likewise, loss or mutation of either *Arabidopsis* *FtsZ1* or *FtsZ2* leads to blocked chloroplast division resulting in fewer enlarged chloroplasts in the plant cell (McAndrew et al. 2008; Osteryoung and McAndrew 2001; Osteryoung and Pyke 1998; Osteryoung et al. 1998; Osteryoung and Vierling 1995; Stokes et al. 2000; Yoder et al. 2007). FtsZ2 proteins share a C-terminal motif with bacterial FtsZ, while FtsZ1 proteins are possibly plant-specific (Miyagishima et al. 2003a). FtsZ1 and FtsZ2 are tightly co-localized to rings at mid-plastid adjacent to the chloroplast inner envelope

membrane (Vitha et al. 2001). Immunofluorescence microscopy of plant cells under- or over-expressing either FtsZ1 or FtsZ2 shows disorganized Z-filaments (Vitha et al. 2001) suggesting the stoichiometry between FtsZ1 and FtsZ2 is critical for proper Z-filament formation. However, it is unknown if FtsZ1 and FtsZ2 form homofilaments or heterofilaments when assembled (Osteryoung and McAndrew 2001).

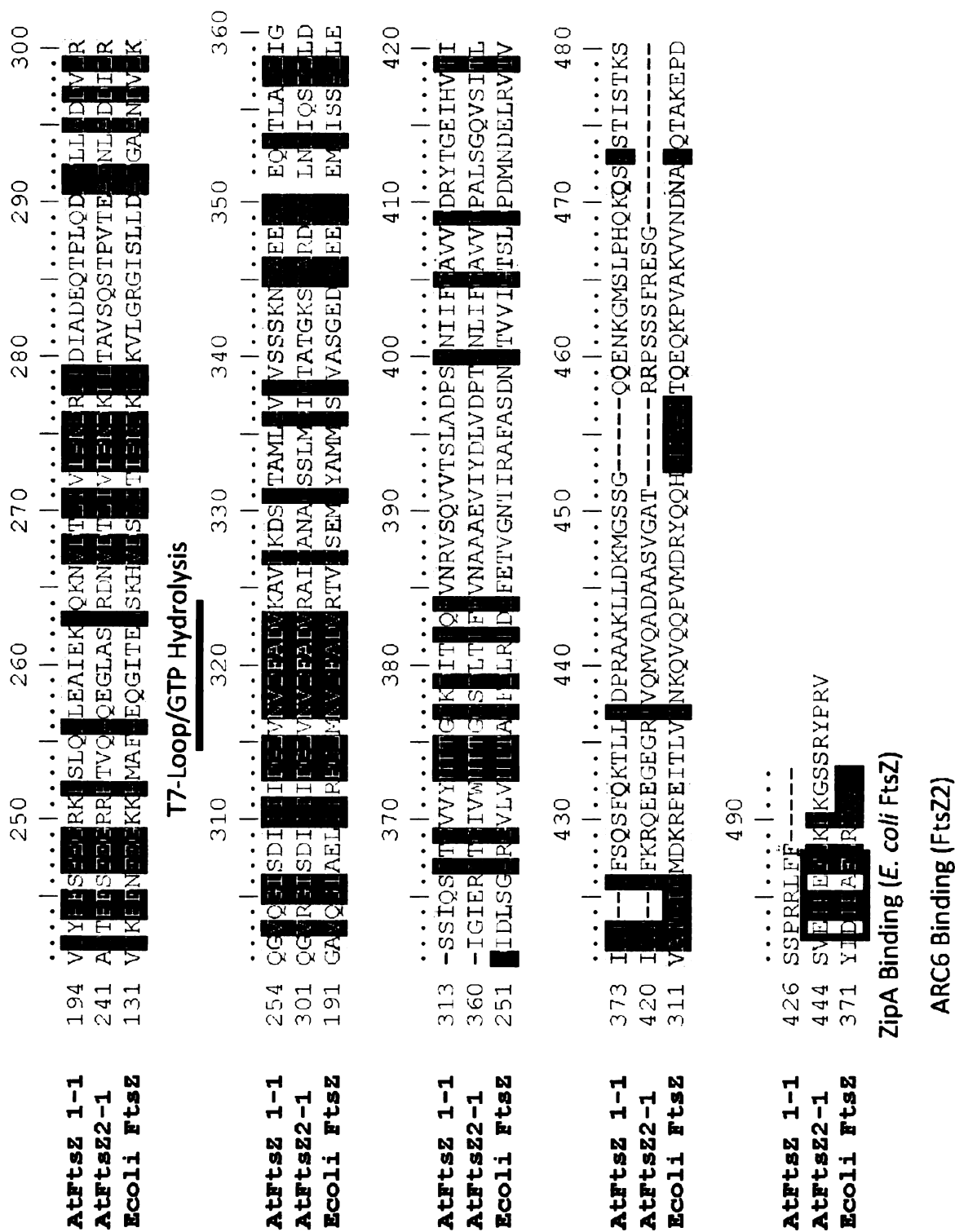
FtsZ1 and FtsZ2 proteins interact *in vivo* in a stable complex with the chloroplast division proteins ARC6 and ARC3 (Maple et al. 2005; McAndrew et al. 2008). FtsZ1 and FtsZ2 are functionally distinguished by differential binding to ARC3 and ARC6, respectively (Maple et al. 2005). ARC3 has been speculated to be important for mid-plastid positioning of the Z-ring (Glynn et al. 2007; Maple et al. 2007) while ARC6 organizes and probably stabilizes Z-filaments at mid-plastid (Vitha et al. 2003). If FtsZ1 and FtsZ2 form heterofilaments, FtsZ1/FtsZ2 co-localized Z-rings could be simultaneously regulated by ARC3 and ARC6 via discrete interactions with FtsZ1 and FtsZ2, respectively.

Bacterial FtsZ and $\alpha\beta$ -tubulin share a common ancestor despite having limited sequence similarity (Erickson 1995, 1997; Nogales et al. 1998a). All FtsZ and tubulin proteins share an N-terminal glycine-rich GTP binding motif that is also conserved in plant FtsZ (Figure 3.1)(Nogales et al. 1998a). The GTPase active site of FtsZ and $\alpha\beta$ -tubulin is completed by the T7-loop of a second FtsZ or tubulin molecule. Thus, two GTP-bound monomers (or two pairs of $\alpha\beta$ -tubulin dimers) are required to complete one GTPase active site.

Figure 3.1: Sequence alignment of AtFtsZ1-1, AtFtsZ2-2 and *E. coli* FtsZ.

The ChloroP predicted transit peptide cleavage sites are indicated by arrows, but the predicted AtFtsZ1-1 cleavage site would remove part of the base recognition motif, so a more probable transit peptide cleavage site was chosen (see text). The N-termini of all proteins contain a non-canonical, glycine-rich, GTP binding motif that in tubulin literature is termed the tubulin-signature motif. All three FtsZ proteins contain all residues in the T7 loop known to be required for GTP hydrolysis; however, the T7 loop of β -tubulin is variant and prevents trans-GTPase hydrolysis in the α -subunit. Plant FtsZ2 and *E. coli* FtsZ share a conserved C-terminal motif and in tubulin these C-terminal extensions have been shown to stick out of the microtubule and are responsible for binding MAPs (microtubule associated proteins). In bacteria, ZipA, which contains a MAP-Tau-like domain, binds this motif, while in plants ARC6 binds this motif in FtsZ2. The function of the FtsZ1 C-terminus is unknown. Note the alignment is split between the N-terminus on page 93 and the C-terminus on page 94.

Figure 3.1 (Continued)



Tubulin differs from bacterial FtsZ because the T7-loop of β -tubulin has an amino acid substitution GxxNxDxxE \rightarrow GxxNxxDxxK which makes the α -subunit incapable of GTP hydrolysis (Nogales et al. 1998a). In addition, lack of GTP hydrolysis by the α -subunit prevents $\alpha\beta$ -tubulin dimers from dissociating, resulting in strict heterodimerization of $\alpha\beta$ -tubulin. Bacterial FtsZ filaments are formed exactly like tubulin, except there is only one type of FtsZ. Because tubulin and FtsZ have *trans* GTP binding sites, the ends of FtsZ and tubulin filaments are biochemically distinct. The plus end of a growing microtubule or FtsZ filament is GTP-capped by the glycine-rich, GTP binding motif. Filament growth occurs when the T7-loop of an incoming subunit completes the active site at the plus end. In contrast, filament growth is kinetically disfavored on the T7-loop-containing minus ends of the filament. Thus, FtsZ and microtubules grow primarily at their plus ends. Due to biochemically distinct ends of FtsZ and tubulin, T7-loop mutations block incoming subunit addition, thus preventing protofilament elongation, but T7-loop mutations do not affect lateral interaction with other protofilaments (Redick et al. 2005; Scheffers et al. 2002). For the purposes of this study, T7 loop mutations will be used to probe the difference between head-to-tail protofilament interaction and lateral stabilization of FtsZ1/FtsZ2 co-polymers.

Bacterial FtsZ assembly is mechanistically similar to tubulin assembly, differing mainly in kinetics of each step in the process. During cytokinesis, a maximum of 35% of monomeric FtsZ is assembled into division rings (Anderson et al. 2004; Stricker et al. 2002). Thus, most unassembled FtsZ is monomeric and GDP-bound. *In vitro*, the

assembly of FtsZ is modeled as follows: GDP-FtsZ exchanges nucleotide resulting in GTP-FtsZ, which dimerizes (Chen et al. 2005; Huecas et al. 2007a; Rivas et al. 2001; Rivas et al. 2000; Romberg et al. 2001). Dimeric GTP-FtsZ cooperatively assembles onto protofilament plus-ends. The incoming T7-loop from dimeric FtsZ (or $\alpha\beta$ -tubulin) completes the active site of the plus-end and GTP hydrolysis begins. GTP hydrolysis is rate-limiting in FtsZ (Romberg and Mitchison 2004) and hydrolysis is not required for assembly (Scheffers et al. 2000). Bacterial FtsZ immediately hydrolyzes GTP upon assembly (Chen and Erickson 2005; Huecas et al. 2007b; Romberg and Mitchison 2004; Scheffers and Driessen 2002), but in tubulin, the GTPase activity lags behind the rate of polymerization (Nogales 1999). In the absence of fresh GTP, FtsZ polymers rapidly hydrolyze GTP and disassemble. FtsZ has a faster GTP hydrolysis rate and FtsZ polymers are less stable than tubulin (Mukherjee and Lutkenhaus 1999). Unlike tubulin, FtsZ is able to maintain its polymerized state by exchanging fresh GTP within the polymer, preventing disassembly. Likewise, polymerized FtsZ (but not tubulin) filaments can be disassembled by addition of GDP which exchanges into polymerized FtsZ (Mingorance et al. 2001). In contrast, tubulin stability is maintained by a slow GTPase activity and the action of many microtubule regulating proteins (Nogales 1999). Tubulin laterally associates into bundled tubes by the lateral interaction primarily between α - and β -subunits (Nogales 1999). FtsZ filament bundling is believed to occur, but lateral association of FtsZ filaments in the absence of stabilizing agents has not been observed *in vitro*. It is unclear how lateral association between FtsZ filaments would affect filament stability and GTP hydrolysis and exchange.

The aims of this study are to determine if both FtsZ1 and FtsZ2 are GTPases and capable of assembly similar to bacterial FtsZ and tubulin, and to distinguish between assembly into homopolymers or heteropolymers. To answer these questions, FtsZ1 and FtsZ2 were produced recombinantly and without their putative chloroplast transit peptides to study their biochemical properties *in vitro*. In the following series of experiments, we report that FtsZ1 and FtsZ2 stably polymerize into heterofilaments that laterally associate into ribbons under dynamic conditions.

Experimental Procedures

Expression and purification of recombinant FtsZ proteins

Previous attempts to characterize the biochemical properties of plant FtsZ (El-Kafafi et al. 2005; Gaikwad et al. 2000) did not remove the chloroplast transit peptides, which interfere with their function. Additionally, FtsZ2 examined by El-Kafafi and colleagues (El-Kafafi et al. 2005) had a C-terminal truncation that removed at least ~25 amino acids conserved with bacterial FtsZ. Moreover, the ChloroP predicted transit peptide of FtsZ1 would remove part of its glycine rich GTP-binding domain (Figure 3.1), so we sought to produce physiologically relevant forms of FtsZ1 and FtsZ2 (design is discussed in the results). FtsZ1 and FtsZ2 were amplified by PCR from cDNA clones of AtFtsZ1-1 (ABRC clone U09686) and full length AtFtsZ2-1 (McAndrew et al. 2001). Note, previous results from our lab with a cDNA for AtFtsZ1-1 (McAndrew et al. 2001; Stokes et al. 2000) (Vitha et al. 2001) contains the mutation S115F in its GTP binding domain, which interferes with its polymerization properties (not shown), but ABRC clone U09686

was sequenced matches the gene sequence annotated in TAIR (<http://www.arabidopsis.org>). FtsZ1 and FtsZ2 were amplified without their transit peptides with the primers 5'-AGTGGTCCATGGCCAGGTCTAAGTCGATGCGATTG-3' and 5'-TGCACCCTCGAGCTAATGATGATGATGATGATGGAAGAAAAGTCTACGGGGA-3' for FtsZ1 and 5'-AGTGGTCCATGGCCGCGCTCAGAAATCTGAATC-3' and 5'-TGCACCCTCGAGTTAATGATGATGATGATGATGGACTCGGGGATAACGAGAGCTG-3' for FtsZ2. These FtsZ1 and FtsZ2 constructs result in the deletion of the putative N-terminal chloroplast transit peptide (57 and 48 amino acids respectively, CTP choice discussed in results) and addition of the amino acids "MA" to complete an NcoI cloning site and insert an ATG start codon for translation. On the C-terminus, a 6X His tag with a stop codon followed by an XhoI site was inserted in the primers. FtsZ1 and FtsZ2 PCR fragments were digested with NcoI and XhoI and the digested fragments were sub-cloned into the NcoI and XhoI sites of the expression vector pDB38 (McAndrew et al. 2008). Note that cloning into the NcoI site removes an HFKT-tag in pDB328. Prior to expression, the constructed gene was confirmed by DNA sequencing. Finally, AtFtsZ2-1 and AtFtsZ2-2 can substitute for one another *in vivo*, indicating they are biochemically redundant (Aaron Schmitz, in preparation); therefore, we used only AtFtsZ2-1 in this study.

For expression of recombinant proteins, FtsZ expression plasmids were transformed into Rosetta(DE3) cells (Novagen) harboring pBS58, which overexpresses the *E. coli ftsQAZ* operon and suppresses filamentation of the cells during expression (Jeong and Lee 2003). Plant FtsZ was optimally expressed as follows: an overnight

culture of cells was grown at 37°C in LB supplemented with 100 µg/ml carbenicillin, 50 µg/ml spectinomycin and 50 µg/ml chloramphenicol and then sub-cultured 1:1000 into fresh LB media containing 50 µg/ml carbenicillin, 25 µg/ml spectinomycin and 12.5 µg/ml chloramphenicol, grown to an OD600 of ~0.6 and expression was induced with 0.5 mM IPTG for 4h at 37°C. Several different temperatures and conditions were tested for expression, but we consistently found that >80% of the protein was found in inclusion bodies. Because protein purified from the soluble fraction typically had contaminating ATPase activity that was difficult to remove by high-salt washes or other chromatographic techniques we chose to refold plant FtsZ from inclusion bodies. After expression, cells were harvested at 9,000 *g* for 10 min at 4°C and dry pellets were stored at -80°C until extraction and purification of recombinant protein.

Frozen cell pellets were thawed on ice and resuspended in 0.01 volumes the initial culture volume in ice-cold extraction buffer (25 mM TrisCl pH 8.0, 500 mM NaCl, 5 mM imidazole with Roche Complete EDTA-free protease inhibitors). Triton-X 100 was added to 0.1% and the cells were sonicated six times for 30 sec at full tip power using a Bronson microtip sonicator. Insoluble debris and inclusion bodies were collected by centrifugation at 18,000 *g* for 20 min at 4°C, the supernatant typically contained <20% of the expressed protein and was discarded. Inclusion bodies were resuspended in extraction buffer and sonicated again. Urea was added to 6 M and prior to affinity chromatography, insoluble material was removed by centrifugation at 18,000 *g* for 20 min at 4°C.

FtsZ1 and FtsZ2 proteins were purified by affinity chromatography using Ni-Sepharose (GE Healthcare) under denaturing conditions. Crude lysates were applied directly to a 15 ml Ni-Sepharose column (GE Healthcare) at 1 ml/min and washed with 2 column volumes of buffer A (25 mM TrisCl pH 8.0, 500 mM NaCl, 6 M urea). FtsZ was eluted with a linear gradient of 0-1 M imidazole in buffer A at 5 ml/min; FtsZ proteins typically eluted between ~100 and 300 mM imidazole and were pooled prior to refolding.

FtsZ1 and FtsZ2 were refolded by dialysis. Because the high concentration of imidazole from elution interferes with protein refolding, imidazole was first removed by dialysis against 25 mM TrisCl pH 8.0, 500 mM NaCl, 3 M urea. Following imidazole removal, ~1 mM GDP was added directly to the dialysis bag and plant FtsZ was dialyzed against three changes of 25 mM TrisCl pH 8.0, 500 mM NaCl, 500 mM GDP. GDP was required to prevent aggregation during refolding. Some protein aggregation was sometimes observed once the concentration of urea fell below ~1 M; this was removed by centrifugation at 14,000 *g* for 20 min at 4°C. Following dialysis, FtsZ protein was concentrated by ultrafiltration (Amicon Centricon, molecular weight cut-off of 30 kDa) to approximately 15 μM and glycerol was added to 10% before storage at -80°C until use. Prior to assay, FtsZ proteins were thawed on ice and centrifuged for 20 min at 12,000 *g* at 4°C to remove aggregated protein. Bacterial FtsZ proteins are typically purified with a round of assembly-based purification to select for active protein. However, we find that FtsZ1 and FtsZ2 assemble individually with poor efficiency.

Typically, ~25% of the plant FtsZ is recovered by CaCl₂, assembly-based purification individually, whereas we typically find >90% of *E. coli* FtsZ is recovered by assembly-based purification. Initially, poor recovery of FtsZ1 and FtsZ2 by assembly-based purification suggested our plant FtsZ preparations were not functional, but the low recovery was found to result from both FtsZ1 and FtsZ2 being required for efficient assembly (see Results). Instead, aggregated protein was removed by desalting with a HiPrep 26/10 column at 10 ml/min equilibrated with TMK (25 mM TrisCl pH 7.0, 0.1 mM MgCl₂, 100 mM KCl). The yield of plant FtsZ from desalting is 50-80% greater than assembly based purification, but there was little difference in protein activity. Following gel filtration into TMK, FtsZ protein was concentrated to approximately 15-20 μM using an Amicon Centricon (30 kDa molecular weight cut-off) and additional aggregated protein was removed by centrifugation at 18,000 *g* for 20 min at 4°C (typically less than 2% of the protein was aggregated). To verify proper refolding, FtsZ1 and FtsZ2 were subjected to sucrose density gradient fractionation with a linear 0-20% gradient prepared in HMK and both FtsZ1 and FtsZ2 fractionated near the 67 kDa marker (not shown).

SDS-PAGE and quantitative amino acid analysis (QAAA) were used to assess the purity of recombinant FtsZ. A typical plant FtsZ preparation was >95% pure. QAAA demonstrated FtsZ1 and FtsZ2 mature proteins are underestimated by the BCA assay by 20%, similar to *E. coli* FtsZ. This result is also consistent with our previous standardization for quantification (McAndrew et al. 2008). Occasionally, FtsZ2 protein

preparations would have a secondary lower MW band, likely due to initiation off of a downstream ATG codon in *E. coli*. The truncated protein was removed by reverse phase chromatography using a Source RPC 3.1/300 column (GE Healthcare) with a linear gradient of 0.1% trifluoroacetic acid (TFA) to 1:10:90, TFA:H₂O:acetonitrile over 20 CV. The eluted protein was refolded as described above and purity was typically >98%.

E. coli FtsZ was prepared by established methods and immediately before assay was subjected to a round of calcium stabilized polymerization and depolymerization (Lu and Erickson 1998; Lu et al. 1998). *E. coli* FtsZ was typically >90% pure as assessed by Coomassie staining SDS-PAGE gels.

Site-directed mutagenesis

Expression plasmids for FtsZ1 and FtsZ2 were mutagenized using established methods (Fisher and Pei 1997). Briefly, primer pairs 5'-GTCAATGTGGATTTTGCAGCTGTGAAGGCAGTCATGAAA-3' and 5'-TTTCATGACTGCCTTCACAGCTGCAAAATCCACATTGAC-3' or 5'-GTGAATGTGGATTTTGCTGCTGTGAGAGCTATAATGGCA-3' and 5'-TGCCATTATAGCTCTCACAGCAGCAAAATCCACATTCAC-3' were used to make D275A or D322A mutations in FtsZ1 or FtsZ2. This results in the T7-loop mutation NVDFAD to NVDFAA. Plasmids were amplified with Ex-Taq (Takara) using the manufacturer's buffers for 14 cycles. Following amplification, the parental plasmid was digested with DpnI (New England Biolabs) for 1h at 37°C. 2 µl of the digestion was used to transform competent DH5α and the mutation was confirmed by sequencing.

GTP binding and hydrolysis assays

Nucleotide binding to FtsZ proteins was performed as previously described (Redick et al. 2005). The GDP content of assembled FtsZ was assayed using the same technique developed for *E. coli* FtsZ (Chen and Erickson 2008; Romberg and Mitchison 2004; Small and Addinall 2003). Briefly, a GTP regeneration system is established with pyruvate kinase that phosphorylates GDP from phosphoenolpyruvate to make GTP. Thus, non-polymer bound GDP is rapidly converted to GTP and the GDP measured is only that bound to polymerized FtsZ. Instead of using radioactive GTP, we detected GDP and GTP by HPLC (Romberg and Mitchison 2004). 5 μ M FtsZ was polymerized in the presence of 0.5 mM GTP in HMK, deproteinated with a 5-fold excess of ice-cold 1 M perchloric acid and centrifuged for 20 min at 4°C. The supernatant was injected into a 0.5 ml sample loop on a AKTA Purifier HPLC and loaded onto a TOSOH DEAE 5P-5W 0.7 mm x 7 mm anion exchange column equilibrated with 100 mM NH_4HCO_3 at 1 ml/min at 25°C and detected by absorbance at 254 nm. Nucleotide was eluted with a linear gradient to 0.5 M NH_4HCO_3 at 1 ml/min over 3 column volumes. The anion-exchange column was calibrated before and after nucleotide binding assays with GDP and GTP. GDP and GTP elute as two closely spaced peaks at ~13.5 and 14.5 ml, respectively, and we estimated the GDP in the polymer by integrating the area underneath the base-line corrected peak corresponding to GDP in Unicorn 5.1 software (GE Healthcare). GDP concentration was calculated using the extinction coefficient $13,700 \text{ M}^{-1} \text{ cm}^{-1}$. Control experiments were performed on *E. coli* FtsZ and our results were consistent with

previous estimates of GDP content (Chen and Erickson 2008; Romberg and Mitchison 2004).

GTPase activity was initially measured with the malachite green assay (Redick et al. 2005). However, because the activity of FtsZ1 and FtsZ2 requires high GTP concentrations, which are incompatible with the malachite green assay, most GTPase assays were performed with a GTP regeneration assay (Ingerman and Nunnari 2005). *E. coli* FtsZ was routinely used as a positive control (Lu and Erickson 1998; Lu et al. 1998). *E. coli* FtsZ was assayed under conditions optimal for plant FtsZ (lower temperature). Optimal FtsZ1 and FtsZ2 GTPase activity was found between 25 and 30°C in 50 mM HEPES-KOH pH 7.0, 100 mM KCl and 5 mM MgSO₄ (HMK), similar to optimal conditions for *E. coli* FtsZ. However, *E. coli* FtsZ is typically assayed at 37°C (Lu and Erickson 1998; Lu et al. 1998), whereas in this study, *E. coli* FtsZ is assayed at 30°C.

Polymerization assays

Electron microscopy of FtsZ polymers was conducted with either 2.5 or 5 μM FtsZ (total FtsZ1 plus FtsZ2). To stabilize FtsZ1, FtsZ2 and *E. coli* FtsZ they were polymerized under non-dynamic conditions in HMKCa (HMK with 5 mM CaCl₂). FtsZ1/FtsZ2 co-polymers were stable without CaCl₂ conditions and were polymerized in HMK. All buffers were filtered through a 0.22 μm filter. Before nucleotide was added, polymerization reactions were centrifuged for 10 min at 14,000 *g*

Table 3.1: GTP binding and hydrolysis properties of FtsZ1 and FtsZ2 compared to *E.*

***coli* FtsZ**

	GTP Binding	ATP Binding	GTPase Specific Activity^A	GTPase Specific Activity^B	Activity with GDP^C	Activity with GTP and EDTA^D	Activity with ATP^E	GDP content of polymers
FtsZ1	1.05 ±0.03	N/D	0.14	0.028	N/D	N/D	N/D	-
FtsZ1D275A	1.15 ±0.25	N/D	N/D	N/D	N/D	N/D	N/D	-
FtsZ2	0.98 ±0.22	N/D	0.14	0.046	N/D	N/D	N/D	-
FtsZ2D322A	0.95 ±0.12	N/D	N/D	N/D	N/D	N/D	N/D	-
FtsZ1/FtsZ2	-	N/D	0.15	-	N/D	N/D	N/D	~10-20%
<i>E. coli</i> FtsZ	1.09 ± 0.17	N/D	2.51	-	N/D	N/D	N/D	~40-50%

Notes

A) Maximum activity observed using a coupled GTPase assay at 25°C reported in this column

B) Activity determined with a malachite green phosphate assay

C) Activity determined with a malachite green phosphate assay

D) Determined with both a malachite green phosphate assay and coupled assay

at 25°C to remove contaminants. After nucleotide was added, plant FtsZ was polymerized for 20 min at 25°C or 30°C; results were similar at both temperatures. *E. coli* FtsZ was used as a positive control and results in HMKCa were consistent with previous reports (Erickson et al. 1996; Mukherjee and Lutkenhaus 1994, 1998). 2 µl of a polymerization reaction was pipetted onto a formvar coated 200-mesh nickel grid and negative stained with 0.5% or 2% uranyl acetate. FtsZ polymers were examined with a JEOL100 CXII (Japan Electron Optics Laboratories) transmission electron microscope at an accelerating voltage of 100 kV at 10,000-450,000X magnification as indicated.

90° light-scattering assays were conducted as previously described for bacterial FtsZ (Mukherjee and Lutkenhaus 1999) using a Photon Technologies Incorporated fluorescence spectrophotometer equipped with a model 814 photomultiplier operated in digital mode at 1000V. Assays were performed with a 0.5 nm excitation and 1 nm emission slit widths and 350 nm excitation and emission wavelengths. Polymerization was conducted in HMK buffer at room temperature unless otherwise specified; all buffers were filtered through a 0.22 µm filter prior to use and all protein preparations were centrifuged for 10 min at 14,000 *g* at 25°C immediately before assay. Polymerization rates were derived by linear regression fit of the linear increase in light-scattering.

Results

Production and refolding of recombinant Arabidopsis FtsZ1-1 and FtsZ2-1

In contrast to previous studies (El-Kafafi et al. 2005; Gaikwad et al. 2000), the putative chloroplast transit peptides of FtsZ1 and FtsZ2 were removed from recombinant FtsZ1 and FtsZ2 (Figure 3.1). ChloroP (Emanuelsson et al. 1999) predicts a 48 amino acid transit peptide for AtFtsZ2-1. AtFtsZ2-1 was aligned with several cyanobacterial FtsZ proteins and the predicted 48 amino acid transit peptide extended beyond the alignments (not shown), suggesting the ChloroP transit peptide prediction for AtFtsZ2-1 is correct. Moreover, removal of the AtFtsZ2-1 putative transit peptide results in a predicted mass of ~46 kDa, which is close to the ~45 kDa mass of AtFtsZ2-1 determined by immunoblotting of Arabidopsis proteins (McAndrew et al. 2008; Stokes et al. 2000). Arabidopsis has two FtsZ2 genes, AtFtsZ2-1 and AtFtsZ2-2 (McAndrew et al. 2008; Osteryoung et al. 1998). The amino acid sequences of these two proteins are 92% similar and 85% identical without their ChloroP predicted transit sequences. In Arabidopsis, *AtFtsZ2-1* and *AtFtsZ2-2* are genetically redundant (Aaron Schmitz et al., in preparation) but *AtFtsZ2-1* is more abundant than *AtFtsZ2-2* (McAndrew et al. 2008) so *AtFtsZ2-1* was chosen as a biochemical representative of the FtsZ2 family from Arabidopsis.

ChloroP predicts a 90 amino acid transit peptide for AtFtsZ1-1. Removal of 90 amino acids from the N-terminus of AtFtsZ1-1 would remove half of the glycine-rich, GTP binding motif (Figure 3.1) (de Boer et al. 1992a; Erickson 1995; Mukherjee et al. 1993; Mukherjee and Lutkenhaus 1994; RayChaudhuri and Park 1992). Moreover, FtsZ1 without 90 N-terminal amino acids has a predicted mass of ~36 kDa, significantly smaller than ~40 kDa determined for AtFtsZ1-1 by immunoblotting Arabidopsis proteins (Stokes

et al. 2000). A better approximation of the AtFtsZ1-1 chloroplast transit peptide length was made with the following information: the native AtFtsZ1-1 mass is ~40 kDa, AtFtsZ1-1 alignments with other FtsZ1 proteins (Stokes and Osteryoung 2003) and chloroplast transit peptides are typically cleaved near charged/arginine residues (Archer and Keegstra 1993; Bruce 2000). These factors together resulted in a new AtFtsZ1-1 transit peptide estimate of 57 amino acids. Finally, a AtFtsZ1-1 57 amino acid transit peptide does not remove important structural elements (Nogales et al. 1998a) from a homology based structural model for AtFtsZ1-1 (Yoder et al. 2007).

Plant FtsZ proteins are cytotoxic when recombinantly expressed in *E. coli*, resulting in long filamented cells (not shown) and low protein expression. Co-expression of the *E. coli ftsQAZ* operon during plant FtsZ expression suppressed cell filamentation and resulted in significantly increased expression of plant FtsZ (Jeong and Lee 2003). Recombinant FtsZ proteins were found predominantly in inclusion bodies (>80%). The small amounts of soluble recombinant FtsZ1 or FtsZ2 were difficult to efficiently separate from contaminating proteins, so plant FtsZ proteins were purified from inclusion bodies. Both FtsZ1 and FtsZ2 were purified by Ni-Sepharose (GE Healthcare) affinity chromatography in 6 M urea (denaturing conditions). Both FtsZ1 and FtsZ2 typically elute from Ni-Sepharose between ~100-300 mM imidazole (not shown). Bacterial FtsZ refolds to an active form when removed from denaturing conditions (Andreu et al. 2002; Santra and Panda 2003) and a similar approach was used to refold plant FtsZ1 and FtsZ2. In some preparations, FtsZ2-1 was contaminated with a small amount of protein initiated from a downstream ATG codon. The truncated,

contaminating FtsZ2-1 protein was removed by reverse phase chromatography prior to refolding. Truncated FtsZ2-1 eluted first from a reverse phase column in ~25% acetonitrile, while FtsZ2-1 eluted later in ~40-45% acetonitrile (not shown). FtsZ1 and FtsZ2 purity was assessed by QAAA and was typically >95% pure after refolding. These preparations did not have significant secondary bands when examined by SDS-PAGE and silver-staining (not shown). FtsZ2 prepared by reverse phase chromatography was typically >98% pure.

Both FtsZ1 and FtsZ2 bind and hydrolyze GTP

Plant FtsZ1 and FtsZ2 contain FtsZ-consensus, N-terminal GTP-binding motifs (Osteryoung and McAndrew 2001). All FtsZ proteins, including plant FtsZ1 and FtsZ2, contain the GTP hydrolysis motif GxxNxDxxD/E in their T7-loops (Mukherjee et al. 1993; Nogales et al. 1998a; RayChaudhuri and Park 1992; Scheffers et al. 2002) (Figure 3.1). To test for GTP binding, FtsZ1 and FtsZ2 were mixed with fresh GTP and unbound nucleotide was removed by gel filtration (Redick et al. 2005). FtsZ1, FtsZ2 and *E. coli* FtsZ bound 1.05 ± 0.03 , 0.98 ± 0.22 and 1.09 ± 0.17 mol of GTP per FtsZ respectively (Table 3.1). To test for nucleotide binding specificity, the experiment was repeated with ATP. FtsZ1, FtsZ2 or *E. coli* FtsZ did not bind detectable levels of ATP (Table 3.1) consistent with previous findings (de Boer et al. 1992a; RayChaudhuri and Park 1992). Together, these data confirm that FtsZ1 and FtsZ2 are properly folded and both are capable of specifically binding GTP like other FtsZ proteins.

FtsZ1 and FtsZ2 were tested for GTP hydrolysis with two assays commonly used with *E. coli* FtsZ. First, the malachite green assay for inorganic phosphate (P_i) was used to measure free and unbound P_i, but this assay cannot be used with high GTP concentrations (Redick et al. 2005). Second, GTP hydrolysis was measured with a regenerative GTPase assay that measures GDP release (Ingerman and Nunnari 2005) presumably from subunit dissociation (Chen and Erickson 2008; Small and Addinall 2003). At 0.5 mM GTP, FtsZ1 and FtsZ2 have low specific activities of 0.028 ±0.002 and 0.046 ±0.002 GTP min⁻¹ FtsZ⁻¹ (Table 3.1). The GTPase activities of FtsZ1 and FtsZ2 were confirmed in a coupled GTPase assay (Ingerman and Nunnari 2005). At higher concentrations of GTP, both FtsZ1 and FtsZ2 have specific GTPase activities of 0.14 GTP min⁻¹ FtsZ⁻¹ (Figure 3.2A, Table 3.1). As a control for GTPase activity, T7-loop mutant proteins were created, FtsZ1D275A and FtsZ2D322A. These proteins have mutated the T7 loops changing GxxNVDFAD to GxxNVDFAA. This mutation in *E. coli* FtsZ abolishes GTP hydrolysis, but GTP binding is unaffected (Redick et al. 2005; Scheffers et al. 2002). FtsZ1D275A and FtsZ2D322A mutant proteins also were able to bind 1.15 ±0.25 and 0.95 ±0.12 molecules of GTP per FtsZ, but did not hydrolyze GTP above background levels. In additional control experiments, hydrolysis was not detected above background when FtsZ1, FtsZ2 and *E. coli* FtsZ were assayed with GDP, ATP or with GTP and 1 mM EDTA (Table 3.1).

The GTP hydrolysis kinetics of FtsZ1 and FtsZ2 differ from each other and from *E. coli* FtsZ. GTP hydrolysis for FtsZ1 and FtsZ2 was examined at 2.5 μM total protein,

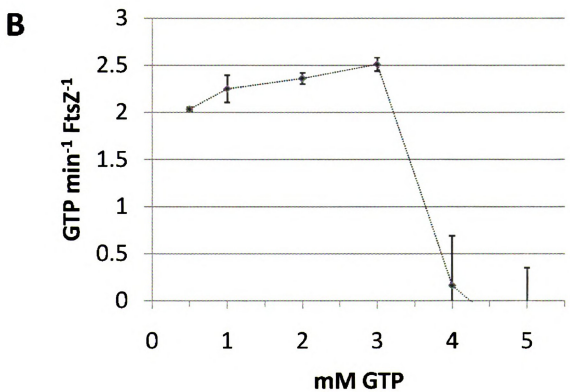
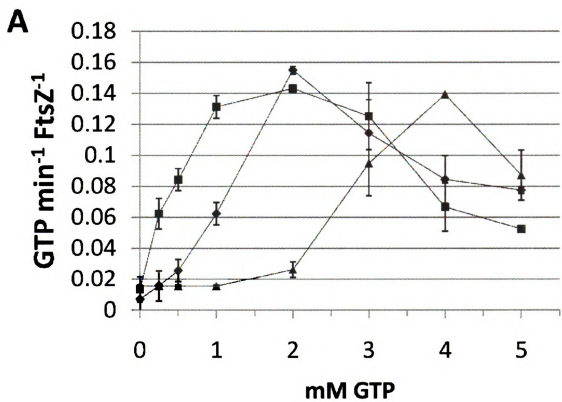
which is within a linear correlation between activity and protein concentration (not shown) and this FtsZ concentration is similar to the predicted FtsZ concentration in chloroplasts (McAndrew et al. 2008). The maximum GTPase activity of FtsZ1 (0.14 GTP min⁻¹ FtsZ⁻¹) was found between ~1-3 mM GTP (Figure 3.2A, ■) while the maximum GTPase activity of FtsZ2 (0.14 GTP min⁻¹ FtsZ⁻¹) was between ~3-4 mM GTP (Figure 3.2A, ▲). In contrast, the maximum specific GTPase activity of equally mixed FtsZ1 and FtsZ2 was slightly increased to 0.15 GTP min⁻¹ FtsZ⁻¹ and found near ~2 mM GTP (Figure 3.2A, ◆). GTP hydrolysis kinetics were distinctly different for FtsZ1 and FtsZ2 (Figure 3.2A). In control experiments, *E. coli* FtsZ GTP hydrolysis was faster as the concentration of GTP increased (Figure 3.2B) from ~2 GTP min⁻¹ FtsZ⁻¹ to ~2.5 GTP min⁻¹ FtsZ⁻¹. At >4 mM GTP, *E. coli* FtsZ GTP hydrolysis was abolished (Figure 3.2B). *E. coli* FtsZ did not demonstrate the GTP concentration-dependent increase in activity (Figure 3.2B) observed for FtsZ1 and FtsZ2 (Figure 3.2A). These results demonstrate that plant have slower rates of GTP hydrolysis compared to *E. coli* FtsZ. Moreover, the GTPase activity of plant FtsZ is stimulated at high GTP concentrations, which could result from different GTP binding or catalytic properties compared to *E. coli* FtsZ.

Do FtsZ1 and FtsZ2 assemble?

FtsZ1/FtsZ2 co-assembly EM and light-scattering

Figure 3.2: GTPase kinetics of FtsZ1, FtsZ2, equally mixed FtsZ1/FtsZ2 and *E. coli* FtsZ

(A) Kinetic GTPase activity of 5 μ M FtsZ1 (■), FtsZ2 (▲) and 5 μ M of equally mixed FtsZ1 and FtsZ2 (◆) were examined at various GTP concentrations. (b) 5 μ M *E. coli* FtsZ was assayed in parallel as a control. The line connecting the points in both panels is interpolated and does not reflect a curve fit.



Both FtsZ1 and FtsZ2 bind and hydrolyze GTP (Table 3.1), which predicts they assemble like bacterial FtsZ. 1 mM GTP was added to 5 μ M of equally mixed FtsZ1 and FtsZ2 in HMK, and after a \sim 100 sec lag light-scattering rapidly increased (Figure 3.3B, \square). The lag before light-scattering rapidly increased is suggestive of cooperative assembly (Caplan and Erickson 2003; Chen et al. 2005; Gonzalez et al. 2005; Huecas and Andreu 2003, 2004; Romberg et al. 2001). As a control, the experiment was repeated with 1 mM GDP instead of GTP and \sim 90% less light-scattering was observed (Figure 3.3B, \blacksquare). 5 μ M of equally mixed FtsZ1 and FtsZ2 were polymerized under identical conditions and polymer topology was examined by EM. FtsZ1 and FtsZ2 co-polymerized with 1 mM GTP assembled into bundled ribbon-like structures reminiscent of tubulin (Figure 3.4D and E). FtsZ1/FtsZ2 co-polymers are \sim 15-20 filaments in width (Figure 3.4E), or \sim 150 nm wide. FtsZ1/FtsZ2 co-polymers typically range from 1-20 μ m in length (Figure 3.4D). FtsZ1/FtsZ2 ribbons are significantly longer than those observed with bacterial FtsZ even in the presence of stabilizing CaCl_2 . In contrast, *E. coli* FtsZ was polymerized in the same conditions as FtsZ1 and FtsZ2 and was found to assemble into single protofilament polymers (not shown) consistent with previous findings (Chen et al. 2005; Huecas et al. 2007a; Romberg et al. 2001). In the absence of nucleotide, or in the presence of 1 mM GDP, assembled filaments were not observed for equally mixed FtsZ1 and FtsZ2 or *E. coli* FtsZ (not shown).

Figure 3.3: 90° Light-scattering polymerization assays of FtsZ1 and FtsZ2.

Symbols on the traces in the figures were added to distinguish between experiments. In panels A and B, the vertical axis light scattering data are $\times 10^3$. All experiments were performed in HMK unless noted otherwise. (A) 5 μM of equally mixed FtsZ1 with FtsZ2 was monitored for light-scattering polymerization in the presence of various concentrations of GTP. In the presence of GDP (\blacklozenge), polymerization was observed but was lower than observed when GTP was added. At 0.5 mM GTP (\square), FtsZ1/FtsZ2 polymerization steadily increased and saturated as the time approached 2h (not shown). At 1 mM (\diamond), 2 mM (\triangle) and 5 mM (\blacksquare) GTP, polymerization saturated more quickly. (B) FtsZ1 with FtsZ2 polymerizes most efficiently when both are present compared to similar concentrations of FtsZ1 or FtsZ2 alone. 2.5 μM FtsZ1 with 2.5 μM FtsZ2 was polymerized with 1 mM GTP (\square), 5 μM FtsZ1 was polymerized with 1 mM GTP (\diamond), 5 μM FtsZ2 was polymerized with 1 mM GTP (\triangle) and as a control, 2.5 μM FtsZ1 with 2.5 μM FtsZ2 was mixed with 1 mM GDP (\blacksquare). (C) The rate of polymerization at various GTP concentrations was determined from panel A. The rate of polymerization was maximal with 0.5 mM GTP (when GTP hydrolysis is slow, Figure 3.2) and as the GTP concentration increased (when GTP hydrolysis is faster, Figure 3.2), the rate of polymerization steadily decreased. (D) the rate of polymerization was calculated for the rapid linear increase in polymerization observed for the traces in panel C. Polymerization is maximal only when both FtsZ1 and FtsZ2 are present with GTP. ΔLS = change in light scattering.

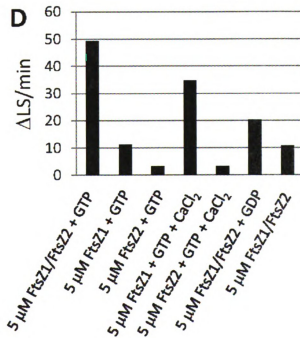
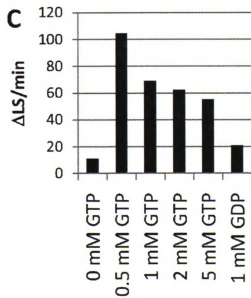
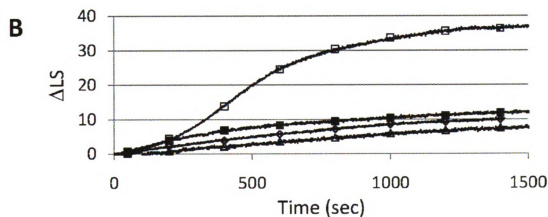
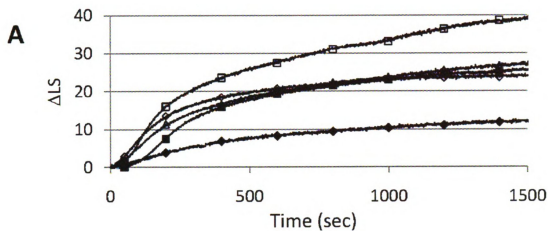
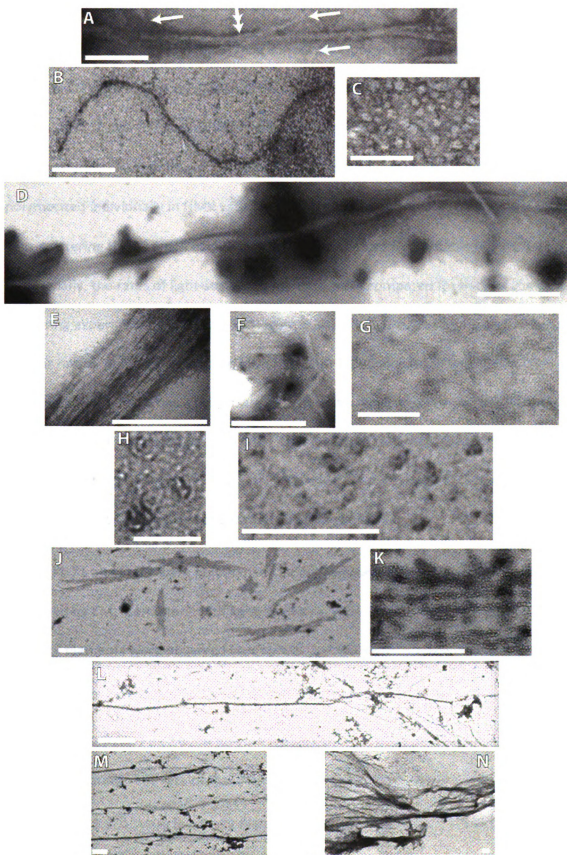


Figure 3.4: Negative stain electron micrographs of FtsZ1 and FtsZ2

(A) FtsZ1 in HMKCa with 1 mM GTP. Single arrow indicates single protofilament example and double arrow indicates double protofilament example. Bar=200 nm. (B) FtsZ2 in HMKCa with 1 mM GTP. Bar=200 nm. (C) FtsZ2 in HMKCa with 1 mM GDP as an example of unassembled plant FtsZs. Bar=200 nm. (D) Wide-field view of FtsZ1/FtsZ2 in equal amounts with 0.5 mM GTP in HMK. Bar= 200 nm. (E) Close-up view of FtsZ1/FtsZ2 from paned D. Bar=1 μ m. (F) FtsZ1/FtsZ2 in equal amounts in 2 mM GTP in HMK. Bar=1 μ m. (G) 2.5 μ M each of FtsZ1 with FtsZ2D322A in HMK with 1 mM GTP. Bar=200 nm. (H) FtsZ2D322A in HMKCa with 1 mM GTP. Bar=200 nm. (I) FtsZ1D275A in HMKCa with 1 mM GTP. Bar=200 nm. (J) FtsZ1/FtsZ2 mixed at 1:5 with 1 mM GTP in HMK. Bar=1 μ m. (K) FtsZ1/FtsZ2 mixed at 5:1 with 1 mM GTP in HMK. Bar= 1 μ m. (L) Polymers in K stabilized in HMKCa. Bar=1 μ m. (M) 2:1, FtsZ1/FtsZ2 in HMKCa with 1 mM GTP. Bar=1 μ m. (N) 1:2, FtsZ1/FtsZ2 in HMKCa with 1 mM GTP. Bar=1 μ m.



FtsZ1 and FtsZ2 homofilaments are unstable

2.5 μM each of mixed FtsZ1/FtsZ2 in HMK co-polymerize into ribbon-like structures (Figure 3.4D and E, Figure 3.3B, \square), but do FtsZ1 and FtsZ2 polymerize individually? 1 mM GTP was added to either FtsZ1 or FtsZ2 individually in HMK and light-scattering was monitored. 5 μM FtsZ1 (Figure 3.3B, \diamond) or FtsZ2 (Figure 3.3B, \triangle) polymerized individually in HMK with 1 mM GTP exhibits approximately 70% less total light-scattering than 2.5 μM each of FtsZ1/FtsZ2 in the same conditions (Figure 3.3B, \square). Additionally, the rates of light-scattering increase were compared for each of the light-scattering experiments in Figure 3.3B (Figure 3.3D). FtsZ1/FtsZ2 with 1 mM GTP has a greater rate of polymerization than either FtsZ1 or FtsZ2 individually with 1 mM GTP. Moreover, FtsZ1/FtsZ2 has a faster rate of light scattering in the presence of GDP than do FtsZ1 and FtsZ2 individually with GTP. Thus, FtsZ1/FtsZ2 co-polymerizes in greater quantity and faster than either FtsZ1 or FtsZ2 alone. In summary, FtsZ1 and FtsZ2 are both required for maximum, cooperative polymerization.

FtsZ1 and FtsZ2 were polymerized individually in HMK with 1 mM GTP and examined by EM. Consistent with light-scattering experiments, very few individual, 10 nm thick filaments were observed (not shown, but identical to those shown in 3.4A and B). To stabilize individual FtsZ1 and FtsZ2 filaments, 5 mM CaCl_2 was added to HMK (HMKCa). FtsZ1 and FtsZ2 were polymerized individually with 1 mM GTP and monitored by light-scattering. The rate of FtsZ2 light-scattering did not increase in the presence of CaCl_2 (Figure 3.3D). Very few FtsZ2 filaments were observed by EM in HMKCa (Figure

3.4B). FtsZ2 filaments in HMKCa were typically $\sim 1 \mu\text{m}$ long and $\sim 10 \text{ nm}$ in width; filaments greater than $1 \mu\text{m}$ in length were not observed. In contrast, FtsZ1 light-scattering increased in HMKCa compared to HMK (Figure 3.3D). FtsZ1 polymer abundance correlated to light-scattering when examined by EM. FtsZ1 polymerized into long thin filaments or pairs of filaments in both HMKCa and HMK, but the abundance of filaments was greater in HMKCa (Figure 3.4A, single filament indicated with one arrow and a double filament indicated with two arrows). FtsZ1 filaments were significantly longer in HMKCa and were typically $\sim 1\text{-}2 \mu\text{m}$ long and $\sim 10 \text{ nm}$ wide consistent with single filaments. FtsZ1 sometimes polymerized into a loose polymer network (not shown) similar to FtsZ1-GFP over-expression in *Physcomitrella patens* (Reski 2002). In the absence of nucleotide, or in the presence of GDP, both FtsZ1 and FtsZ2 appear monomeric (Figure 3.4C, FtsZ2 with 1 mM GDP as an example), similar to results with *E. coli* FtsZ (Mukherjee and Lutkenhaus 1994). FtsZ1 and FtsZ2 have low GTPase activity individually, which should correlate to more stable polymers. However, FtsZ1 and FtsZ2 do not polymerize by themselves unless CaCl_2 is present. In contrast, when FtsZ1 and FtsZ2 are mixed and polymerized with GTP, ribbon-like structures are observed (Figure 3.4D and E). Together, these results further support the hypothesis of FtsZ1 and FtsZ2 co-polymerization.

FtsZ1/FtsZ2 co-polymer length correlates to GTPase activity

At 0.5 mM GTP, the GTPase activity of FtsZ1/FtsZ2 is slow, but at $> 1 \text{ mM}$ the GTPase activity is faster (Figure 3.2A). This result predicts that maximum assembly

should occur at low GTP concentrations, but less polymerization should occur at higher concentrations of GTP. This question was addressed by using light-scattering and EM to examine FtsZ1 and FtsZ2 co-polymerized at various concentrations of GTP. 2.5 μ M of FtsZ1 and FtsZ2 in HMK were polymerized with increasing concentrations of GTP. FtsZ1/FtsZ2 have the highest light-scattering signal in the presence of 0.5 mM GTP, (Figure 3.3A, \square) and the fastest rate of increase in signal (Figure 3.3C). In addition, FtsZ1/FtsZ2 light-scattering plateaus between \sim 1.5-2h (not shown). However, as the concentration of GTP is increased above 1 mM, the lag of FtsZ1/FtsZ2 polymerization increases (Figure 3.3A; 1 mM: \diamond ; 2 mM, \triangle and 5 mM, \blacksquare) and the rate of polymerization decreases (Figure 3.3C) but the amount of light-scattering plateaus at the same point between 1-5 mM GTP. Significantly, 1-5 mM correlates to the maximum FtsZ1/FtsZ2 GTPase activity (Figure 3.2A). Controls were incubated with 1 mM GDP (Figure 3.3A, \blacklozenge) or no nucleotide and had low levels of light-scattering (not shown).

Does increased GTP concentration correlate to shorter FtsZ1/FtsZ2 ribbons, or less bundling between individual filaments? Light-scattering experiments demonstrate that the amount of FtsZ1/FtsZ2 co-polymerization plateaus at high GTP concentrations (Figure 3.3A). Also, at these concentrations of GTP, FtsZ1/FtsZ2 hydrolyze GTP faster. This predicts that FtsZ1/FtsZ2 ribbons would be shorter, which was tested by examining FtsZ1/FtsZ2 co-polymers by EM in 2 and 5 mM GTP. The width of FtsZ1/FtsZ2 co-polymers was \sim 150 nm and the same as the ribbons polymerized in 0.5 mM GTP (Figure 3.4E). However, FtsZ1/FtsZ2 polymerized in 2 or 5 mM GTP were shorter, never longer than 1 μ m, than those polymerized at 0.5 mM (compare Figure 3.4F to Figure 3.4D).

Because the width is unaffected we hypothesize that these polymers may be treadmilling (Cleveland 1982; Larsen et al. 2007; Margolin 2007; Margolis and Wilson 1998).

The critical concentration for polymerization

When mixed equally, FtsZ1 and FtsZ2 display a kinetic lag in polymerization that lengthens as the concentration of GTP increases. This suggests FtsZ1/FtsZ2 co-assemble cooperatively. Bacterial FtsZ cooperatively assembles with a critical concentration of $\sim 1 \mu\text{M}$ (Anderson et al. 2004; Redick et al. 2005; Stricker and Erickson 2003). The critical concentration for FtsZ1/FtsZ2 mixtures was determined by light-scattering (Mukherjee and Lutkenhaus 1999). The concentration of FtsZ1/FtsZ2 was varied between 0.125 and 2.5 μM (total FtsZ1/FtsZ) and plotted versus the rate of polymerization. Polymerization was not observed when the concentration of FtsZ1/FtsZ2 was below 0.5 μM in HMK. To verify that assembled protein could be detected at this FtsZ concentration, the experiment was repeated in HMKCa with 1 mM GTP. In HMKCa, 0.5 μM FtsZ1/FtsZ2 light-scattering increased (not shown), demonstrating the lack of light-scattering in HMK correlates to a lack of significant assembly. A linear regression was used to fit data points above 0.5 μM FtsZ1/FtsZ2 (Figure 3.5). The x-intercept of the regression predicts a critical concentration of $\sim 0.7 \mu\text{M}$ for co-assembly of FtsZ1/FtsZ2. The plant FtsZ1/FtsZ2 critical concentration is consistent with calculations of $\sim 0.5\text{-}1 \mu\text{M}$ for *E. coli* FtsZ (Anderson et al. 2004; Redick et al. 2005; Stricker and Erickson 2003).

FtsZ1/FtsZ2 co-polymers are larger and more stable than E. coli FtsZ

polymers

Polymerization of equally mixed FtsZ1 and FtsZ2 (Figure 3.6, top trace) was compared with that of bacterial FtsZ by light-scattering assays in HMK. 5 μ M *E. coli* FtsZ was assayed for light-scattering with 1 mM GTP (Figure 3.6, bottom trace, arrow indicates GTP addition). The signal increased when GTP was added and then returned to baseline within \sim 10 minutes. Moreover, *E. coli* FtsZ light-scattering did not increase when GDP or no nucleotide was added (not shown). All *E. coli* FtsZ experiments were consistent with previous results (Mukherjee and Lutkenhaus 1994). Moreover, when 5 mM GTP was added to 5 μ M *E. coli* FtsZ, the light-scattering signal increased in proportion to the GTP concentration. The light-scattering signal persisted longer than with 1 mM GTP (Figure 3.6, middle trace). In contrast, plant FtsZ1/FtsZ2 mixtures have a higher light-scattering signal (Figure 3.6, top trace) in HMK with 1 mM GTP. When examined by EM under these same conditions, *E. coli* FtsZ was found to assemble into single filaments as previously reported (Caplan and Erickson 2003; Huecas et al. 2007a). Thus, plant FtsZ1/FtsZ2 polymerizes significantly more, and is more stable than *E. coli* FtsZ. This result is consistent with the difference in GTP hydrolysis rates between plant FtsZ1/FtsZ2 and *E. coli* FtsZ.

Figure 3.5: Critical concentration for FtsZ1/FtsZ2 polymerization monitored by 90° light-scattering.

FtsZ1 and FtsZ2 were mixed equally and 1 mM GTP was added to the cuvette. Rates of polymerization were derived from light scattering data and plotted versus the FtsZ concentration. All data points except those corresponding to 0.5 and 0.25 μM FtsZ, where polymerization was essentially not observed, were fit with the linear regression $y = 5.0328x - 3.7318$ ($R^2 = 0.9413$). These results predict a critical concentration for FtsZ1/FtsZ2 polymerization of $\sim 0.7 \mu\text{M}$.

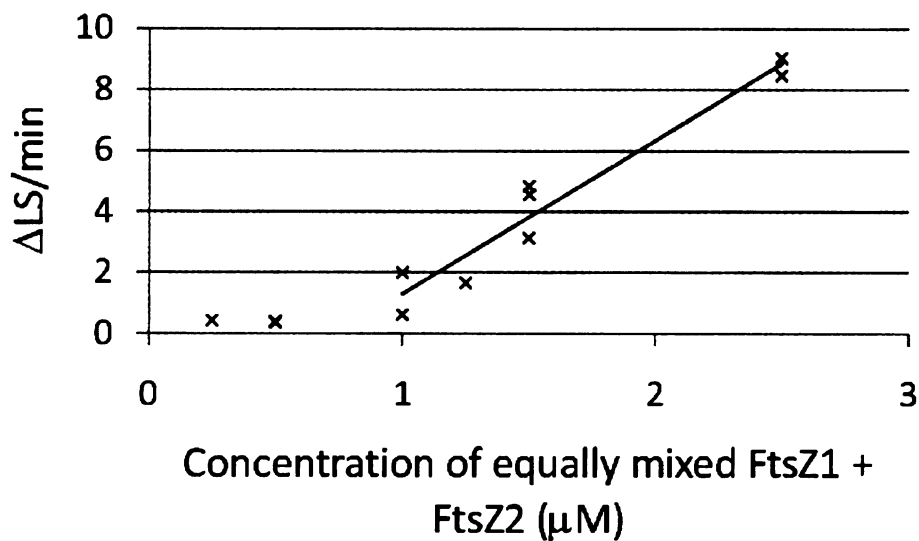
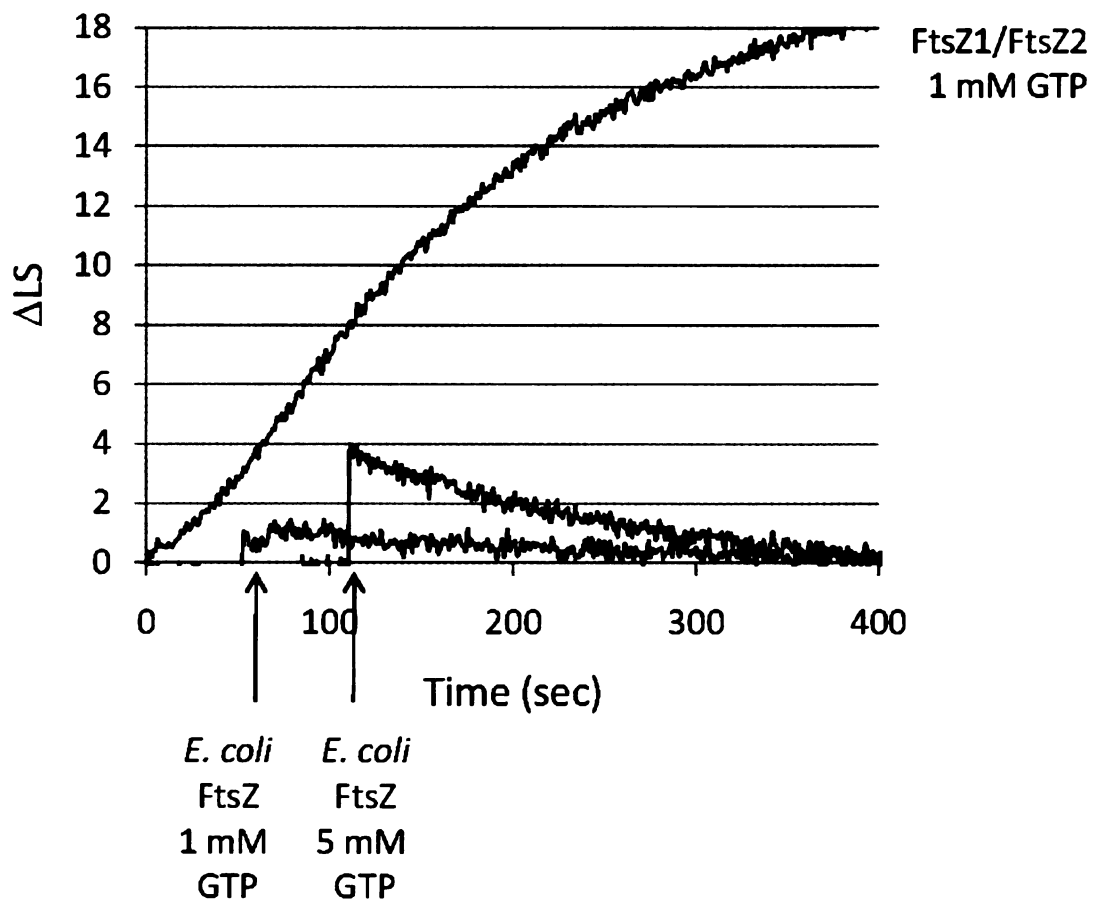


Figure 3.6: Light-scattering comparison of polymerization of *E. coli* FtsZ and FtsZ1 with FtsZ2 both at 5 μ M in HMK buffer.

(A) FtsZ1 with FtsZ2 (upper curve) polymerizes extensively and does not disassemble over the assay monitoring time of 1 h. In contrast, *E. coli* FtsZ rapidly polymerizes, but disassembles rapidly, likely correlating to the concentration of GTP since a second polymerization of EcFtsZ with 5 mM GTP (middle curve) was performed and the extent of polymerization was higher than with 1 mM GTP (lower curve). Arrows indicate GTP addition to *E. coli* FtsZ.



FtsZ1/FtsZ2 copolymers are not disassembled by GDP

Polymerized *E. coli* FtsZ exchanges nucleotide within the polymer, unlike $\alpha\beta$ -tubulin polymers. As a result, *E. coli* FtsZ can readily be depolymerized by the addition of GDP (Huecas and Andreu 2004). In contrast, plant FtsZ1/FtsZ2 co-polymers are significantly more stable and have higher signals in light-scattering assays than *E. coli* FtsZ (Figure 3.6). Additionally, FtsZ1/FtsZ2 laterally bundle in the absence of stabilizing agents (Figure 3.4D and E). One possible difference between plant FtsZ and *E. coli* FtsZ could be nucleotide exchange within assembled polymers. FtsZ1 and FtsZ2 were co-polymerized with 0.5 mM GTP for 30 min at 25°C and then light-scattering was monitored for ~5 min. 5 mM GDP was added to the cuvette (Figure 3.7, marked) and the light-scattering signal decreased slightly, but recovered in <100 sec. As a control, light-scattering returned to baseline when 2 mM EDTA was added to FtsZ1/FtsZ2 co-polymers (Figure 3.7, marked).

To investigate the GDP content of FtsZ1/FtsZ2 co-polymers, *E. coli* FtsZ and FtsZ1/FtsZ2 co-polymers were maintained in a GTP regeneration system previously used to estimate the GDP content of *E. coli* FtsZ and TubZ (Chen and Erickson 2008; Romberg and Mitchison 2004). 5 μ M EcFtsZ was found to contain 2-2.5 μ M GDP after incubation for 20 minutes with 0.5 μ M GTP, while 5 μ M FtsZ1/FtsZ2 contained 0.2-1 μ M GDP in the same conditions. These results suggest that the consequence of a low GTPase activity of plant FtsZ is a reduced content of GDP within the polymer and provide evidence of why plant FtsZ1/FtsZ2 co-polymers are significantly more stable in HMK than *E. coli* FtsZ.

Stoichiometric requirements for GTPase activity and polymerization

Adding additional FtsZ1 or FtsZ2 to FtsZ1/FtsZ2 polymerization assays

decreases the extent of polymerization

If FtsZ1 and FtsZ2 form a head-to-tail heterofilament, varying the ratio of FtsZ1 to FtsZ2 should result in reduced polymerization. This possibility was tested by varying the ratio between FtsZ1 and FtsZ2, keeping the total FtsZ concentration at 5 μ M and monitoring light-scattering. In the first series of experiments, excess FtsZ1 was added to FtsZ2. As the concentration of FtsZ1 increased, the light-scattering signal decreased (Figure 3.8A: 1:1, \square ; 10:1, \circ ; 3:1, \triangle ; 2:1 \diamond). Moreover, the rate of light-scattering decreased proportionally to the increase in FtsZ1 levels (Figure 3.8C). In a series of related experiments, excess FtsZ2 was added to FtsZ1 while keeping the total concentration of protein at 5 μ M. Adding excess FtsZ2 decreased light-scattering (Figure 3.8B: 1:1, \square ; 1:10, \circ ; 1:3, \triangle ; 1:2, \diamond) and decreased the initial rate of light-scattering (Figure 3.8C). Light-scattering predicts that excess FtsZ1 or FtsZ2 would result in shorter filaments when examined by EM. FtsZ1 and FtsZ2 were mixed at 1:5 or 5:1 in HMK and examined by EM. FtsZ1 mixed 1:5 with FtsZ2, shortened and reduced lateral association of filaments (Figure 3.4J) and the reduction in polymerization correlated to the light-scattering signals. In contrast, FtsZ1 mixed 5:1 with FtsZ2, lateral association was almost entirely abolished, and filament length was slightly shortened, but filament quantity was not reduced (Figure 3.4K). These results demonstrate that FtsZ2 may

mediate bundling with FtsZ1, but FtsZ1 does not mediate significant bundling between FtsZ1 and FtsZ2.

FtsZ2-1 promotes lateral bundling of FtsZ1-1/FtsZ2-1 ribbons

FtsZ1/FtsZ2 were co-polymerized at varied ratios and examined by EM in the presence of CaCl₂ to stabilize the polymers. When the ratio of FtsZ1 to FtsZ2 is 2:1 (and as high as 5:1, not shown) and polymerized in HMKCa with 1 mM GTP, thin filaments are typically observed (Figure 3.4L) similar to polymerizing FtsZ1 only (Figure 3.4A), but filament pairs were observed more often. In contrast, when the ratio between FtsZ1 and FtsZ2 is 1:2, FtsZ1/FtsZ2 ribbons increasingly have individual filaments dissociating from the larger cable itself, sometimes crossing from ribbon-to-ribbon (Figure 3.4M). FtsZ1 and FtsZ2 were also mixed at a 1:5 ratio. When examined by EM, these polymers adopt a fan-like structure, and bundling is loosened between cable filaments (Figure 3.4N). Moreover, many short ribbon-fragments with fewer bundled filaments are laterally dissociated from the cable. In summary, by stabilizing FtsZ1/FtsZ2 polymerized at different ratios two different polymer morphologies were observed. Excess FtsZ1 results in thinner filaments, and sometimes filament pairs. In contrast, excess FtsZ2 results in cables with disrupted lateral interaction. In addition, the cable stays somewhat intact, but the lateral disruption is proportional to the increase in ratio. We interpret this result to suggest lateral interactions are predominantly between FtsZ2 and FtsZ1.

Figure 3.7: Equally mixed FtsZ1 and FtsZ2 are not depolymerized by GDP.

5 μ M total FtsZ1 and FtsZ2 were equally mixed in HMK and polymerized in the presence of 2 mM GTP for 30 min at 25°C. FtsZ1 and FtsZ2 were co-assembled for 30 min in the presence of 0.5 mM GTP and then placed into a spectrofluorimeter to measure light-scattering. After \sim 6 min of monitoring light-scattering in the presence of GTP, 5 mM GDP (in 25 mM HEPES-KOH pH 7.0) was added to the cuvette and monitored for an additional \sim 6 min. To verify that FtsZ1 and FtsZ2 co-polymers were able to be disassembled, 2 mM EDTA was then added to the cuvette and light-scattering was monitored for \sim 45 min longer at 25°C. In the presence of 2 mM EDTA, FtsZ1/FtsZ2 co-polymers rapidly disassembled, whereas GDP only decreased the light scattering slightly and then rapidly recovered

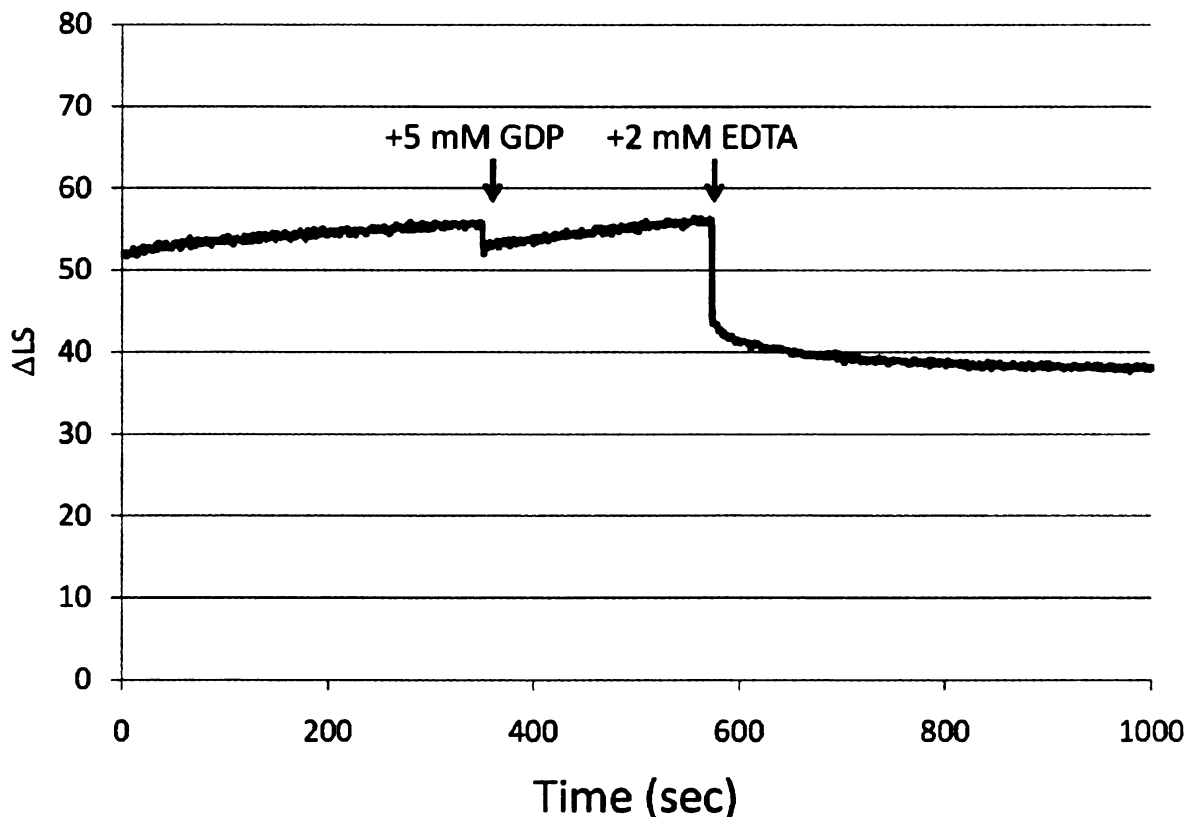


Figure 3.8: The effect of varying the ratio between FtsZ1 and FtsZ2, while keeping the total FtsZ concentration at 5 μ M monitored by light-scattering.

(A) Adding excess FtsZ1 to the polymerization reaction decreases the total polymerization. The total concentration of FtsZ1 and FtsZ2 was maintained at 5 μ M while varying the ratio from 1:1 (\square), 10:1 (\circ), 3:1 (\triangle), 2:1 (\diamond). (B) Excess FtsZ2 also decreases the amount of polymerization proportional to the amount of excess FtsZ2 added to the cuvette, although the decrease in polymerization is greater than the effect of adding FtsZ1. The total concentration of FtsZ1 and FtsZ2 was maintained at 5 μ M while varying the ratio from 1:1 (\square), 1:10 (\circ), 1:3 (\triangle), 1:2 (\diamond). (C) In addition to decreasing the total polymerization of FtsZ1 and FtsZ2, the rate of assembly is decreased by adding excess FtsZ1 or FtsZ2. Rates of polymerization were measured for the light-scattering traces in A and B and compared to each other. Again, adding more FtsZ2 decreases the rate of polymerization more than similar experiments adding excess FtsZ1 suggesting a possible capping role for FtsZ2.

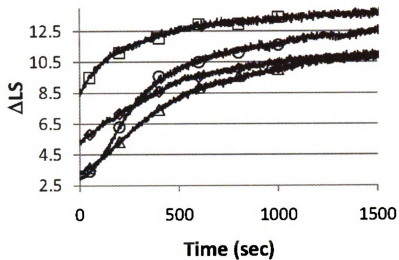
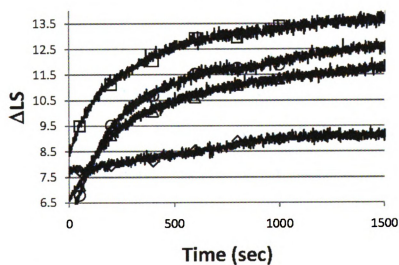
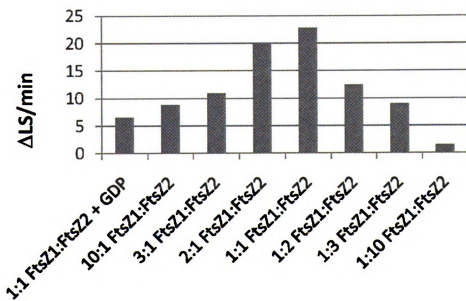
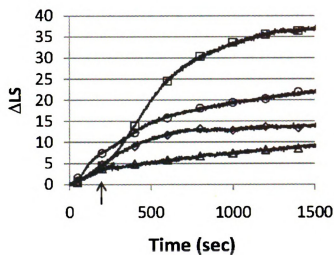
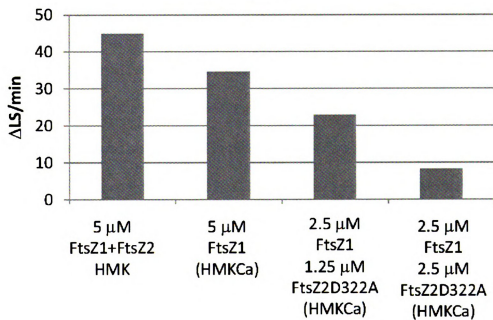
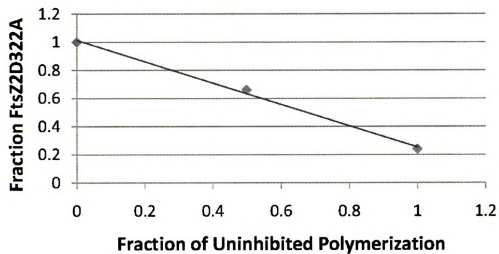
A**B****C**

Figure 3.9: Inhibition of FtsZ1 polymerization by FtsZ2D322A.

To distinguish between lateral and longitudinal inhibition of polymerization, a T7 loop capping mutation, FtsZ2D322A, was tested for competition to FtsZ1 polymerization. (A) Adding FtsZ2D322A steadily decreases the extent of FtsZ1 polymerization. 5 μ M FtsZ1/FtsZ2 in HMK with 1 mM GTP (\square), 2.5 μ M FtsZ1 in HMKCa with 1.25 μ M FtsZ2D322A (\diamond), 2.5 μ M FtsZ1 in HMKCa with 2.5 μ M FtsZ2D322A (\triangle), the arrow indicates when FtsZ2D322A was added to the cuvette for this trace only to demonstrate specific dynamic inhibition. 5 μ M FtsZ1 in HMKCa with 1 mM GTP (\circ). (B) Moreover, the rate of polymerization of 5 μ M total FtsZ1/FtsZ2D322A is 85% less than if 5 μ M total FtsZ1/FtsZ2 is polymerized in the presence of 1 mM GTP. Again, the strong competitive effect of FtsZ2D322A on FtsZ1 polymerization suggests FtsZ2 may cap FtsZ1/FtsZ2 heterofilaments. (C) Linear relationship between the fraction of FtsZ2D322A in the reaction and the fraction of the initial rate of polymerization observed in panel A. The data were fit by the equation $y = -0.76x + 1.0136$, $R^2 = 0.9962$.

A**B****C**

FtsZ2D322A competitively inhibits the polymerization of FtsZ1

Polymerization of plant FtsZ with excess FtsZ1 or FtsZ2 results in shorter polymers. These results suggest FtsZ1/FtsZ2 have a heterofilament polymer topology. Mutations in the T7-loop of FtsZ1 and FtsZ2 were used to probe the heterofilament interface. In *E. coli*, these mutations were previously used to show that the *E. coli* FtsZ filament interface is similar to that in tubulin (Redick et al. 2005; Scheffers et al. 2002), but lateral incorporation into Z-rings is maintained *in vivo* suggesting lateral interaction between filaments is not disrupted (Redick et al. 2005). Thus, our FtsZ1D275A and FtsZ2S322A T7-loop mutants should act as sub-stoichiometric competitive inhibitors (Redick et al. 2005) of GTPase activity and filament formation if FtsZ1 and FtsZ2 are heterofilaments. FtsZ1 was polymerized in HMKCa to stabilize the filaments in the presence of increasing concentrations of FtsZ2D322A. FtsZ1 polymerization is inhibited at increased concentrations of FtsZ2D322A (Figure 3.9A). Furthermore, the reduction in polymerization is proportional to sub-stoichiometric amounts of FtsZ2D322A added to the polymerization assay (Figure 3.9C) and plotting the fraction of FtsZ2D322A (inhibitor) versus the fraction of the initial rate of polymerization for the uninhibited results in a slope of 0.8. Thus, there is a negative linear correlation between the presence of FtsZ2D322A and the initial rate of polymerization. Taken together these data support an FtsZ1/FtsZ2 heterofilament morphology. Moreover, the extent of inhibition of FtsZ1 by FtsZ2D322A is strongly inhibited near a 1:1 ratio, suggestive of a strict heterofilament topology. In a parallel line of experiments, the addition of less than a 1:5 ratio of FtsZ1D275 to FtsZ2 reduced FtsZ2 polymerization in HMKCa below

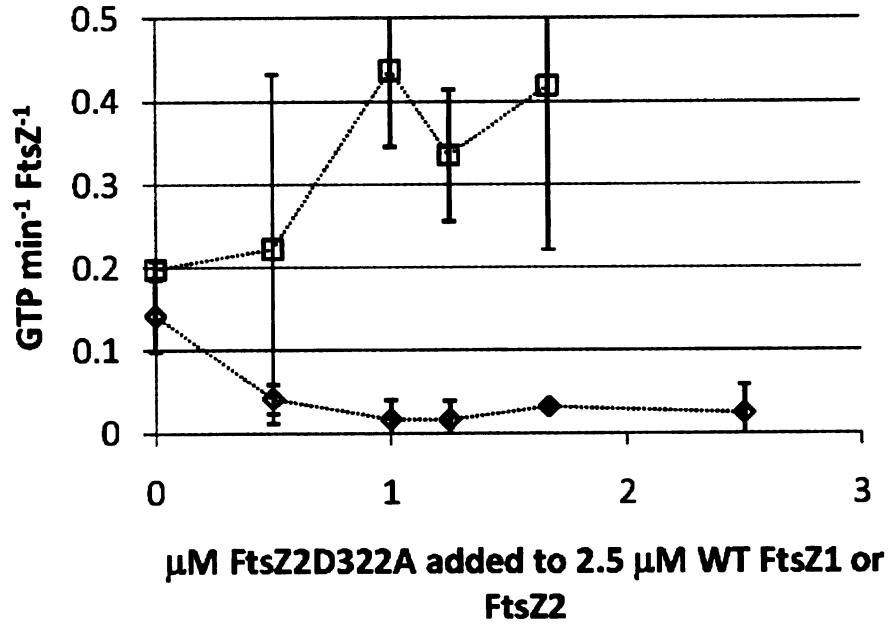
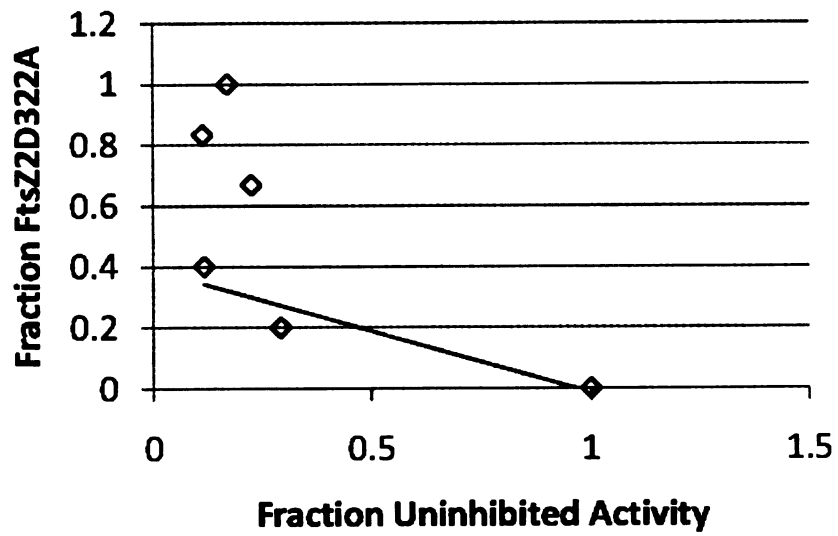
detectable levels suggesting the converse of this experiment is true, but the results are difficult to interpret, because FtsZ2 does not polymerize efficiently by itself.

FtsZ2D322A inhibits the GTPase activity of FtsZ1, but not FtsZ2

In a parallel line of experimentation, the effects of adding increased amounts of FtsZ2D322A to FtsZ1 and FtsZ2 were examined in coupled GTPase assays (Figure 3.10). FtsZ2D322A inhibited the GTPase activity of FtsZ1 in 2 mM GTP in HMK as the concentration of FtsZ2D322A increased (Figure 3.10, \diamond). The negative correlation between the fraction of inhibitor and activity is plotted in Figure 3.10B and has a slope of ~ 0.4 , suggesting half the active sites are inhibited consistent with co-polymerization. When examined by EM, filaments were significantly shortened (Figure 3.4G). Activity was at background levels when the concentration of FtsZ2D322A was greater than 1 μM . In contrast, the GTPase activity of FtsZ2 is stimulated in the presence of FtsZ2D322A. This may result from lateral allosteric activation of the non-mutated protein. At high concentrations of FtsZ2D322A with FtsZ2, visible aggregates were present and were not plotted. Moreover, the high error in the activity estimates for FtsZ2 with FtsZ2D322A is due to signal drift from accumulation of mesh-like structures (seen when examined by EM in parallel). This is suggestive of laterally associated FtsZ2/FtsZ2D322A. Thus the increased GTPase activity of FtsZ2/FtsZ2D322A probably results lateral interactions, not head-to-tail protofilament interactions.

Figure 3.10: Inhibition of the GTPase activity of FtsZ1 and FtsZ2 by FtsZ2D322A in 2 mM GTP in a coupled GTPase assay.

(A) FtsZ1 (\diamond) and FtsZ2 (\square) were assayed for GTPase activity in the presence of increasing concentrations of FtsZ2D322A. Above 1 μ M FtsZ2D322A, FtsZ1 activity was at background levels while FtsZ2 activity was slightly enhanced. (B) The fraction of FtsZ2D322A assayed with FtsZ1 is plotted against the fraction of activity observed. The first three points correlating to detectable levels of activity were fit with the line $y = -0.4041x + 0.3899$, $R^2 = 0.892$. The large error observed for FtsZ2D322A with FtsZ2 is due to the formation of aggregates/mesh-like structures in the presence of high FtsZ2D322A concentrations with FtsZ2 when examined by EM (Figure 3.4H)

A**B**

Plant FtsZ and T7-loop mutants assemble into rings in E. coli

To verify that FtsZ1D275A and FtsZ2D322A mutations do not disrupt protein structure, identical mutations were made in FtsZ1-GFP and FtsZ2-GFP expression vectors in *E. coli*. At an OD₆₀₀ of 1.0, cells harbouring FtsZ-GFP expression plasmids were induced with 0.1 μM IPTG for 2 h. FtsZ1-GFP, FtsZ2-GFP, FtsZ1D275A and FtsZ2D322A were independently visualized by fluorescence microscopy. All four proteins assembled into rings equally spaced along filamented *E. coli* cells (Figure 3.11A and B) reminiscent of the native *E. coli* FtsZ-GFP (Ma et al. 1996). Because all four proteins localize to identical ring-like structures, the same result as performing a similar experiment with *E. coli* FtsZ-GFP (Redick et al. 2005), we conclude the T7-loop mutations do not disrupt the plant FtsZ proteins. GFP color variants of *E. coli* FtsZ are not available, and so plant FtsZ could not be co-localized to native *E. coli* FtsZ rings. Preliminary results also suggest FtsZ1D275A and FtsZ2D322A interact with FtsZ1 and FtsZ2 in the yeast two-hybrid assay.

Discussion

Previous in vitro studies

Two previous studies examined the polymerization of FtsZ1 and FtsZ2 with their transit peptides (FtsZ2 was also C-terminally truncated removing 80 C-terminal amino acids) (El-Kafafi et al. 2005; Gaikwad et al. 2000). In contrast, we constructed AtFtsZ1-1 and AtFtsZ2-1 expression constructs lacking their putative chloroplast transit peptides to be more relevant to physiological forms of FtsZ1 and FtsZ2. For this study, we chose to

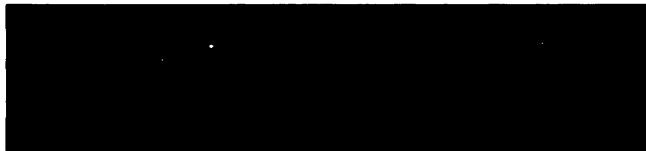
use C-terminally His-tagged proteins. In parallel, we examined N-terminally His-tagged proteins that are thrombin cleavable. Although protein recovery rates from this approach were less, we found that the GTPase activity and assembly of untagged plant FtsZ proteins to be indistinguishable from those of C-terminally His-tagged plant FtsZ (not shown). Moreover, C-terminal His-tags have previously been reported not to affect the polymerization or GTPase activities of various bacterial FtsZs (Huecas et al. 2007a; Oliva et al. 2003). It was previously suggested that full-length FtsZ1 and FtsZ2 do not efficiently polymerize without glutaraldehyde cross-linking (El-Kafafi et al. ; Gaikwad et al. 2000) and our results are consistent with this finding. Here we report that both FtsZ1 and FtsZ2 are required for efficient polymerization (Figure 3.3).

FtsZ1 and FtsZ2 possess all residues known to be important for GTP binding and hydrolysis (Osteryoung and McAndrew 2001) (Figure 3.1), and GTP hydrolysis and GTP binding assays confirmed that both are GTPases (Figure 3.2, Table 3.1). However, plant FtsZ1 and FtsZ2 have significantly slower rates of GTP hydrolysis than *E. coli* FtsZ (Figure 3.2) and FtsZ1/FtsZ2 polymers are far more stable than *E. coli* FtsZ protofilaments. This is not unprecedented; *M. tuberculosis* FtsZ also has low GTPase activity and slow polymer turnover kinetics compared to those of *E. coli* FtsZ (Anand et al. 2004; Borhani and White 2004; Chen et al. 2007; White et al. 2000). Consistent with the stability of the FtsZ1/FtsZ2 filaments *in vitro*, we have observed that Z-rings are visible by immunofluorescence at the mid-plastid in most chloroplasts even in cells in which chloroplasts are not actively dividing (Vitha et al. 2001). Thus, a consequence of a lower GTPase activity may be stabilized Z-rings *in vivo*.

Figure 3.11: Fluorescence microscopy of plant FtsZs fused to GFP expressed in *E. coli*

FtsZ1-GFP, FtsZ2-GFP, FtsZ1D275A-GFP and FtsZ2D322A-GFP are localized to regularly spaced ring-like structure in *E. coli*. This is similar to previous results with T7-loop mutants of *E. coli* FtsZ (Redick et al.). Bar=10 μ m.

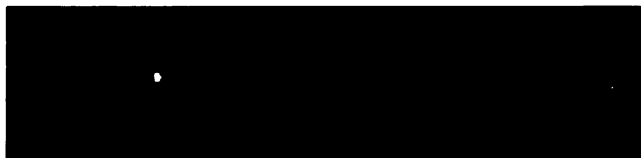
FtsZ1-GFP



FtsZ1D322A-GFP



FtsZ2-GFP



FtsZ2D275A-GFP



This contrasts with *E. coli* Z-rings, which are short-lived during the cell cycle, appearing only just before fission and then disassembling just before the completion of fission (Addinall et al. 1996; Bi and Lutkenhaus 1990a, 1991; den Blaauwen et al. 2003; Harry et al. 1999; Lin et al. 1997; Regamey et al. 2000). The low GTPase activity and stability of FtsZ1/FtsZ2 polymers suggests that plant FtsZ1 and FtsZ2 polymer dynamics may be subject to regulation *in vivo*.

FtsZ1 and FtsZ2 polymerize into heterofilaments

FtsZ1 and FtsZ2 have been shown by immunofluorescence to tightly co-localize to rings at mid-plastid (Vitha et al. 2001), but it was not known if FtsZ1 and FtsZ2 assemble into homofilaments that laterally associate, or if they assemble into heterofilaments (Osteryoung and McAndrew 2001). FtsZ1 and FtsZ2 assemble inefficiently individually, but when mixed equally they assemble faster and more extensively (Figure 3.3) suggesting that FtsZ1 and FtsZ2 are both required for optimum filament formation. In previous work, our lab has shown that manipulation of FtsZ levels disrupts chloroplast division and FtsZ filament morphology *in vivo* (McAndrew et al. 2001; McAndrew et al. 2008; Stokes et al. 2000; Yoder et al. 2007) and performing similar experiments *in vitro* led to the same conclusion: changing the ratio between FtsZ1 and FtsZ2 interferes with polymerization.

Varying the ratio of FtsZ1 and FtsZ2 disrupts the FtsZ1/FtsZ2 co-polymerization longitudinally. In addition, T7-loop mutations were created in FtsZ1 and FtsZ2 that disrupt GTP hydrolysis but not binding (Table 3.1)(Redick et al. 2005; Scheffers et al.

2002). T7-loop mutations in *E. coli* FtsZ specifically disrupt the interface between head-to-tail subunits, impairing protofilament elongation (Redick et al. 2005; Scheffers et al. 2002). Moreover, there is genetic evidence that T7-loop mutations behave analogously in Arabidopsis. Because T7-loop mutants inhibit polymerization, we expect similar mutations to be dominant-negative alleles *in vivo*. As indicated in Appendix A (Yoder et al. 2007), an FtsZ1 mutant, *ftsZ1G267R*, was found to have a mutated T7-loop, GxxNx₂DxxD to RxxNx₂DxxD, and to be dominant-negative. In addition, immunofluorescence of AtFtsZ1-1 and AtFtsZ2-1 showed significantly shortened Z-filaments in homozygous mutants (in young tissue, where the level of the mutant protein is similar to AtFtsZ1-1 levels in wild type plants). We conclude that *ftsZ1G267R* exerts a dominant-negative effect by inhibiting polymerization of FtsZ1/FtsZ2 heteropolymer elongation.

The T7-loop mutation FtsZ2D322A acts as a competitive inhibitor of FtsZ1, but slightly enhances GTP hydrolysis by FtsZ2 (Figure 3.10), suggesting FtsZ2D322A is competing for the head-to-tail GTPase active site of FtsZ1, but does not interfere with the head-to-tail active site formation between FtsZ2 monomers. Moreover, FtsZ2D322A at sub-stoichiometric levels proportionately reduces the polymerization of FtsZ1 (Figure 3.9). FtsZ2 does not efficiently polymerize by itself and FtsZ2D322A did not affect FtsZ2 polymerization (not shown). But interpretation of these results is difficult because FtsZ2 does not efficiently assemble by itself. Taken together these data support a heterofilament model of FtsZ1/FtsZ2 co-polymers (Figure 3.12). Additionally, and while

a ratio of 1:1 FtsZ1/FtsZ2 in bundled heterofilaments is the more stable form of FtsZ, there is no absolute specificity for a strict heterofilament.

If FtsZ1 and FtsZ2 form heterofilaments, the minimum subunit for assembly would be predicted to be an FtsZ1/FtsZ2 dimer, similar to $\alpha\beta$ -tubulin (Caplow and Fee 2002). Indeed, we previously have examined the composition and molecular mass of the FtsZ containing complex (Chapter 2)(McAndrew et al. 2008). We found that FtsZ1, FtsZ2, ARC3 and ARC6 and possibly a protein that cross-reacts with ZipA (Chapter 4) co-fractionate in a salt-stable complex with a mass of ~ 240 kDa. Using the molecular masses of the individual components, this predicts a minimal stoichiometry of the unassembled complex of 1:1:1:1:1, FtsZ1/FtsZ2/ARC3/ARC6/"ZipA". This suggests that the minimal assembly unit found *in vivo* is a dimer of FtsZ1 and FtsZ2 (also with the additional FtsZ binding factors). These facts further support our hypothesis that FtsZ1 and FtsZ2 form heterofilament polymers.

The in vivo stoichiometry of FtsZ1 and FtsZ2

In Chapter 2 (McAndrew et al. 2008) FtsZ1 and FtsZ2 are found to be in a ratio of $\sim 1:2$. Moreover the total FtsZ1 and FtsZ2 concentration in the chloroplast stroma is estimated to average about $1.3 \mu\text{M}$ to $2.6 \mu\text{M}$ (depending on the volume occupied by thylakoids) in three-week old Arabidopsis plants. FtsZ1/FtsZ2 co-polymers assemble rapidly with a critical concentration of $\sim 0.7 \mu\text{M}$. Moreover, maximal assembly of FtsZ1/FtsZ2 ribbons was found at 0.5 mM GTP, which is close to the 0.2 mM concentration of GTP found in the chloroplast (Krause and Heber 1976). Additionally,

0.2 mM GTP in the chloroplast stroma would correlate to very low FtsZ1/FtsZ2 GTP hydrolysis (Figure 3.2A). Thus, under physiological conditions the assembly of FtsZ1/FtsZ2 co-polymers is strongly favored, except that the ratio between FtsZ1 and FtsZ2 is approximately 1:2 (McAndrew et al. 2008). *In vitro*, this ratio would inhibit polymerization of FtsZ1/FtsZ2 co-polymers. So how do FtsZ1 and FtsZ2 attain maximum polymerization into cables? One answer may be that ARC6, an FtsZ2-interacting protein, may stabilize FtsZ filaments and Z-rings *in vivo* (Vitha et al. 2003) by regulating FtsZ2 availability or activity.

In chloroplasts, ARC3 is essential for proper Z-ring positioning to mid-plastid (Glynn et al. ; Maple and Moller 2007a) and is a chimera of an FtsZ GTP-binding domain and a PIP-5-kinase (Shimada et al. 2004). ARC3 specifically interacts with FtsZ1. How might ARC3 function in plastids? In the absence of FtsZ1 *in vitro*, FtsZ2 filament formation is disfavored and stabilization factors are required to visualize polymers by EM (Figure 3.4B). Thus, ARC3 may be an FtsZ1 GTP-exchange factor that stimulates GTP exchange, and hence stabilizes FtsZ rings at mid-plastid. Alternatively ARC3 may sequester FtsZ1 from FtsZ2, thus promoting Z-ring disassembly at sites other than the mid-plastid. However, the finding that ARC3 is localized to mid-plastid rings strongly favors a role of ARC3 being integral to the Z-ring and acting as a GTP exchange factor. The precise localization of ARC3 in the plastid will need to be further clarified to understand its biochemical effects on Z-rings.

Curiously, despite the reduced rate of GTP hydrolysis (13-53 fold less than that of *E. coli* FtsZ) by FtsZ1/FtsZ2 *in vitro*, the *in vivo* dynamics measured by FRAP of FtsZ1-GFP are about 3-times slower (a preliminary measurement) (Vitha et al. 2005) than the *in vivo* dynamics of bacterial FtsZ-GFP (Stricker et al. 2002). This suggests that FtsZ1/FtsZ2 co-polymerization may not be regulated by their internal GTP hydrolysis and assembly rates but possibly by modulation of their biochemical properties by accessory factors such as ARC3 and ARC6. Future *in vitro* work will be essential to defining the biochemical roles of ARC3 and ARC6 and their effect on FtsZ1/FtsZ2 filaments.

Heterofilament bundling

FtsZ1/FtsZ2 heterofilaments bundle into ribbons when examined by EM. When excess FtsZ2 is co-polymerized with FtsZ1 (and stabilized with CaCl₂), FtsZ1/FtsZ2 ribbons appear to spread into fan-like structures with many intersecting individual unbundled filaments apparent (Figure 3.4M and N). The results were similar in the absence of CaCl₂; mixing FtsZ1 and FtsZ2 at 1:5 causes FtsZ1/FtsZ2 filaments within ribbons to “fray” (Figure 3.4J), whereas excess FtsZ1 completely disrupts lateral interactions when mixed at 5:1 in HMK (Figure 3.4K). This suggests a lack of availability for FtsZ2 to laterally interact with FtsZ1, since the amount of FtsZ1 is reduced. This result is different than tubulin, where lateral interactions are α - α and β - β (Nogales 2000). However, we interpret lateral stabilization within FtsZ1/FtsZ2 ribbons to be primarily between FtsZ2 and FtsZ1 (Figure 3.12). Further site-directed mutagenesis

studies will be important to deciphering lateral bundling interactions between FtsZ1 and FtsZ2.

FtsZ1/FtsZ2 are different than tubulin and bacterial FtsZ

Plant FtsZ1 and *E. coli* FtsZ share 41% identity and 61% similarity and FtsZ2 and *E. coli* FtsZ share 37% identity and 61% similarity. This suggests plant and bacterial FtsZ should be biochemically similar. Indeed, plant and bacterial FtsZ both bind and hydrolyze GTP and assemble into protofilaments with similar critical concentrations. However, the biochemical details differ between FtsZ1/FtsZ2 and *E. coli* FtsZ. The most obvious difference is that plant FtsZ1/FtsZ2 assemble more stably than *E. coli* FtsZ and form ribbon-like structures in the presence of GTP without stabilizing agents. In contrast, *E. coli* FtsZ has a high GTPase activity (Figure 3.2B, Table 3.2) and *E. coli* FtsZ filaments disassemble rapidly (Mukherjee and Lutkenhaus 1999) and do not bundle in the absence of stabilizing agents. FtsZ1/FtsZ2 bundling may block nucleotide exchange, perhaps explaining why plant FtsZ1/FtsZ2 polymers cannot be disassembled by GDP.

FtsZ1/FtsZ2 share some similarities with bacterial FtsZ, but in other ways also resemble tubulin. Tubulin forms strict head-to-tail heterofilaments that laterally associate into tubes (Nogales 1999). Laterally associated FtsZ1/FtsZ2 heterofilament ribbons look similar to tubulin when examined by EM (Figure 3.4D and E). However, because FtsZ1 and FtsZ2 are both GTPases and can assemble independently, they probably are not strict heterodimers. However, co-assembled FtsZ1/FtsZ2 is clearly more stable. $\alpha\beta$ -tubulin heterofilament formation is a direct result of a mutation in the

T7-loop of the β -subunit, disrupting GTP hydrolysis in α -tubulin (Nogales 1999). Thus, the most kinetically stable form of tubulin is a strict heterodimer that subsequently assembles into heterofilaments. Likewise, FtsZ1 and FtsZ2 polymerize into a heterofilament (Figure 3.12).

In conclusion, plant FtsZ has retained many similarities to bacterial FtsZ, but has evolved to polymerize more stably like eukaryotic tubulin. Likewise, $\alpha\beta$ -tubulin has evolved an extremely complex regulatory network of accessory proteins, nucleation complexes and depolymerization factors to strictly regulate microtubule assembly spatially and temporally (Nogales 1999). For plant FtsZ1/FtsZ2 heterofilaments the regulation point seems to be at remodeling and disassembly. ARC3 and ARC6 are strong candidates to perform this function.

Why do plants require two types of FtsZ?

Taken together, this study allows speculation as to the evolutionary driving force that resulted in two types of FtsZ in plants. There is precedent for gene expansion of cytoskeletal proteins, notably as FtsZ evolved to tubulin, the array of tubulin types has expanded significantly (Dutcher 2001). Thus, two hypotheses could explain the divergence of two FtsZ types in plants. First, the simplest hypothesis is that there are two types of FtsZ in plants to help overcome dimerization/nucleation for assembly like $\alpha\beta$ -tubulin. In this work, we demonstrate maximum cooperative assembly of FtsZ1 and FtsZ2 requires equal amounts of both. A second hypothesis is that two types of FtsZ are required for Z-ring regulation. Indeed, FtsZ1 and FtsZ2 differ in their specific binding to

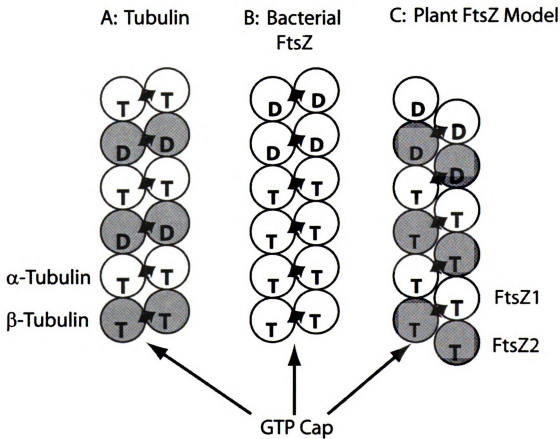
ARC3 and ARC6, respectively. Moreover, ARC3 is a eukaryotically created chimera of an FtsZ, GTP binding domain and a eukaryotic C-terminus. ARC3 binds FtsZ1 and specifies mid-cell positioning of the Z-ring (Glynn et al. ; Maple and Moller 2007a). In contrast, ARC6 specifically binds FtsZ2 to stabilize and organize Z-rings at mid-plastid. Finally, despite two possible explanations for the evolution of two FtsZ types, it is most likely that both nucleation and assembled Z-ring control by the eukaryotic host drove the divergence of two FtsZ types. Future experiments clarifying plant FtsZ nucleation and the biochemical roles of ARC3 and ARC6 will be crucial to further understanding why two types of FtsZ are used for chloroplast division.

Acknowledgements

Special thanks to Dr. Alicia Pastor for training and support of electron microscopy. Dr. Joseph Leykam was an invaluable resource to discuss protein purification and Dr. William Wedemeyer consulted on protein refolding confirmation. Jonathan Glynn consulted in many useful discussions and helpful reading of the manuscript and thanks to Aaron Schmitz for helpful discussions and sharing preliminary findings. This work was supported by fellowships from the MSU Plant Sciences Fellowship program and an N. E. Tolbert memorial fellowship to B.J.S.C. Olson. This work was supported by grant numbers 0092448 and 0544676 from the National Science Foundation.

Figure 3.12: Model of plant FtsZ heterofilament interactions.

(A) Lateral association between $\alpha\beta$ -tubulin is α - α and β - β . $\alpha\beta$ -tubulin is capped by β -tubulin bound to GTP. (B) Bacterial FtsZ protofilaments are believed to laterally interact, but the mechanism is unknown. (C) Model of the FtsZ1/FtsZ2 heterofilament. FtsZ1/FtsZ2 lateral interaction is between FtsZ1 and FtsZ2, differing from tubulin. FtsZ1/FtsZ2 filaments are also GTP capped, but the cap could be either FtsZ1 or FtsZ2.



CHAPTER FOUR

THE SEARCH FOR AN ANALOGUE TO THE BACTERIAL CELL DIVISION PROTEIN ZIPA BY COMPUTATIONAL AND EXPERIMENTAL APPROACHES

B. J. S. C. Olson performed all experiments except those outlined Figures 4.6 and 4.7 and wrote the chapter.

Introduction

The division of chloroplasts is mediated by two families of FtsZ proteins, FtsZ1 and FtsZ2, which are homologues of the bacterial cell division protein FtsZ (Osteryoung 2000; Osteryoung and McAndrew 2001; Osteryoung and Pyke 1998; Stokes et al. 2000). Plant and bacterial FtsZ share significant sequence similarity (Osteryoung 2001), supporting the endosymbiotic origin of chloroplasts (Margulis 1971, 1975), and FtsZ2 family proteins share a conserved C-terminal motif with bacterial FtsZ (Osteryoung and McAndrew 2001). Despite the conservation of FtsZ in the division of chloroplasts, several bacterial cell division proteins have no obvious homologues in plants, such as ZipA, FtsA and MinC (discussed in chapter 1). A key question is: have new proteins evolved to replace the functions of these “missing” proteins, or have the progenitors of these proteins retained their core structures, but diverged enough in their sequences to be no longer detectable by sequence similarity searches? The work described here attempted to address this question and possibly identify a plant analogue to the bacterial cell division protein ZipA.

In bacteria, FtsZ proteins are anchored to the membrane by two proteins, ZipA and FtsA; the later is in the same structural super-family as actin/HSP70 proteins (Bork et al. 1992; van den Ent and Lowe 2000). Both ZipA and FtsA interact with the extreme carboxyl terminus of *E. coli* FtsZ (Addinall and Lutkenhaus 1996; Hale and de Boer 1999; Hale and de Boer 1997; Haney et al. 2001; Liu et al. 1999; Wang et al. 1997; Yan et al. 2000) and anchor the FtsZ ring to the inside of the cell membrane by an integral

membrane domain (Hale and de Boer 1997). In contrast, FtsA is a peripheral membrane protein (Addinall and Lutkenhaus 1996). Both FtsA and ZipA are required for interaction with downstream cell division proteins (Pichoff and Lutkenhaus 2002). The crystal structure of ZipA complexed with the carboxyl terminus of FtsZ has been solved (Mosyak et al. 2000). Based on the quaternary structure of tubulin (Li et al. 2002) the ZipA/FtsZ interacting domain is believed to stick out of assembled FtsZ filaments (Nogales 2000).

Despite the conservation of the ZipA/FtsA binding motif in FtsZ2 (chapter 1, Figure 1.1)(Osteryoung 2001), neither ZipA nor FtsA have been identified in plants, though both functions together are essential to bacterial cell division. The presence of the ZipA binding domain in FtsZ2 suggested that a ZipA-like protein may be involved in chloroplast division. In an attempt to identify a ZipA protein in chloroplasts, two parallel approaches were utilized. First, a partially purified FtsZ-containing complex from pea chloroplasts (McAndrew et al. 2008) was probed by immunoblotting with an antibody to *E. coli* ZipA. The antibody detected a protein of ~35 kDa that co-fractionates with FtsZ through various purification steps. Although the identity of the protein that cross-reacts with the ZipA antibody was not determined, future efforts may elucidate its identity now that the work described below tightly links this protein to the pea FtsZ complex. Second, a novel structural search algorithm was developed and utilized to identify a putative Arabidopsis protein, Ssz1, with structural similarity to ZipA. However functional analysis of this gene did not unequivocally link it to a role in chloroplast division.

Results

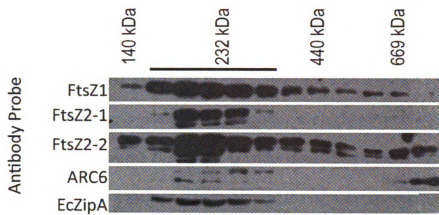
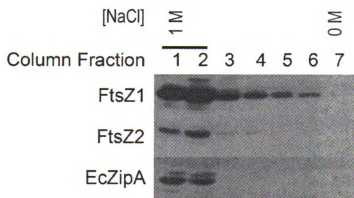
Chloroplasts contain a protein that cross-reacts with a ZipA antibody and co-fractionates with FtsZ during partial purification

To find if a ZipA-like protein is involved in chloroplast division, an antibody to *E. coli* ZipA was obtained (Hale and de Boer 1999) and tested for cross-reactivity with chloroplastic proteins. The ZipA-specific antibody did not recognize a protein in isolated intact *Arabidopsis* chloroplasts, but recognized a ~35 kDa protein in isolated pea chloroplasts (R. S. McAndrew, unpublished observation). To test if the ZipA cross-reactive protein may have a role in chloroplast division, n-dodecyl- β -D-maltoside (DDM) solubilized pea chloroplasts were separated by sucrose density gradient fractionation as described above (chapter 2)(McAndrew et al. 2008). Sucrose density gradient fractions were probed by immunoblot with antibodies to FtsZ1, FtsZ2, ARC6 and ZipA. Proteins recognized by these antibodies co-fractionated near the top of the sucrose density gradient between 210-240 kDa (Figure 4.1A). In separate experiments these proteins were also found to co-fractionate with ARC3 (McAndrew et al. 2008).

To further investigate interaction between the protein recognized by the ZipA antibody and FtsZ1 and FtsZ2, a series of additional purification steps were performed after sucrose density gradient fractionation. First, fractions 3-10 from the sucrose

Figure 4.1: FtsZ1, FtsZ2, ARC6 and a protein that cross-reacts with an antibody to *E. coli* ZipA cofractionate in sucrose density gradients, native PAGE and by hydrophobic interaction chromatography.

Isolated pea chloroplasts were lysed in the presence of DDM and soluble proteins were fractionated on a sucrose density gradient. Proteins in the fractions shown were acetone-precipitated and analyzed by SDS-PAGE and immunoblotting using AtFtsZ1-1, AtFtsZ2-1 and AtFtsZ2-2 specific antibodies as described (McAndrew et al. 2008). (A) Analysis of fractions from a 5-20% sucrose density gradient. FtsZ1, FtsZ2, ARC6 and a protein that cross-reacts with an *E. coli* ZipA antibody co-sedimented in a mass range of ~210-240 kDa, indicated with a bar above the immunoblots. (B) The peak FtsZ-containing fractions (indicated by the bar in panel A) were pooled and subjected to native PAGE and analyzed by immunoblot. FtsZ1, FtsZ2 and the protein that cross-reacts with the *E. coli* ZipA antibody again co-separate at ~220 kDa. (C) The peak FtsZ-containing fractions indicated by the bar in panel A were pooled and subjected to hydrophobic interaction chromatography using a 1 M to 0 M NaCl elution gradient. FtsZ1, FtsZ2, and a protein that cross-reacts with the *E. coli* ZipA antibody co-eluted in the same fractions, between 1 M and 0.8 M NaCl, indicated by the bar above the immunoblots

A**B****C**

density gradient corresponding to ~210-240 kDa were pooled (McAndrew et al. 2008)(Chapter 2, Figure 2.7), concentrated by ultrafiltration, separated by native PAGE and analyzed by immunoblot using antibodies to FtsZ1, FtsZ2 and ZipA (Figure 4.1B). The mass of this complex is approximately 220 kDa, significantly higher than the 35 kDa mass of the protein recognized by the ZipA antibody under denaturing conditions, suggesting they are in a complex together. The stability of the complex containing FtsZ1, FtsZ2 and the ZipA cross-reactive protein was investigated by performing hydrophobic interaction chromatography on sucrose density gradient fractions containing these proteins (Figure 4.1B indicated with a bar). Immunoblot analysis of hydrophobic interaction chromatography fractions eluted with a 1 M to 0 M NaCl gradient shows that FtsZ1, FtsZ2 and the ZipA cross-reactive protein co-elute (Figure 4.1C).

In order to identify the protein that cross-reacts with the ZipA-specific antibody, a series of proteomic experiments were employed on various fractions containing FtsZ and ZipA. First, bands from the native PAGE gel, at a molecular mass of ~220 kDa where FtsZ1, FtsZ2 and the ZipA cross-reactive protein migrated, were cut out of the gel, digested with trypsin and subjected to tandem mass-spectrometry. Proteins were identified by molecular ion fingerprinting using the predicted mass fragments of proteins in the Arabidopsis genome (even though the protein was isolated from pea). The positive control for the experiment is identification of either FtsZ1 or FtsZ2 in the complex; however, neither protein was identified and none of the other identified proteins were strong candidates to be ZipA (not shown). Moreover, most of the strong

fingerprints identified were that of the chloroplast metabolic pathways and probably contaminants.

A series of additional experiments were attempted by immunoprecipitation of the FtsZ complex from sucrose density gradient fractions (Figure 4.1A, indicated by the bar) and then performing proteomic analysis. However, no strong candidates for a putative ZipA were identified (not shown). The current identity of the ZipA cross-reactive protein is unknown, but the recent 454 sequencing of a pea cDNA library recently created at Michigan State University (Andreas Weber and Andrea Braeutigam, personal communication) could be pursued to identify the ZipA cross-reactive protein in pea.

Identification of a structural analogue to the bacterial cell division protein

ZipA

In bacteria, the FtsZ ring is believed to be organized near the membrane at the division site by the action of two essential division proteins, ZipA and FtsA. FtsZ2 family proteins contain a conserved C-terminal domain that in bacteria is responsible for binding to these proteins. This suggests that ZipA and/or FtsA homologues are involved in chloroplast division. Attempts to identify a homologue of bacterial ZipA in plants based on sequence similarity has been unsuccessful due to the general lack of conservation of primary amino acid sequence among known ZipA proteins (Du and Arvidson 2003).

Figure 4.2: Overview of the structural threading search algorithm used to identify a putative Arabidopsis chloroplastic protein with structural similarity to ZipA, Ssz1.

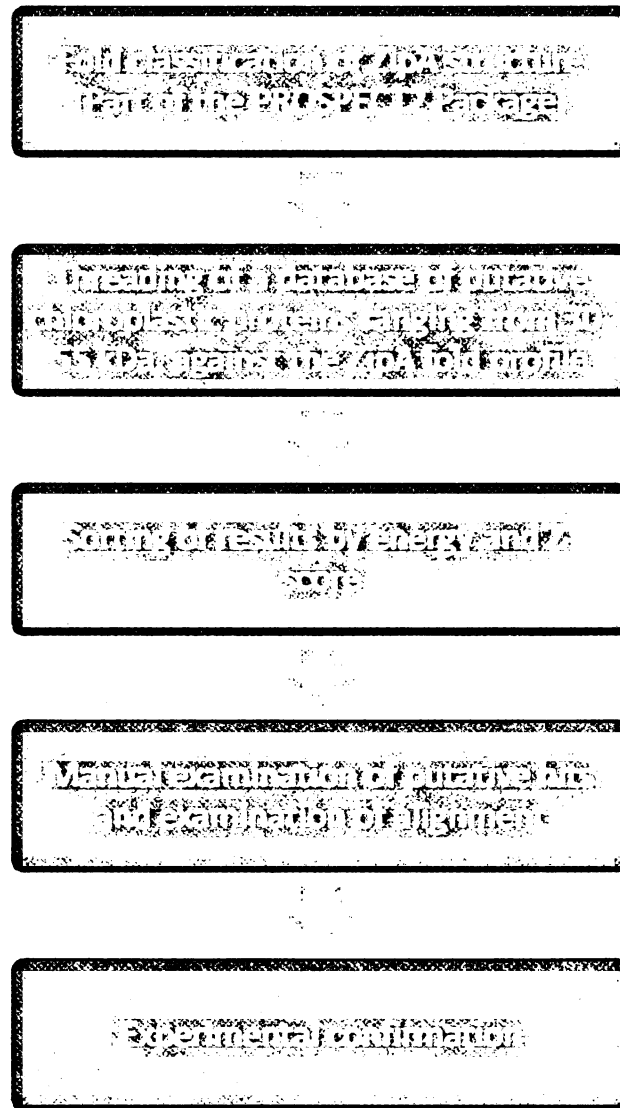


Table 4.1: Candidate proteins structurally similar to *E. coli* ZipA.

List of high-ranking proteins from a database of putative chloroplastic Arabidopsis proteins in the filtered database that had a high likelihood of being the same structure as the C-terminus of ZipA (1f46). Z-score is a measure of likelihood that the structure is correct and a number greater than 6 is significant. Asterisk indicates the gene for Ssz1. Genes where an associated T-DNA insertion was available and examined are listed.

<u>Gene (AGI Number)</u>	<u>Z-score</u>	<u>Annotation in TAIR</u>	<u>Chloroplast Division Phenotype?</u>
AT4G08790	5.35	Nitrilase activity, nitrogen compound metabolic process	No*
AT3G19680	6.45	Chloroplast protein, molecular function unknown, biological process unknown	No*
AT1G50040	4.85	Chloroplast protein, molecular function unknown, biological process unknown	Not Available
AT3G51930	4.43	Transducin family protein / WD-40 repeat family protein	Not Available
AT1G79050	9.65	DNA repair protein recA; Identical to DNA repair protein recA homolog 1, chloroplast precursor (RECA)	Not Examined
AT4G33540*	12.9	Metallo-beta-lactamase family protein; similar to hypothetical protein OsJ_008663	Slightly fewer enlarged chloroplasts
AT1G37063	7.57	Transposable element gene; transposase-related, weak similarity to Tam3-transposase	Not available

*Genotype was only confirmed once, both homozygous and heterozygous plants were examined.

Since there is a crystal structure for *E. coli* ZipA (EcZipA, Mosyak et al. 2000; Moy et al. 2000) I attempted to detect a structural analogue of ZipA in a database of proteins predicted to be targeted to chloroplasts (overview of the approach, Figure 4.2). The amino acid sequence for *E. coli* ZipA was used to produce a structural profile using the threading algorithm in the PROSPECT2 software package (Xu and Xu 2000). *E. coli* ZipA has a MW of 36.4 kD so a database of approximately 4,000 predicted chloroplast proteins was filtered for those that had a MW range of 35-55 kD. The logic was that a chloroplastic ZipA homologue would have to acquire a chloroplast transit peptide, thus lengthening the protein. Moreover, an *E. coli* ZipA-specific antibody recognizes a protein of about 35 kDa in pea. A filtered database was used for this analysis because of the large amount of computational time required for the analysis. Proteins in the database were threaded into the crystal structure for *E. coli* ZipA. The threaded structures were then sorted and analyzed by their z-scores. Seven strong hits were identified as putative candidates (Table 4.1). Analysis of the structural alignments between known ZipA proteins and these candidates revealed that the locus At4g33540 (called Ssz1, structurally similar to ZipA, Ssz1) was a strong candidate to contain the C-terminal FtsZ binding domain of ZipA. Examination of the threaded Ssz1 structures showed that structural contacts between *E. coli* ZipA and *E. coli* FtsZ would be conserved if Ssz1 were to bind AtFtsZ2, thus further supporting this locus as a candidate ZipA analogue (Figure 4.3, Table 4.2). Of note is the fact that only the carboxyl terminal region of the Ssz1 is structurally similar to ZipA and that Ssz1 lacks an amino terminal transmembrane domain believed to be involved in anchoring ZipA to the membrane.

Ssz1 on the other hand has weak similarity to β -lactamases and glyoxylases. It is unclear if Ssz1 has β -lactamase or glyoxylase activity. However, β -lactamases are found in the cell wall of bacteria and there is some evidence that chloroplasts may have bacterial cell wall material (murein) at the division site (Katayama et al. 2003; Machida et al. 2006).

Phenotype of a T-DNA insertional mutant for ssz1

The SALK T-DNA insertional line 039451 contains a T-DNA insertion annotated as being in exon 4 of Ssz1 (Figure 4.4). This insertion is expected to abolish expression or produce a truncated Ssz1 protein. Seeds were obtained from the ABRC at Ohio State University, grown in soil and analyzed for their genotype and phenotype. Out of 37 plants initially grown, line number 17 was found to be homozygous for the T-DNA insertion based on PCR analysis of the At4g33540 locus (Figure 4.4B). Samples from the leaves of these plants were examined by microscopy (Figure 4.5A). Compared to three-week-old wild-type plants there are slightly fewer, enlarged chloroplasts in three-week-old SALK_039451 plants (Figure 4.5B), suggesting that Ssz1 may be involved in chloroplast division. Furthermore, analysis of chloroplast number per cell plan area showed fewer chloroplasts per cell area. In the future the phenotype needs to be unequivocally linked to the genotype by backcrossing the SALK_039451-171 into a wild-type background.

Ssz1 is a Stromal Chloroplast protein

In order to interact with FtsZ2 in the chloroplast, Ssz1 would have to be stromal-localized like FtsZ2. To test if Ssz1 is a chloroplastic protein, it was translated *in vitro* in the presence of [³⁵S]-methionine and imported into chloroplasts as previously done to determine stromal localization of AtFtsZ1-1, AtFtsZ2-1 and AtFtsZ2-2 (McAndrew et al. 2001) and inner envelope membrane localization of ARC6 (Vitha et al. 2003). Following import, chloroplasts were treated with thermolysin and trypsin, which digests proteins outside the chloroplast and in the inner membrane space (Cline et al. 1984). Chloroplasts were fractioned into membrane and stromal fractions and analyzed by SDS-PAGE and autoradiography.

The Ssz1 translation product (Figure 4.6A, TP) migrates near its predicted molecular mass of ~50 kDa. A band corresponding to the translation product (indicated as “pSsz1”) was observed in chloroplasts that were untreated by thermolysin as well as a lower mass band (indicated by “mSsz1”, Figure 4.6A). The upper mass band was not present in chloroplasts treated with thermolysin or trypsin, but the lower band was present and corresponds to the ~40 kDa mass predicted for Ssz1 without its putative transit peptide (53 amino acids)(Figure 4.6A, lanes 4 and 6). Lysing the chloroplasts with Triton X-100 resulted in the digestion of both pSsz1 and mSsz1 (not shown), demonstrating that the proteases were active. In control experiments, the small-subunit of RuBisCo (Figure 4.6B) was also found in the stroma, demonstrating Ssz1 is an imported protein.

Figure 4.3: Alignment of *E. coli* ZipA with its potential structural analogue in *Arabidopsis*.

Identities are highlighted in black, similarities determined by a PAM250 matrix are highlighted in gray. ZipA is structurally similar to AT4G33540 from residue 190-328 in ZipA. Columns marked with "+" indicate residues in *E. coli* ZipA that are involved in interacting with FtsZ (Mosyak et al., 2000) and are chemically similar in AT4G33540 and predicted to maintain favorable contact with the C-terminal region of AtFtsZ2-1. Columns marked with a "~" are not chemically identical, but in AT4G33540 they would make favorable contacts to AtFtsZ2-1. Columns marked with a "#" would not be favorable contacts. A full alignment of a sub-set of proteins with sequence similarity to Ssz1 is in Figure 4.8.

1
-----MMQDL--R-LILLIIVGAI-AIIALLVHGFWTSRKERSMFRDRPLAR---MKSKR--DDDSY--DE---
MASAFSAVSSLSYQFRSKEAIFSSKASCFSSTALSGRRVFGSIKAAQVTSHEPRTONVEGDI FVDNTCIDCDTCRW
1

55
-----DV-EDDEGVGEV-RVERVNH---APA-NAQE---HEAAR-PSPOHQY-OPPYASAQPRQPVPQPPPAQ-VPP
MVPPIRKQIFSDLSSQDLFTRVDNMSAVTKQPTCKEIRLNALQALLSCTGSIINTQTPPADIGMAQTFPLVVDKDTLFPV
81

116
QHAP--HHPAQ-PVQQPAAVQPPEQLQQPVSPQVAPAPQPVHSAIPQA-QQAEPQPAEPVAAPOPEPVAEPAPV-M--DK
LFNPLSFHFFFRMVINNRVVEKLAGKIMKGGVRYMFLTHRDDVADHKKWADREKSTRILHEDDDVEPSTSDVELKLEGS
161

188
+ + + + +
PKRK-EAVITMNVAAHHGSEFNGELLNBIQQAG-FIEGDMNTYHRHSPDGGSPAFELSLANMVKPGTFDPEMKDFTTPG
PWSIYEDVELIHTPGHSEVSI-SNC--KNHKNKCSIEGVCMPHKSJ-----K--ALFFKGDHVIMTEHGLSILHQYNHGS
241

266
~ ++ + + +
VTIFMQVPSYGDDELQNFKLMLOSAQHIADDEVGVVLDQORRMTP-OKLREYODIIREVVKDANA 328
VPLQANVEKLINI-DENWLIPEGRRVHFKDC-D-KAKNLEALVOKHREKOLVSFSKSGKA 371
312

Table 4.2: Residue contact comparison between ZipA bound to *E. coli* FtsZ and Ssz1 bound to the plant FtsZ2 C-terminus.

Residues in the structures of the *E. coli* FtsZ C-terminus that contact residues in *E. coli* ZipA (from structure 1f46) compared to how the threaded structure of Ssz1 (Structural based sequence alignment in Figure 4.3) would contact the AtFtsZ2-1 C-terminus.

<i>Amino Acid in the EcZipA crystal structure or equivalent residue in Ssz1</i>		<i>Interacts with this amino acid in EcFtsZ or AtFtsZ2-1</i>		
<u>EcZipA</u>	<u>Ssz1</u>	<u>EcFtsZ</u>	<u>AtFtsZ2-1</u>	<u>Notes</u>
R305/R306	K348/N349	Y371	S460	
M248	V294	L372	V461	
K250	M296	D373	E462	Contact is between the non-polar portion of K250, this would be a similar in the AtFtsZ2-1 and AT4G33540 interaction
T267	P313	None	None	Side chain is solvent exposed
I196	I250	I374	I463/P464	
		P375	P464	Solvent exposed, locks a side chain turn in place
		A376	E465	A376 of EcFtsZ interacts with the hydrophobic region of R379 in EcFtsZ, in AtFtsZ2-1 E465 would interact favorably with K468. Also see F269 in ZipA
M226	V272	F377	F466	F377 in EcFtsZ interacts with L378 in EcFtsZ, in AtFtsZ2-1 this would be F466 interacting with L467
V194	V248	L378	L467	See the above note
F269	Q315	A376/F377	E465/F466	See the note for A376 in EcFtsZ
		R379	K468	Solvent Exposed
		K380	K469	Solvent Exposed
M226	V278	Q381	K470	In ZipA, EcFtsZ interaction the interaction is between the hydrophobic part of Q381 and M226, The charged part of the side chain is solvent exposed; a similar interaction would be expected between V278 of AT4G33940 and AtFtsZ2-1 with the charged head group solvent exposed.

Following import, protease protection and protease removal, chloroplasts were hypotonically lysed and fractionated into soluble and membrane fractions. The membrane fractions were washed four times with lysis buffer to remove residual soluble protein and analyzed by SDS-PAGE and autoradiography. Ssz1 was found to be a soluble stromal protein and in the soluble fraction (Figure 4.6A, lane 4 and 6). These results confirm the prediction that Ssz1 is indeed a stromal chloroplast protein as predicted from bioinformatic analysis opening up the potential to be involved in chloroplast division.

Removal of the Ssz1 homologue in *Synechococcus elongatus* does not disrupt FtsZ filament morphology

The phenotype of an Arabidopsis T-DNA insertion in Ssz1 is slightly fewer and enlarged chloroplasts. Ssz1 was identified on the basis of being a candidate FtsZ2 interacting protein with structural similarity to bacterial ZipA. This predicts that Ssz1 mutants would exhibit perturbed Z-ring morphology (McAndrew et al. 2001) as has been observed for disruptions in the FtsZ2 binding protein ARC6 (Vitha et al. 2003). Ssz1 has an ortholog in the cyanobacterium *Synechococcus elongatus* (locus syc1416) and disruption of the gene should lead to a perturbed Z-ring morphology. A knockout allele, *Ssz1* Δ , was created by homologous recombination mutation using the cloned *Ssz1* allele with a resistance marker to spectinomycin inserted into the middle of the gene. After segregation of the knockout line by selection on spectinomycin *Ssz1* transcript was no

longer observed (not shown) and the wild-type *Ssz1* could not be detected by PCR (not shown). *Ssz1*Δ mutants and wild-type cells were analyzed by immunofluorescence microscopy with an antibody to FtsZ (Miyagishima et al. 2005) and the Z-ring morphology was the same in both wild-type and *Ssz1*Δ strains of *Synechococcus* PCC 7942 (Figure 4.7).

Ssz1 does not interact with FtsZ2 in the yeast-two hybrid assay

To test if *Ssz1* interacts with plant FtsZ2, an initial yeast two-hybrid assay was performed between *Ssz1* and FtsZ2 in the Matchmaker I® system (Clontech). Initial results suggested the proteins interact (not shown). However, when *Ssz1* was re-tested against an empty vector it was found to autoactivate the His reporter (not shown). Problems with autoactivation are well known in this yeast two-hybrid system and so this interaction was re-tested in an alternate system with fewer technical problems.

Figure 4.4: PCR analysis to identify a homozygous SALK_039451 mutant of in *Ssz1*.

(A) PCR analysis of SALK_039451-17 (homozygous), SALK_039451-18

(heterozygous) and WT Col-0. For each line, two PCR reactions were performed. The first reaction probed for the presence of an intact WT allele (primers gAt4g33540-L and gAt4g33540-R, expected product size 1685 bp) and the second reaction confirmed the presence of the T-DNA in the gene (primers LBb1 and gAt4g33540-R). Arrows indicate the PCR product for the WT allele and T-DNA PCR products. (B) Diagram of the gene structure for *SSZ1* (At4g33540) and the position of PCR primers used to analyze the T-DNA insertion of SALK_039451 and the expected bands for WT and insertional alleles. In addition, the location of the T-DNA is indicated in exon 4.

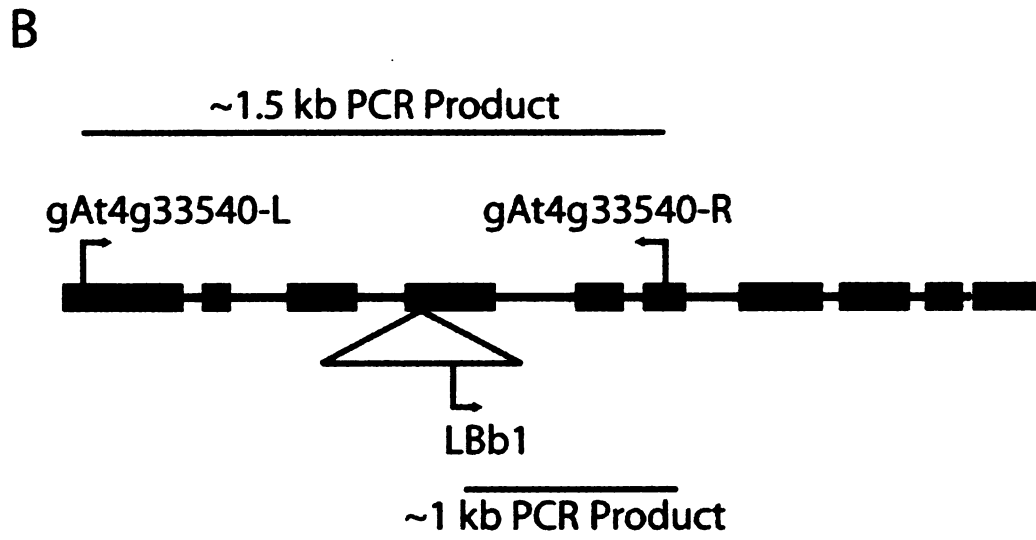
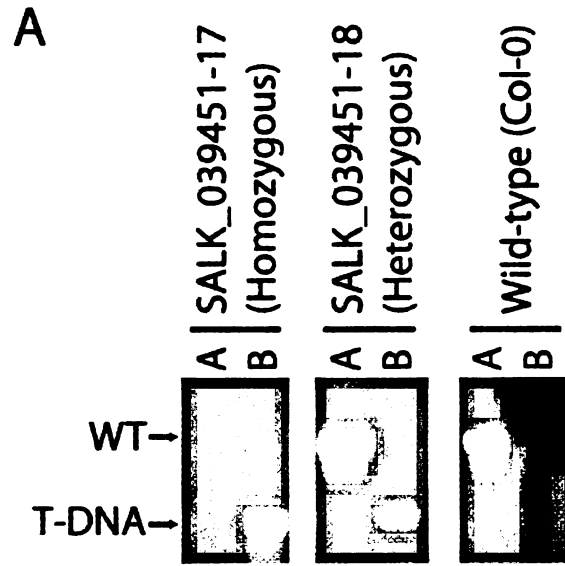
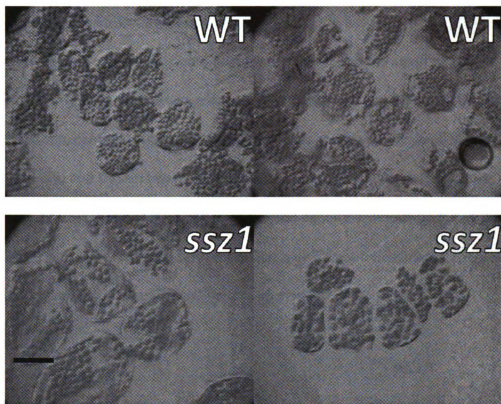


Figure 4.5: Comparison of WT and Salk 039451 cells.

(A) Photomicrographs of fixed Arabidopsis tissue under 40X magnification of either WT Col-0 or Salk 039451 (labeled *ssz1*). Bar=50 μm . (B) The chloroplast number versus cell area was measured and plotted for thirteen cells for either WT (○) or Salk_039451 (□) and fit with a linear regression. R^2 for WT is 0.71 and for Salk 039451 is 0.55.

A



B

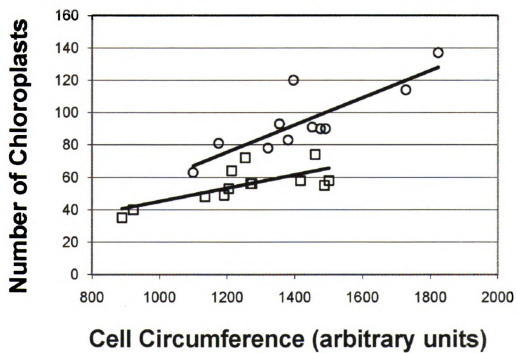


Figure 4.6: Chloroplast import assay of Ssz1.

Autoradiograph of SDS-PAGE of import assays of Ssz1 and the small subunit of rubisco (SS). "TP" = in vitro translation product; "P" = Pellet fraction; "S" = soluble protein after 10 min. centrifugation at 20,000 g. Ssz1 was soluble and protected from thermolysin (lane 4) and trypsin treatment (lane 6). Pre-Ssz1 (pSsz1) migrated at ~50 kDa, mature Ssz1 (mSsz1) migrated at ~40 kDa. Control experiments with SS found the mature SS (mSS) was protected from both thermolysin and trypsin treatment. These results demonstrate both Ssz1 and SS are soluble stromal proteins.

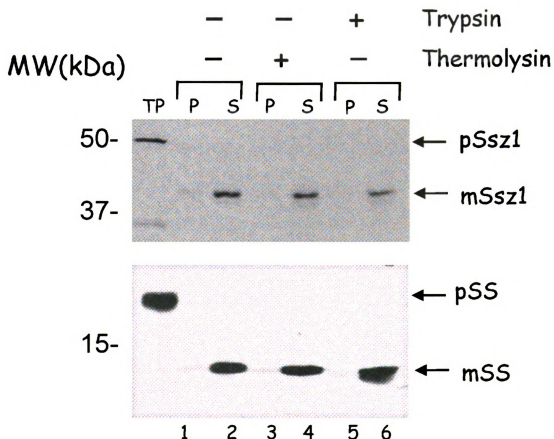
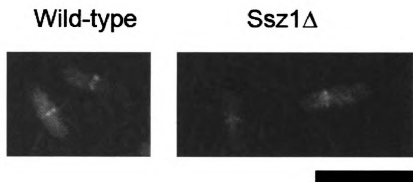


Figure 4.7: Immunolocalization of FtsZ in wild-type and Ssz1 Δ *Synechococcus* PCC 7942.

FtsZ ring morphology at mid-cell is not disrupted by the disruption of Ssz1 with spectinomycin resistance. Black bar = 20 μ m



In order to re-test if FtsZ2 and Ssz1 might directly interact, they were tested for interaction in the Matchmaker III yeast-two-hybrid assay from Clontech®. Ssz1 was found not to autoactivate this His reporter (Table 4.3). Moreover, Ssz1 did not interact with FtsZ2 (Table 4.3). The positive control worked as reported (Maple et al. 2005) (ARC6-E4 against FtsZ2, indicated by “+++++”). Negative controls (empty vectors) had weak autoactivation (indicated by a “+”). While initially promising for an interaction between FtsZ2 and Ssz1, more rigorous testing demonstrates that it is unlikely that FtsZ2 and Ssz1 directly interact (Table 4.3).

Discussion

Structure Similarity Search Algorithm Development

One significant limitation of homology-based database searches is that they do not take into account 3D protein folding information for identification of homologues. There are many examples of protein families with similar functional activity or structure but lacking sequence homology (e.g. Fribourg and Conti 2003; Matsuo et al. 1996). With a large portion of the sequenced eukaryotic genomes having no known sequence homologues, I sought to develop a novel method for identifying proteins by structural homology. Most proteins do not have an experimentally determined structure; in lieu of experimental data an algorithm must be used for structural prediction *in silico*. Currently, most algorithms utilize sequence homology to predict structure (e.g. Guex and Peitsch 1997). Since the interest of this analysis focuses on

Table 4.3: Summary of a yeast two-hybrid interaction assay between Ssz1 and FtsZ2.

The interaction between both proteins was assayed with a His-reporter growth assay as previously described (Maple et al. 2005). Ssz1 was cloned without its putative 53 amino acid transit peptide into pGADT7 or pGBKT7 and tested against either FtsZ2-1 without its transit peptide or just the C-terminus of the protein (Maple et al. 2005). As a positive control, exon 4 of ARC6 was tested for interaction with FtsZ2-1(CTD) (Jonathan Glynn, personal communication). “++++” reports overgrowth of the yeast streaked on a drop-out plate lacking His. “+” reports less than five colonies when streaked on a drop-out plate lacking His. “None” reports that no colonies grew on the plate after four days at 30°C. All assays were performed in parallel on the same drop-out plate lacking His.

<u>Bait (in pGADT7)</u>	<u>Prey (in pGBKT7)</u>	<u>Growth on +His</u>	<u>Growth on -His</u>
Ssz1Δ53	FtsZ2-1	+++++	None
Ssz1Δ53	FtsZ2-1(CTD)	+++++	None
Ssz1Δ53	pGBKT7(Empty vector)	+++++	+
pGADT7(Empty Vector)	FtsZ2-1	+++++	None
ARC6-E4	FtsZ2-1CTD	+++++	None
pGADT7(Empty Vector)	pGBKT7(Empty Vector)	+++++	+
ARC6-E4	FtsZ2-1	+++++	+++++

proteins without sequence homology an algorithm was needed that could predict 3D structures accurately, quickly and without homology information. Protein threading algorithms address these needs by placing the sequence of an unknown structure into the solved structure and evaluate the likelihood that this structure is correct (Xu and Xu 2000). This is then repeated for an entire database of solved structures and key candidate structural models are created. Threading relies on the fact that functionally related proteins often contain the same structural folds while not necessarily having similar sequences (Gerstein and Levitt 1997).

All plant FtsZ2 proteins contain C-terminal domain conserved with bacteria (Osteryoung and McAndrew 2001). In bacteria this conserved domain interacts with the cell division proteins ZipA and FtsA. Thus, we deduce that ZipA and/or FtsA function are conserved in chloroplast division. Previous attempts to identify a ZipA homologue in plants based on sequence homology have been unsuccessful. This might follow from a report that suggests the sequence of ZipA is not well conserved in bacteria (Nishida et al. 2003). One possibility is that the function of ZipA has been replaced by other proteins such as the actin-like protein FtsA. Work in bacteria has shown that FtsA can perform functions attributed to ZipA in *E. coli* (Geissler et al. 2003). In light of our limitations in identifying proteins based on structural homology, I developed an algorithm to search a database of proteins for structural homology instead of sequence homology. This analysis resulted in the identification of the putative ZipA-like protein Ssz1.

Ssz1 displays fewer and slightly enlarged chloroplasts (Figure 4.5), initially suggesting Ssz1 may play a role in chloroplast division. Ssz1 was confirmed as a chloroplastic protein (Figure 4.6). However, Ssz1 did not interact with FtsZ2 in the yeast two-hybrid assay and a knockout of Ssz1 in the cyanobacterium *Synechococcus* PCC 7942 did not show a cell division defect phenotype, nor was the FtsZ filament morphology disrupted (Figure 4.7). Multiple attempts at generating plants expressing a GFP-tagged version of the Ssz1 have been unsuccessful. Additional attempts were made to pull down either FtsZ1 or FtsZ2 with recombinant GST-Ssz1 added to plant extracts. These attempts were not successful. Moreover, based on the inability of Ssz1 to interact with FtsZ2 in a yeast-two-hybrid assay would suggest Ssz1 is probably not localized to mid-plastid division rings. Additionally, an attempt to complement a temperature-sensitive strain of *E. coli* ZipA with Ssz1 also was unsuccessful, further excluding Ssz1 from a ZipA function. While, the attempted identification of a protein structurally similar to ZipA in plants was a worthwhile endeavor, ultimately, Ssz1 cannot be linked to a role in chloroplast division.

An explanation for the mild division phenotype of the Salk insertional mutant is the recent identification of Ssz1 as responsive to arsenic treatment of plant (which inhibits phosphate transport)(Catarcha et al. 2007) and instead the fewer chloroplasts per cell observed in the mutant may instead be a result of a stressed metabolic transport network within the plant cell.

An antibody to *E. coli* ZipA cross-reacts with a protein of about 35 kDa, and is close to the mass of *E. coli* ZipA and suggests a ZipA-like protein may be present in chloroplasts even if it is not Ssz1. The protein that cross-reacts with the *E. coli* ZipA antibody co-fractionates with FtsZ1, FtsZ2, ARC3 and ARC6 on sucrose density gradients and further co-fractionates with FtsZ1 and FtsZ2 and ARC3 by anion exchange chromatography (Figure 4.1C) and co-fractionates by native PAGE with FtsZ1 and FtsZ2. While attempts at identifying the *E. coli* cross reactive protein by tandem mass spectrometric fingerprinting against proteins from the Arabidopsis genome failed, future work to identify the protein using a pea cDNA library recently would be a worthwhile effort in the future. The case for a non-ARC6 ZipA-like protein in chloroplast is strong and this protein awaits identification by future experimental efforts

Materials and Methods

Generation of a Ssz1 Δ strain of Synechococcus PCC 7942

About 1.3 kb fragment of a gene with sequence similarity to Ssz1 was amplified from *Synechococcus* PCC 7942 genomic DNA by primers TGGCTTCTTCTGCGATCAAC and TTTTGGATGGTCTGTGGGC. The product was cloned into pGEM-T vector. The cloned genomic fragment was cut with MscI and a SmaI fragment of omega interposon (conferring spectinomycin resistance) cut from pRL453 (a kind gift from Peter Wolk) was inserted to the MscI site. A clone in which the omega interposon is inserted in the same direction of Ssz1 gene was transformed into *Synechococcus* PCC 7942 using previously described methods (Miyagishima et al. 2005). Ssz1 Δ was segregated on by

selection on spectinomycin and FtsZ was detected in the mutant by immunofluorescence microscopy as previously described (Miyagishima et al. 2005).

Database of Putative Chloroplast Proteins for Threading

The genome of the *Arabidopsis thaliana* was searched for proteins that are putatively targeted to the chloroplast by the analysis done by the MIPS project (<http://mips.gsf.de/proj/thal/db/index.html>). This database consisted of 3972 entries and are listed in "Supplementary Data". These proteins were then filtered for proteins with a predicted MW range of 35-55 kD thus reducing the database used for analysis to 1535 protein sequence and is available in "Supplementary Data".

Threading of the Unknown Chloroplast Proteins

The 1535 putative chloroplast proteins were threaded against the structure of ZipA complexed with FtsZ (PDB structure 1f46). The top 100 proteins based on the energy function report from the threading algorithm in PROSPECT2 from this analysis were then reanalyzed 100 times to get z-score information and then sorted. These data were sorted for those with a high z-score, ranked top in the quality of the structural similarity and by the Arabidopsis genome annotation provided by MIPS (Table 4.2). Analysis was performed on a SGI Octane 2 IRIX workstation with dual 400 MHz MIPS processors and took approximately 52 h of computational time.

Growth Conditions of Plants

SALK T-DNA insertional lines of *Arabidopsis thaliana* or wild type ecotype Columbia-0, were obtained from ABRC. Plants were grown as previously described (Osteryoung et al. 1998).

Microscopy of Fixed Arabidopsis Tissue

Three week old Arabidopsis plants had leaf sections removed and fixed as previously described (Osteryoung et al. 1998). The tissue was then squashed onto a glass microscopy slide and intact cells examined on an Olympus BH-2 microscope under 40X magnification. Intact cells were photographed with a Nikon Coolpix 9200 digital camera under constant focal length for comparison amongst pictures. Pictures were analyzed for cell size and chloroplast number using the ImageJ software package (<http://rsbweb.nih.gov/ij/>). Data was analyzed using Microsoft Excel XP for Windows XP.

Genotype of SALK insertions in Ssz1

Three week old leaves from T3 plants were extracted with the DNAzol procedure to obtain RNA free DNA (Chomczynski et al. 1997). Approximately 100 ng of DNA was subjected to PCR using TaKaRa ExTaq (distributed by PanVera) either the primer combination of gAT4G33540-L, 5'-TCTTCTCTGCGGTTTCTTCGCTCTCG-3' and gAT4G33540-R, 5'-CGAACACCACCCTTCATCTCGATCTTTCCA-3' to confirm the presence of a WT allele or gAT4G33540-R and LBb1, 5'-GCAGCAAGCGGTCCACGCTGGTT3' to confirm the presence of a T-DNA insertion within the gene. Thermocycling was performed for 1 min at 96°C, 32 cycles of 15 sec at 94°C, 30 sec at 65°C and 2 min at 72°C, and a final

extension of 4 min at 72°C. Under these conditions plants with a signal for the T-DNA insertion but lacking a signal for the gene (due to the incorporation of the T-DNA) were deemed homozygous for the T-DNA insertion, whereas a WT plant will contain a gene specific signal but no signal for the T-DNA.

Yeast-two Hybrid Assay

Ssz1 without its 53 amino acid predicted chloroplast transit peptide was amplified by PCR from the cDNA U17949 (ABRC Stock, <http://www.arabidopsis.org>) with the primers 5'-GGGGACAAGTTTGTACAAAAAAGCAGGCTCAAATCCTAGAAGACGAACTCAG-3' and 5'-

CTTGTTTCCTTTAGCAAATCCGGGAAAGCTGACCCAGCTTCTTGACAAAGTGGTCCCC-3'.

Following PCR, Ssz1 Δ 53 was recombined into the vector pDONR207 (Invitrogen) with BP clonase using standard Gateway[®] system protocols (Invitrogen) to create pDONR207-Ssz1 Δ 53. The yeast-two-hybrid vectors pGAD-T7 and pGBK-T7 from the Clontech[®] Matchmaker III[®] system were both digested with SmaI and the Gateway[®] RfB conversion cassette (Invitrogen) was ligated and transformed into DB3.1 cells, which are resistant to the *ccdB* gene harbored in the RfB cassette. The new yeast-two-hybrid vectors, pGAD-T7-DEST and pGBK-T7-DEST, now Gateway[®] Destination compatible, were verified by restriction mapping and sequencing and place the GAL4 activation and GAL4 DNA binding domains in frame with the Gateway[®] system. Ssz1 Δ 53 bait and prey plasmids were created by recombining pDONR207-Ssz1 Δ 53 into pGAD-T7-DEST and pGBK-T7-DEST to create Ssz1 Δ 53-pGAD and Ssz1 Δ 53-pGBK respectively.

Figure 4.8: ClustalW alignment of plant and cyanobacterial Ssz1 homologues

Ssz1 Δ 53-pGAD and Ssz1 Δ 53-pGBK were tested for interaction with FtsZ2-1 and FtsZ2-1-CTD created exactly as previously described (Maple et al. 2005) and tested for activation of the histidine reporter on SD-ULHT as previously described (Maple et al. 2005). Each experiment was repeated twice independently. ClustalW alignment of a subset of proteins found to be similar to Ssz1 by a BLAST search of the NCBI NR database. Note that rice has two genes similar to Ssz1 (this is true in both Indica and Japonica cultivars). GenBank accession numbers are as follows: *Arabidopsis thaliana* Col-0, 22329127; Spruce (*Picea sitchensis*), 116792143; *Oryza sativa* cv. Japonica, 125584249; *Oryza sativa* cv. Japonica, 115450011; *Nostoc* sp. PCC 7120, 17228723; *Synechococcus* sp. 48242153; *Synechocystis* sp. PCC 6803, 16331548.

Figure 4.8 (continued)

	190	200	210	220	230	240
Arabidopsis
Spruce	VDSPRYVEKLA	GRTEKGGVRYMFL	THRD	DVADHKKWAER	FRKSTRILHSDDDV	PEPSTSDV
Rice A	VDSPEKELAS	QDELGGGAR	YMFLSHRD	DVADHKKWAER	RLSCORILAH	NEVQSHYADV
Rice B	VDSPRYTKLAN	IEELGGAR	YMFLTHRD	DVADHKKWAER	LKCRERI	IHSGDVERAVYDV
Nostoc	VDSPRYTKLAN	IEKLGGAR	YMFLTHM	DVADHKKWAER	LKCRERI	IHSGDVDDVYADV
Synechococcus	IIIVPRSAFLAR	LIOSMGGS	AVLTHRD	DVADHQR	FAGVLCORILH	DETSAQTRNV
Synechocystis	ILCFANHEDNE	AMLGEQ	EFVRMLCL	THRDGHC	QKVKVTIQ	ERLSCQVFWVQEQEAYLLP
	250	260	270	280	290	300
Arabidopsis
Spruce	ETKLEGGPWS	IYEDVELI	HTPGHSEGS	VQVPHKSL	KALFTGDH	VIMT--ESG--LSIL
Rice A	EMKLECGPWS	LDPEIDL	IHTPGHTEGS	VSLEFKVP	KALFTGDH	IYAS--HNG--ELAYF
Rice B	ERKLTNGPWN	IGADFEL	IHTPGHTQ	SGSVCLFYKVP	KALFTGDH	VAKS--EESDDIYLF
Nostoc	EMKLTNGPND	IGADFEL	IHTPGHTEGS	VCLFYKVP	KALFTGDH	VAKS--EESDDIYLF
Synechococcus	ETQLTTEPFL	QPDVLI	HTVPGHTR	CHTVLYKNI	KFLFTGDH	LWAS--ENRHLQAF
Synechocystis	EHQLNGSDA	EIAPEL	LIPTPGHT	AGSICAVL	GEARCVL	SGDHLIMNI--AFQQVLYCS
	310	320	330	340	350	36
Arabidopsis
Spruce	ECYNHGSVP	QLEAVEK	ELIN---	LDNRNML	IPGHGRV	VHFKDGDFAKNI
Rice A	EGYNYSV	QVENIR	PEIQ---	MDFLAL	LPHGRI	IKFENINEK
Rice B	LMYSRC	QVLSQDS	MRKLLK---	LDDFEFL	PHGGRY	IHYKDVHAK
Nostoc	LMYSRC	QVLSQDS	MRKLLK---	LDDFEFL	PHGGRY	IHYKDVHAK
Synechococcus	RDCVYS	WABQIR	SMRRIAD---	YSDF	VWLP	PHGRFRFHAD
Synechocystis	KHYCWN	FERQIR	SKLQD---	LDVAWL	PPHG	GHFRFAP
	370	380	390	400	410	420
Arabidopsis
Spruce	KTFHPR	QOAS	VEKITH	RMLDEK	NLPLRA	VQPC
Rice A
Rice B
Nostoc
Synechococcus
Synechocystis

CHAPTER FIVE

SUMMARY AND FUTURE DIRECTIONS

Summary

This dissertation aims to advance the knowledge of the biochemical properties of plant FtsZ1 and FtsZ2. When this work was initiated there was a limited amount of function information for FtsZ1 and FtsZ2. Moreover, the putative plant FtsZ regulatory proteins ARC3 and ARC6 were not yet discovered. Thus the aim of these studies was to use a biochemical approach to understand why plants use two types of FtsZ proteins. To understand the composition of the FtsZ complex *in vivo*, FtsZ was purified from pea stroma. Pea FtsZ1 and FtsZ2 co-fractionate with the chloroplast division proteins ARC3 and ARC6 when separated by sucrose density gradient, anion-exchange chromatography, size-exclusion chromatography and native polyacrylamide gel electrophoresis. In addition, a ZipA-antibody cross-reactive protein was found to co-fractionate with FtsZ1/FtsZ2/ARC3/ARC6-containing complexes. Finally, FtsZ levels were quantified in isolated *Arabidopsis thaliana* chloroplasts and FtsZ1 and FtsZ2 were found at a constant ratio of ~1:2. FtsZ1 and FtsZ2 were also found to be co-immunoprecipitated from pea stroma.

Plant FtsZ2 contains a C-terminus similar to the ZipA-binding C-terminus of bacterial FtsZ. However, ZipA had not been identified in plants. A structural search algorithm was created find a chloroplastic protein that is structurally similar to ZipA. This algorithm identified a strong ZipA candidate, Ssz1, but Ssz1 could not be definitively linked to a role in chloroplast division. Moreover, exon 4 of ARC6 has recently been found to be structurally similar to ZipA and binds the C-terminus of FtsZ2.

To understand the biochemical properties of plant FtsZ, recombinant FtsZ1 and FtsZ2 were produced individually in *E. coli*. FtsZ1 and FtsZ2 were both found to be GTPases, but approximately 15-fold slower than the GTPase activity of *E. coli* FtsZ. When mixed equally FtsZ1 and FtsZ2 co-assemble into bundled ribbon-like structures. Maximal FtsZ1/FtsZ2 co-assembly requires an equal concentration of both proteins. In addition, a T7-loop mutant, FtsZ2D322A, was found to be a sub-stoichiometric competitive inhibitor of FtsZ1, but not FtsZ2. Together these results support a FtsZ1/FtsZ2 heterofilament model similar to $\alpha\beta$ -tubulin.

In summary, work described in this dissertation advances our knowledge of biochemical properties of FtsZ1 and FtsZ2. More importantly, this work lays the groundwork for future study of the stromal chloroplast division machinery. FtsZ1 and FtsZ2 co-polymerize into heteropolymers and can be co-purified with ARC3, ARC6 and a ZipA cross-reactive protein. ARC3 and ARC6 are known to regulate FtsZ filament morphology *in vivo* (Glynn et al. 2007; Vitha et al. 2003). Thus a logical model is that FtsZ1/FtsZ2 heterofilaments are directly bound to proteins that regulate their assembly, organization and dynamics. Future work will be needed to test this new model of FtsZ dynamics and regulation.

Future Directions

Structural Search Algorithms

Sequence alignment search tools such as BLAST (Altschul et al. 1990; Gish and States 1993) infer structural and functional similarity from sequence similarity, and not

protein structural similarity. This approach works well for closely related genes and proteins. However, sequence alignment searches generally do not work well when sequences differ substantially. The result of this problem is that approximately 40% (as of 2007) of the Arabidopsis genome remains functionally unannotated because these genes (or deduced proteins) do not have sequence similarity to other proteins (Swarbreck et al. 2007). However, the inability to annotate genes in plant genomes may result from some of these genes being plant-specific.

Plants contain stromal targeted homologues to some bacterial cell division proteins such as FtsZ, MinD, MinE and SulA. However, plants lack homologues to several bacterial cell division proteins that have been predicted to exist, such as MinC and ZipA. This prompted the concept of searching for proteins with similar function, not by sequence similarity, but by structural similarity. Searching a database for proteins with structural similarity has not been previously done to my knowledge. Instead of developing a new computational framework to do this analysis, the threading algorithm of the PROSPECT2 software package was used to find a structural analogue of *E. coli* ZipA in plants. While one candidate, Ssz1, looked promising (Chapter 4), ultimately Ssz1 could not be definitively linked to chloroplast division. However, the prediction that plants contain a structural analogue of ZipA has been borne out. Recent work in our laboratory by Jonathan Glynn has found that a *de novo* derived structure of a short portion of ARC6 is structurally similar to ZipA. Furthermore, this portion of ARC6 also interacts with the FtsZ2 C-terminal motif similar to the *E. coli* FtsZ ZipA binding motif, and ARC6 has a role in remodeling and organizing FtsZ filaments (Vitha et al. 2003),

indicating ARC6 had functional as well as partial structural similarity to ZipA. recent studies from our laboratory have revealed that ARC6 bears a domain with structural and functional similarity to ZipA (J. Glynn, unpublished).

In the future, structural similarity algorithms may become useful, especially as more genomes are sequenced with high throughput mechanisms. In order for this approach to be successful in the future, the major weakness of this approach should be addressed, the threading algorithm itself. This analysis used the threading algorithm from the structure prediction software package PROSPECT2, which is designed for structural modeling and not database searching. Future structural search algorithms should instead focus on a different approach such as comparing the arrangement and content of α and β sheets in a secondary structure prediction or other methods without a sequence similarity bias.

Finally, a good lesson from this work is that while computation predictions can be extremely useful for making scientific progress, there is no substitute for the power of the scientific experiment itself.

The protein that cross-reacts with the E. coli ZipA antibody

An antibody to *E. coli* ZipA specifically recognizes a ~35 kDa protein in pea chloroplasts, similar to the mass of the *E. coli* ZipA protein. The identification of this putative chloroplastic protein is an exciting prospect. In the research presented here, this protein has been shown to be tightly associated with the FtsZ-containing complex by sucrose density gradient fractionation, native PAGE, anion exchange and

hydrophobic interaction chromatography, suggesting this protein might be a chloroplast division protein.

Unfortunately, due to a lack of an appropriate molecular ion template database, a strong candidate for the 35 kDa ZipA cross-reactive protein was not identified. The pea orthologues of ARC6 and its homologue ASH1 can be ruled out as candidates for the ZipA cross-reactive protein because of their high molecular masses (80-100 kDa based on the Arabidopsis sequences and detection on immunoblots; McAndrew et al. 2008; Yue Yang, unpublished). Future experiments should focus on identifying the ZipA cross-reactive protein by proteomic identification from α -ZipA immunoprecipitation, instead using a recently generated pea cDNA library to generate molecular ions for identification (Andreas Weber, personal communication).

Chloroplast division protein purification from inclusion bodies

Chloroplastic proteins are difficult to produce recombinantly in *E. coli*. Most stromal proteins are encoded in the nucleus, translated in the cytoplasm and imported into the chloroplast. Further, most chloroplast proteins have a chloroplast targeting sequence on their N-terminus that is cleaved as the protein is imported into the chloroplast (Bruce 2000). Moreover, prediction of the presence of the chloroplast transit peptide is generally straightforward (although many proteins may be missed), but the prediction of the cleavage site for the chloroplast targeting sequence is still enigmatic. For example, the predicted cleavage site of the FtsZ1 transit peptide is at amino acid 90 and would result in the removal of half of the Rossman-fold GTP binding

motif that is characteristic of FtsZ and tubulin (see Chapter 3 for more detail). Indeed, this cleavage site was chosen for yeast-two-hybrid constructs between plant FtsZs (Maple et al. 2005) and while it does not appear to have affected interaction between the FtsZs themselves, it does call into question the interaction between FtsZ1 and ARC3, since ARC3 contains an FtsZ Rossmann-fold GTP binding domain that may be compensating for this missing domain in the FtsZ1 construct. So how should researchers approach this in the future?

The expression of plastid division proteins (such as FtsZ1, FtsZ2, ARC6 and ARC3 and many others) recombinantly in *E. coli* has been an extremely difficult procedure because A) the proteins frequently block *E. coli* cell division and are thus cytotoxic; B) due to toxicity, they are frequently found in inclusion bodies and C) stromal plastid division proteins tend to bind tightly to the native *E. coli* division machinery and are difficult to remove, similar to the difficulty of purifying *E. coli* FtsZ beyond 90% under native conditions (Lu and Erickson 1998). Typically, accessory factor proteins bind extremely tightly and are not removed even under the high salt conditions of anion and cation exchange chromatography.

The work described here makes a significant leap forward in the ability for plant FtsZ proteins to be purified in an active form. The key to this process is the co-expression of the *ftsQAZ* operon from *E. coli* during expression (Jeong and Lee 2003) to prevent a block in cell division. Further, expression levels are increased in strains

overexpressing the *ftsQAZ* operon suggesting blocked cell division reduces protein expression.

The approach to expression and purification of FtsZ1 and FtsZ2 recombinantly in *E. coli* has also been successful for expressing the stromal, soluble domain of ARC6 and fragments of ARC3 (Bradley Olson, unpublished observations). Moreover, refolding protocol derivatives of those used to refold plant FtsZ1 and FtsZ2 (Chapter 3) are successful at refolding ARC6 and ARC3 from inclusion bodies and have significantly increased the capacity to study cytotoxic chloroplast division proteins *in vitro*, by purification of recombinant proteins.

FtsZ biochemistry

Future biochemical study of FtsZ should be focused in three areas. First, the biochemical relationship between FtsZ1 and FtsZ2 in head-to-tail protofilaments should be defined in detail. These experiments can be complemented with *in vivo* assessment of the T7-loop mutations (FtsZ2 described in Chapter 3) and others that target the interface between FtsZ1 and FtsZ2. Second, defining lateral interactions between FtsZ1 and FtsZ2 will need to be addressed. Third, what are the biochemical effects of FtsZ interacting proteins such as ARC6 and ARC3?

Probing heterofilament formation by FtsZ1 and FtsZ2

In Chapter 2, FtsZ1 and FtsZ2 were found in a salt-stable complex that represents unassembled FtsZ (McAndrew et al. 2008). Moreover, the molecular mass of the native FtsZ complex suggests the presence of one each of FtsZ1, FtsZ2, ARC6 and ARC3

(McAndrew et al. 2008) and possibly the presence of a protein that cross-reacts with ZipA (Chapter 4). In Chapter 3, FtsZ1 and FtsZ2 were found to assemble into heterofilaments. Thus, ignoring ARC3 and ARC6, the basic unit of plant FtsZ assembly is a head-to-tail dimer of FtsZ1 and FtsZ2 similar to $\alpha\beta$ -tubulin. In contrast to tubulin, both FtsZ1 and FtsZ2 are GTPases, thus there is not an obvious explanation for why FtsZ1/FtsZ2 polymerize into heterofilaments. One possibility is that plant FtsZ disassembly is regulated, contrasting with bacterial FtsZ which is assembly regulated. FtsZ1/FtsZ2 head-to-tail polymerization should be explored for a mechanistic explanation.

Several structures of $\alpha\beta$ -tubulin dimers have been solved and described in detail (Nogales 1999, 2000; Nogales et al. 1998a; Nogales and Wang 2006; Nogales et al. 1999; Nogales et al. 1998b). FtsZ1 and FtsZ2 homology based structures (Yoder et al. 2007) should be examined for residues that might mediate head-to-tail interactions. The residues that are found to be in the FtsZ1/FtsZ2 interface should be sequentially mutated and tested for the effect on polymerization and GTPase activity, in a similar approach that was used with T7-loop mutations (Chapter 3). These experiments will provide significant insight into the exact specificity for heterofilament formation. Moreover, they could yield insight into the head-to-tail filament specificity for bacterial FtsZ and $\alpha\beta$ -tubulin. In concert with these experiments, it would be useful to collaborate with a structural lab to attempt to crystallize an FtsZ1/FtsZ2 dimer.

There is growing evidence that bacterial FtsZ polymers are assembled by the addition of FtsZ dimers, not monomers (Chen et al. 2005; Chen and Erickson 2005; Huecas et al. 2007a). This is kinetically similar to $\alpha\beta$ -tubulin, with the exception that the $\alpha\beta$ -tubulin dimer is initiated by chaperones (Lewis et al. 1997). In the bacterial FtsZ model, there is growing evidence that *E. coli* FtsZ exists as a dimer and not monomers (Chen et al. 2005; Chen and Erickson 2005; Huecas et al. 2007a; Rivas et al. 2001). After dimer formation there is a kinetic lag (cooperativity) to add a FtsZ dimers onto a growing protofilament (Caplan and Erickson 2003; Chen et al. 2005; Huecas and Andreu 2003, 2004; Huecas et al. 2007a; Romberg and Levin 2003). If true for plant FtsZ, this would predict that FtsZ1/FtsZ2 dimerization is the minimal subunit of filament formation, and addition of FtsZ1/FtsZ2 dimers to heterofilaments is cooperative, as observed by light-scattering in Chapter 3.

FtsZ1/FtsZ2 dimerization can be examined with multiple approaches. First, variants of FtsZ1 and FtsZ2 recombinant proteins described in Chapter 3 have been created that allow N-terminal fluorescent tags to be attached to Cys residues. These Cys residues correspond to the plus-side of the growing protofilament and would be GTP-capped. To probe for dimerization, fluorescently labeled FtsZ1 could be tested for quenching upon mixing with unlabelled FtsZ2 (or the converse). This approach can be used to measure the dissociation constant between head-to-tail associated FtsZ, since the fluorescent tagging site lies in the FtsZ1/FtsZ2 interface. Indeed, preliminary data to this effect have been generated. N-terminal fluorescently labeled FtsZ1 and FtsZ2 are biochemically indistinguishable from unlabelled proteins (Bradley Olson, unpublished

observation). Preliminary experiments demonstrate the fluorescent tags are quenched when mixed in *trans*, but a technical hurdle of photobleaching needs to be overcome to measure the dissociation constant in detail (Bradley Olson, unpublished observations). If fluorescent tagging does not work, an approach such as calorimetry (Caplan and Erickson 2003; Huecas et al. 2007b) could be used to confirm the energy of FtsZ1/FtsZ2 heterofilament polymerization.

Second, non-hydrolyzable fluorescent GTP analogues could be used to probe the nucleotide dissociation constants for FtsZ1 and FtsZ2 individually and mixed (Huecas et al. 2007b). These experiments will answer the question of which nucleotide binding site is in the interface between FtsZ1 and FtsZ2. In Chapter 3, there is evidence that polymerized plant FtsZ does not exchange nucleotide for free nucleotide. In this future line of experiments, the nucleotide binding sites would be probed with non-hydrolyzable, fluorescent nucleotide analogues similar to previous approaches (Huecas and Andreu 2003, 2004; Huecas et al. 2007b). The site that is found within the interface between FtsZ1 and FtsZ2 would be found to have a lower dissociation constant. To distinguish between FtsZ1 and FtsZ2 nucleotide binding sites, FtsZ1 and FtsZ2 could be mutated in their glycine-rich N-terminal domain to convert them to ATP binding proteins as has been done previously for *E. coli* FtsZ (RayChaudhuri and Park 1994). Thus, ATP-binding and GTP-binding variants of FtsZ1 and FtsZ2 could be mixed and analyzed for fluorescence nucleotide quenching to determine which nucleotide binding site is in the interface.

Finally, an Arabidopsis *FtsZ1-1* mutant was found to have the mutation, G267R which is in its T7-loop (Appendix A)(Yoder et al. 2007). In lines or tissues where *ftsZ1G267R* is expressed at normal levels, this allele is dominant-negative. Moreover, *ftsZ1G267R* leads to short disorganized filaments, suggesting it is blocking polymerization of FtsZ1/FtsZ2 heterofilaments. An important confirmation of the hypothesis that FtsZ1 and FtsZ2 polymerize into heterofilaments would be to attempt to rescue *ftsZ1* and *ftsZ2* knockouts (Aaron Schmitz, in preparation) with T7-loop mutants similar to those described in Chapter 3. If FtsZ1 and FtsZ2 do polymerize into heterofilaments *in vivo*, it would be expected that *FTSZ1D275A* would act dominant-negatively in an *ftsZ1* knockout mutant and exacerbate the knockout phenotype. Moreover, overexpression of *FTSZ2D275A* should lead to strong depolymerization of wild-type FtsZ2 when observed by immunofluorescence. Important to these experiments will be doing the reciprocal experiment and controls with wild-type alleles.

FtsZ1 and FtsZ2 lateral interactions

The lateral interactions between bacterial FtsZ are poorly understood, mostly because in the absence of stabilizing agent, bacterial FtsZ only assembles into single protofilaments (Chen et al. 2005; Mukherjee and Lutkenhaus 1994). Moreover, most of the differences in amino acid sequence between FtsZ1 and FtsZ2 (Stokes and Osteryoung 2003) lie in regions predicted to be solvent-exposed in putative structures created by homology modeling (FtsZ1 model in Yoder et al. 2007). Residues found to be putatively within the interface between plant FtsZ filaments should be probed with site-

directed mutagenesis and analysis of the mutation effect analyzed by light-scattering and electron microscopy, similar to the techniques used in Chapter 3. In this set of experiments, mutations that decrease filament bundling should be identified and characterized further. It should also be pointed out that the inherent stability of plant FtsZ1/FtsZ2 co-polymers may be an experimental advantage over *E. coli* FtsZ for understanding FtsZ lateral interactions.

In a second line of experiments, an approach such as partial proteolysis of polymerized FtsZ1/FtsZ2 could be used to define filament interfaces. The idea behind this experiment is that residues that lie within the interface between FtsZ1 and FtsZ2 would be protease-protected, but solvent exposed faces would be protease sensitive. These experiments could be followed by fluorescently labeling residues on various surfaces of FtsZ1 and FtsZ2 (similar to experiments proving the interface head-to-tail above) and testing for quenching after polymer bundling. These experiments could use results from a previous study with *E. coli* FtsZ as a guide (Lu et al. 2001).

In conclusion, the experiments described above aim to structurally define the relationship between FtsZ1 and FtsZ2 in more detail. These experiments will be extremely useful for furthering our understanding of FtsZ and tubulin polymerization. Finally, these experiments will describe the assembly of a component of the chloroplast fission machinery in detail and be a scaffold for understanding the role of other division factors such as ARC3 and ARC6.

The biochemical effects of ARC6 and ARC3

A series of biochemical experiments based on light-scattering and EM should be performed to define the biochemical effects of ARC6 and ARC3 on the GTPase activity and polymerization of FtsZ1/FtsZ2. Based on genetic analysis showing that ARC6 promotes (Vitha et al. 2003) and ARC3 inhibits FtsZ filament formation (Glynn et al. 2007) in chloroplasts, we hypothesize that ARC6 should promote and ARC3 inhibit the polymerization of FtsZ1/FtsZ2 *in vitro* through their respective interactions with FtsZ2 and FtsZ1. Based on the presence of both proteins in the FtsZ-containing complex described in (McAndrew et al. 2008)(Chapter 2), we might further expect ARC6 and ARC3 to act antagonistically on polymerization when mixed.

There is evidence that ARC6 may also promote the polymerization of FtsZ2 in the absence of FtsZ1. In antisense *AtFtsZ1-1* and *AtFtsZ2-1* lines, the reduction of *AtFtsZ1-1* or *AtFtsZ2-1* have different effects on Z-filament topology (Vitha et al. 2001). The loss of *AtFtsZ2-1* leads to short disorganized *AtFtsZ1-1* filaments (Vitha et al. 2001). In contrast, loss of *AtFtsZ1-1* leads to long spiral *AtFtsZ2-1* filaments (Vitha et al. 2003). This suggests that FtsZ2 is capable of forming long Z-filaments on its own, or that ARC6 is promoting FtsZ2 filament stability in the absence of *AtFtsZ1-1*. *In vitro*, it was found that FtsZ2 does not assemble efficiently on its own (Chapter 3) and this would suggest the long FtsZ2-filaments observed in the absence of *AtFtsZ1-1* are due to the stabilization effects of ARC6. This idea could be tested by creating an *ftsZ1/arc6* double mutant and performing immunofluorescence for *AtFtsZ2-1*. If ARC6 is in fact promoting FtsZ2 stability, short *AtFtsZ2-1* Z-filaments would be expected to be observed in the *ftsZ1/arc6* double mutant (Vitha et al. 2001).

Finally, ARC3 has a role in the positioning of the Z-ring properly to mid-plastid. Immunolocalization of FtsZ in the *arc3* mutant shows evenly spaced, multiple Z-rings (Glynn et al. 2007) suggesting ARC3 may have a MinC-like function (Glynn et al. 2007; Maple and Moller 2007a). Additionally, ARC3 localizes both to the pole (Maple et al. 2007) and mid-plastid (Maple et al. 2007; Shimada et al. 2004). ARC3 contains an N-terminal, FtsZ-type GTP binding domain and could either modulate the GTP activity or cap FtsZ filaments. This could be tested *in vitro* by examining the GTPase activity and polymerization of FtsZ1 and FtsZ1/FtsZ2 in the presence of increasing concentrations of ARC3.

Concluding remarks

The establishment of an *in vitro* system to study plant FtsZ biochemistry will open a new functional understanding of chloroplast division at a biochemical level. Current efforts in understanding chloroplast division have been focused on identifying the molecular players involved. However as more chloroplast division genes are identified, their functional role in plastid division will need to be understood. This dissertation contributes significantly to this goal.

APPENDIX A

Yoder, D. W^{*}, D. Kadirjan-Kalbach^{*}, B. J. S. C. Olson, S. Y. Miyagishima, S. L. Deblasio, R. P. Hangarter, K. W. Osteryoung and S. Vitha (2007). "Effects of mutations in Arabidopsis FtsZ1 on plastid division, FtsZ ring formation and positioning, and FtsZ filament morphology in vivo." Plant and Cell Physiology **48**(6): 775-791.

^{*}These authors contributed equally to this work

Note: This reprint is reproduced under license number 1912310855884 from Oxford University Press granted to B. J. S. C. Olson and Michigan State University.

B. J. S. C. Olson contributed the following: performed the initial immunoblots for this paper (immunoblots for publication including *atFtsZ1-1-Δ1* were performed by D. W. Yoder); built the homology-based structure and created the structure-based alignment between plant and bacterial FtsZs; made the discovery that *pmi4* is semi-dominant; made the discovery that expression levels of the mutant proteins vary in young versus old leaf tissues; interpreted the possible effect of the mutations; wrote the early drafts of the discussion and contributed editorial assistance to the final manuscript.

Effects of Mutations in Arabidopsis *FtsZ1* on Plastid Division, FtsZ Ring Formation and Positioning, and FtsZ Filament Morphology in vivo

David W. Yoder^{1,4}, Deena Kadirjan-Kalbach^{1,4}, Bradley J. S. C. Olson^{1,2}, Shin-ya Miyagishima^{1,5}, Stacy L. DeBlasio^{3,6}, Roger P. Hangarter³ and Katherine W. Osteryoung^{1,*}

¹ Department of Plant Biology, Michigan State University, East Lansing, MI 48824, USA

² Department of Biochemistry and Molecular Biology, Michigan State University, East Lansing, MI 48824, USA

³ Department of Biology, Indiana University, Bloomington, IN 47405, USA

In plants, chloroplast division FtsZ proteins have diverged into two families, FtsZ1 and FtsZ2. FtsZ1 is more divergent from its bacterial counterparts and lacks a C-terminal motif conserved in most other FtsZs. To begin investigating FtsZ1 structure–function relationships, we first identified a T-DNA insertion mutation in the single *FtsZ1* gene in *Arabidopsis thaliana*, *AtFtsZ1-1*. Homozygotes null for *FtsZ1*, though impaired in chloroplast division, could be isolated and set seed normally, indicating that *FtsZ1* is not essential for viability. We then mapped five additional *atftsZ1-1* alleles onto an *FtsZ1* structural model and characterized chloroplast morphologies, FtsZ protein levels and FtsZ filament morphologies in young and mature leaves of the corresponding mutants. *atftsZ1-1(G267R)*, *atftsZ1-1(R298Q)* and *atftsZ1-1(Δ404–433)* exhibit reduced FtsZ1 accumulation but wild-type FtsZ2 levels. The semi-dominant *atftsZ1-1(G267R)* mutation caused the most severe phenotype, altering a conserved residue in the predicted T7 loop. *atftsZ1-1(G267R)* protein accumulates normally in young leaves but is not detected in rings or filaments. *atftsZ1-1(R298Q)* has midplastid FtsZ1-containing rings in young leaves, indicating that R298 is not critical for ring formation or positioning despite its conservation. *atftsZ1-1(D159N)* and *atftsZ1-1(G366A)* both have overly long, sometimes spiral-like FtsZ filaments, suggesting that FtsZ dynamics are altered in these mutants. However, *atftsZ1-1(D159N)* exhibits loss of proper midplastid FtsZ positioning while *atftsZ1-1(G366A)* does not. Finally, truncation of the FtsZ1 C-terminus in *atftsZ1-1(Δ404–433)* impairs chloroplast division somewhat but does not prevent midplastid Z ring formation. These alleles will facilitate understanding of how the in vitro biochemical properties of FtsZ1 are related to its in vivo function.

Keywords: *arc10* — FtsZ — *pmi4*.

Abbreviations. *arc*, accumulation and replication of chloroplasts; CAPS, cleaved amplified polymorphic sequences; CTD, C-terminal domain; DIC, differential interference contrast;

EMS, ethylmethane sulfonate; FITC, fluorescein isothiocyanate; *pmi*, plastid mobility impaired; NTD, N-terminal domain; RT PCR, reverse transcription PCR; SSLP, simple sequence length polymorphism.

Introduction

Plastids arose from an ancestral cyanobacterial endosymbiont and have retained a division apparatus reminiscent of that in cyanobacterial cell division (Osteryoung and Vierling 1995, Osteryoung et al. 1998, Colletti et al. 2000, Itoh et al. 2001, Maple et al. 2002, Vitha et al. 2003, Maple et al. 2004, reviewed in Osteryoung and Nunnari 2003, Aldridge et al. 2005). Plastid division requires assembly of FtsZ1 and FtsZ2, plant-specific homologs of the tubulin-like bacterial cytoskeletal protein FtsZ (Osteryoung et al. 1998), into a ring (the Z ring) at the midplastid division site (Vitha et al. 2001). The Z ring is localized to the midplastid through the activity of the FtsZ-positioning proteins MinD and MinE (Colletti et al. 2000, Itoh et al. 2001, Maple et al. 2002) and is thought to be stabilized by the J-domain-like protein ARC6 (Vitha et al. 2003). Midplastid positioning of the Z ring presumably ensures that normal plastid populations are maintained in all plant cells.

Bacterial FtsZ has two functional domains, an N-terminal domain (NTD) and a C-terminal domain (CTD), that fold independently of one another (Oliva et al. 2004). The NTD contains a Rossman fold for GTP binding (Löwe 1998, Löwe and Amos 1998), and the CTD contains a T7 loop for GTP hydrolysis (de Boer et al. 1992, RayChaudhuri and Park 1992, Löwe 1998, Löwe and Amos 1998, Scheffers et al. 2002). The CTD also contains at its extreme C-terminus a short conserved stretch of amino acids that has been shown to interact with the bacterial cell division proteins FtsA and ZipA (Ma and Margolin 1999, Vaughan et al. 2004). Similar to tubulin, longitudinal contacts in FtsZ polymers are made between the region of

⁴These authors contributed equally to this work.

⁵Present address: Miyagishima Initiative Research Unit, Frontier Research System, RIKEN, 2-1 Hirosawa, Wako, Saitama, 351-0198 Japan.

⁶Present address: Department of Microbiology, The State University of New York, Stony Brook, NY 11794, USA.

*Corresponding author: E-mail, osteryou@msu.edu; Fax, +1-517-353-1926

the CTD bearing the T7 loop in one monomer and the GTP-binding site in the NTD of the next monomer. The GTP-hydrolytic site is formed by interaction between two monomers, and GTP hydrolysis is stimulated by FtsZ polymerization (Erickson 1998, Löwe and Amos 1998, Nogales et al. 1998, Oliva et al. 2004).

FtsZ1 and *FtsZ2* arose early in plant evolution by duplication of a common ancestral *FtsZ* gene of cyanobacterial origin. *FtsZ1* is more divergent from its cyanobacterial counterparts than is *FtsZ2*, and is unique to plants and green algae (Stokes and Osteryoung 2003, Wang et al. 2003, Rensing et al. 2004). *FtsZ1* also lacks the short C-terminal motif found in most bacterial *FtsZ* proteins; this motif is conserved in *FtsZ2* proteins (Fig. 2A), where it mediates an *FtsZ2*-specific interaction with ARC6 (Maple et al. 2005). Thus *FtsZ1* and *FtsZ2* are functionally as well as phylogenetically divergent. Nevertheless, except for lack of the C-terminal conserved motif, *FtsZ1* has all the hallmarks of a typical *FtsZ* and is predicted to be a GTPase (Osteryoung and McAndrew 2001). Consistent with this observation, recombinant *FtsZ1* has been reported to undergo GTP-dependent multimerization and assembly into filament-like structures in vitro and to complement a cell division defect in an *Escherichia coli ftsZ* mutant (Gaikwad et al. 2000, El-Kafafi et al. 2005). However, the structural requirements for *FtsZ1* chloroplast division activity in vivo have not been investigated.

To investigate further *FtsZ1* function in plants and begin defining the features important for its chloroplast division activity, we compared the predicted secondary and tertiary structures of *FtsZ1* with those of bacterial *FtsZ*. We show that *FtsZ1* contains predicted α -helices, loops and β -sheets that in bacteria form a Rossman fold for GTP binding and a T7 loop for GTP hydrolysis. We also isolated six mutant alleles of the single *FtsZ1* gene in *Arabidopsis thaliana*, *AtFtsZ1-1* (*At1g55280*), including a null allele. Four alleles alter conserved amino acids, and one truncates *AtFtsZ1-1* near its C-terminus. Analysis of chloroplast morphologies, *FtsZ1* and *FtsZ2* protein levels, and *FtsZ* ring and filament morphologies in the mutant backgrounds show that: (i) plants homozygous for the *FtsZ1* null allele are viable and *FtsZ2* protein levels are not affected; (ii) predicted structural features in *FtsZ1* homologous to those in bacterial *FtsZ* are important for *FtsZ* filament (Z filament) and chloroplast morphology in vivo, and some residues may be important for accumulation of *FtsZ1*, including the C-terminus; (iii) *FtsZ2* is capable of forming rings in very small chloroplasts in the absence of a functional *FtsZ1* protein; (iv) changes in *FtsZ1* protein level or function do not alter expression of *FtsZ2*, but do affect *FtsZ2* filament morphology; and (v) mutations in key residues appear to impact *FtsZ* polymer dynamics in vivo.

Results

atftsZ1-1-Δ1 is a null allele of *AtFtsZ1*

A search of the SIGNAL 'T-DNA Express' database (<http://signal.salk.edu/cgi-bin/tdnaexpress>) revealed a mutant line, SALK_073878 (Alonso et al. 2003), harboring a T-DNA insertion in the first exon of *AtFtsZ1-1* (Fig. 1A). We have designated this gene *atftsZ1-1-Δ1*. The genotype of the homozygous T-DNA insertion mutant was verified by PCR. *atftsZ1-1-Δ1* mutant plants exhibit altered chloroplast morphology and a block in chloroplast division, as indicated by a dramatic reduction in chloroplast numbers compared with wild-type Columbia (Col-0; Fig. 1B, C). Leaf mesophyll cells in *atftsZ1-1-Δ1* typically contain an average of five chloroplasts per cell, with a range of 1–12 chloroplasts (Table 1), compared with a mean of 41 in wild-type Col-0. These chloroplasts are enlarged and exhibit heterogeneity in size and number from cell to cell (Fig. 1D). No aplastidic cells were detected in any leaf samples. Homozygous mutants set seed and produced viable plants. In order to confirm that the PCR-detected T-DNA insertion caused the mutant phenotypes, *atftsZ1-1-Δ1* plants were transformed with wild-type *AtFtsZ1-1* under control of its native promoter. Wild-type chloroplast morphology and number were restored in the transformant, confirming that the T-DNA insertion is the cause of the mutant phenotypes (data not shown).

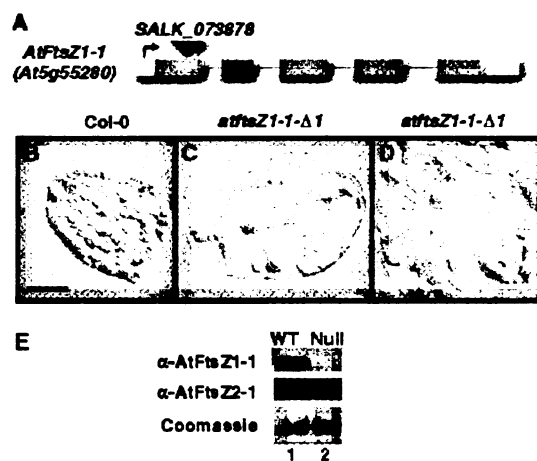


Fig. 1 (A) *AtFtsZ1-1* gene depicting the position of the T-DNA insertion in *atftsZ1-1-Δ1* (Salk_073878) in the 3' region of exon 1. Light micrographs representing chloroplast morphology in wild-type Col-0 (B) and *atftsZ1-1-Δ1* (C and D). (E) Immunoblot of protein extracts from mature leaves of Col-0 and the null allele (*atftsZ1-1-Δ1*) using α -*AtFtsZ1-1* (top panel), α -*AtFtsZ2-1* (middle panel), and Coomassie-stained gel for loading comparison (bottom panel).

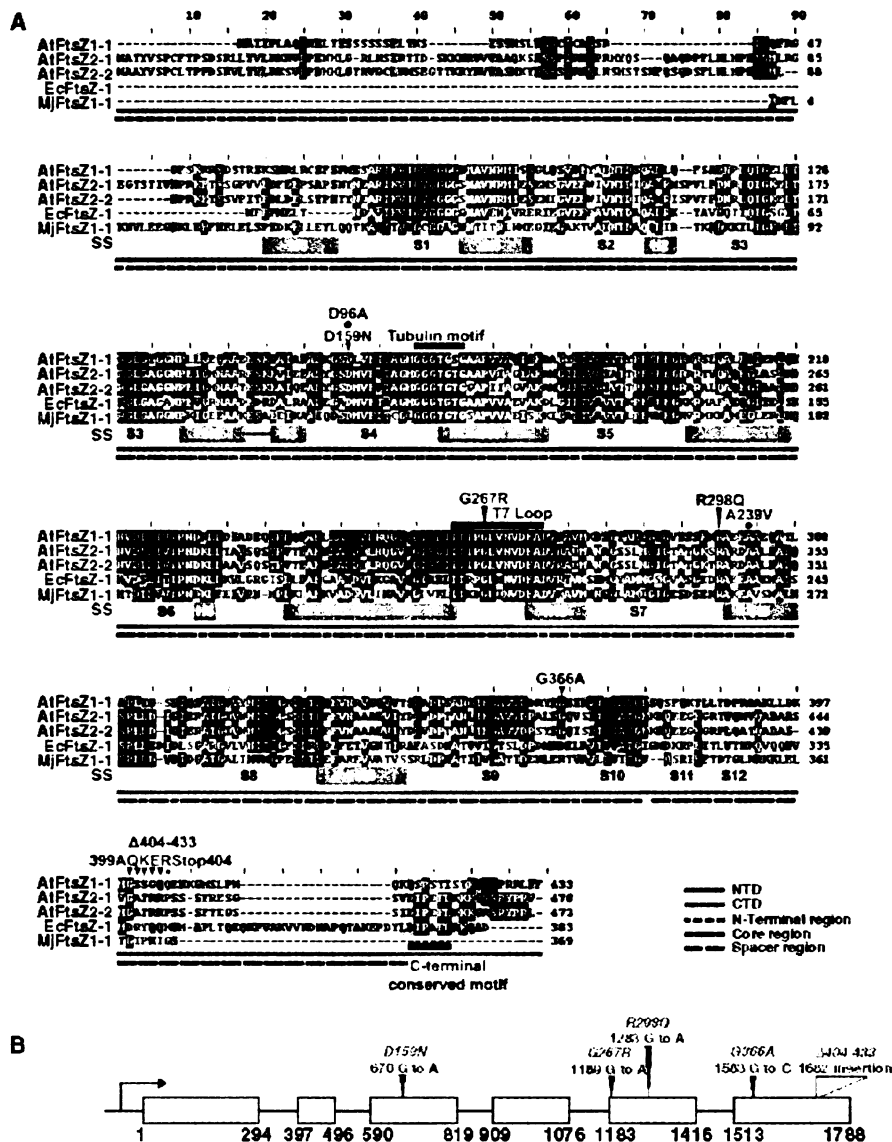


Fig. 2 (A) Amino acid alignment of AtFtsZ1-1 (NP_200339), AtFtsZ2-1 (NP_190843), AtFtsZ2-2 (NP_565839), EcFtsZ (AAC73206) and MjFtsZ (Q57816) proteins with predicted secondary structure. Dark gray bars represent α -helices and light gray arrows represent β -strands, with all structures labeled based on the homologous structures from *Methanococcus jannaschii* (Lowe, 1998). Black dots above the sequence indicate equivalent bacterial mutations. D96A (Redick et al. 2005) is a mutation equivalent to D159, and A239V represents both *ts1* in *Bacillus subtilis* (Michie et al. 2006) and *ftsZ2863* in *Escherichia coli* (Addinall et al. 2005). The positions of the five mutant alleles are indicated by black arrows and the amino acid changes are indicated above the alignment. Black bars above the alignment are the tubulin motif (GCCGTGT/SG) (Raychaudhuri and Park 1992) and T7 loop. The C-terminal conserved motif is indicated by a black bar below the alignment. The legend indicates the NTD, CTD, N-Terminal region, core region and spacer region. (B) The transcript or unit of At5g55280, with the positions of each mutation indicated above with black arrows. At, *Arabidopsis thaliana*; Ec, *Escherichia coli*; Mj, *Methanococcus jannaschii*.

Table 1 *atftsZ1-1* mutant phenotypes and morphologies in leaves from 3-week-old plants

Line	Chloroplast morphology			Seed set (%) ^c	Z filament morphology	Mutation
	Phenotype	Mean number ^a	Range ^b			
Col-0						
Wild type	–	41	30–50	97.6	Midplastid FtsZ rings	–
null	Giant chloroplasts, some smaller chloroplasts	5	1–12	99.2	No FtsZ1 protein, FtsZ2 filaments are long and randomly distributed	T-DNA insertion, exon 1
D159N	Heterogeneous, one greatly enlarged with numerous smaller chloroplasts	14	7–20	99.1	Long, possibly parallel Z filaments, some midplastid rings in smaller chloroplasts	EMS, lateral surface
G267R	Giant chloroplasts	1	1–3	97.9	Reduced FtsZ1 protein levels, punctate FtsZ1, long and randomly distributed FtsZ2 filaments	EMS, T7 loop
R298Q	Heterogeneous	19	12–25	96.1	Faint FtsZ1 rings in young tissue, midplastid FtsZ2 rings and filaments; reduced FtsZ1 protein level	EMS, N-terminal of H9
Ws-2						
Wild type	–	55	25–75	99.2	Midplastid FtsZ rings	–
G366A	Heterogeneous, one greatly enlarged with numerous smaller chloroplasts	23	11–31	98.2	Midplastid FtsZ filaments with some rings in smaller chloroplasts	Untagged T-DNA, between S9 and S10
Δ404	Slightly enlarged	22	15–29	95.9	Truncated FtsZ1 protein with reduced protein level; midplastid FtsZ rings and filaments	T-DNA insertion, 30 residue truncation

^aMean number of chloroplasts in 100 cells counted through a single median focal plane.

^bThe minimum and maximum number of chloroplasts detected in any one cell.

^cPercentage of wild-type seeds. The difference from 100% represents aborted or abnormal seeds.

Immunoblot analysis of protein extracts from mature leaf tissue of homozygous *atftsZ1-1-Δ1* individuals was performed using AtFtsZ1-1-specific antibodies (Stokes et al. 2000) (Fig. 1E). AtFtsZ1-1 protein was not detected in the mutant (Fig. 1E, lane 2), demonstrating that *atftsZ1-1-Δ1* is a null allele of *AtFtsZ1-1*, consistent with the site of T-DNA insertion (Fig. 1A). There was no detectable difference in the AtFtsZ2-1 protein level in this mutant when compared with the wild type (Fig. 1B, lanes 1 and 2). These data show that AtFtsZ1-1 is not essential for the survival of Arabidopsis or the propagation of plastids. The null allele of *FtsZ1* also provided a basis for phenotypic comparisons among the other *FtsZ1* mutant alleles described below and served as a negative control for Z filament morphology and immunoblot assays.

Mutant alleles of *AtFtsZ1-1*

In addition to *atftsZ1-1-Δ1*, we identified five novel mutant alleles of *AtFtsZ1-1* from several mutant populations, four recessive and one semi-dominant. The positions of mutations in the predicted structures of FtsZ1 and the *AtFtsZ1-1* gene are shown (Figs. 2A, B, and 3). Chloroplast phenotypes and FtsZ morphologies in the mutants were compared with those in their respective wild types—Col-0 for *atftsZ1-1-Δ1*, *atftsZ1-1(D159N)*, *atftsZ1-1(G267R)* and *atftsZ1-1(R298Q)* (Figs. 4A–M, Q, U, and 5A–M, Q, U), and Wassiljevskija (Ws-2) for *atftsZ1-1(G366A)* and *atftsZ1-1(Δ404–433)* (Figs. 4N–P, R–T, V–X, and 5N–P, R–T, V–X). All phenotypic data have been compiled in Table 1.

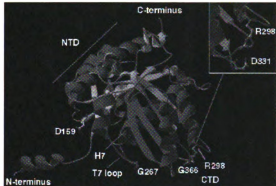


Fig. 3 Predicted three-dimensional structure of AtFtsZ1-1 based upon *M. jannaschii* FtsZ (Q57816) with D159, C267, R298 and C366 indicated with side chains. The chloroplast transit peptide and C-terminal conserved motif are not in the resolved structure of *M. jannaschii* FtsZ and do not appear in this model. Inset: close up view of R298 with the side chain pointing towards the side chain of D331.

Two recessive alleles of *AtFtsZ1-1*, *atfz1-1(D159N)* and *atfz1-1(R298Q)*, were identified in a visual microscopy-based screen for chloroplast division mutants from an M_2 ethylmethane sulfonate (EMS)-mutagenized Col-0 population (Miyagishima et al. 2006). These two mutations, which conferred altered chloroplast morphology in leaf mesophyll cells, were crossed into *Ler*, and F_2 plants were tested for linkage to known plastid division genes using PCR-based markers. The mutant phenotypes were linked to a 1.5-Mb region on chromosome 5 that included *AtFtsZ1-1*. This linkage excluded all other known plastid division genes, and subsequent sequencing uncovered point mutations at *At5g55280* in both mutants. *atfz1-1(D159N)* exhibits variability in chloroplast size (Fig. 4C) and has a mean number of 14 chloroplasts per cell (Table 1). The mutation results from a G-to-A transition at nt 6,701 in exon 3 (Fig. 2B) that alters an aspartate residue conserved in the NTD of all FtsZ proteins (Stokes and Osteryoung 2003) (Fig. 2A). *atfz1-1(R298Q)* also exhibits heterogeneity of chloroplast size (Fig. 4M), but the mesophyll cell chloroplasts are typically less variable in size than those in *atfz1-1(D159N)* (Fig. 4C), and contain more chloroplasts per mesophyll cell, having a mean number of 19 (Table 1). *atfz1-1(R298Q)* harbors a G-to-A transition at nt 1,283 in exon 2 (Fig. 2B), altering an arginine residue in the CTD that is highly conserved among *E. coli* FtsZ, cyanobacterial FtsZ and plant FtsZ proteins, but is loosely conserved among plant FtsZ2 proteins (Stokes and Osteryoung 2003) (Fig. 2A).

An allele of *AtFtsZ1-1*, originally designated *pmi4*, was isolated in a screen for plastid movement pupaired (*pmi*)

mutants (DeBiasio et al. 2005). *pmi4* mutants are defective in blue light-induced chloroplast movements; in *pmi4*, this defect results from a severe block in chloroplast division (DeBiasio et al. 2005). Leaf mesophyll cells of *pmi4* contain a mean of one (Table 1), but sometimes two or three, greatly enlarged chloroplasts (Fig. 4D). F_1 plants from a *pmi4* × *Ler* mapping cross exhibited a mixture of small and large chloroplasts, indicating that *pmi4* is a semi-dominant mutation (Supplementary Fig. S1). *pmi4* was mapped to a 58 kb region on chromosome 5 that included *AtFtsZ1-1*. Sequence analysis of *AtFtsZ1-1* from *pmi4* genomic DNA revealed a G-to-A transition at nt 1,189 in exon 5 (Fig. 2B), altering G267 in the CTD to R (Fig. 2A). Henceforth, we refer to this mutant as *atfz1-1(G267R)*.

are10, a recessive mutant isolated previously in a screen for mutants with defects in accumulation and replication of chloroplasts (arc) (Pyke and Leech 1994), exhibits reduced numbers of chloroplasts that are heterogeneous in size, similar to *atfz1-1(D159N)*, with a mean number of 23 chloroplasts compared with 55 in wild-type *Ws-2* (Table 1). Leaf mesophyll cells from this mutant typically contain one greatly enlarged chloroplast and numerous smaller chloroplasts (Fig. 4O) (Rutherford 1996, Pyke 1999). We mapped *are10* to a 311 kb region on chromosome 5 containing *AtFtsZ1-1* (*At5g55280*). Sequence analysis of this locus revealed a G-to-C transversion at nt 1,583 in exon 6 (Fig. 2B) that resulted in a missense mutation in the CTD, G366A (Fig. 2A). This mutation alters a glycine residue that is highly conserved among plant FtsZ1 and cyanobacterial FtsZ proteins (Stokes and Osteryoung 2003). To confirm that the chloroplast division phenotype in *are10* is a consequence of the *atfz1-1* missense mutation, *are10* plants were transformed with wild-type *AtFtsZ1-1* as in the null mutant. Wild-type chloroplast morphology and number were restored in the transformant, confirming that *AtFtsZ1-1* complements *are10* (data not shown). We refer to the *are10* mutation hereafter as *atfz1-1(G366A)*.

Lastly, *atfz1-1(A404 433)* was isolated by PCR-based screening of a T-DNA insertion population in the *Ws-2* background (Sussman et al. 2000). Mesophyll cell chloroplasts in this mutant are reduced in number [a mean of 22 (Table 1)] and are larger than in the wild type (Fig. 4P), but do not exhibit heterogeneity in size. Sequence analysis showed a T-DNA insertion in the last exon at nt 1,682 in this mutant (Fig. 2B), resulting in a loss of the final 30 amino acids of AtFtsZ1-1 and altering the amino acid sequence at the point of insertion from 399GSSGQQ404 to 399AQKERStop404 (Fig. 2A).

FtsZ1 and mutant alleles can be modeled onto bacterial FtsZ secondary and three-dimensional structures

Plant and bacterial FtsZ proteins share considerable sequence similarity (Stokes and Osteryoung 2003) (Fig. 2A).

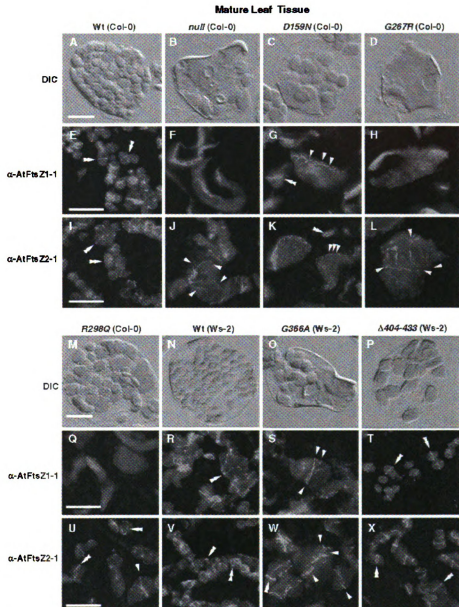


Fig. 4 DIC light micrographs of chloroplast phenotypes (A–D and M–P) and immunofluorescence micrographs of chloroplasts using AtFtsZ1-1 antibodies (E–H and Q–T) and AtFtsZ2-1 antibodies (I–L and U–X) from *Arabidopsis* mature leaf mesophyll cells of Col-0 samples; wild type (A, E and I), null allele (*atfz1-1-d1*) (B, F and J), *atfz1-1(D159N)* (C, G and K), *atfz1-1(G267H)* (D, H and L) and *atfz1-1(R298Q)* (M, Q and U), and Ws-2 samples; wild type (N, R and V), *atfz1-1(G366A)* (O, S and W), and *atfz1-1(Δ404–433)* (P, T and X). Arrows indicate FtsZ filaments, and double arrows indicate midplastid FtsZ rings. Bar sizes are equal to 20 μ m.

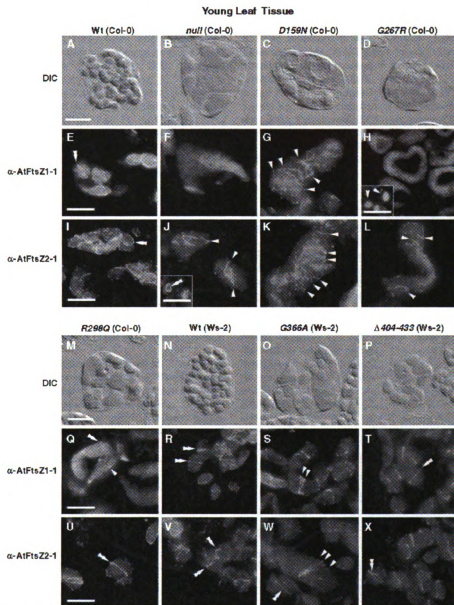


Fig. 5 DIC light micrographs of chloroplast phenotypes (A–D and M–P) and immunofluorescence micrographs of chloroplasts using AtFtsZ1-1 antibodies (E–H and Q–T) and AtFtsZ2-1 antibodies (I–L and U–X) from *Arabidopsis* young leaf mesophyll cells of Col-0 samples; wild type (A, E and I), null allele (*atftsZ1-1*) (B, F and J), *atftsZ1-1(D159N)* (C, G and K), *atftsZ1-1(G267R)* (D, H and L), and *atftsZ1-1(R298Q)* (M, Q and U), and Ws-2 samples; wild type (N, R and V), *atftsZ1-1(G365A)* (O, S and W), and *atftsZ1-1(Δ404–433)* (P, T and X). Arrows indicate FtsZ filaments, and double arrows indicate midplastid FtsZ rings. Bar sizes are equal to 20 μ m for DIC and 10 μ m for immunofluorescence.

We mapped the sequence of the Arabidopsis FtsZ1 protein, AtFtsZ1-1, onto the atomic structure of *Methanococcus jannaschii* FtsZ (Löwe 1998, Löwe and Amos 1998) (Q57816) using the structure prediction programs SWISS-MODEL and DeepView (Peitsch et al. 1995, Guex and Peitsch 1997, Schwede et al. 2003) (Fig. 3). Structural features corresponding to those in the bacterial protein can be identified in both the secondary and tertiary structural models of AtFtsZ1-1 (Figs. 2A, 3). According to the nomenclature used by Löwe (1998) and Löwe and Amos (1998), the NTD comprises α -helices H0–H7 and β -strands S1–S6 (Fig. 2A), which constitute a putative Rossmann fold for GTP binding. The CTD encompasses the portion of the protein downstream of helix H7, including α -helices H8–H10 and β -strands S7–S12. All secondary structures present in bacterial FtsZ (Löwe 1998, Löwe and Amos 1998) are predicted in AtFtsZ1-1. A T7 loop that overlaps with α -helix H8 is predicted at the beginning of the AtFtsZ1-1 CTD (Figs. 2A, 3). In the *E. coli* protein, the T7 loop contacts the γ -phosphate of GTP in the adjacent FtsZ molecule to catalyze GTP hydrolysis (de Boer et al. 1992, RayChaudhuri and Park 1992, Scheffers et al. 2002). In the bacterial FtsZ polymer, the T7 loop, α -helix H8, β -strand S9 and α -helix H10 make contacts with the GTP-binding domain in the NTD of the adjacent monomer (Oliva et al. 2004).

Using a different nomenclature based on alignment of sequences from a wide range of organisms, Vaughan et al. (2004) delineated four regions in FtsZ proteins: a variable N-terminus, a highly conserved core region, a highly variable spacer and a C-terminal region. The latter region, defined in part by the presence of the C-terminal conserved motif, is not found in FtsZ1 (Vaughan et al. 2004); instead, FtsZ1 proteins have a divergent C-terminus of roughly similar length (Rensing et al. 2004) (Fig. 2A). Some residues within this region are largely conserved within the plant FtsZ1 family, however (Rensing et al. 2004), suggesting that the divergent C-terminus and specific features within it are important for FtsZ1 function.

All of the mutant alleles, with the exception of *atftsZ1-1-41*, have been mapped onto the secondary and tertiary predicted structures. The *atftsZ1-1-D159N* mutation changes a highly conserved, negatively charged aspartate to an uncharged polar asparagine (Fig. 2A). This residue is predicted to be on the lateral surface of the protein in β -strand S4 of the NTD (Figs. 2A, 3) based on the position of the equivalent residue in *E. coli* FtsZ, D96 (Redick et al. 2005). The equivalent mutation in *E. coli* FtsZ, D96A, does not impair the ability of FtsZ to form protofilaments *in vitro*, though it does prevent complementation of the *E. coli* mutant *ftsZ84* (RayChaudhuri and Park 1994, Lu et al. 2001, Redick et al. 2005). The altered chloroplast morphology exhibited by *atftsZ1-1-D159N* (Fig. 4C)

suggests that this charged residue is important for AtFtsZ1 function.

The mutation in *atftsZ1-1(G267)* alters a highly conserved glycine, G267 (Stokes and Osteryoung 2003), positioned near the junction of the NTD and CTD, in the predicted GTP-hydrolytic T7 loop (Figs. 2A, 3). Mutations in the T7 loop of bacterial FtsZ inhibit GTP hydrolysis activity and cannot complement null mutations (Scheffers et al. 2002, Redick et al. 2005). Mutation of the equivalent glycine has not been described in bacteria, suggesting that this may be lethal. However, mutation of an adjacent proline in *E. coli ftsZ9124* blocks cell division, impairs formation of FtsZ rings and filaments, and prevents *in vitro* polymerization (Addinall et al. 2005).

R298 is predicted to correspond to a highly conserved arginine residue on the N-terminal side of α -helix H9 (Figs. 2A, 3) (Löwe, 1998, Löwe and Amos, 1998, Stokes and Osteryoung, 2003, Vaughan et al., 2004). The side chain of R298 points directly at D331 in the three-dimensional model (Fig. 3, inset), suggesting a potential ionic interaction between the two oppositely charged side chains in the predicted tertiary structure. Mutation of this residue in *atftsZ1-1(R298Q)* may disrupt this ionic interaction, which could disrupt the structure of the protein in the immediate region. Mutation of the equivalent arginine has not been reported in bacteria, perhaps due to possible lethality, though mutations in a nearby residue have been shown to be important for cell division but not GTP binding or hydrolysis in *E. coli* and *Bacillus subtilis* (Lu et al. 2001, Addinall et al. 2005, Michie et al. 2006). The affected arginine in *atftsZ1-1(R298Q)* is invariant in FtsZ1 and cyanobacterial FtsZ proteins (Stokes and Osteryoung 2003), and is conserved in both *E. coli* and *M. jannaschii* FtsZs (Fig. 2A), indicating that this residue is important for FtsZ function in general.

G366 has its hydrogen side chain positioned on the inside of a tight turn between β -strands S9 and S10 (Figs. 2A, 3) at the C-terminal end of the conserved core region, and apparently cannot be substituted by alanine in the mutant *atftsZ1-1(G366A)*. In the bacterial FtsZ polymer, β -strand S9 is involved in mediating interaction between the CTD and the NTD in the next monomer (Oliva et al. 2004). Because G366 is near the equivalent β -strand in FtsZ1, this residue may play a role in longitudinal contacts between FtsZ monomers in the chloroplast.

Finally, the T-DNA insertion mutant *atftsZ1-1(4404-433)* truncates the last 30 residues of AtFtsZ1-1, altering the resulting five C-terminal amino acids (Fig. 2A). Although FtsZ1 lacks the C-terminal conserved motif, truncation of the extreme C-terminus of FtsZ1 does alter chloroplast morphology (Fig. 4P), suggesting a role for this divergent region in FtsZ1 function.

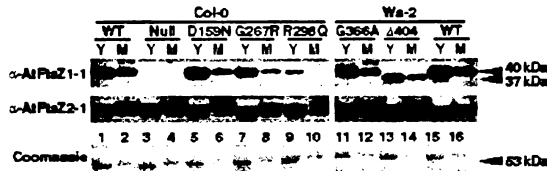


Fig. 6 Immunoblot of protein extracts from young (Y) and 3-week-old mature (M) leaves, using AtFtsZ1-1 (A, top row) and AtFtsZ2-1 (A, middle row) antibodies, from Col-0 samples; wild type (lanes 1 and 2), *atftsZ1-1-Δ1* (lanes 3 and 4), *atftsZ1-1(D159N)* (lanes 5 and 6), *atftsZ1-1(G267R)* (lanes 7 and 8), *atftsZ1-1(R298Q)* (lanes 9 and 10), and Ws-2 samples: *atftsZ1-1(G366A)* (lanes 11 and 12) and *atftsZ1-1(Δ404-433)* (lanes 13 and 14), and wild type (lanes 15 and 16). The arrows indicate the truncated ~37 kDa protein in *atftsZ1-1(Δ404-433)* vs the expected ~40 kDa size of the mature AtFtsZ1-1.

Analysis of FtsZ protein levels in *atftsZ1-1* mutants

To investigate further the phenotypes of the mutants, we evaluated FtsZ1 and FtsZ2 protein levels by immunoblotting of protein extracts from Arabidopsis leaves (Fig. 6). Because we have observed that FtsZ protein levels in wild types are higher in young leaf tissue than in mature leaf tissue (Fig. 6, lanes 1, 2, 15 and 16; Osteryoung laboratory, unpublished), we analyzed both young and mature leaves of homozygous mutants. We defined young leaves as the first leaf pair from 15-day-old plants and mature leaves as the first two leaf pairs from plants older than 21 d. Although some biological variability was observed in replicate experiments, AtFtsZ2-1 (Fig. 6, middle panel) and AtFtsZ2-2 protein levels (not shown) did not differ consistently in the mutants. FtsZ2 protein levels in the mutants were similar to those in the respective wild types; therefore, only the AtFtsZ2-1 levels are shown to represent FtsZ2 protein. Assays for immunoblot experiments were performed using *atftsZ1-1-Δ1* as a negative control (Fig. 6, lanes 3 and 4), and appropriate positive wild-type controls: Col-0 (Fig. 6, lanes 1, 2) for *atftsZ1-1-Δ1*, *atftsZ1-1(D159N)*, *atftsZ1-1(G267R)* and *atftsZ1-1(R298Q)* (Fig. 6, lanes 3, 10), and Ws-2 (Fig. 6, lanes 15 and 16) for *atftsZ1-1(G366A)* and *atftsZ1-1(Δ404-433)* (Fig. 6, lanes 11, 14).

Two of the mutants, *atftsZ1-1(D159N)* and *atftsZ1-1(G366A)*, consistently exhibited relatively wild-type levels of FtsZ1 protein (Fig. 6, lanes 5, 6, 11 and 12), indicating that the mutations in these lines do not affect protein expression or stability. In contrast, three of the mutants exhibited FtsZ1 levels that were lower than in the wild type. FtsZ1 was not detected in protein extracts from either young or mature leaves from *atftsZ1-1-Δ1* (Fig. 6, lanes 3 and 4), as previously demonstrated for this null allele (Fig. 1E). A relatively wild-type level of FtsZ1 was detected in young leaves of *atftsZ1-1(G267R)* (Fig. 6, lane 7).

However, in mature leaves, the level of FtsZ1 protein was consistently much lower than in mature leaves of the wild type (Fig. 6, lane 8), and in some biological replicates the detection was marginal, suggesting either that the protein is not stable or that expression is altered. In *atftsZ1-1(R298Q)*, very little FtsZ1 protein was detected in young leaves, and was undetectable in mature leaves (Fig. 6, lanes 9 and 10). *atftsZ1-1(Δ404-433)* exhibited slightly reduced levels of FtsZ1 protein in both young and mature leaves (Fig. 6, lanes 13 and 14). Consistent with the position of the T-DNA insertion, this truncated protein migrates faster on SDS PAGE than does FtsZ1 from Ws-2 (Fig. 6, lanes 15 and 16), with a predicted band size of ~37 kDa compared with ~40 kDa for wild-type FtsZ1. In all other samples where FtsZ1 protein was detected, the migration of the FtsZ1 cross-reacting bands was similar to that of wild-type FtsZ1. Our interpretation of these data is that the detected mutant FtsZ1 proteins are targeted to chloroplasts and their transit peptides processed.

Analysis of FtsZ transcripts in *atftsZ1-1* mutants with reduced FtsZ1 protein levels

To investigate whether the reduced protein levels in *atftsZ1-1(G267R)*, *atftsZ1-1(R298Q)* and *atftsZ1-1(Δ404-433)* might result from reduced transcription of the mutant genes, we compared AtFtsZ1-1 transcript levels with those in the wild type using reverse transcription PCR (RT-PCR). Since AtFtsZ2-1 protein levels were unchanged in these mutants, AtFtsZ2-1 transcript levels and actin-2 were used as controls. Reverse transcription reactions were performed on equal quantities of total RNA for AtFtsZ1-1 and AtFtsZ2-1 primers, and a half quantity for Actin-2 primers. PCR amplification was done using gene-specific primers designed to generate products that would span multiple introns to ensure PCR products were not generated from contaminating genomic DNA. Although there was some biological variability, the PCRs from the mutant samples all yielded bands that were at least as intense as the wild-type controls at 26 cycles (Fig. 7, lanes 3 and 6). We conclude that transcription is not significantly altered in any of the mutants exhibiting reduced FtsZ1 protein levels, and, with the exception of the null allele, the chloroplast morphologies observed in the mutants result specifically from changes in the FtsZ1 amino acid sequence.

Young leaf mesophyll cells exhibit chloroplast morphologies similar to those in mature leaf mesophyll cells

Typically, morphological defects in chloroplast division mutants are reported for mesophyll cells of mature, fully expanded leaves. However, some of the mutants in this study exhibited FtsZ1 protein levels that were dramatically altered when comparing young and mature leaf tissue, or exhibited variability or heterogeneity of

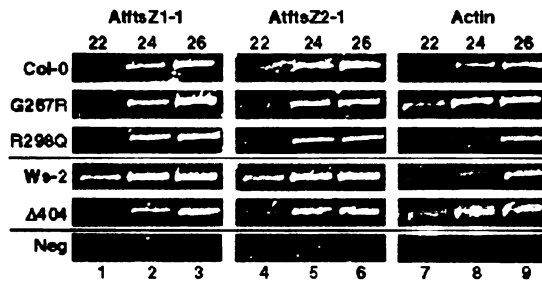


Fig. 7 RT-PCR analysis of *AtftsZ1-1* alleles comparing 22, 24 and 26 cycles of amplification using gene-specific primers for *AtftsZ1-1*; as controls, *AtftsZ2-1* and *Actin-2* primers were used. All samples reached saturation by 26 cycles, suggesting that the mutants do not exhibit altered transcript levels. Wild-type Col-0 and Ws-2 controls appear above the relevant mutants, and a single negative (Neg) reaction set is also shown. The FtsZ RT-PCRs were initiated with double the starting material when compared with the actin control reactions due to the low level of FtsZ transcript.

chloroplast morphology. In order to determine if there were developmental differences in chloroplast morphology between young and mature leaves, we examined young mesophyll cells from leaves that were similar in size and age to leaves used for immunoblot analysis. In each of the mutants, the chloroplast morphologies observed in young leaf mesophyll cells (Fig. 5A D, M P) were similar to those in mature leaf mesophyll cells (Fig. 4A D, M P). This suggests that the chloroplast division defects present early, and chloroplast morphology is not further affected by changes in FtsZ1 protein level as the leaf matures.

Analysis of FtsZ filament morphology in *atftsZ1-1* mutants

Next, we evaluated FtsZ1 localization and filament morphology by immunofluorescence staining of mature leaves (Fig. 4E H, Q T) and in young leaves (Fig. 5E H, Q T). In order to compare Z filament morphologies directly between all of the mutants, we also show micrographs of FtsZ2 immunofluorescent staining (Figs. 4I L, U X, 5I L, U X). Since Z filament patterns for AtFtsZ2-1 and AtFtsZ2-2 were similar in each mutant (data not shown), only AtFtsZ2-1 is used for comparison. With the exception of *atftsZ1-1-Δ1*, *atftsZ1-1(G267R)* and *atftsZ1-1(R298Q)* (Figs. 4F, H, Q, 5F, H), FtsZ1 filament morphologies were similar to the corresponding FtsZ2 filament morphology in the respective mutants. Control assays for localization experiments were performed with the appropriate wild types Col-0 (Figs. 4E, I, 5E, I) for *atftsZ1-1-Δ1*, *atftsZ1-1(D195N)*, *atftsZ1-1(G267R)* and *atftsZ1-1(R298Q)* (Figs. 4F H, J L, Q, U, 5F H, J L, Q, U); Ws-2 (Figs. 4R, V, 5R, 5V) for *atftsZ1-1(G366A)* and *atftsZ1-1(Δ404-433)* (Figs. 4S, T, W, X, 5S, T, W, X). *atftsZ1-1-Δ1* also served as a negative control for FtsZ1 localization.

Immunolocalization of FtsZ proteins in both mature leaves (Fig. 4F) and young leaves (Fig. 5F) did not detect FtsZ1 in *atftsZ1-1-Δ1*, consistent with immunoblot data (Figs. 1E and 6, upper panel lanes 3 and 4). However, FtsZ2 was detected as abnormally long, random filaments in both tissues (Figs. 4J, 5J). Our localization data are consistent with previous antisense suppression studies of *AtftsZ1-1* (Vitha et al. 2001) and further confirm that *atftsZ1-1-Δ1* is a null allele. Interestingly, occasional FtsZ2 rings could be detected in smaller chloroplasts, such as those found in the vasculature of the leaf (Fig. 5J, inset). This suggests that the size of the chloroplast and the ability to form a Z ring are inversely related when FtsZ1 is lacking. In other words, as the chloroplast becomes larger, fewer Z rings are formed.

The only mutant recovered with a mutation in the NTD that also expresses FtsZ1 protein, *atftsZ1-1(D159N)*, exhibited enlarged chloroplasts (Fig. 4C) containing FtsZ1 and FtsZ2 filaments that were long, and not positioned exclusively to the midplastid, though some do appear to be parallel (Fig. 4G, K). A similar Z filament phenotype was also observed in young leaves (Fig. 5G, K). This indicates that the predicted lateral surface residue D159 is not required for Z filament formation, but is important for proper Z ring positioning. However, it is possible that this mutation might hyperstabilize FtsZ filaments, which might also impact FtsZ dynamics. Interestingly, the smaller chloroplast population did exhibit some Z rings that appear to be positioned at the midplastid (Fig. 4G, double arrow). The most severe disruption of Z ring morphology was consistently correlated with the largest chloroplasts.

Of all the *atftsZ1-1* alleles in this study, including the null allele, the most severe phenotype is exhibited by *atftsZ1-1(G267R)*. In young leaves, as in protein extracts from young leaves (Fig. 6, lane 7), mutant FtsZ1 protein was detected by immunofluorescent staining in *atftsZ1-1(G267R)* (Fig. 5H), but not in mature leaves (Fig. 4H). However, unlike staining of chloroplasts from young Col-0 leaves where FtsZ was localized to rings (Fig. 5E, I), the mutant FtsZ1 protein was localized to punctate structures with a diffuse pattern (Fig. 5H). This pattern was most obvious in the small chloroplasts found in the vascular tissues in young leaves (Fig. 5H, inset). Intriguingly, the FtsZ2 protein in the young leaves did not exhibit a dispersed punctate localization pattern, but rather formed abnormally long, random filaments (Fig. 5L). Consistent with the reduced detection of FtsZ1 protein from immunoblotting of mature leaf protein extracts (Fig. 6, lane 8), the mutant FtsZ1 protein was barely detectable by immunostaining in the enlarged chloroplasts of expanded leaves, and cannot be distinguished from background labeling (Fig. 4H). FtsZ2 protein in these chloroplasts was also detected as abnormally long, disorganized filaments, many

of which appeared fragmented or discontinuous (Fig. 4L). In addition, the phenotypes exhibited in *atftsZ1-1(G267R)* are consistent with antisense lines that suppress AtFtsZ1-1 and AtFtsZ2-1 expression (Osteryoung et al. 1998). However, it should be noted that the number and size of chloroplasts in *atftsZ1-1-A1* and antisense FtsZ lines were much more variable compared with the phenotype of *atftsZ1-1(G267R)*, which is consistently severe (1–3 chloroplasts).

In young leaves of *atftsZ1-1(R298Q)*, FtsZ1 and FtsZ2 were both localized to rings and filaments (Fig. 5Q, U). However, the FtsZ1 filaments were faint and difficult to detect, consistent with immunoblot data (Fig. 6, lane 9). Despite a significant reduction in FtsZ1 protein in mature leaves, however, FtsZ2 was detected in Z rings at the midplastid (Fig. 4U), while FtsZ1 was not detected (Fig. 4Q). This phenotype is in stark contrast to the chloroplast morphology of antisense AtFtsZ1 lines that exhibit greatly enlarged chloroplasts and disrupted FtsZ2 filament morphology when FtsZ levels are reduced (Osteryoung et al. 1998, Vilha et al. 2001). However, there is an important difference between *atftsZ1-1(R298Q)* and antisense or null lines. In the null mutant, AtFtsZ1-1 protein is not produced, and in the antisense line the level of protein is regulated at the level of transcription. However, *atftsZ1-1(R298Q)* does generate a transcript, and the AtFtsZ1-1 protein that is produced is properly targeted to the chloroplast and processed based on the migration of the mutant FtsZ1 protein by SDS-PAGE (Fig. 6, lanes 1 and 9). This shows that the regulation of FtsZ1 protein level in this mutant is post-transcriptional, and there appears to be sufficient protein entering the chloroplast to form the faintly detected Z filaments despite the reduced accumulation of FtsZ1 protein.

Immunofluorescence labeling in mature and young leaves of *atftsZ1-1(G366A)* detected FtsZ1 and FtsZ2 primarily at the midplastid (Figs. 4S, W, 5S, W). The largest chloroplasts exhibited multiple rings or possibly spiral-shaped Z filaments that sometimes appeared to branch (Fig. 4S, W). The Z filaments appeared as more normal Z rings in the smaller plastids of the mutant (Fig. 4W). In the young leaves, many more chloroplasts were observed to contain Z rings that did not appear branched or as spirals (Fig. 5S, W). This finding is consistent with FtsZ2 rings seen in small chloroplasts of the null mutant (Fig. 5J, inset), and Z rings detected in the smaller chloroplasts of *atftsZ1-1(D159N)* (Fig. 4K, double arrow). These data further support a relationship between chloroplast size and Z ring formation. The results indicate that G366 is not essential for midplastid positioning of FtsZ1 or FtsZ2 or for FtsZ filament formation, but does influence Z ring morphology.

Z ring positioning and morphology were relatively normal in the slightly enlarged chloroplasts of

atftsZ1-1(A404–433), with nearly all chloroplasts containing FtsZ rings detected at the midplastid in both mature and young leaves (Figs. 4T, X, 5T, X). These data show that the extreme C-terminus is not required for positioning, polymerization or ring formation of FtsZ. However, the increased chloroplast size suggests that the last 30 residues of FtsZ1 may play a role in chloroplast division unrelated to Z ring assembly, perhaps via interaction with downstream division factors. These residues may also be important for FtsZ1 stability based on the reduced level of this C-terminally truncated FtsZ1 protein. It should be noted that this mutation does not truncate any portion of the core protein and that the encoded protein structurally resembles FtsZ from *M. jannaschii* in lacking a C-terminal conserved motif (Fig. 2A).

Viability of *atftsZ1-1* mutants

Since none of the mutants in this study exhibited aplastic cells, including the null and *atftsZ1-1(G267R)* mutants, we concluded that plastid division is occurring at some basal level so that each cell inherits some chloroplasts. In order to confirm that the disruption of chloroplast division does not alter the inheritance of plastids in the next generation, we examined seed set (Table 1). For each mutant and its respective wild type, we compared the number of mature seeds in five siliques from five individual plants. For each mutant there was no significant difference in the percentage of viable seed set in the mutant when compared with the respective wild-type seed set, indicating that FtsZ1 is not required for plant viability or propagation.

Discussion

Although most prokaryotes have a single *FtsZ* gene, *FtsZ* has undergone several independent gene duplication events, leading to the evolution of multiple FtsZ paralogs in some organisms (Vaughan et al. 2004). The evolution of FtsZ1 and FtsZ2 in plants and green algae from an FtsZ of cyanobacterial origin represents one such event. All FtsZ proteins share a common domain architecture that includes the variable N-terminal region, a conserved core region and a highly variable spacer region (Vaughan et al. 2004) (Fig. 2A). The majority of FtsZs, including all known cyanobacterial FtsZs and plant FtsZ2, also contain a C-terminal region that mediates interaction with specific accessory proteins (Ma et al. 1996, Ma et al. 1997, Maple et al. 2005). However, FtsZ1 is more divergent from its cyanobacterial counterparts than is FtsZ2 (Stokes and Osteryoung 2003, Rensing et al. 2004) and is among a number of FtsZ proteins from several unrelated taxa that lack the conserved C-terminal motif found in the majority of FtsZs (Vaughan et al. 2004). To our knowledge, the study on FtsZ1 presented here is the first in which the

functional consequences of mutations in an FtsZ that lacks the C-terminal region have been investigated. The results suggest important roles for specific regions and residues of FtsZ1 in chloroplast division.

FtsZ1 is not essential

Previously, we reported that plants expressing an *AtFtsZ1-1* antisense transgene were impaired in chloroplast division, but were not grossly affected in overall growth or morphology (Osteryoung et al. 1998, Vittha et al. 2001). However, in the antisense plants we could not rule out the possibility that low levels of *AtFtsZ1-1* expression persisted. Our finding in the present study that homozygous *atftsZ1-1-Δ1* null mutants can be isolated and propagated shows conclusively that FtsZ1 is not essential for viability in *Arabidopsis*. This is perhaps surprising given the conservation of FtsZ1 in plants. Multiple chloroplasts were often observed in a single cell in the null mutant and, as in the antisense plants, no leaf cells lacking chloroplasts were seen, further indicating that chloroplasts can be propagated during cell division in the absence of FtsZ1. How this occurs in *FtsZ1* or other large-chloroplast mutants is not yet known; alternative mechanisms of plastid partitioning in addition to binary fission, such as budding, have been reported (Pyke 1999, Forth and Pyke 2006). However, in all the *FtsZ1* mutants investigated, abnormal Z filament or chloroplast morphologies were evident in both young and mature leaves, indicating that FtsZ1, though not essential for viability, is necessary for maintenance of normal Z rings throughout leaf development. Also, when FtsZ1 filament morphology was disrupted, FtsZ2 filament morphology was also perturbed, consistent with previous co-localization and interaction studies, indicating an interaction between FtsZ1 and FtsZ2 (Vittha et al. 2001, Maple et al. 2005).

The chloroplast morphology phenotypes in the null mutant are more heterogeneous than we have observed previously in *AtFtsZ1-1* antisense lines (Osteryoung et al. 1998). This may be because the lines propagated for analysis in the early study were selected in part for their phenotypic consistency.

G267 and α -helix H9 are important for FtsZ1 accumulation

Comparisons of FtsZ1 levels between young and mature leaves of wild-type plants show a decrease in FtsZ1 protein levels as the leaves mature and expand (Fig. 6). *atftsZ1-1(G267R)* and *atftsZ1-1(R298Q)* exhibit reduced FtsZ1 accumulation relative to the wild type. These mutations alter residues in the predicted T7 loop and near α -helix H9 of FtsZ1, respectively, suggesting that these regions may be important for FtsZ1 accumulation in leaves. *FtsZ1* transcript levels are not reduced in these mutants relative to those in the wild type, showing that the changes in protein levels are post-transcriptional. It is possible that

the reduced FtsZ1 levels result from decreased translational efficiency of the transcripts, but we suggest that these changes are more likely to reflect enhanced degradation, perhaps because the mutant proteins are less likely to be present in assembled polymers due to their conformational defects. Consistent with this idea, FtsZ1 is not detected in rings or filaments in *atftsZ1-1(G267R)*, and fewer FtsZ1-containing rings and filaments are detected in *atftsZ1-1(R298Q)* than in the other *FtsZ1* mutants (excluding the null mutant) described in this study. Future *in vitro* biochemical studies will be important for investigating the ability of these and other mutants to assemble into polymers.

*The semi-dominant mutation in *atftsZ1-1(G267R)* alters a conserved glycine in the predicted T7 loop*

The mutation at G267 in *atftsZ1-1(G267R)* is semi-dominant. The glycine at this position is conserved in the T7 loop of plant and bacterial FtsZs, which comprises part of the active site for GTP hydrolysis (Löwe and Amos 1999, Lu et al. 2001, Scheffers et al. 2002). Mutations in the equivalent residue have not been reported for the bacterial proteins, but other T7 loop mutants in *E. coli* FtsZ exhibit reduced polymerization and/or GTP hydrolysis *in vitro*. Further, the mutant *E. coli* proteins retain their ability to interact with and suppress the GTPase activity of wild-type FtsZ (Scheffers et al. 2002). The mutant FtsZ1 protein in *atftsZ1-1(G267R)* may be similarly impaired, which would explain both the dominant-negative phenotype in the heterozygote and the fact that the homozygote consistently exhibits a more severe chloroplast division phenotype than does the *atftsZ1-1-Δ1* null mutant. Our results show that FtsZ1 cannot tolerate an arginine substitution at G267, and suggest that the equivalent T7 loop glycine may be critical for the activity of other FtsZs as well.

**atftsZ1-1(R298Q)* phenotype suggests that FtsZ1 may be more important in young than mature leaves*

An apparent contradiction of our results is that *atftsZ1-1(R298Q)* has a less severe chloroplast division phenotype but lower FtsZ1 protein levels than the other mutants described here except for *atftsZ1-1(Δ404–433)*. The low level of FtsZ1 in *atftsZ1-1(R298Q)* suggests that the lesion destabilizes the protein, possibly through the loss of a predicted ionic interaction between R298 and D331 (Fig. 3, inset). However, in young leaves, enough mutant FtsZ1 protein is apparently available and sufficiently competent to allow the formation of some midplastid FtsZ1-containing Z rings *in vivo*, although FtsZ1 is not detected in mature leaves. In addition, FtsZ2 ring morphology is not altered in leaf mesophyll chloroplasts of *atftsZ1-1(R298Q)*. These results show that R298 is not required for Z ring formation or positioning, and suggest that FtsZ1

activity may be most important for propagation of chloroplasts during early leaf development.

D159 and G366 are important for FtsZ1 dynamics

In order for the Z ring to contract during binary fission and be repositioned to the middle of the new daughter chloroplasts, FtsZ polymers must undergo dynamic rearrangement. Two of the mutants in this study may be defective in FtsZ1 dynamics. *atftsZ1-1(D159N)* exhibits a unique Z filament morphology of overly long, possibly branched filaments (Figs. 4G, K, 5G, K), suggesting that FtsZ polymers may be hyperstabilized in this mutant. D159 is a lateral surface residue just N-terminal of the conserved tubulin motif (GGGTGT/SG). Mutation of the equivalent residue in *E. coli* FtsZ, D96, reduces GTP binding and hydrolysis, and the mutant protein cannot rescue the *ftsZ84* mutant though it is able to polymerize in vitro (Lu et al. 2001, Redick et al. 2005). One possible explanation for the aberrant FtsZ morphology in *atftsZ1-1(D159N)* is that substitution of a negatively charged side chain with a polar uncharged side chain at D159 excessively stabilizes FtsZ1 interactions, perhaps with adjacent Z filaments or unknown accessory factors, inhibiting disassembly and resulting in a loss of control of FtsZ midplastid positioning.

atftsZ1-1(G366A) also appears to have excess FtsZ1 filaments, but these are properly positioned in rings or possibly spirals (Fig. 4S, W), indicating that G366 is not required for midplastid positioning of FtsZ1. However, the filament morphology suggests that the mutant G366A protein may be impaired in its ability to be remodeled or repositioned. Interestingly, the FtsZ filament morphology in *atftsZ1-1(G366A)* resembles that of a recently described temperature-sensitive *B. subtilis* FtsZ mutant, *ts1* (Michie et al. 2006). At the non-permissive temperature, the mutant FtsZ protein in *ts1* forms spiral-like Z filaments that localize to the midcell. The spirals in the *ts1* mutant are hypothesized to represent a trapped FtsZ intermediate with reduced ability to be reorganized into rings (Michie et al. 2006). Although G366 is not near the affected residue in the *ts1* mutant, the Z filament morphology in *atftsZ1-1(G366A)* suggests that G366 may play a similar role in reorganizing FtsZ1 in the chloroplast. Consistent with this possibility, we have observed FtsZ1- and FtsZ2-containing spirals extending from the midplastid Z ring in deeply constricted plastids in wild-type, *pdv1*, *pdv2* and *arc5*, suggesting that a spiral intermediate could be part of a mechanism for redeploying chloroplast FtsZs to the new division site in newly divided chloroplasts (Vitha et al. 2001, Miyagishima et al. 2006).

FtsZ1 as well as FtsZ2 is abnormally localized in *atftsZ1-1(D159N)* and *atftsZ1-1(G366A)* (Fig. 4G, K, S, W), though FtsZ1 protein levels are not dramatically reduced in these mutants, particularly in young leaves

(Fig. 6, lanes 5, 6, 11 and 12). These findings suggest a role for FtsZ1 in regulating FtsZ2 filament morphology in vivo.

The extreme C-terminus of FtsZ1 is not required for FtsZ1 ring formation or positioning

The presence of FtsZ1 in midplastid rings and filaments in *atftsZ1-1(Δ404-433)* indicates that the FtsZ1 C-terminus is not involved in regulation of Z ring morphology or positioning in chloroplasts. This is consistent with the complete lack of a corresponding C-terminal region in *M. jamaicensis* (Fig. 2A) and other Archaea FtsZ proteins (Vaughan et al. 2004), and the finding that the C-terminal region in *E. coli* FtsZ is not required for Z ring assembly (Wang et al. 1997, Osawa and Erickson 2005). However, there appears to be a conservation of C-terminal amino acids unique to plant FtsZ1 proteins (Rensing et al. 2004), suggesting that this region is important for another aspect of FtsZ1 function such as interaction with other division factors, similar to the C-terminal regions of *E. coli* FtsZ and plant FtsZ2 (Ma and Margolin 1999, Maple et al. 2005). The C-terminus of FtsZ1 may also be important for FtsZ1 accumulation based on the reduced FtsZ1 protein levels in *atftsZ1-1(Δ404-433)*, but as the transcript lacks the native 3'-untranslated region, the decreased protein accumulation may be a consequence of reduced translational efficiency. Nevertheless, reduction of FtsZ1 per se. at least to the level in *atftsZ1-1(Δ404-433)*, does not prevent Z ring formation and midplastid positioning.

Heterogeneity of chloroplast size suggests a relationship between chloroplast size and Z ring formation

atftsZ1-1(D159N), *atftsZ1-1(R298Q)* and *atftsZ1-1(G366A)* exhibit chloroplast size heterogeneity. This probably reflects the fact that chloroplast compartment volume is maintained at a constant proportion of cell size through a combination of chloroplast division and chloroplast expansion (Pyke 1997, Pyke 1999). In *Arabidopsis* leaf mesophyll cells, chloroplasts do not divide synchronously; only a subset of chloroplasts can be observed undergoing division in expanding cells (Pyke 1997, Pyke 1999). We suggest that, in the *FtsZ1* mutants, individual chloroplasts that cannot divide normally because of impaired FtsZ function would nevertheless continue to expand. Once the prescribed chloroplast compartment volume is reached, division of all chloroplasts would be inhibited. Consistent with this likelihood, altered Z filament morphology was primarily detected in the enlarged chloroplasts of *atftsZ1-1(D159N)* and *atftsZ1-1(G366A)* (Fig. 4G, S), and much less frequently in smaller chloroplasts (Fig. 4G, double arrow; Fig. 5S, W). In addition, FtsZ2 rings were detected in the very small chloroplasts of the null mutant (Fig. 5J, inset). As the chloroplasts increase in size, the altered Z ring morphology becomes more pronounced, culminating

in the observed phenotypes. In this study, all the mutants, with the exception of *atftsZ1-1(G267R)* and *atftsZ1-1(Δ404-433)*, exhibited some degree of chloroplast size heterogeneity.

In conclusion, we have found that mutations in FtsZ1 impact FtsZ1 protein level, FtsZ1 filament morphology, chloroplast size and number, and FtsZ2 filament morphology, but not FtsZ2 protein levels. The latter demonstrates that FtsZ2 protein levels are regulated independently of FtsZ1 protein level. The *in vivo* results reported here can be compared with the results of *in vitro* biochemical assays on recombinant FtsZ1 proteins once such assays become available (work in progress). However, D159 and G366 appear to be important for FtsZ dynamics during chloroplast division. We have also found that plants completely lacking FtsZ1 (null) or having a dominant-negative phenotype [*atftsZ1-1(G267R)*] are viable and that each mesophyll cell contains at least one chloroplast, indicating that FtsZ1 is not essential to plant viability or chloroplast propagation. However, FtsZ1 is essential for maintaining wild-type chloroplast numbers. A key advantage of many small chloroplasts over a few large ones in land plants is probably their ability to be repositioned in response to light stimulus, both to maximize light absorption under low light and to minimize photoinhibition under high light. Consistent with this idea, Jeong et al. (2002) showed that large chloroplasts in tobacco plants overexpressing tobacco *FtsZ1* are defective in movement and more susceptible to photodamage than in the wild type. Our finding here that the *pmi4* mutant is an allele of *FtsZ1* further emphasizes the relationship between chloroplast division and chloroplast movement.

Materials and Methods

Plant material

Seed stock from *A. thaliana* seed for SALK_073878 and the *arc10* mutant (CS282) were obtained from the Arabidopsis Biological Resource Center (Ohio State University, Columbus, OH, USA) (<http://www.arabidopsis.org/abrc/>). The *arc10* mutant was isolated from a T-DNA mutagenized population of Ws-2 (Pyke and Leech 1994). Seed of *pmi4* was obtained from an EMS-mutagenized population of Col-0 (DeBlasio et al. 2005). Seed of *atftsZ1-1(D159N)* and *atftsZ1-1(R298Q)* were obtained from a plastid division mutant screen from an EMS-mutagenized M₂ population of Col-0 seed (Lehle Seeds). Seed of *atftsZ1-1(Δ404-433)* was obtained through a PCR-based screening of the T-DNA insertion population of Ws-2 (Sussman et al. 2000).

All mutants and wild-type seeds were sown in 1/2x Hoagland's soaked soil and grown in a chamber at 21°C with a day/night cycle of 16/8 h for 3-4 weeks as previously described (Osteryoung et al. 1998). The young expanding leaves from the inner rosette, expanding leaves from the outer rosette and fully expanded leaves were harvested for immunoblotting or immunostaining analysis (Stokes et al. 2000).

Identification of a Salk T-DNA insertion mutant

A mutant bearing a T-DNA insertion within *AtFtsZ1-1* (At5g55280; SALK_073878) was identified through a database search of the Salk Institute Genomic Analysis Laboratory website (<http://signal.salk.edu/cgi-bin/tdnaexpress>) (Fig. 1A). To determine the genotype of plants bearing the T-DNA insertion, the following primers were used: *AtFtsZ1-1* LP, 5'-CAGAGCTTGGCAATCCGTGTT-3'; *AtFtsZ1-1* RP, 5'-AAGCATGCGCAAA GTCAGTCG-3'; and a T-DNA left border primer LBb1, 5'-GCGTGGACCGCTTGCTGCAACT-3'. The presence of a wild-type allele was determined by PCR using the gene-specific primers that flanked the insertion site (LP and RP), while a combination of a T-DNA left border primer and RP was used to identify the mutant allele. The nucleotide sequences of the DNA fragments resulting from PCR amplification using primers specific for the T-DNA left border and one of the flanking sequences was determined.

FtsZ1-1 screen of the Wisconsin T-DNA insertion population

An insertion mutant *atftsZ1-1(Δ404-433)* was obtained by PCR-based screening of the T-DNA insertion population from the Arabidopsis Knockout Facility at the University of Wisconsin-Madison (Sussman et al. 2000) using the following primers: LB 5'-CATTTATAATAACGCTGCGGACATCTAC-3', and flanking primers forward 5'-CCACTCGATCTCTCACCTTTCCTTT GTG-3', and reverse 5'-AGAAAAGTCTACGGGGAGAAGAC GATTTG-3'. The population consists of 72,960 BASTA-resistant lines in ecotype Ws-2 transformed with an activation-Tag vector, pSK1015. Using the recommended methods, several rounds of PCR screening were followed by Southern blotting analysis, and further confirmation by sequence analysis identified a T-DNA insertion in *AtFtsZ1-1*.

pmi4 mutant screen

pmi4 was isolated from M₂ EMS-mutagenized Col-0 population screened for plastid mobility impaired mutants and crossed into *Ler* for genetic mapping (DeBlasio et al. 2005). F₂ progeny exhibiting altered chloroplast movement responses were then screened microscopically to confirm the homozygous chloroplast division phenotype. Division-defective F₂s were mapped to a 58 kb region of chromosome 5 between MCO15B at 22,416 kb and MET17A at 22,474 kb, which includes *At5g55280*. The *At5g55280* locus was PCR amplified from *pmi4* genomic DNA and the resultant sequence was compared with that of Col-0. All original simple sequence length polymorphism (SSLP) markers were made with the polymorphic database on TAIR (<http://www.arabidopsis.org/>) and from the CEREBON database (Jander et al. 2002).

EMS plastid division mutant screen

Two mutants defective in plastid division were isolated by a visual microscopy-based screen of leaves from an M₂ population of EMS-mutagenized Col-0 (Lehle Seeds). Mutants with defective chloroplast division phenotypes were analyzed for linkage to known plastid division genes, followed by sequencing the plastid division gene with significant linkage. Two new alleles of *AtFtsZ1-1* were identified in this screen and designated *atftsZ1-1(D159N)* and *atftsZ1-1(R298Q)*.

Genetic mapping of *arc10*, *atftsZ1-1(D159N)* and *atftsZ1-1(R298Q)*

arc10, *atftsZ1-1(D159N)* and *atftsZ1-1(R298Q)* were crossed into *Ler* to generate mapping populations. F₂ plants

identified by DIC (differential interference contrast) microscopy to have the corresponding mutant phenotype were used for mapping. CER436625 (5'-TACICCGTTTGGGCGTTTAT-3' and 5'-TGGTAGTCTGAATAACGAAACG-3') and SHIG015 (5'-TGCTAACGTTTCGAACATGG-3' and 5'-GGTTTGATGAGCAACATGG-3') on chromosome 5 tightly linked *arc10* to *AtFtsZ1-1*, and markers CER436625 and CER456386 (5'-AGTAACTCAAACCAAACAAGGAC-3' and 5'-TTTGATGCATCATAACAGAAAGTC-3') linked *atftsZ1-1D159N* and *atftsZ1-1R298Q* to *AtFtsZ1-1*. Mapping primers for CAPS (cleaved amplified polymorphic sequences) and SSLP markers created from the polymorphic database on TAIR (<http://www.arabidopsis.org>) and from the CERON database (Jander et al. 2002) were obtained from Invitrogen (Carlsbad, CA, USA). CAPS markers were digested for 1 h in 20 µl reactions using 10 µl of PCR product with sufficient enzyme to achieve proper digestion. SSLP and digested CAPS marker fragments were then resolved by agarose gel electrophoresis and the resultant banding patterns analyzed.

Complementation of *atftsZ1-1-A1* and *arc10*

Both lines were transformed with *AtFtsZ1-1* under the control of 500 bp of the putative upstream native promoter. Full-length *AtFtsZ1-1* was PCR amplified from Col-0 genomic DNA with *PfiTurbo* (Stratagene, La Jolla, CA, USA) using primer pair 5'-TCAGACAAGAACAACCTCAAAC-3' and 5'-TACATCCAGTTAGAACCAATCAT-3'. The PCR product was cloned into pGEM-T Easy (Promega) and the subsequent subclone digested with *NotI* and further subcloned into the *NotI* site of pMLBART, a derivative of pART27 (Gleave 1992) that confers resistance to the herbicide glufosinate as a selectable marker. *Agrobacterium*-mediated transformation of Arabidopsis and selection of T₁ transformants were performed as described previously (Vitha et al. 2001). The resulting T₁ plants were selected for BASTA resistance, and chloroplast morphology in leaf mesophyll cells was assessed as described previously.

Secondary and three dimensional structure modeling

Full-length amino acid sequences of AtFtsZ1-1 (NP_200539), AtFtsZ2-1 (NP_190843), AtFtsZ2-2 (NP_565839), EcFtsZ (AAC73206) and MjFtsZ (Q57816) were used for structure prediction. The AtFtsZ1-1 structure was generated from SWISS-MODEL and analyzed with the accompanying DeepView software (Peitsch et al. 1995, Guex and Peitsch 1997, Schwede et al. 2003). The WHAT_CHECK report generated for the predicted structure determined that there were no major problems with the structure.

Analysis of chloroplast phenotype

Leaf tissue was fixed and macerated to separate individual cells as described previously (Osteryoung et al. 1998). Mesophyll cells were viewed using an Olympus BH2 microscope equipped with DIC optics and a 40× objective. Images were captured with a Leica DFC320 digital camera.

Immunofluorescence microscopy

Tissue samples were embedded in Steedman's wax, sectioned and immunostained essentially as previously described in Vitha et al. (2001), except that the sections were incubated with anti-FtsZ antibody diluted 1:3,500 overnight at room temperature, and a second blocking step, identical to the first, was added prior to incubation with secondary antibody. The samples were then incubated with goat anti-rabbit Alexa Fluor 488 conjugate

(Molecular Probes) for 4 h at room temperature at 1:300 dilution. Samples were viewed with a Leica DMRA2 fluorescence microscope equipped with 100×/1.35 and 63×/1.32 oil immersion objectives using fluorescein isothiocyanate (FITC, excitation 460–500 nm, emission 512–545 nm) and Cy3 (excitation 510–560 nm, emission 572–647 nm) filter sets. The fluorescence collected through the Cy3 filter set was used to visualize chloroplast shape in expanding leaves. Stacks of optical sections were captured using VolumeScan software (Vaytek, Fairfield, IA, USA) and a Retiga 1350xi cooled CCD camera (Qimaging, Burnaby, BC, Canada), with the z-step set to 0.4 µm for mature leaf tissue and to 0.25 µm for young leaf tissue. The FITC and Cy3 image stacks were processed using ImageJ ver. 1.37v software (<http://rsb.info.nih.gov/ij/>) by unsharp masking (mask weight 0.55, Gaussian radius 4 and 15 for FITC and Cy3, respectively), merged to RGB and then projected to achieve extended depth of focus (brightest point method). Assembly and annotation of figures and final adjustment of brightness and contrast were performed using Adobe Photoshop version 6.0.

Western blotting and immunoblotting

Western blot analysis of FtsZ levels in FtsZ mutants and wild-type controls was performed as previously described in Stokes et al. (2000), with the following modifications in sample preparation. Leaves from 3-week-old plants were snap-frozen in liquid nitrogen, crushed with a mortar and pestle, and then suspended in 1.5× plant extraction buffer [1.5× plant extraction buffer is 90 mM Tris HCl (pH 8.0), 3% SDS, 22.5% sucrose, protease inhibitors (5 mM *ε*-amino-*N*-caproic acid and 1 mM benzamide) and 100 mM dithiothreitol (DTT)]. The samples were then heated at 90°C for 10 min and the insoluble debris was pelleted by centrifugation for 10 min at 16,000×g at room temperature. The supernatant from each sample was loaded based on equal fresh weight on a 10% SDS polyacrylamide gel for subsequent analysis.

RT-PCR analysis

Total RNA was isolated from 8-day-old shoots grown on MS plates under the same growth conditions as for soil-grown plants above. The shoots were snap-frozen in liquid nitrogen, ground in a mortar and pestle, and total RNA extracted using an RNeasyTM kit (Qiagen Inc., Valencia, CA, USA). Reverse transcription was performed on 5 µg of total RNA using SuperScript IITM (Invitrogen) according to the manufacturer's recommendations with oligo(dT) primers. *AtFtsZ1-1* and *AtFtsZ2-1* transcripts were amplified using the following primer pairs: 18,897 (5'-ATAAACACGGATTTCGCAAGCTC-3') and 8,080 (5'-CCGATCAATGGAGCCAAAGTTG-3'); 9,137 (5'-TCGAAGAAGA ACTGTTTCAGGCTC-3') and 9,179 (5'-GGTTATGCTTACTTGAACCG-3') from 1.0 µl of final reverse transcription product in 22, 24 and 26 cycles. *Actin 2* was amplified using the primer pair: ACT2-1 (5'-GGCTCCTCTTAACCCAAAGG-3') and ACT2-2 (5'-TTCTCGATGGAAGAGCTGGT-3') from 0.5 µl of final reverse transcription product in 22, 24 and 26 cycles. The band intensities from each of the mutant allele RT-PCRs were compared with the respective wild-type and actin controls.

Seed set analysis

The siliques from fully mature Arabidopsis plants were harvested, placed on a microscope slide using double-sided tape and gently opened to expose the developed seeds. The numbers of mature, abnormal and aborted seeds were counted and the percentage of mature seeds was calculated based on the sum of all the potential seeds. The difference in the percentage of seed set

from 100% represents the percentage of seeds that were abnormal or aborted.

Supplementary material

Supplementary material mentioned in the article is available to online subscribers at the journal website www.pcp.oxfordjournals.org.

Acknowledgments

The authors thank Dr. Stanislav Vitha for technical assistance in processing immunolocalization micrographs, Joyce Bowyer for assisting with analysis of the null allele, and Eric Greenberg for seed set analysis. This research was funded by US National Science Foundation grants NSF-0313520 and CMB-0544676 (to K.W.O.) and IBN-0080783 (to R.P.H.).

References

- Addinall, S.G., Small, E., Whitaker, D., Sturrock, S., Donachie, W.D. and Khattar, M.M. (2005) New temperature-sensitive alleles of *ftsZ* in *Escherichia coli*. *J. Bacteriol.* 187: 358–365.
- Aldridge, C., Maple, J. and Moller, S.G. (2005) The molecular biology of plastid division in higher plants. *J. Exp. Bot.* 56: 1061–1077.
- Alonso, J.M., Stepanova, A.N., Llesse, T.J., Kim, C.J., Chen, H., et al. (2003) Genome-wide insertional mutagenesis of *Arabidopsis thaliana*. *Science* 301: 653–657.
- Colletti, K.S., Tattersall, E.A., Pyke, K.A., Froehlich, J.E., Stokes, K.D. and Osteryoung, K.W. (2000) A homologue of the bacterial cell division site-determining factor MmD mediates placement of the chloroplast division apparatus. *Curr. Biol.* 10: 507–516.
- DeBlasio, S.L., Luesse, D.L. and Hangarter, R.P. (2005) A plant-specific protein essential for blue-light-induced chloroplast movements. *Plant Physiol.* 139: 101–114.
- de Boer, P., Crossley, R. and Rothfield, L. (1992) The essential bacterial cell-division protein *FtsZ* is a GTPase. *Nature* 359: 254–256.
- El-Kafafi, E.S., Mukherjee, S., El-Shami, M., Putaux, J.L., Block, M.A., Pignot-Paintrand, I., Lerbs-Mache, S. and Falconet, D. (2005) The plastid division proteins, FtsZ1 and FtsZ2, differ in their biochemical properties and sub-plastid localization. *Biochem. J.* 387: 669–676.
- Erickson, H.P. (1998) Atomic structures of tubulin and FtsZ. *Trends Cell Biol.* 8: 133–137.
- Forth, D. and Pyke, K.A. (2006) The *suffulta* mutation in tomato reveals a novel method of plastid replication during fruit ripening. *J. Exp. Bot.* 57: 1971–1979.
- Gaikwad, A., Babbarwal, V., Pant, V. and Mukherjee, S.K. (2000) Pea chloroplast FtsZ can form multimers and correct the thermosensitive defect of an *Escherichia coli ftsZ* mutant. *Mol. Gen. Genet.* 263: 213–221.
- Gleave, A.P. (1992) A versatile binary vector system with a T-DNA organizational structure conducive to efficient integration of cloned DNA into the plant genome. *Plant Mol. Biol.* 20: 1203–1207.
- Guex, N. and Peitsch, M.C. (1997) SWISS-MODEL and the Swiss-PdbViewer: an environment for comparative protein modeling. *Electrophoresis* 18: 2714–2723.
- Itoh, R., Fujiwara, M., Nagata, N. and Yoshida, S. (2001) A chloroplast protein homologous to the eubacterial topological specificity factor MmE plays a role in chloroplast division. *Plant Physiol.* 127: 1644–1655.
- Jander, G., Norris, S.R., Rounsley, S.D., Bush, D.F., Levin, I.M. and Last, R.L. (2002) *Arabidopsis* map-based cloning in the post-genome era. *Plant Physiol.* 129: 440–450.
- Jeong, W.J., Park, Y.-I., Suh, K., Raven, J.A., Yoo, O.J. and Liu, J.R. (2002) A large population of small chloroplasts in tobacco leaf cells allows more effective chloroplast movement than a few enlarged chloroplasts. *Plant Physiol.* 129: 112–121.
- Löwe, J. (1998) Crystal structure determination of FtsZ from *Methanococcus jannaschii*. *J. Struct. Biol.* 124: 235–243.
- Löwe, J. and Amos, L.A. (1998) Crystal structure of the bacterial cell-division protein FtsZ. *Nature* 391: 203–206.
- Löwe, J. and Amos, L.A. (1999) Tubulin-like protofilaments in Ca²⁺-induced FtsZ sheets. *EMBO J.* 18: 2364–2371.
- Lu, C., Stricker, J. and Erickson, H.P. (2001) Site-specific mutations of FtsZ—effects on GTPase and in vitro assembly. *BMC Microbiol.* 1: 7.
- Ma, X., Ehrhardt, D.W. and Margolin, W. (1996) Colocalization of cell division proteins FtsZ and FtsA to cytoskeletal structures in living *Escherichia coli* cells by using green fluorescent protein. *Proc. Natl. Acad. Sci. USA* 93: 12998–13003.
- Ma, X. and Margolin, W. (1999) Genetic and functional analyses of the conserved C-terminal core domain of *Escherichia coli* FtsZ. *J. Bacteriol.* 181: 7531–7544.
- Ma, X., Sun, Q., Wang, R., Singh, G., Jonietz, E.L. and Margolin, W. (1997) Interactions between heterologous FtsA and FtsZ proteins at the FtsZ ring. *J. Bacteriol.* 179: 6788–6797.
- Maple, J., Aldridge, C. and Moller, S.G. (2005) Plastid division is mediated by combinatorial assembly of plastid division proteins. *Plant J.* 43: 811–823.
- Maple, J., Chua, N.H. and Moller, S.G. (2002) The topological specificity factor AtMinE1 is essential for correct plastid division site placement in *Arabidopsis*. *Plant J.* 31: 269–277.
- Maple, J., Fujiwara, M.T., Kitahata, N., Lawson, T., Baker, N.R., Yoshida, S. and Moller, S.G. (2004) GIANT CHLOROPLAST 1 is essential for correct plastid division in *Arabidopsis*. *Curr. Biol.* 14: 776–781.
- Machte, K.A., Monahan, L.G., Beech, P.L. and Harry, E.J. (2006) Trapping of a spiral-like intermediate of the bacterial cytokinetic protein FtsZ. *J. Bacteriol.* 188: 1680–1690.
- Miyajima, S.Y., Froehlich, J.E. and Osteryoung, K.W. (2006) PDV1 and PDV2 mediate recruitment of the dynamin-related protein ARC5 to the plastid division site. *Plant Cell* 18: 2517–2530.
- Nogales, E., Downing, K.H., Amos, L.A. and Löwe, J. (1998) Tubulin and FtsZ form a distinct family of GTPases. *Nat. Struct. Biol.* 5: 451–458.
- Oliva, M.A., Cordell, S.C. and Lowe, J. (2004) Structural insights into FtsZ protofilament formation. *Nat. Struct. Mol. Biol.* 11: 1243–1250.
- Osawa, M. and Erickson, H.P. (2005) Probing the domain structure of FtsZ by random truncation and insertion of GFP. *Microbiology* 151: 4033–4043.
- Osteryoung, K.W. and McAndrew, R.S. (2001) The plastid division machine. *Annu. Rev. Plant Physiol. Plant Mol. Biol.* 52: 315–333.
- Osteryoung, K.W. and Nunnari, J. (2003) The division of endosymbiotic organelles. *Science* 302: 1698–1704.
- Osteryoung, K.W., Stokes, K.D., Rutherford, S.M., Percival, A.L. and Lee, W.Y. (1998) Chloroplast division in higher plants requires members of two functionally divergent gene families with homology to bacterial *ftsZ*. *Plant Cell* 10: 1991–2004.
- Osteryoung, K.W. and Vierling, E. (1995) Conserved cell and organelle division. *Nature* 376: 473–474.
- Peitsch, M.C., Wells, T.N., Stampf, D.R. and Sussman, J.L. (1995) The Swiss-3DImage collection and PDB-Browser on the World-Wide Web. *Trends Biochem. Sci.* 20: 82–84.
- Pyke, K.A. (1997) The genetic control of plastid division in higher plants. *Amer. J. Bot.* 84: 1017–1027.
- Pyke, K.A. (1999) Plastid division and development. *Plant Cell* 11: 549–556.
- Pyke, K.A. and Leach, R.M. (1994) A genetic analysis of chloroplast division and expansion in *Arabidopsis thaliana*. *Plant Physiol.* 104: 201–207.
- RayChaudhuri, D. and Park, J.T. (1992) *Escherichia coli* cell-division gene *ftsZ* encodes a novel GTP-binding protein. *Nature* 359: 251–254.
- RayChaudhuri, D. and Park, J.T. (1994) A point mutation converts *Escherichia coli* FtsZ septation GTPase to an ATPase. *J. Biol. Chem.* 269: 22941–22944.
- Redick, S.D., Stricker, J., Briscoe, G. and Erickson, H.P. (2005) Mutants of FtsZ targeting the protofilament interface: effects on cell division and GTPase activity. *J. Bacteriol.* 187: 2727–2736.

- Rensing, S.A., Kessler, J., Reski, R. and Decker, E.L. (2004) Diversification of ftsZ during early land plant evolution. *J. Mol. Evol.* 58: 154–162.
- Rutherford, S.M. (1996) The genetic and physical analysis of mutants of chloroplast number and size in *Arabidopsis thaliana*. Department of Biology, University of York.
- Scheffers, D.J., de Wit, J.G., der Blaauwen, T. and Driessen, A.J. (2002) GTP hydrolysis of cell division protein FtsZ: evidence that the active site is formed by the association of monomers. *Biochemistry* 41: 521–529.
- Schwede, T., Kopp, J., Guex, N. and Peitsch, M.C. (2003) SWISS-MODEL: an automated protein homology-modeling server. *Nucleic Acids Res.* 31: 3381–3385.
- Stokes, K.D., McAndrew, R.S., Figueroa, R., Vitha, S. and Osteryoung, K.W. (2000) Chloroplast division and morphology are differentially affected by overexpression of *FtsZ1* and *FtsZ2* genes in *Arabidopsis*. *Plant Physiol.* 124: 1668–1677.
- Stokes, K.D. and Osteryoung, K.W. (2003) Early divergence of the FtsZ1 and FtsZ2 plastid division gene families in photosynthetic eukaryotes. *Gene* 320: 97–108.
- Sussman, M.R., Amasino, R.M., Young, J.C., Krysan, P.J. and Austin-Phillips, S. (2000) The *Arabidopsis* knockout facility at the University of Wisconsin-Madison. *Plant Physiol.* 124: 1465–1467.
- Vaughan, S., Wickstead, B., Gull, K. and Adainall, S.G. (2004) Molecular evolution of FtsZ protein sequences encoded within the genomes of archaea, bacteria, and eukaryota. *J. Mol. Evol.* 58: 19–29.
- Vitha, S., Froehlich, J.E., Kokstarova, O., Pyke, K.A., van Erp, H. and Osteryoung, K.W. (2003) ARC6 is a J-domain plastid division protein and evolutionary descendant of the cyanobacterial cell division protein FtsZ. *Plant Cell* 15: 1918–1933.
- Vitha, S., McAndrew, R.S. and Osteryoung, K.W. (2001) FtsZ ring formation at the chloroplast division site in plants. *J. Cell Biol.* 153: 111–119.
- Wang, D., Kong, D., Wang, Y., Hu, Y., He, Y. and Sun, J. (2003) Isolation of two plastid division ftsZ genes from *Chlamydomonas reinhardtii* and its evolutionary implication for the role of FtsZ in plastid division. *J. Exp. Bot.* 54: 1115–1116.
- Wang, X., Huang, J., Mukherjee, A., Cao, C. and Lutkenhaus, J. (1997) Analysis of the interaction of FtsZ with itself, GTP, and FtsA. *J. Bacteriol.* 179: 5551–5559.

(Received January 4, 2007; Accepted April 17, 2007)

REFERENCES

- Addinall, S.G., Bi, E. and Lutkenhaus, J. (1996) FtsZ ring formation in *fts* mutants. *J. Bacteriol.* 178: 3877-3884.
- Addinall, S.G. and Lutkenhaus, J. (1996) FtsA is localized to the septum in an FtsZ-dependent manner. *J. Bacteriol.* 178: 7167-7172.
- Ahmad, F.J., Yu, W., McNally, F.J. and Baas, P.W. (1999) An essential role for katanin in severing microtubules in the neuron. *J. Cell Biol.* 145: 305-315.
- Aldridge, C., Maple, J. and Moller, S.G. (2005) The molecular biology of plastid division in higher plants. *J. Exp. Bot.* 56: 1061-1077.
- Alonso, J.M., Stepanova, A.N., Leisse, T.J., Kim, C.J., Chen, H., et al. (2003) Genome-wide insertional mutagenesis of *Arabidopsis thaliana*. *Science* 301: 653-657.
- Altschul, S.F., Gish, W., Miller, W., Myers, E.W. and Lipman, D.J. (1990) Basic local alignment search tool. *J. Mol. Biol.* 215: 403-410.
- Anand, S., Rajeswari, H., Gupta, P., Srinivasan, R., Indi, S. and Ajitkumar, P. (2004) A C-terminal deletion mutant of *Mycobacterium tuberculosis* FtsZ shows fast polymerization in vitro. 150: 1119-1121.
- Anderson, D.E., Gueiros-Filho, F.J. and Erickson, H.P. (2004) Assembly dynamics of FtsZ rings in *Bacillus subtilis* and *Escherichia coli* and effects of FtsZ-regulating proteins. *J. Bacteriol.* 186: 5775-5781.
- Anderson, D.J. and Blobel, G. (1983) Immunoprecipitation of proteins from cell-free translations. *Methods Enzymol.* 96: 111-120.
- Andreu, J.M., Oliva, M.A. and Monasterio, O. (2002) Reversible unfolding of FtsZ cell division proteins from archaea and bacteria. Comparison with eukaryotic tubulin folding and assembly. *J. Biol. Chem.* 277: 43262-43270.
- Archer, E.K. and Keegstra, K. (1993) Analysis of chloroplast transit peptide function using mutations in the carboxyl-terminal region. *Plant Mol. Biol.* 23: 1105-1115.
- Arnon, D.I. (1949) Copper enzymes in isolated chloroplasts. Polyphenoloxidase in *Beta Vulgaris*. *Plant Physiol.* 24: 1-15.

- Barak, I. and Wilkinson, A.J. (2007) Division site recognition in *Escherichia coli* and *Bacillus subtilis*. *FEMS Microbiol. Rev.* 31: 311-326.
- Belmont, L.D. and Mitchison, T.J. (1996) Identification of a protein that interacts with tubulin dimers and increases the catastrophe rate of microtubules. *Cell* 84: 623-631.
- Bernhardt, T.G. and de Boer, P.A.J. (2005) SlmA, a nucleoid-associated, FtsZ binding protein required for blocking septal ring assembly over chromosomes in *E. coli*. *Mol. Cell* 18: 555-564.
- Bi, E. and Lutkenhaus, J. (1990a) FtsZ regulates frequency of cell division in *Escherichia coli*. *J. Bacteriol.* 172: 2765-2768.
- Bi, E. and Lutkenhaus, J. (1990b) Interaction between the min locus and ftsZ. *J. Bacteriol.* 172: 5610-5616.
- Bi, E. and Lutkenhaus, J. (1991) FtsZ ring structure associated with division in *Escherichia coli*. *Nature* 354: 161-164.
- Bi, E. and Lutkenhaus, J. (1993) Cell division inhibitors Sula and MinCD prevent formation of the FtsZ ring. *J. Bacteriol.* 175: 1118-1125.
- Bleazard, W., McCaffery, J.M., King, E.J., Bale, S., Mozdy, A., Tieu, Q., Nunnari, J. and Shaw, J.M. (1999) The dynamin-related GTPase Dnm1 regulates mitochondrial fission in yeast. *Nat. Cell Biol.* 1: 298-304.
- Borhani, D.W. and White, E.L. (2004) Polymerization of C-terminally truncated *Mycobacterium tuberculosis* FtsZ is unlikely to be physiologically relevant. *Microbiology* 150: 3903-3906.
- Bork, P., Sander, C. and Valencia, A. (1992) An ATPase domain common to prokaryotic cell cycle proteins, sugar kinases, actin, and hsp70 heat shock proteins. *Proc. Natl. Acad. Sci. U. S. A.* 89: 7290-7294.
- Bruce, B.D. (2000) Chloroplast transit peptides: structure, function and evolution. *Trends in Cell Biology* 10: 440-447.
- Bruce, B.D., Perry, S., Froehlich, J. and Keegstra, K. (1994) *In vitro* import of proteins into chloroplasts. In *Plant Molecular Biology Manual J1*. Edited by Gelvin, S.B. and Schilperoort, R.B. pp. 1-15. Kluwer Academic Publishers, Boston.
- Caplan, M. and Erickson, H.P. (2003) Apparent cooperative assembly of the bacterial cell-division protein FtsZ demonstrated by isothermal titration calorimetry. *J. Biol. Chem.* 278: 13784-13784.

Caplow, M. and Fee, L. (2002) Dissociation of the tubulin dimer is extremely slow, thermodynamically very unfavorable, and reversible in the absence of an energy source. *Mol. Biol. Cell* 13: 2120-2131.

Catarecha, P., Segura, M.D., Franco-Zorrilla, J.M., Garcia-Ponce, B., Lanza, M., Solano, R., Paz-Ares, J. and Leyva, A. (2007) A mutant of the Arabidopsis phosphate transporter PHT1;1 displays enhanced arsenic accumulation. *Plant Cell* 19: 1123-1133.

Chau, M.F., Radeke, M.J., de Ines, C., Barasoain, I., Kohlstaedt, L.A. and Feinstein, S.C. (1998) The microtubule-associated protein tau cross-links to two distinct sites on each alpha and beta tubulin monomer via separate domains. *Biochemistry* 37: 17692-17703.

Chen, Y., Anderson, D.E., Rajagopalan, M. and Erickson, H.P. (2007) Assembly dynamics of *Mycobacterium tuberculosis* FtsZ. *J. Biol. Chem.* 282: 27736-27743.

Chen, Y., Bjornson, K., Redick, S.D. and Erickson, H.P. (2005) A rapid fluorescence assay for FtsZ assembly indicates cooperative assembly with a dimer nucleus. *Biophys. J.* 88: 505-514.

Chen, Y. and Erickson, H.P. (2005) Rapid in vitro assembly dynamics and subunit turnover of FtsZ demonstrated by fluorescence resonance energy transfer. *J. Biol. Chem.*: M500895200.

Chen, Y. and Erickson, H.P. (2008) *In vitro* assembly studies of FtsZ/Tubulin-like proteins (TubZ) from Bacillus Plasmids: Evidence for a capping mechanism. *J. Biol. Chem.* 283: 8102-8109.

Chomczynski, P., Mackey, K., Drews, R. and Wilfinger, W. (1997) DNAzol: a reagent for the rapid isolation of genomic DNA. *BioTechniques* 22: 550-553.

Chung, K.-M., Hsu, H.-H., Yeh, H.-Y. and Chang, B.-Y. (2007) Mechanism of regulation of prokaryotic tubulin-like GTPase FtsZ by membrane protein EzrA. *J. Biol. Chem.* 282: 14891-14897.

Cleveland, D.W. (1982) Treadmilling of tubulin and actin. *Cell* 28: 689-691.

Cline, K., Werner-Washburne, M., Andrews, J. and Keegstra, K. (1984) Thermolysin is a suitable protease for probing the surface on intact pea chloroplasts. *Plant Physiol.* 75: 675-678.

Clos, J. and Brandau, S. (1994) pJC20 and pJC40--two high-copy-number vectors for T7 RNA polymerase-dependent expression of recombinant genes in *Escherichia coli*. *Protein Expr. Purif.* 5: 133-137.

Colletti, K.S., Tattersall, E.A., Pyke, K.A., Froelich, J.E., Stokes, K.D. and Osteryoung, K.W. (2000) A homologue of the bacterial cell division site-determining factor MinD mediates placement of the chloroplast division apparatus. *Curr. Biol.* 10: 507-516.

Cordell, S.C., Anderson, R.E. and Lowe, J. (2001) Crystal structure of the bacterial cell division inhibitor MinC. *EMBO J.* 20: 2454-2461.

Dai, K. and Lutkenhaus, J. (1992) The proper ratio of FtsZ to FtsA is required for cell division to occur in *Escherichia coli*. *J. Bacteriol.* 174: 6145-6151.

David-Pfeuty, T., Erickson, H.P. and Pantaloni, D. (1977) Guanosinetriphosphatase activity of tubulin associated with microtubule assembly. *Proceedings of the National Academy of Sciences* 74: 5372-5376.

de Boer, P., Crossley, R. and Rothfield, L. (1992a) The essential bacterial cell-division protein FtsZ is a GTPase. *Nature* 359: 254-256.

de Boer, P.A., Crossley, R.E. and Rothfield, L.I. (1989a) A division inhibitor and a topological specificity factor coded for by the minicell locus determine proper placement of the division septum in *E. coli*. *Cell* 56: 641-649.

de Boer, P.A., Crossley, R.E. and Rothfield, L.I. (1992b) Roles of MinC and MinD in the site-specific septation block mediated by the MinCDE system of *Escherichia coli*. *J. Bacteriol.* 174: 63-70.

de Boer, P.A.J., Crossley, R.E. and Rothfield, L.I. (1989b) A division inhibitor and a topological specificity factor coded for by the minicell locus determine proper placement of the division septum in *E. coli*. *Cell* 56: 641-649.

den Blaauwen, T., Aarsman, M.E.G., Vischer, N.E. and Nanninga, N. (2003) Penicillin-binding protein PBP2 of *Escherichia coli* localizes preferentially in the lateral wall and at mid-cell in comparison with the old cell pole. *Mol. Microbiol.* 47: 539-547.

Derry, W.B., Wilson, L. and Jordan, M.A. (1998) Low potency of taxol at microtubule minus ends: implications for its antimetabolic and therapeutic mechanism. *Cancer Res.* 58: 1177-1184.

Dewar, S.J., Begg, K.J. and Donachie, W.D. (1992) Inhibition of cell division initiation by an imbalance in the ratio of FtsA to FtsZ. *J. Bacteriol.* 174: 6314-6316.

Diaz, J.F., Kralicek, A., Mingorance, J., Palacios, J.M., Vicente, M. and Andreu, J.M. (2001) Activation of cell division protein FtsZ. Control of switch loop T3 conformation by the nucleotide gamma-phosphate. *J. Biol. Chem.* 276: 17307-17315.

Dougherty, C.A., Himes, R.H., Wilson, L. and Farrell, K.W. (1998) Detection of GTP and Pi in wild-type and mutated yeast microtubules: implications for the role of the GTP/GDP-Pi cap in microtubule dynamics. *Biochemistry* 37: 10861-10865.

Downing, K.H. and Nogales, E. (1998a) New insights into microtubule structure and function from the atomic model of tubulin. *Eur Biophys J* 27: 431-436.

Downing, K.H. and Nogales, E. (1998b) Tubulin and microtubule structure. *Curr. Opin. Cell Biol.* 10: 16-22.

Downing, K.H. and Nogales, E. (1998c) Tubulin structure: insights into microtubule properties and functions. *Curr. Opin. Struct. Biol.* 8: 785-791.

Du, Y. and Arvidson, C.G. (2003) Identification of ZipA, a signal recognition particle-dependent protein from *Neisseria gonorrhoeae*. *J. Bacteriol.* 185: 2122-2130.

Dutcher, S.K. (2001) The tubulin fraternity: alpha to eta. *Curr. Opin. Cell Biol.* 13: 49-54.

Edwards, D.H., Thomaidis, H.B. and Errington, J. (2000) Promiscuous targeting of *Bacillus subtilis* cell division protein DivIVA to division sites in *Escherichia coli* and fission yeast. *EMBO J.* 19: 2719-2727.

El-Kafafi, E.S., Mukherjee, S., El-Shami, M., Putaux, J.L., Block, M.A., Pignot-Paintrand, I., Lerbs-Mache, S. and Falconet, D. (2005) The plastid division proteins, FtsZ1 and FtsZ2, differ in their biochemical properties and sub-plastidial localisation. *Biochem. J.* 387: 669-676.

El-Kafafi, S., Karamoko, M., Pignot-Paintrand, I., Grunwald, D., Mandaron, P., Lerbs-Mache, S. and Falconet, D. (2008) Developmentally regulated association of plastid division protein FtsZ1 with thylakoid membranes in *Arabidopsis thaliana*. *Biochem. J.* 409: 87-94.

Emanuelsson, O., Nielsen, H. and von Heijne, G. (1999) ChloroP, a neural network-based method for predicting chloroplast transit peptides and their cleavage sites. *Protein Sci.* 8: 978-984.

Erickson, H.P. (1995) FtsZ, a prokaryotic homolog of tubulin? *Cell* 80: 367-370.

Erickson, H.P. (1997) FtsZ, a tubulin homologue in prokaryote cell division. *Trends Cell Biol* 7: 362-367.

Erickson, H.P. and Stoffler, D. (1996) Protofilaments and rings, two conformations of the tubulin family conserved from bacterial FtsZ to alpha/beta and gamma tubulin. *J. Cell Biol.* 135: 5-8.

- Erickson, H.P., Taylor, D.W., Taylor, K.A. and Bramhill, D. (1996) Bacterial cell division protein FtsZ assembles into protofilament sheets and minirings, structural homologs of tubulin polymers. *Proc Natl Acad Sci USA* 93: 519-523.
- Fisher, C.L. and Pei, G.K. (1997) Modification of a PCR-based site-directed mutagenesis method. *BioTechniques* 23: 570-571, 574.
- Fitzpatrick, L.M. and Keegstra, K. (2001) A method for isolating a high yield of *Arabidopsis* chloroplasts capable of efficient import of precursor proteins. *Plant J* 27: 59-65.
- Fribourg, S. and Conti, E. (2003) Structural similarity in the absence of sequence homology of the messenger RNA export factors Mtr2 and p15. *EMBO Rep.* 4: 699-703.
- Fu, X., Shih, Y.L., Zhang, Y. and Rothfield, L.I. (2001) The MinE ring required for proper placement of the division site is a mobile structure that changes its cellular location during the *Escherichia coli* division cycle. *Proc. Natl. Acad. Sci. U. S. A.* 98: 980-985.
- Fujiwara, M. and Yoshida, S. (2001) Chloroplast targeting of chloroplast division FtsZ2 proteins in *Arabidopsis*. *Biochem. Biophys. Res. Commun.* 287: 462-467.
- Fujiwara, M.T., Nakamura, A., Itoh, R., Shimada, Y., Yoshida, S. and Moller, S.G. (2004) Chloroplast division site placement requires dimerization of the ARC11/AtMinD1 protein in *Arabidopsis*. *J. Cell Sci.* 117: 2399-2410.
- Gaikwad, A., Babbarwal, V., Pant, V. and Mukherjee, S.K. (2000) Pea chloroplast FtsZ can form multimers and correct the thermosensitive defect of an *Escherichia coli* ftsZ mutant. *Mol Gen Genet* 263: 213-221.
- Gao, H., Kadirjan-Kalbach, D., Froehlich, J.E. and Osteryoung, K.W. (2003) ARC5, a cytosolic dynamin-like protein from plants, is part of the chloroplast division machinery. *Proc. Natl. Acad. Sci. U. S. A.* 100: 4328-4333.
- Geissler, B., Elraheb, D. and Margolin, W. (2003) A gain-of-function mutation in *ftsA* bypasses the requirement for the essential cell division gene *zipA* in *Escherichia coli*. *Proc. Natl. Acad. Sci. U. S. A.* 100: 4197-4202.
- Geissler, S., Siegers, K. and Schiebel, E. (1998) A novel protein complex promoting formation of functional alpha- and gamma-tubulin. *EMBO J.* 17: 952-966.
- Gerstein, M. and Levitt, M. (1997) A structural census of the current population of protein sequences. *Proc. Natl. Acad. Sci. U. S. A.* 94: 11911-11916.

- Gish, W. and States, D.J. (1993) Identification of protein coding regions by database similarity search. *Nat. Genet.* 3: 266-272.
- Glynn, J.M., Miyagishima, S., Yoder, D.W., Osteryoung, K.W. and Vitha, S. (2007) Chloroplast division. *Traffic* 8: 451-461.
- Gonzalez, J., Velez, M., Jimenez, M., Alfonso, C., Schuck, P., Mingorance, J., Vicente, M., Minton, A. and Rivas, G. (2005) Cooperative behavior of *Escherichia coli* cell-division protein FtsZ assembly involves the preferential cyclization of long single-stranded fibrils. *102*: 1895-1900.
- Gonzalez, J.M., Jimenez, M., Velez, M., Mingorance, J., Andreu, J.M., Vicente, M. and Rivas, G. (2003) Essential cell division protein FtsZ assembles into one monomer-thick ribbons under conditions resembling the crowded intracellular environment. *J. Biol. Chem.* 278: 37664-37671.
- Gray, M.W. (1993) The endosymbiont hypothesis revisited. *Int. Rev. Cytol* 141: 233-357.
- Gueiros-Filho, F.J. and Losick, R. (2002) A widely conserved bacterial cell division protein that promotes assembly of the tubulin-like protein FtsZ. *Genes Dev.* 16: 2544-2556.
- Guex, N. and Peitsch, M.C. (1997) SWISS-MODEL and the Swiss-PdbViewer: an environment for comparative protein modeling. *Electrophoresis* 18: 2714-2723.
- Hale, C.A. and de Boer, P.A. (1999) Recruitment of ZipA to the septal ring of *Escherichia coli* is dependent on FtsZ and independent of FtsA. *J. Bacteriol.* 181: 167-176.
- Hale, C.A. and de Boer, P.A.J. (1997) Direct binding of FtsZ to ZipA, an essential component of the septal ring structure that mediates cell division in *E. coli*. *Cell* 88: 175-185.
- Hale, C.A., Meinhardt, H. and de Boer, P.A. (2001) Dynamic localization cycle of the cell division regulator MinE in *Escherichia coli*. *EMBO J.* 20: 1563-1572.
- Haney, S.A., Glasfeld, E., Hale, C., Keeney, D., He, Z. and de Boer, P. (2001) Genetic analysis of the *Escherichia coli* FtsZ•ZipA interaction in the yeast ywo-hybrid system. Characterization of FtsZ residues essential for the interactions with ZipA and with FtsA. *J. Biol. Chem.* 276: 11980-11987.
- Harry, E.J., Rodwell, J. and Wake, R.G. (1999) Co-ordinating DNA replication with cell division in bacteria: a link between the early stages of a round of replication and mid-cell Z ring assembly. *Mol. Microbiol.* 33: 33-40.

Hartman, J.J., Mahr, J., McNally, K., Okawa, K., Iwamatsu, A., Thomas, S., Cheesman, S., Heuser, J., Vale, R.D. and McNally, F.J. (1998) Katanin, a microtubule-severing protein, is a novel AAA ATPase that targets to the centrosome using a WD40-containing subunit. *Cell* 93: 277-287.

Higashitani, A., Ishii, Y., Kato, Y. and Koriuchi, K. (1997) Functional dissection of a cell-division inhibitor, SulA, of *Escherichia coli* and its negative regulation by Lon. *Mol Gen Genet* 254: 351-357.

Hirata, D., Masuda, H., Eddison, M. and Toda, T. (1998) Essential role of tubulin-folding cofactor D in microtubule assembly and its association with microtubules in fission yeast. *EMBO J.* 17: 658-666.

Howell, B., Larsson, N., Gullberg, M. and Cassimeris, L. (1999) Dissociation of the tubulin-sequestering and microtubule catastrophe-promoting activities of oncoprotein 18/stathmin. *Mol. Biol. Cell* 10: 105-118.

Hu, Z. and Lutkenhaus, J. (1999) Topological regulation of cell division in *Escherichia coli* involves rapid pole to pole oscillation of the division inhibitor MinC under the control of MinD and MinE. *Mol. Microbiol.* 34: 82-90.

Hu, Z. and Lutkenhaus, J. (2000) Analysis of MinC reveals two independent domains involved in interaction with MinD and FtsZ. *J. Bacteriol.* 182: 3965-3971.

Hu, Z. and Lutkenhaus, J. (2001) Topological regulation of cell division in *E. coli*. spatiotemporal oscillation of MinD requires stimulation of its ATPase by MinE and phospholipid. *Mol. Cell* 7: 1337-1343.

Hu, Z., Mukherjee, A., Pichoff, S. and Lutkenhaus, J. (1999) The MinC component of the division site selection system in *Escherichia coli* interacts with FtsZ to prevent polymerization. *Proc. Natl. Acad. Sci. U. S. A.* 96: 14819-14824.

Huang, J., Cao, C. and Lutkenhaus, J. (1996) Interaction between FtsZ and inhibitors of cell division. *J. Bacteriol.* 178: 5080-5085.

Huecas, S. and Andreu, J. (2003) Energetics of the cooperative assembly of cell division protein FtsZ and the nucleotide hydrolysis switch.: 46146-46154.

Huecas, S. and Andreu, J. (2004) Polymerization of nucleotide-free, GDP- and GTP-bound cell division protein FtsZ: GDP makes the difference. *FEBS Lett.* 569: 43-48.

Huecas, S., Llorca, O., Boskovic, J., Martin-Benito, J., Valpuesta, J.M. and Andreu, J.M. (2007a) Energetics and geometry of FtsZ polymers: nucleated self-assembly of single protofilaments. *Biophys. J.:* biophysj.107.115493.

- Huecas, S., Schaffner-Barbero, C., Garcia, W., Yebenes, H., Palacios, J.M., Diaz, J.F., Menendez, M. and Andreu, J.M. (2007b) The interactions of cell division protein FtsZ with guanine nucleotides. *J. Biol. Chem.* 282: 37515-37528.
- Ingerman, E. and Nunnari, J. (2005) A continuous, regenerative coupled GTPase assay for dynamin-related proteins. *Methods Enzymol.* 404: 611-619.
- Ingerman, E., Perkins, E.M., Marino, M., Mears, J.A., McCaffery, J.M., Hinshaw, J.E. and Nunnari, J. (2005) Dnm1 forms spirals that are structurally tailored to fit mitochondria. *J. Cell Biol.* 170: 1021-1027.
- Itoh, R., Fujiwara, M., Nagata, N. and Yoshida, S. (2001) A chloroplast protein homologous to the eubacterial topological specificity factor minE plays a role in chloroplast division. *Plant Physiol.* 127: 1644-1655.
- Jeong, K.J. and Lee, S.Y. (2003) Enhanced production of recombinant proteins in *Escherichia coli* by filamentation suppression. *Appl. Environ. Microbiol.* 69: 1295-1298.
- Justice, S.S., Garcia-Lara, J. and Rothfield, L.I. (2000) Cell division inhibitors Sula and MinC/MinD block septum formation at different steps in the assembly of the *Escherichia coli* division machinery. *Mol. Microbiol.* 37: 410-423.
- Katayama, N., Takano, H., Sugiyama, M., Takio, S., Sakai, A., Tanaka, K., Kuroiwa, H. and Ono, K. (2003) Effects of Antibiotics that Inhibit the Bacterial Peptidoglycan Synthesis Pathway on Moss Chloroplast Division. *Plant Cell Physiol.* 44: 776-781.
- Koksharova, O.A. and Wolk, C.P. (2002) A novel gene that bears a DnaJ motif influences cyanobacterial cell division. *J. Bacteriol.* 184: 5524-5528.
- Kollman, J.M., Zelter, A., Muller, E.G.D., Fox, B., Rice, L.M., Davis, T.N. and Agard, D.A. (2008) The structure of the γ -tubulin small complex: implications of its architecture and flexibility for microtubule nucleation. *Mol. Biol. Cell* 19: 207-215.
- Krause, G.H. and Heber, U. (1976) Topics in Photosynthesis. Edited by Barber, J. pp. 171-214. Elsevier.
- Kuroiwa, H., Mori, T., Takahara, M., Miyagishima, S.Y. and Kuroiwa, T. (2002) Chloroplast division machinery as revealed by immunofluorescence and electron microscopy. *Planta* 215: 185-190.
- Laemmli, U.K. (1970) Cleavage of structural protein during the assembly of the head of bacteriophage T4. *Nature* 227: 680-685.

- Larsen, R.A., Cusumano, C., Fujioka, A., Lim-Fong, G., Patterson, P. and Pogliano, J. (2007) Treadmilling of a prokaryotic tubulin-like protein, TubZ, required for plasmid stability in *Bacillus thuringiensis*. *Genes Dev.* 21: 1340-1352.
- Leech, R.M., Thomson, W.W. and Platt-Aloia, K.A. (1981) Observations on the mechanism of chloroplast division in higher plants. *New Phytol.* 87: 1-9.
- Levin, P.A., Kurtser, I.G. and Grossman, A.D. (1999) Identification and characterization of a negative regulator of FtsZ ring formation in *Bacillus subtilis*. *Proc. Natl. Acad. Sci. U. S. A.* 96: 9642-9647.
- Levin, P.A., Schwartz, R.L. and Grossman, A.D. (2001) Polymer stability plays an important role in the positional regulation of FtsZ. *J. Bacteriol.* 183: 5449-5452.
- Lewis, S.A., Tian, G. and Cowan, N.J. (1997) The α - and β -tubulin folding pathways. *Trends in Cell Biology* 7: 479-484.
- Li, H., DeRosier, D.J., Nicholson, W.V., Nogales, E. and Downing, K.H. (2002) Microtubule structure at 8 Å resolution. *Structure (Camb)* 10: 1317-1328.
- Lin, D.C., Levin, P.A. and Grossman, A.D. (1997) Bipolar localization of a chromosome partition protein in *Bacillus subtilis*. *Proc. Natl. Acad. Sci. U. S. A.* 94: 4721-4726.
- Liu, Z., Mukherjee, A. and Lutkenhaus, J. (1999) Recruitment of ZipA to the division site by interaction with FtsZ. *Mol. Microbiol.* 31: 1853-1861.
- Lohret, T.A., McNally, F.J. and Quarmby, L.M. (1998) A role for katanin-mediated axonemal severing during *Chlamydomonas* deflagellation. *Mol. Biol. Cell* 9: 1195-1207.
- Lohse, S., Hause, B., Hause, G. and Fester, T. (2006) FtsZ characterization and immunolocalization in the two phases of plastid reorganization in arbuscular mycorrhizal roots of *Medicago truncatula*. *Plant Cell Physiol.* 47: 1124-1134.
- Löwe, J. (1998) Crystal structure determination of FtsZ from *Methanococcus jannaschii*. *J Struct Biol* 124: 235-243.
- Lowe, J. and Amos, L.A. (1998) Crystal structure of the bacterial cell-division protein FtsZ. *Nature* 391: 203-206.
- Lowe, J. and Amos, L.A. (1999) Tubulin-like protofilaments in Ca²⁺-induced FtsZ sheets. *EMBO J.* 18: 2364-2371.
- Lu, C. and Erickson, H.P. (1998) Purification and assembly of FtsZ. *Methods Enzymol.* 298: 305-313.

Lu, C., Reedy, M. and Erickson, H.P. (2000) Straight and curved conformations of FtsZ are regulated by GTP hydrolysis. *J. Bacteriol.* 182: 164-170.

Lu, C., Stricker, J. and Erickson, H.P. (1998) FtsZ from *Escherichia coli*, *Azotobacter vinelandii*, and *Thermotoga maritima*—quantitation, GTP hydrolysis, and assembly. *Cell Motility And The Cytoskeleton* 40: 71-86.

Lu, C., Stricker, J. and Erickson, H.P. (2001) Site-specific mutations of FtsZ—effects on GTPase and in vitro assembly. *BMC Microbiol* 1: 7.

Lutkenhaus, J. (2007) Assembly dynamics of the bacterial MinCDE system and spatial regulation of the Z ring. *Annu. Rev. Biochem.* 76: 539-562.

Ma, X., Ehrhardt, D.W. and Margolin, W. (1996) Colocalization of cell division proteins FtsZ and FtsA to cytoskeletal structures in living *Escherichia coli* cells by using green fluorescent protein. *Proc. Natl. Acad. Sci. U. S. A.* 93: 12998-13003.

Machida, M., Takechi, K., Sato, H., Chung, S.J., Kuroiwa, H., Takio, S., Seki, M., Shinozaki, K., Fujita, T., Hasebe, M. and Takano, H. (2006) Genes for the peptidoglycan synthesis pathway are essential for chloroplast division in moss. *Proceedings of the National Academy of Sciences* 103: 6753-6758.

Maple, J., Aldridge, C. and Moller, S.G. (2005) Plastid division is mediated by combinatorial assembly of plastid division proteins. *The Plant Journal* 43: 811-823.

Maple, J., Chua, N.H. and Moller, S.G. (2002) The topological specificity factor AtMinE1 is essential for correct plastid division site placement in Arabidopsis. *Plant J* 31: 269-277.

Maple, J., Fujiwara, M., Kitahata, N., Lawson, T., Baker, N., Yoshida, S. and Moller, S. (2004) GIANT CHLOROPLAST 1 is essential for correct plastid division in Arabidopsis. *Curr. Biol.* 14: 776-781.

Maple, J. and Moller, S.G. (2007a) Plastid division coordination across a double-membraned structure. *FEBS Lett.*

Maple, J. and Moller, S.G. (2007b) Plastid division: evolution, mechanism and complexity. *Ann Bot (Lond)* 99: 565-579.

Maple, J., Vojta, L., Soll, J. and Moller, S.G. (2007) ARC3 is a stromal Z-ring accessory protein essential for plastid division. *EMBO Rep.* 8: 293-299.

Margolin, W. (2000) Themes and variations in prokaryotic cell division. *FEMS Microbiol. Rev.* 24: 531-548.

- Margolin, W. (2002) Bacterial sporulation: FtsZ rings do the twist. *Curr. Biol.* 12: R391-392.
- Margolin, W. (2005a) Bacterial mitosis: actin in a new role at the origin. *Curr. Biol.* 15: R259-261.
- Margolin, W. (2005b) FtsZ and the division of prokaryotic cells and organelles. *Nat. Rev. Mol. Cell Biol.* 6: 862-871.
- Margolin, W. (2007) Bacterial cytoskeleton: not your run-of-the-mill tubulin. *Curr. Biol.* 17: R633-636.
- Margolis, R.L. and Wilson, L. (1998) Microtubule treadmilling: what goes around comes around. *BioEssays* 20: 830-836.
- Margulis, L. (1971) The origin of plant and animal cells. *Am Sci* 59: 230-235.
- Margulis, L. (1975) Symbiotic theory of the origin of eukaryotic organelles; criteria for proof. *Symp Soc Exp Biol*: 21-38.
- Marston, A.L. and Errington, J. (1999) Selection of the midcell division site in *Bacillus subtilis* through MinD-dependent polar localization and activation of MinC. *Mol. Microbiol.* 33: 84-96.
- Marston, A.L., Thomaides, H.B., Edwards, D.H., Sharpe, M.E. and Errington, J. (1998) Polar localization of the MinD protein of *Bacillus subtilis* and its role in selection of the mid-cell division site. *Genes Dev.* 12: 3419-3430.
- Matsuo, Y., Yamada, A., Tsukamoto, K., Tamura, H.O., Ikeawa, H., Nakamura, H. and Nishikawa, K. (1996) A distant evolutionary relationship between bacterial sphingomyelinase and mammalian DNase I. *Protein Sci.* 5: 2459-2467.
- Mazouni, K., Domain, F., Cassier-Chauvat, C. and Chauvat, F. (2004) Molecular analysis of the key cytokinetic components of cyanobacteria: FtsZ, ZipN and MinCDE. *Mol. Microbiol.* 52: 1145-1158.
- McAndrew, R.S., Froehlich, J.E., Vitha, S., Stokes, K.D. and Osteryoung, K.W. (2001) Colocalization of plastid division proteins in the chloroplast stromal compartment establishes a new functional relationship between FtsZ1 and FtsZ2 in higher plants. *Plant Physiol.* 127: 1656-1666.
- McAndrew, R.S., Olson, B.J.S.C., Kadirjan-Kalbach, D., Chi-Ham, C.L., Vitha, S., Froehlich, J.E. and Osteryoung, K.W. (2008) *In vivo* quantitative relationship between plastid

division proteins FtsZ1 and FtsZ2 and identification of ARC6 and ARC3 in a native FtsZ complex. *Biochem. J.* In Press.

McNally, F.J., Okawa, K., Iwamatsu, A. and Vale, R.D. (1996) Katanin, the microtubule-severing ATPase, is concentrated at centrosomes. *J. Cell Sci.* 109 (Pt 3): 561-567.

McNally, F.J. and Thomas, S. (1998) Katanin is responsible for the M-phase microtubule-severing activity in *Xenopus* eggs. *Mol. Biol. Cell* 9: 1847-1861.

Melki, R., Fievez, S. and Carlier, M.F. (1996) Continuous monitoring of Pi release following nucleotide hydrolysis in actin or tubulin assembly using 2-amino-6-mercapto-7-methylpurine ribonucleoside and purine-nucleoside phosphorylase as an enzyme-linked assay. *Biochemistry* 35: 12038-12045.

Menendez, M., Rivas, G., Diaz, J.F. and Andreu, J.M. (1998) Control of the structural stability of the tubulin dimer by one high affinity bound magnesium ion at nucleotide N-site. *J. Biol. Chem.* 273: 167-176.

Michie, K. and Lowe, J. (2006) Dynamic filaments of the bacterial cytoskeleton. *Annu. Rev. Biochem.* 75: 467-492.

Mingorance, J., Rueda, S., Gomez-Puertas, P., Valencia, A. and Vicente, M. (2001) *Escherichia coli* FtsZ polymers contain mostly GTP and have a high nucleotide turnover. *Mol. Microbiol.* 41: 83-91.

Miroux, B. and Walker, J.E. (1996) Over-production of proteins in *Escherichia coli*: mutant hosts that allow synthesis of some membrane proteins and globular proteins at high levels. *J. Mol. Biol.* 260: 289-298.

Miyagishima, S., Kuroiwa, H. and Kuroiwa, T. (2001a) The timing and manner of disassembly of the apparatuses for chloroplast and mitochondrial division in the red alga *Cyanidioschyzon merolae*. *Planta* 212: 517-528.

Miyagishima, S., Nishida, K. and Kuroiwa, T. (2003a) An evolutionary puzzle: chloroplast and mitochondrial division rings. *Trends Plant Sci.* 8: 432-438.

Miyagishima, S., Takahara, M. and Kuroiwa, T. (2001b) Novel filaments 5 in diameter constitute the cytosolic ring of the plastid division apparatus. *The Plant Cell* 13: 707-721.

Miyagishima, S., Takahara, M., Mori, T., Kuroiwa, H., Higashiyama, T. and Kuroiwa, T. (2001c) Plastid division is driven by a complex mechanism that involves differential transition of the bacterial and eukaryotic division rings. *Plant Cell* 13: 2257-2268.

- Miyagishima, S., Wolk, C. and Osteryoung, K. (2005) Identification of cyanobacterial cell division genes by comparative and mutational analyses. *Mol. Microbiol.* 56: 126-143.
- Miyagishima, S.Y., Froehlich, J.E. and Osteryoung, K.W. (2006) PDV1 and PDV2 mediate recruitment of the dynamin-related protein ARC5 to the plastid division site. *Plant Cell* 18: 2517-2530.
- Miyagishima, S.Y., Nishida, K., Mori, T., Matsuzaki, M., Higashiyama, T., Kuroiwa, H. and Kuroiwa, T. (2003b) A plant-specific dynamin-related protein forms a ring at the chloroplast division site. *Plant Cell* 15: 655-665.
- Moritz, M., Braunfeld, M.B., Sedat, J.W., Alberts, B. and Agard, D.A. (1995) Microtubule nucleation by gamma-tubulin-containing rings in the centrosome. *Nature* 378: 638-640.
- Mosyak, L., Zhang, Y., Glasfeld, E., Haney, S., Stahl, M., Seehra, J. and Somers, W.S. (2000) The bacterial cell-division protein ZipA and its interaction with an FtsZ fragment revealed by X-ray crystallography. *EMBO J.* 19: 3179-3191.
- Moy, F.J., Glasfeld, E., Mosyak, L. and Powers, R. (2000) Solution structure of ZipA, a crucial component of *Escherichia coli* cell division. *Biochemistry* 39: 9146-9156.
- Mukherjee, A., Cao, C. and Lutkenhaus, J. (1998) Inhibition of FtsZ polymerization by Sula, an inhibitor of septation in *Escherichia coli*. *Proc. Natl. Acad. Sci. U. S. A.* 95: 2885-2890.
- Mukherjee, A., Dai, K. and Lutkenhaus, J. (1993) *Escherichia coli* cell division protein FtsZ is a guanine nucleotide binding protein. *Proc. Natl. Acad. Sci. U. S. A.* 90: 1053-1057.
- Mukherjee, A. and Lutkenhaus, J. (1994) Guanine nucleotide-dependent assembly of FtsZ into filaments. *J. Bacteriol.* 176: 2754-2758.
- Mukherjee, A. and Lutkenhaus, J. (1998) Dynamic assembly of FtsZ regulated by GTP hydrolysis. *EMBO J.* 17: 462-469.
- Mukherjee, A. and Lutkenhaus, J. (1999) Analysis of FtsZ assembly by light scattering and determination of the role of divalent metal cations. *J. Bacteriol.* 181: 823-832.
- Musser, S.M. and Theg, S.M. (2000) Proton transfer limits protein translocation rate by the thylakoid Δ pH/Tat machinery. *Biochemistry* 39: 8228-8233.
- Nielsen, E., Akita, M., Davila-Aponte, J. and Keegstra, K. (1997) Stable association of chloroplastic precursors with protein translocation complexes that contain proteins from both envelope membranes and a stromal Hsp100 molecular chaperone. *EMBO J.* 16: 935-946.

- Nishida, K., Takahara, M., Miyagishima, S.Y., Kuroiwa, H., Matsuzaki, M. and Kuroiwa, T. (2003) Dynamic recruitment of dynamin for final mitochondrial severance in a primitive red alga. *Proc. Natl. Acad. Sci. U. S. A.* 100: 2146-2151.
- Nogales, E. (1999) A structural view of microtubule dynamics. *Cell. Mol. Life Sci.* 56: 133-142.
- Nogales, E. (2000) Structural insights into microtubule function. *Annu. Rev. Biochem.* 69: 277-302.
- Nogales, E., Downing, K.H., Amos, L.A. and Lowe, J. (1998a) Tubulin and FtsZ form a distinct family of GTPases. *Nat Struct Biol* 5: 451-458.
- Nogales, E. and Wang, H.-W. (2006) Structural intermediates in microtubule assembly and disassembly: how and why? *Curr. Opin. Cell Biol.* 18: 179-184.
- Nogales, E., Whittaker, M., Milligan, R.A. and Downing, K.H. (1999) High-resolution model of the microtubule. *Cell* 96: 79-88.
- Nogales, E., Wolf, S.G. and Downing, K.H. (1998b) Structure of the alpha beta tubulin dimer by electron crystallography. *Nature* 391: 199-203.
- Oliva, M., Cordell, S. and Lowe, J. (2004) Structural insights into FtsZ protofilament formation. *Nat. Struct. Mol. Biol.*
- Oliva, M.A., Huecas, S., Palacios, J.M., Martin-Benito, J., Valpuesta, J.M. and Andreu, J.M. (2003) Assembly of archaeal cell division protein FtsZ and a GTPase-inactive mutant into double-stranded filaments. *J. Biol. Chem.* 278: 33562-33570.
- Olson, B.J.S.C. and Markwell, J.P. (2007) Assays for determination of protein concentration. In *Current Protocols in Protein Science*. Edited by Coligan, J.E., Dunn, B.M., Speicher, D.W. and Wingfield, P.T. pp. 3.4.1-3.4.29. John Wiley & Sons, Inc.
- Olson, B.J.S.C. and Osteryoung, K.W. (2007) Biochemical analysis of FtsZ1 and FtsZ2. In *Plant Biology and Botany 2007 Joint Congress*, Chicago, IL.
- Osawa, M., Anderson, D.E. and Erickson, H.P. (2008) Reconstitution of contractile FtsZ rings in liposomes. *Science* In press.
- Osteryoung, K.W. (2000) Organelle fission: crossing the evolutionary divide. *Plant Physiol.* 123: 1213-1216.
- Osteryoung, K.W. (2001) Organelle fission in eukaryotes. *Curr Opin Microbiol* 4: 639-646.

- Osteryoung, K.W. and McAndrew, R.S. (2001) The plastid division machine. *Annu Rev Plant Physiol Plant Mol Biol* 52: 315-333.
- Osteryoung, K.W. and Pyke, K.A. (1998) Plastid division: evidence for a prokaryotically derived mechanism. *Curr Opin Plant Biol* 1: 475-479.
- Osteryoung, K.W., Stokes, K.D., Rutherford, S.M., Percival, A.L. and Lee, W.Y. (1998) Chloroplast division in higher plants requires members of two functionally divergent gene families with homology to bacterial *ftsZ*. *Plant Cell* 10: 1991-2004.
- Osteryoung, K.W. and Vierling, E. (1995) Conserved cell and organelle division. *Nature* 376: 473-474.
- Pichoff, S. and Lutkenhaus, J. (2001) Escherichia coli division inhibitor MinCD blocks septation by preventing Z-ring formation. *J. Bacteriol.* 183: 6630-6635.
- Pichoff, S. and Lutkenhaus, J. (2002) Unique and overlapping roles for ZipA and FtsA in septal ring assembly in Escherichia coli. *EMBO J.* 21: 685-693.
- Pradel, N., Santini, C.-L., Bernadac, A., Fukumori, Y. and Wu, L.-F. (2006) Biogenesis of actin-like bacterial cytoskeletal filaments destined for positioning prokaryotic magnetic organelles. *PNAS* 103: 17485-17489.
- Pyke, K.A. and Leech, R.M. (1994) A genetic analysis of chloroplast division and expansion in *Arabidopsis thaliana*. *Plant Physiol.* 104: 201-207.
- Pyke, K.A., Marrison, J.L. and Leech, R.M. (1991) Temporal and spatial development of the cells of the expanding first leaf of *Arabidopsis thaliana* (L.) Heynh. *J. Exp. Bot.* 42: 1407-1416.
- Raskin, D.M. and de Boer, P.A. (1997) The MinE ring: an FtsZ-independent cell structure required for selection of the correct division site in *E. coli*. *Cell* 91: 685-694.
- Raskin, D.M. and de Boer, P.A. (1999a) MinDE-dependent pole-to-pole oscillation of division inhibitor MinC in *Escherichia coli*. *J. Bacteriol.* 181: 6419-6424.
- Raskin, D.M. and de Boer, P.A. (1999b) Rapid pole-to-pole oscillation of a protein required for directing division to the middle of *Escherichia coli*. *Proc. Natl. Acad. Sci. U. S. A.* 96: 4971-4976.
- RayChaudhuri, D. and Park, J.T. (1992) *Escherichia coli* cell-division gene *ftsZ* encodes a novel GTP-binding protein. *Nature* 359: 251-254.

RayChaudhuri, D. and Park, J.T. (1994) A point mutation converts *Escherichia coli* FtsZ septation GTPase to an ATPase. *J. Biol. Chem.* 269: 22941-22944.

Raynaud-Messina, B. and Merdes, A. (2007) γ -tubulin complexes and microtubule organization. *Curr. Opin. Cell Biol.* 19: 24-30.

Raynaud, C., Cassier-Chauvat, C., Perennes, C. and Bergounioux, C. (2004a) An Arabidopsis homolog of the bacterial cell division inhibitor SulA is involved in plastid division. *Plant Cell* 16: 1801-1811.

Raynaud, C., Cassier-Chauvat, C., Perennes, C. and Bergounioux, C. (2004b) An Arabidopsis homolog of the bacterial cell division inhibitor SulA is involved in plastid division. *Plant Cell* 16: 1801-1811.

Redick, S.D., Stricker, J., Briscoe, G. and Erickson, H.P. (2005) Mutants of FtsZ targeting the protofilament interface: effects on cell division and GTPase activity. *J. Bacteriol.* 187: 2727-2736.

Regamey, A., Harry, E.J. and Wake, R.G. (2000) Mid-cell Z ring assembly in the absence of entry into the elongation phase of the round of replication in bacteria: co-ordinating chromosome replication with cell division. *Mol. Microbiol.* 38: 423-434.

Rensing, S.A., Kiessling, J., Reski, R. and Decker, E.L. (2004) Diversification of *ftsZ* during early land plant evolution. *J. Mol. Evol.* 58: 154-162.

Reski, R. (2002) Rings and networks: the amazing complexity of FtsZ in chloroplasts. *Trends Plant Sci.* 7: 103-105.

Rivas, G., Fernandez, J.A. and Minton, A.P. (2001) Direct observation of the enhancement of noncooperative protein self-assembly by macromolecular crowding: Indefinite linear self-association of bacterial cell division protein FtsZ. *Proc. Natl. Acad. Sci. U. S. A.* 98: 3150-3155.

Rivas, G., Lopez, A., Mingorance, J., Ferrandiz, M.J., Zorrilla, S., Minton, A.P., Vicente, M. and Andreu, J.M. (2000) Magnesium-induced linear self-association of the FtsZ bacterial cell division protein monomer. The primary steps for FtsZ assembly. *J. Biol. Chem.* 275: 11740-11749.

Robertson, E.J., Rutherford, S.M. and Leech, R.M. (1996) Characterization of chloroplast division using the Arabidopsis mutant *arc5*. *Plant Physiol.* 112: 149-159.

Romberg, L. and Levin, P.A. (2003) Assembly dynamics of the bacterial cell division protein FtsZ: poised at the edge of stability. *Annu. Rev. Microbiol.* 57: 125-154.

Romberg, L. and Mitchison, T.J. (2004) Rate-limiting guanosine 5'-triphosphate hydrolysis during nucleotide turnover by FtsZ, a prokaryotic tubulin homologue involved in bacterial cell division. *Biochemistry* 43: 282-288.

Romberg, L., Simon, M. and Erickson, H.P. (2001) Polymerization of FtsZ, a bacterial homolog of tubulin. is assembly cooperative? *J. Biol. Chem.* 276: 11743-11753.

Rothfield, L., Justice, S. and Garcia-Lara, J. (1999) Bacterial cell division. *Annu. Rev. Genet.* 33: 423-448.

Rothfield, L., Taghbalout, A. and Shih, Y.-L. (2005) Spatial control of bacterial division-site placement. *Nat Rev Micro* 3: 959-968.

Rowland, S.L., Fu, X., Sayed, M.A., Zhang, Y., Cook, W.R. and Rothfield, L.I. (2000) Membrane redistribution of the *Escherichia coli* MinD protein induced by MinE. *J. Bacteriol.* 182: 613-619.

Rueda, S., Vicente, M. and Mingorance, J. (2003) Concentration and assembly of the division ring proteins FtsZ, FtsA, and ZipA during the *Escherichia coli* cell cycle. *J. Bacteriol.* 185: 3344-3351.

Sackett, D.L. (1995) Structure and function in the tubulin dimer and the role of the acidic carboxyl terminus. *Subcell Biochem* 24: 255-302.

Sackett, D.L., Bhattacharyya, B. and Wolff, J. (1985) Tubulin subunit carboxyl termini determine polymerization efficiency. *J. Biol. Chem.* 260: 43-45.

Santra, M.K. and Panda, D. (2003) Detection of an intermediate during unfolding of bacterial cell division protein FtsZ: loss of functional properties precedes the global unfolding of FtsZ. *J. Biol. Chem.* 278: 21336-21343.

Scheffers, D. and Driessen, A.J. (2001) The polymerization mechanism of the bacterial cell division protein FtsZ. *FEBS Lett.* 506: 6-10.

Scheffers, D.J., de Wit, J.G., den Blaauwen, T. and Driessen, A.J. (2002) GTP hydrolysis of cell division protein FtsZ: evidence that the active site is formed by the association of monomers. *Biochemistry* 41: 521-529.

Scheffers, D.J., den Blaauwen, T. and Driessen, A.J. (2000) Non-hydrolysable GTP-gamma-S stabilizes the FtsZ polymer in a GDP-bound state. *Mol. Microbiol.* 35: 1211-1219.

Scheffers, D.J. and Driessen, A.J. (2002) Immediate GTP hydrolysis upon FtsZ polymerization. *Mol. Microbiol.* 43: 1517-1521.

Shih, Y.L., Fu, X., King, G.F., Le, T. and Rothfield, L. (2002) Division site placement in *E.coli*: mutations that prevent formation of the MinE ring lead to loss of the normal midcell arrest of growth of polar MinD membrane domains. *EMBO J.* 21: 3347-3357.

Shimada, H., Koizumi, M., Kuroki, K., Mochizuki, M., Fujimoto, H., Ohta, H., Masuda, T. and Takamiya, K.-i. (2004) ARC3, a chloroplast division factor, is a chimera of prokaryotic FtsZ and part of eukaryotic phosphatidylinositol-4-phosphate 5-kinase. *Plant Cell Physiol.* 45: 960-967.

Singh, J.K., Makde, R.D., Kumar, V. and Panda, D. (2007) A membrane protein, EzrA, regulates assembly dynamics of FtsZ by interacting with the C-Terminal tail of FtsZ. *Biochemistry* 46: 11013-11022.

Small, E. and Addinall, S.G. (2003) Dynamic FtsZ polymerization is sensitive to the GTP to GDP ratio and can be maintained at steady state using a GTP-regeneration system. *Microbiology* 149: 2235-2242.

Small, E., Marrington, R., Rodger, A., Scott, D.J., Sloan, K., Roper, D., Dafforn, T.R. and Addinall, S.G. (2007) FtsZ polymer-bundling by the *Escherichia coli* ZapA orthologue, YgfE, involves a conformational change in bound GTP. *J. Mol. Biol.* 369: 210-221.

Sossong, T.M., Jr., Brigham-Burke, M.R., Hensley, P. and Pearce, K.H., Jr. (1999) Self-activation of guanosine triphosphatase activity by oligomerization of the bacterial cell division protein FtsZ. *Biochemistry* 38: 14843-14850.

Stokes, K.D., McAndrew, R.S., Figueroa, R., Vitha, S. and Osteryoung, K.W. (2000) Chloroplast division and morphology are differentially affected by overexpression of FtsZ1 and FtsZ2 genes in Arabidopsis. *Plant Physiol.* 124: 1668-1677.

Stokes, K.D. and Osteryoung, K.W. (2003) Early divergence of the FtsZ1 and FtsZ2 plastid division gene families in photosynthetic eukaryotes. *Gene* 320: 97-108.

Strepp, R., Scholz, S., Kruse, S., Speth, V. and Reski, R. (1998) Plant nuclear gene knockout reveals a role in plastid division for the homolog of the bacterial cell division protein FtsZ, an ancestral tubulin. *Proc. Natl. Acad. Sci. U. S. A.* 95: 4368-4373.

Stricker, J. and Erickson, H.P. (2003) *In vivo* characterization of *Escherichia coli* ftsZ mutants: effects on Z-ring structure and function. *J. Bacteriol.* 185: 4796-4805.

Stricker, J., Maddox, P., Salmon, E.D. and Erickson, H.P. (2002) Rapid assembly dynamics of the *Escherichia coli* FtsZ-ring demonstrated by fluorescence recovery after photobleaching. *Proc. Natl. Acad. Sci. U. S. A.* 99: 3171-3175.

- Swarbreck, D., Wilks, C., Lamesch, P., Berardini, T.Z., Garcia-Hernandez, M., et al. (2007) The Arabidopsis Information Resource (TAIR): gene structure and function annotation. *Nucl. Acids Res.*: gkm965.
- Szeto, T.H., Rowland, S.L. and King, G.F. (2001) The dimerization function of MinC resides in a structurally autonomous C-terminal domain. *J. Bacteriol.* 183: 6684-6687.
- Takada, A., Nagai, K. and Wachi, M. (2005) A decreased level of FtsZ is responsible for inviability of RNase E-deficient cells. *Genes Cells* 10: 733-741.
- Tanaka-Takiguchi, Y., Itoh, T.J. and Hotani, H. (1998) Visualization of the GDP-dependent switching in the growth polarity of microtubules. *J. Mol. Biol.* 280: 365-373.
- Tian, G., Bhamidipati, A., Cowan, N.J. and Lewis, S.A. (1999) Tubulin folding cofactors as GTPase-activating proteins. GTP hydrolysis and the assembly of the alpha/beta-tubulin heterodimer. *J. Biol. Chem.* 274: 24054-24058.
- Tian, G., Huang, Y., Rommelaere, H., Vandekerckhove, J., Ampe, C. and Cowan, N.J. (1996) Pathway leading to correctly folded beta-tubulin. *Cell* 86: 287-296.
- Tian, G., Lewis, S.A., Feierbach, B., Stearns, T., Rommelaere, H., Ampe, C. and Cowan, N.J. (1997) Tubulin subunits exist in an activated conformational state generated and maintained by protein cofactors. *J. Cell Biol.* 138: 821-832.
- Tieu, Q. and Nunnari, J. (2000) Mdv1p is a WD repeat protein that interacts with the dynamin-related GTPase, Dnm1p, to trigger mitochondrial division. *J. Cell Biol.* 151: 353-366.
- Tieu, Q., Okreglak, V., Naylor, K. and Nunnari, J. (2002) The WD repeat protein, Mdv1p, functions as a molecular adaptor by interacting with Dnm1p and Fis1p during mitochondrial fission. *J. Cell Biol.* 158: 445-452.
- van den Ent, F. and Lowe, J. (2000) Crystal structure of the cell division protein FtsA from *Thermotoga maritima*. *EMBO J.* 19: 5300-5307.
- Vandecandelaere, A., Brune, M., Webb, M.R., Martin, S.R. and Bayley, P.M. (1999) Phosphate release during microtubule assembly: what stabilizes growing microtubules? *Biochemistry* 38: 8179-8188.
- Vaughan, S., Wickstead, B., Gull, K. and Addinall, S.G. (2004) Molecular evolution of FtsZ protein sequences encoded within the genomes of archaea, bacteria, and eukaryota. *J. Mol. Evol.* 58: 19-29.

- Vitha, S., Froehlich, J.E., Koksharova, O., Pyke, K.A., van Erp, H. and Osteryoung, K.W. (2003) ARC6 Is a J-Domain plastid pision protein and an evolutionary descendant of the cyanobacterial cell division protein Ftn2. *Plant Cell* 15: 1918-1933.
- Vitha, S., Holzenburg, A. and Osteryoung, K.W. (2005) Assembly dynamics of FtsZ and ARC6 plastid-dividing proteins. *Microsc. Microanal.* 11 (Suppl 2): 1154.
- Vitha, S., McAndrew, R.S. and Osteryoung, K.W. (2001) FtsZ ring formation at the chloroplast division site in plants. *J. Cell Biol.* 153: 111-119.
- Wang, X., Huang, J., Mukherjee, A., Cao, C. and Lutkenhaus, J. (1997) Analysis of the interaction of FtsZ with itself, GTP, and FtsA. *J. Bacteriol.* 179: 5551-5559.
- Wang, X. and Lutkenhaus, J. (1993) The FtsZ protein of *Bacillus subtilis* is localized to the division site and has a GTPase activity that is dependent upon the FtsZ concentration. *Mol. Microbiol.* 9: 435-442.
- Waterman-Storer, C.M. and Salmon, E.D. (1998) How microtubules get fluorescent speckles. *Biophys. J.* 75: 2059-2069.
- Weigel, D. and Glazebrook, J. (2002) *Arabidopsis: A laboratory manual*. Cold Spring Harbor Press, Cold Spring Harbor, New York.
- White, E.L., Ross, L.J., Reynolds, R.C., Seitz, L.E., Moore, G.D. and Borhani, D.W. (2000) Slow polymerization of *Mycobacterium tuberculosis* FtsZ. *J. Bacteriol.* 182: 4028-4034.
- Woldringh, C.L., Mulder, E., Valkenburg, J.A., Wientjes, F.B., Zaritsky, A. and Nanninga, N. (1990) Role of the nucleoid in the toporegulation of division. *Res. Microbiol.* 141: 39-49.
- Xu, Y. and Xu, D. (2000) Protein threading using PROSPECT: design and evaluation. *Proteins* 40: 343-354.
- Yan, K., Pearce, K.H. and Payne, D.J. (2000) A conserved residue at the extreme C-terminus of FtsZ is critical for the FtsA-FtsZ interaction in *Staphylococcus aureus*. *Biochem. Biophys. Res. Commun.* 270: 387-392.
- Yoder, D.W., Kadirjan-Kalbach, D., Olson, B.J.S.C., Miyagishima, S.Y., Deblasio, S.L., Hangarter, R.P., Osteryoung, K.W. and Vitha, S. (2007) Effects of mutations in *Arabidopsis* FtsZ1 on plastid division, FtsZ ring formation and positioning, and FtsZ filament morphology in vivo. *Plant Cell Physiol.* 48: 775-791.

Yoshida, Y., Kuroiwa, H., Misumi, O., Nishida, K., Yagisawa, F., Fujiwara, T., Nanamiya, H., Kawamura, F. and Kuroiwa, T. (2006) Isolated Chloroplast Division Machinery Can Actively Constrict After Stretching. *Science* 313: 1435-1438.

Yu, X.C. and Margolin, W. (1997) Ca^{2+} -mediated GTP-dependent dynamic assembly of bacterial cell division protein FtsZ into asters and polymer networks *in vitro*. *EMBO J.* 16: 5455-5463.

Zheng, Y., Wong, M.L., Alberts, B. and Mitchison, T. (1995) Nucleation of microtubule assembly by a gamma-tubulin-containing ring complex. *Nature* 378: 578-583.

MICHIGAN STATE UNIVERSITY LIBRARIES



3 1293 02956 5946